THE UNIVERSITY
of EDINBURGH

The study of *RIN3*:

A susceptibility gene for Paget's disease of bone

Mahéva VALLET (HND, M.Eng)

A thesis submitted for the degree of Doctor of Philosophy

University of Edinburgh

2017

À mon grand-père.

DECLARATION

I hereby declare that this thesis has been composed by myself and the work described within, except where specifically acknowledged, is my own and that it has not been accepted in any previous application for a degree. The information obtained from sources other than this study is acknowledged in the text or included in the references.

Mahéva VALLET

CONTENTS

Dedication III

Declaration V

Contents VII

Acknowledgements XIII

Publications from this thesis XV

Abbreviations XVII

List of figures XXIII

List of tables XXVI

Abstract XXIX

Lay abstract XXXI

CHAPTER ONE

1 INTRODUCTION 2

1.1 BONE ANATOMY AND FUNCTION 2

1.1.1 Bone structure 2

1.1.2 Bone cells 7

1.1.3 Bone remodelling 17

1.2 PAGET'S DISEASE OF BONE 22

1.2.1 Historical aspect 22

1.2.2 Epidemiology 23

1.2.3 Clinical features 25

1.2.4 Cellular abnormalities 27

1.3 MANAGEMENT OF PAGET'S DISEASE OF BONE 28

1.3.1 Bisphosphonates 28

1.3.2 Other treatments 30

1.3.3 Non-pharmacologic treatments 31

1.3.4 Monitoring 31

1.3.5 Surgery 31

1.4 GENETICS AND PAGET'S 33

1.4.1 Classical Paget's 34

1.4.2 Paget's disease-like disorders 52

1.5 CANDIDATE PATHOPHYSIOLOGICAL MECHANISMS 59
1.5.1 Environmental factors 59
1.5.2 Osteoclastic factors of Paget's disease of bone 64
1.5.3 Autophagy 67
1.5.4 Ephrins 69
1.6 AIMS OF THIS THESIS 70

CHAPTER TWO

2 MATERIALS AND METHODS 72
2.1 MUTATION SCREENING 72
2.1.1 Sanger sequencing 72
2.1.2 Next generation sequencing 80
2.1.3 Frequency analysis 81
2.1.4 Imputation 82
2.1.5 In silico analysis of variant pathogenicity 83
2.2 GENOTYPING FOR ALLELIC ASSOCIATION 85
2.2.1 Cohort 85
2.2.2 Variants analysed 85
2.2.3 Analysis 87
2.3 TISSUE CULTURE 92
2.3.1 Osteoclast cell culture 92
2.3.2 Osteoblast cell culture 95
2.4 RNA RELATED INVESTIGATIONS 100
2.4.1 TRizol® sample collection 100
2.4.2 RNA isolation 101
2.4.3 Reverse transcription 102
2.4.4 Quantitative real-time PCR 103
2.5 PROTEIN RELATED INVESTIGATION 108
2.5.1 Protein isolation 108
2.5.2 Protein quantification 108
2.5.3 Gel elecrophoresis 109
2.5.4 Electrophoretic transfer 109
2.5.5 Immunostaining and antibody detection 110

2.6 IMMUNOFLUORESCENCE 111
2.7 IMMUNOHISTOCHEMISTRY 112
2.8 MICE EXPERIMENTATION 115
2.8.1 Mice 115
2.8.2 Genotyping methods 116
2.8.3 Micro computed tomography 119
2.8.4 Bone histomorphometric analysis 124
2.8.5 Data analysis 132

CHAPTER THREE

3 TARGETED SEQUENCING OF THE PAGET'S DISEASE ASSOCIATED 14Q32 LOCUS 134

3.1 SUMMARY 134
3.2 INTRODUCTION 135
3.3 METHODS 136
3.4 RESULTS 138
3.4.1 Imputation of the 14q32 locus 138
3.4.2 Detection of variants in *RIN3* 140
3.4.3 *In silico* analysis of RIN3 mutations 144
3.5 DISCUSSION 151

CHAPTER FOUR

4 *RIN3* VARIANTS AND DISEASE SEVERITY IN PDB 158

4.1 SUMMARY 158
4.2 INTRODUCTION 159
4.3 METHODS 160
4.4 RESULTS 162
4.4.1 Case and control investigations 162
4.4.2 Association study with disease activity 164
4.5 DISCUSSION 169

CHAPTER FIVE

5 EXPRESSION OF *RIN3* IN BONE AND BONE CELLS 176

5.1 SUMMARY 176

5.2 INTRODUCTION 177

5.3 METHODS 178

5.4 RESULTS 179

5.4.1 Expression of *Rin3* in mouse tissues 179

5.4.2 *Rin3* mRNA is expressed in cells of the bone micro environment 180

5.4.3 RIN3 protein is expressed in the murine bone micro environment 181

5.4.4 RIN3 is expressed through the cytoplasm of osteoclasts cultured from mice 184

5.4.5 RIN3 is highly expressed through the cytoplasm of human osteoclasts 185

5.5 DISCUSSION 187

CHAPTER SIX

6 PHENOTYPE ANALYSIS OF *Rin3* DEFICIENT MICE 194

6.1 SUMMARY 194

6.2 INTRODUCTION 195

6.3 METHODS 197

6.4 RESULTS 198

6.4.1 *Rin3* deficient mice have a normal body weight 198

6.4.2 *Rin3* deficient mice have an increased bone mass and trabecular number 198

6.4.3 *Rin3* deficient mice show an osteoclastic phenotype 206

6.4.4 Osteoblasts cultured from *Rin3* deficient mice 211

6.4.5 Osteoclasts cultured from *Rin3* deficient mice show the same formation and survival pattern than wild type mice 213

6.5 DISCUSSION 216

CHAPTER SEVEN

7 DISCUSSION AND CONCLUSIONS 224

BIBLIOGRAPHY 235

APPENDICES ***261***

Appendix 1. Materials, reagents, technical equipment and software 262

Appendix 2.1. Primer sequences for *RIN3* amplification 270

Appendix 2.2. Solutions for TRAcP staining in culture plates 272

Appendix 2.3. ALP assay solutions 273

Appendix 2.4. Solution for cell lysis 274

Appendix 2.5. Western blot solutions 275

Appendix 2.6. Apathy syrup composition 276

Appendix 4.1. Haplotype diagram 277

Appendix 4.2. Estimated haplotype frequencies for the PRISM cohort 278

Appendix 4.3. Details of the association study for p.T425M in the PRISM cases 279

Appendix 4.4. Details of the association study for p.T425M in the PRISM cases not carrying *SQSTM1* mutations 280

Appendix 4.5. Details of the association study for p.T425M in the PRISM cases carriers of *SQSTM1* mutation 281

Appendix 4.6. Details of the association study for p.R279C in the PRISM cases 282

Appendix 4.7. Details of the association study for p.R279C in the PRISM cases not carrying *SQSTM1* mutations 283

Appendix 4.8. Details of the association study for p.R279C in the PRISM cases carriers of *SQSTM1* mutation 284

Appendix 4.9. Details of the association study for the rare variants in the PRISM cases 285

Appendix 4.10. Details of the association study for the rare variants in the PRISM cases not carrying *SQSTM1* mutations 286

Appendix 4.11. Details of the association study for the rare variants in the PRISM cases carriers of *SQSTM1* mutation 287

Appendix 4.12. Estimated haplotype frequencies for the PRISM cases, including the GWAS hit imported data 288

ACKNOWLEDGEMENTS

Firstly, I would like to express my most sincere gratitude to my primary supervisor Professor Stuart H. Ralston, who has provided the most undivided guidance and support through this PhD and always offered precious advice whenever I needed it. He has been the most inspiring mentor I could have hoped for. I am also extremely grateful to my co-supervisor Dr. Jon P. Warner, for defying all studentship odds to allow me in his lab and showing constant enthusiasm towards my project. They both have not only given me the chance of contributing to scientific research for the first time, but also the possibility to access a new life, in the gorgeous place that is Scotland.

I cannot thank Dr. Antonia Sophocleous enough for her tireless and invaluable support. This thesis would have not been possible without her help and I cannot express how lucky I have felt to have her by my side as a secondary supervisor through this journey. I wish you the best in Cyprus and will miss you. I would also like to express my sincere gratitude to Judith Pagan, who has guided me through the Sanger sequencing work.

I would like to especially thank Dr. Omar Albagha for his work in the imputation, next generation sequencing and analysis of both sequencing techniques, and Dr. Sachin Wani for his help in next generation sequencing. Thank you to Dr. Dinesh Soares for his work on the *in silico* study of *RIN3*. I would also like to thank Dr. Anna Törnqvist and Dr. Asim Azfer for their help and advice with the animal work. Many thanks to Professor Donald Salter and his pathological lab for helping with the immunohistochemistry, especially Helen Caldwell. I would also like to thank Professor Rob Van'T Hof and his technicians Gemma Charlesworth and Amanda Prior for the sections of the *Rin3*$^{-/-}$ mice and for opening your laboratory to me.

Thank you to Dr. Nerea Alonso Lopez for performing the haplotype analyses and severity association from those, and many thanks to Dr. Matthieu Vermeren for his advice and help on immunofluorescence. I would like to express my gratitude to my other colleagues in the bone group. Belinda, Mica, Azim, Barbara, Philip, Ariane, and also Colette - thank you for your constant professional and emotional support. Thank you to Jenna, Tara, Hayley, Nikki, Doreen, David, Ian, Elaine, Lorna, Louise, Austin, Paul and Freddie from the South East Scotland Clinical Genetics Service lab to truly let me be one of yours for a year. I am also very grateful for all patients who kindly participated in this work.

I would like to thank my family for all their love and support, especially my mum for pushing me as far as possible in everything I undertook in my life. You expected nothing but excellence of me, and all those hours of extra homework have finally paid off, thank you. I would also like to thank my extended family, Terry and Claude. I also have a special thought for my grandmother, Paulette and Miquette. Big, big stroke to the fluffy and cuddly Nikita. Finally, I would like to thank my boyfriend, Paul. I would have never done this without your unfailing constant support, topped with perfect cottage pies and mac and cheese. You are the best.

I dedicate this thesis to my grandfather, a man who represents the definition of hard work, with a heart bigger than himself (and to anyone who always has their names underlined in red by Word).

Some figures were adapted and modified from Servier Medical Art (Servier, 2017). This work was funded by the European Research Council (311723-GENEPAD) and by grants from Arthritis Research UK (19799 and 19520).

PUBLICATION FROM THIS THESIS

Papers

Vallet, M., Soares, D. C., Wani, S., Sophocleous, A., Warner, J., Salter, D. M., Ralston, S. H. & Albagha, O. M. (2015) Targeted sequencing of the Paget's disease associated 14q32 locus identifies several missense coding variants in *RIN3* that predispose to Paget's disease of bone. *Hum. Mol. Genet*, 24(11), 3286-3295.

Vallet, M. & Ralston, S. H. (2016) Biology and Treatment of Paget's Disease of Bone. *J Cell Biochem*, 117(2), 289-99

Abstracts, Oral Presentations & Awards

Vallet, M., Soares, D. C., Wani, S., Sophocleous, A., Warner, J., Salter, D. M., Ralston, S. H. & Albagha, O. M., Variants in RIN3 predispose to Paget's disease of bone. Presented at the 41th European Symposium on Calcified Tissues, Prague, Czech Republic, May 2014. **Received: New Investigator Award.**

Vallet, M., Soares, D. C., Wani, S., Sophocleous, A., Warner, J., Salter, D. M., Ralston, S. H. & Albagha, O. M., Targeted sequencing of the Paget's disease associated 14q32 locus identifies several missense coding variants in *RIN3* that predispose to Paget's disease of bone. Presented at the 48th European Society of Human Genetics, Glasgow, Scotland, June, 2015.

Vallet, M., Soares, D. C., Wani, S., Sophocleous, A., Warner, J., Salter, D. M., Ralston, S. H. & Albagha, O. M., Targeted sequencing of the Paget's disease associated 14q32 locus identifies several missense coding variants in *RIN3* that predispose to Paget's disease of bone. Presented at the British-Society-for-Matrix-Biology (BSMB) and Bone-Research-Society (BRS), Edinburgh, Scotland, September, 2015.

ABBREVIATIONS

129/OlaHsd	An inbred mouse strain
°C	Degrees celsius
αMEM	Alpha-minimum essential medium
$\alpha_v\beta_3$	Alpha-v beta-3 integrin
AA	Amino acid
ALP	Alkaline phosphatase
ALS	Amyotrophic lateral sclerosis
ANOVA	Analysis of variance
aPKCs	Atypical PKCs
Arg	Arginine
Asp	Aspartic acid
ATPase	Adenosine triphosphatase
β-GP	Beta-glycerol phosphate
BCA	Bicinchoninic acid
BFR	Bone formation rate
BGP	Bone gla protein
BM	Bone marrow
BMD	Bone mineral density
BMDMs	Bone marrow derived macrophages cells
BMPs	Bone morphogenic proteins
BMU	Basic multicellular unit
bp	Base pair
BV/TV	Trabecular bone volume to total volume
$C_{(t)}$	Threshold cycle
C57BL/6	An inbred mouse strain
Ca^{2+}	Calcium ions
Cath K	Cathepsin K
CD2AP	Adaptor CD2-associated protein
cDNA	Complementary DNA
CDV	Canine distemper virus
CEU	Utah Residents (CEPH) with Northern and Western European Ancestry
C-FMS	Gene encoding the receptor CSF1R
Cl^-	Chloride ions
CNOT4	CCR4-NOT transcription complex, subunit 4
Col1a1	Type 1 collagen
CSF1R	Colony-stimulating factor 1 receptor
Ct	Cortical

Ct.Ar	Cross-sectional cortical area
CYLD	Cylindromatosis (Turban tumor syndrome)
DC-STAMP	Dendritic cells - specific transmembrane protein
DEPC	Diethyl pyrocarbonate
dH_2O	Distilled water
DMSO	Dimethyl sulfoxide
DNA	Deoxyribonucleic acid
dNTP	Deoxynucleotide
DTT	Dithiothreitol
DXA	Dual-energy X-ray absorptiometry
EDTA	Ethylenediaminetetraacetic acid
ERK	Extracellular regulated kinase
ESH	Expansile skeletal hyphosphatasia
F primer	Forward primer
FCS	Fetal calf serum
FEO	Familial expansile osteolysis
FFPE	Formalin-fixed paraffin-embedded
FGF	Fibroblast growth factors
FPP	Farnesyl pyrophosphate
G	Gauge
GAP	GTPase-activating proteins
GCT	Giant cell tumour
GDP	Guanosine diphosphate
GEF	Guanine nucleotide exchange factors
GERP	Genomic evolutionary rate profiling
Gly	Glycine
GOLGA6A	Golgin A6 family, member A
GSTM4	Glutathione S-transferase Mu 4
GTP	Guanosine triphosphate
GTPase	Guanosine triphosphatase
GWAS	Genome wide association study
H^+	Hydrogen ions
HBSS	Hank's balanced salt solution
HCO_3^-	Bicarbonate ions
hnRNP	Heterogeneous nuclear ribonucleoprotein
IBM	Inclusion body myositis
IBMPFD	Inclusion body myopathy, Paget's disease and frontotemporal dementia
ID	Identification number
Ihh	Indian hedgehog
IkB	Inhibitor of NFκB

IKK	Iκβ kinase
IL	Interleukin
IS-RT-PCR	*In situ*-reverse transcriptase-polymerase chain reaction
JPD	Juvenile Paget's disease
kb	Kilo Base
kDa	Kilo Dalton
kg, g, mg, µg, ng	Kilogram, gram, milligram, microgram, nanogram
kV	Kilovolt
l, ml, µl	Litre, millilitre, microlitre
LC3	Light chain 3 gene
LD	Linkage disequilibrium
LL-BMD	Lower limb bone mineral density
LRP	Low-density lipoprotein receptor-related protein
M, mM, µM	Molar, millimolar, micromolar
mA	Milliampere
MACH	Markov chain haplotyping
MAF	Minor allele frequency
MAPK	Mitogen activated protein kinase
MAR	Mineral apposition rate
M-CSF	Macrophage colony stimulating factor
MEA	2-Methoxyethyl acetate
Med.Cav.Dm	Medullary cavity diameter
MEK	MAPK kinase/ERK kinase
mm, nm	Millimetre, nanometre
MMA	Methyl methacrylate
MMP	Metalloproteinase
Mϕ	Macrophage
mRNA	Messenger RNA
MSC	Mesenchymal stem cells
MV	Measles virus
MVNP	MV nucleocapsid
MVs	Matrix vesicles
NEMO	NFκB essential modulator
NFκB	Nuclear factor κB
NRF-2	Nuclear respiratory factor 1
NSAIDs	Non-steroidal anti-inflammatory drugs
NUP 205	Nucleoporin 205
OB	Osteoblast
Ob.N/BS	Osteoblast number per bone surface
OC	Osteoclast
Oc.N/BS	Osteoclast number per bone surface
Oc.S/BS	Active resorption area per bone surface

OCN	Osteocalcin
OPG	Osteoprotegerin
OPN	Osteopontin
OPTN	Optineurin (Optic neuropathy inducing)
OSN	Osteonectin
Osx	Osterix
P	Probability
p62	Protein 62
PBMCs	Peripheral blood mononuclear cells
PBS	Phosphate buffered saline
PCR	Polymerase chain reaction
PDB	Paget's disease of bone
Pi	Inorganic phosphate
PPi	Inorganic pyrophosphate
PKCs	Protein kinase Cs
PML	Promyelocytic leukemia
PNP	p-nitrophenol-phosphate
PRISM	Paget's disease of bone: a randomized trial of intensive versus symptomatic management
PRR	Proline rich region
PTH	Parathyroid hormone
qPCR	Real time quantitative PCR
R primer	Reverse primer
RA	Ras-association
RANK	Receptor activator of NF-κB
RANKL	Receptor activator of NF-κB ligand
RGD	Arg-Gly-Asp tripeptide
RIN	Rab and Ras Interactor
RNA	Ribonucleic Acid
ROI	Region of interest
rpm	Revolutions per minute
rRNA	Ribosomal RNA
RSV	Respiratory syncytial virus
RT-PCR	Reverse transcription PCR
Runx2	Runt-related transcription factor 2
SCF	Stem cell factor
SD	Standard deviation
SEM	Standard error of mean
SH	Src-homology
SNP	Single nucleotide polymorphism
SOST	Sclerostin
Sox9	DNA-binding SRY box 9

SQSTM1	Sequestosome 1
TAFII-17	Transcription factor II D subunit 17
Tb	Trabecular
TBST	Tris-buffered saline and tween
TGF-β	Transforming growth factor-b
TM7SF4	Transmembrane 7 superfamily member 4
TNF	Tumour necrosis factor
TNFRSF	TNF receptor superfamily
TRAcP	Tartrate-resistant acid phosphatase staining
TRAF6	TNF receptor-associated factor 6
TRANCE	TNF-related activation-induced cytokine
TRizol®	Total RNA isolation reagent
UBA	Ubiquitin associated domain
UBD	Ubiquitin-binding domain
MicroCT	Micro computed tomography
UTR	Untranslated region
UV	Ultraviolet
v/v	Volume to volume
VCP	Vasolin-containing protein
VOI	Volume of interest
VPS9	Vacuolar protein sorting 9
w/v	Weight to volume
WT	Wild type
ZiPP	Zoledronate in the prevention of Paget's
ZNF687	Zinc finger protein 687

LIST OF FIGURES

Figure 1.1: Structure of a long bone 3

Figure 1.2: Schematic representation of an osteon structure in cortical bone 5

Figure 1.3: Schema of osteoclast differentiation (Boyle et al, 2003) 8

Figure 1.4: Summary of the osteoclastic resorption (Rosen, 2013)..... 11

Figure 1.5: Schematic illustration of the bone remodelling..... 21

Figure 1.6: Sir James Paget and Paget's disease of bone..... 22

Figure 1.7: Trabecular biopsies of Pagetic bones 25

Figure 1.8: Regulation of the bone resorption activity through the NFκB pathway (Rea et al, 2013)..... 36

Figure 1.9: Schema of GTPase activation cycle (Nielsen et al, 2008)..... 47

Figure 1.10: Schematic illustration of the human *RIN3* gene and its domains..... 51

Figure 1.11: Electron microscopy photography of the nucleus of a Pagetic osteoclast (Mills & Singer, 1976) 60

Figure 2.1: AMPure XP purification process (Beckman Coulter, 2017a)..... 76

Figure 2.2: CleanSEQ purification process (Beckman Coulter, 2017b)..... 78

Figure 2.3: General process of sequencing reaction for *RIN3* 79

Figure 2.4: Summary of the Taqman SNP Genotyping assay (Life Technologies, 2011) 88

Figure 2.5: Summary of bone marrow osteoclast culture 93

Figure 2.6: Summary of calvarial osteoblast culture 97

Figure 2.7: Screenshots of the Opticon Monitor 3.1 quantification curves 106

Figure 2.8: Area deleted of *Rin3* by the Internal Mouse Phenotyping Consortium 115

Figure 2.9: DNA gel electrophoresis to determine *Rin3* mice genotype 118

Figure 2.10: Holders used for the microCT analyses..... 120

Figure 2.11: Summary of the area traced from bone for microCT analysis 122

Figure 2.12: Site of dissection of femur for plastic embedding and histomorphometry 124

Figure 2.13: Process of the TrapHisto software to identify and measure bone and osteoclast parameters 129

Figure 2.14: Images of the calcein labelling analysed by the CalceinHisto software 131

Figure 3.1: Association plots for the 14q32 locus and conditional analysis for rs10498635 139

Figure 3.2: Schematic illustration of missenses on the RIN3 protein sequence 142

Figure 3.3: Screenshot of the Hapmap LD analysis for the GWAS hit against common variants detected in *RIN3* by fine-mapping 142

Figure 3.4: PONDR VL-XT disorder predictions of the coding variants locating in the PRR region of RIN3 146

Figure 3.5: 3D Homology model of the SH2 and VPS9 domains 147

Figure 3.6: Evaluation of the 3D Homology model of the VPS9 domain using MetaMQAPII 148

Figure 3.7: Assessment of the exposition of p.G613A and p.Y793H in the VPS9 domain 148

Figure 3.8: Importance of helical structures in the VPS9 149

Figure 5.1: Expression of mRNA *Rin3* in mouse tissues 179

Figure 5.2: mRNA expression of *Rin3* in the bone microenvironment 180

Figure 5.3: Expression of protein RIN3 in BM, Mϕ and OC under RANKL stimulation 182

Figure 5.4: Expression of protein RIN3 during osteoclast differentiation under RANKL stimulation 183

Figure 5.5: Pictures of cultured M-CSF and RANKL stimulated mouse bone marrow derived-osteoclasts stained by immunofluorescence for RIN3 184

Figure 5.6: Pictures of tissue sections stained by immunohistochemistry for RIN3 186

Figure 6.1: Body weight of *Rin3*$^{-/-}$ female mice at age 8 weeks 198

Figure 6.2: MicroCT results on the *Rin3*$^{-/-}$ mice and WT controls, for the femoral trabecular bone 199

Figure 6.3: MicroCT results on the *Rin3*$^{-/-}$ mice and WT controls, for the tibial trabecular bone 200

Figure 6.4: MicroCT results on the *Rin3*$^{-/-}$ mice and WT controls, for the trabecular bone of the spine 201

Figure 6.5: MicroCT results on the *Rin3*$^{-/-}$ mice and WT controls, for the femoral cortical bone 202

Figure 6.6: 3D remodelling pictures of the scanned bones in *Rin3*$^{-/-}$ and WT controls 205

Figure 6.7: Histomorphometric results on the *Rin3*$^{-/-}$ mice and WT controls for TRAcP staining and osteoclast analysis 207

Figure 6.8: Representative sections of the WT and *Rin3*$^{-/-}$ mice after TRAcP staining 208

Figure 6.9: Dynamic histomorphometric analysis from calcein labelling on *Rin3*$^{-/-}$ mice and WT controls 209

Figure 6.10: Representative sections of the WT and *Rin3*$^{-/-}$ double calcein labelling staining 210

Figure 6.11: Calvarial osteoblasts ALP activity levels from *Rin3*$^{-/-}$ mice and WT controls 211

Figure 6.12: Alizarin red staining of mineralised nodules from *Rin3*$^{-/-}$ mice and WT calvarial osteoblasts 212

Figure 6.13: Osteoclast numbers from RANKL and M-CSF stimulated osteoclast cultures, from *Rin3*$^{-/-}$ and WT control mice 214

Figure 6.14: Survival assay in RANKL and M-CSF stimulated osteoclasts from *Rin3*$^{-/-}$ and WT control mice 215

LIST OF TABLES

Table 1.1: Summary of genes associated with Paget's disease of Bone 34

Table 1.2: Clinical features of rare inherited syndromes similar to Paget's disease of bone 53

Table 2.1: Sequences of the M13 primers used for sequencing PCR reactions 73

Table 2.2: Master mix used for universal PCR 74

Table 2.3: Master mix used for GC rich PCR 75

Table 2.4: PCR conditions used for each exon of the *RIN3* gene 75

Table 2.5: Master mix composition for the sequencing reaction (96 and 384 well plates) 77

Table 2.6: Sequencing mix composition (96 and 384 well plates) 77

Table 2.7: Summary of genotyped variants in *RIN3* 86

Table 2.8: Clinical phenotypes investigated in presence of *RIN3* mutations (Visconti et al, 2010) 90

Table 2.9: qPCR primers of *Rin3* and probe library number and sequence 104

Table 2.10: Sets of primers used for the determination of the mice genotypes 118

Table 2.11: NRecon software parameters for reconstruction (Campbell & Sophocleous, 2014) 120

Table 2.12: Ctan software parameters outcome (Campbell & Sophocleous, 2014) 123

Table 2.13: Embedding process program used with the Leica tissue processor 125

Table 2.14: Composition of the methoxyethyl acetate infiltration solution 125

Table 2.15: MEA resin removal steps in preparation of TRAcP staining 127

Table 2.16: Tartrate-resistant-acid-phosphatase staining solution composition for histomorphometry 128

Table 2.17: Traphisto software outcome data 129

Table 2.18: Calceinhisto software outcome data 132

Table 3.1: Statistical analysis of frequencies from potential pathogenic variants detected by sequencing in *RIN3* 141

Table 3.2: FoldX stability calculations for equivalent residues in template structures 150

Table 4.1: Burden test analysis on rare variants genotyped in *RIN3* 162

Table 4.2: Statistical analysis of frequencies from rare variants genotyped in *RIN3* 163

Table 4.3: Statistical analysis of the severity association on haplotype 1 from PRISM/SQSTM1- cases 166

Table 4.4: Statistical analysis of the severity association on haplotype 7 containing p.T425M from PRISM/SQSTM1– cases 167

Table 4.5: Statistical analysis of the severity association on haplotype 18 containing p.R279C from PRISM/SQSTM1– cases 168

Table 6.1: Summary of statistical analyses of the microCT scanning results on the *Rin3*$^{-/-}$ mice and WT controls 203

THE STUDY OF *RIN3*: A SUSCEPTIBILITY GENE FOR PAGET'S DISEASE OF BONE

Mahéva VALLET

College of Medicine and Veterinary Medicine

Deanery of Molecular, Genetic and Population Health Sciences

University of Edinburgh

ABSTRACT

Paget's disease of bone (PDB) shows a strong genetic component and mutations in *SQSTM1* (Sequestosome 1) are observed in about 10% of sporadic PDB patients.

My PhD investigated the *RIN3* gene (Ras and Rab interactor protein 3), previously implicated in the pathogenesis of PDB by GWAS. The *RIN3* gene encodes a guanine exchange factor (GEF), involved in the activation of GTPases which are crucial in osteoclast activity. It also has a role in endocytosis and recycling of tyrosine kinase receptor. The role of *RIN3* in bone remodelling is unclear, however some investigations revealed some associations with bone: *RIN3* has been associated with high lower limb bone mineral density in children in a meta-analysis of GWAS studies, and was shown to be expressed in primary calvarial osteoblasts. The expression of *RIN3* was down regulated during human primary osteoclast differentiation, and also in iliac bone biopsies from osteoporotic patients compared to healthy postmenopausal donors (Kemp et al, 2014).

In Chapter 1, I present normal bone structure, composition and remodelling before detailing PDB and its genetics. I then introduce *RIN3* as a candidate gene for PDB. In Chapter 2, I describe all methods performed and materials used for the completion of this project. This includes primary cell cultures, RNA and protein work, immunostaining, immunochemistry and phenotype analysis on *Rin3*$^{-/-}$ mice. Chapter 3 presents the fine mapping of *RIN3* using Sanger and next generation sequencing performed on PDB cases and controls. 18 variants were detected and one common variant (p.R279C) showed a strong association with PDB. Rare variants were also over-represented in cases, and many were shown to be on the same haplotype as p.R279C. Chapter 4 details the association study performed on a UK cohort and includes the investigation of the clinical phenotype severity in patients against the *RIN3* mutations. Chapter 5 presents the expression pattern of *RIN3* in bone cells and bone microenvironment. Important variations of *RIN3* mRNA and protein were detected during the differentiation of bone marrow derived osteoclasts. Protein levels of RIN3 were also found in osteoclasts from human osteoclastoma, human osteosarcoma, PDB patients, giant cell tumour (GCT) and healthy controls. Within all the mouse tissues analysed, *Rin3* mRNA was expressed the highest in bone after lung. Chapter 6 focuses on the work performed on mice deficient of the *Rin3* gene. They showed a higher trabecular bone volume and a smaller active resorption surface occupied by osteoclasts in trabecular bone.

In conclusion, the combined *in vitro* and *in vivo* analyses have uncovered that *RIN3* plays a role in bone metabolism and is a strong gene candidate for PDB.

THE STUDY OF *RIN3*: A SUSCEPTIBILITY GENE FOR PAGET'S DISEASE OF BONE

Mahéva VALLET

College of Medicine and Veterinary Medicine

Deanery of Molecular, Genetic and Population Health Sciences

University of Edinburgh

LAY ABSTRACT

Paget's disease of bone (PDB) is a common skeletal disease where too much bone is being formed, and too quickly. Typically, this is caused by an over-activation of osteoclasts, the cells responsible for bone resorption. This results in a weak bone and patients can develop important bone pain and deformities, leading to complications such as nerve compression and fractures.

The origin of PDB is still not fully understood, however it has been shown that specific DNA mutations can predispose to it. The most important gene is *SQSTM1*, but mutations are present in only 10% of patients without family history. More genes need to be investigated to allow a better diagnosis and prevention of the disease in patients. My PhD consisted in investigating a new gene called *RIN3*, thought to be involved in PDB and bone remodelling.

A common mutation and many rare mutations were found to be more present in patients than in controls. The expression of *Rin3* was also confirmed for the first time in osteoclasts generated from mice, and was also the highest in bone tissue from mice compared to all other organs investigated. *RIN3* was also found to be expressed in human osteoclasts in both healthy and Pagetic patients.

I additionally investigated bone changes in mice for which the *Rin3* gene was inactivated. These mice had increased bone mass, as well as a smaller surface area occupied by active osteoclasts compared to control mice.

This confirms that *RIN3* is expressed in mouse and human bone. It also shows that removing the *Rin3* gene in mice provokes changes in bone metabolism, leading us to think that it would normally lower bone mass and increase resorption surface. These being important features of PDB, *RIN3* becomes a strong candidate to consider. The mutations detected follow this trend as well and could, with more investigation, help us understand the complexity of PDB in more depth.

CHAPTER ONE

INTRODUCTION

1 INTRODUCTION

1.1 BONE ANATOMY AND FUNCTION

1.1.1 Bone structure

The skeleton is a strong and supportive structure, made of two connective tissues that are mineralised bone and cartilage. In association with the muscles, the bones offer mechanical strength and motion to the body, as well as organ protection and mineral storage. Based on their structure, bones are organised in four categories: long, short, flat, and irregular (Clarke, 2008).

Long bones are made of a hollow shaft called diaphysis, closed by larger and rounder ends called epiphyses, allowing articulation. The central medullary cavity of the diaphysis contains the haematopoietic marrow which confers a supply of growth factors, cytokines and haematopoiesis for the body. Growth plates are located at the metaphyses, between the diaphysis and the epiphyses of the bone. The joints at the end of long bones are protected by cartilage, while the outer surface of the rest of the bones are covered by a membrane called periosteum. This connective tissue is held tightly against the cortical bone by collagenous fibres called Sharpey's fibers, running through the underlying bone (Figure 1.1). Examples of long bones would be clavicles, humerus, radius, femurs, tibiae, or phalanges. They are involved in weight bearing and movement (Clarke, 2008).

Short bones are usually of cubic shape and are as large as they are wide. They typically include the carpal bones of the wrist and tarsal bones of the feet and are involved in movement. Flat bones can be of many shapes such as the skull, scapulae, sternum or the ribs, and they are involved in internal organ protection.

Irregular bones such as vertebrae, sacrum, or coccyx have complex structures and have a protective role as well (Clarke, 2008).

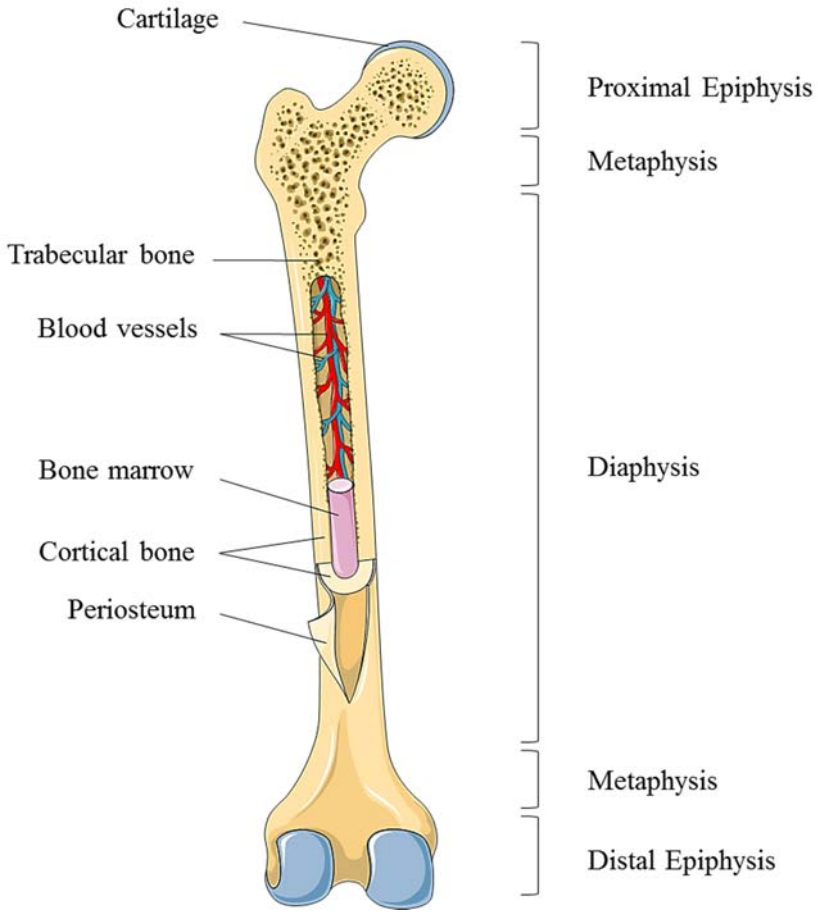

Figure 1.1: Structure of a long bone.
Adapted using Servier medical art (Servier, 2017).

The adult skeleton is made of 80% cortical bone, which has a solid and compact architecture. The rest is made of spongy like cancellous bone, called trabecular bone. The ratio between the two can vary a lot from one bone to the other (Clarke, 2008).

Cortical bone has a white dense characteristic look and is located on the outer side of the bones to protect the marrow. It has low metabolic activity and is made of multiple cylinders called osteons, or Haversian systems. Each cylinder is a succession of concentric lamellae made of collagen fibres, surrounding a Haversian canal where nerve fibres and blood vessels are passing through (Figure 1.2) (Clarke, 2008).

Cancellous bone, also called trabecular or spongy bone, is softer and less dense. It fills the cortical bone and has a spongy aspect. The empty spaces are filled with bone marrow, making trabecular bone more metabolically active than cortical bone. It is highly present in flat bones and in the epiphyses and metaphyses of the long bones (Figure 1.1). Trabecular bone is also constituted of osteons called packets, made of concentric lamellae organised in a parallel fashion (Clarke, 2008).

Bone is made of an inorganic matrix (70-90%), an organic matrix (20-40%), cells (osteoblasts, osteocytes, and osteoclasts) and water (Clarke, 2008). The main mineral compound which constitutes bone is a close analogue of a naturally occurring crystal, called hydroxyapatite ($Ca_{10}[PO_4]_6[OH]_2$) (Rosen, 2013). Additional minerals such as phosphate, carbonate and magnesium are also found, although composition varies with environment and diet (Rosen, 2013).

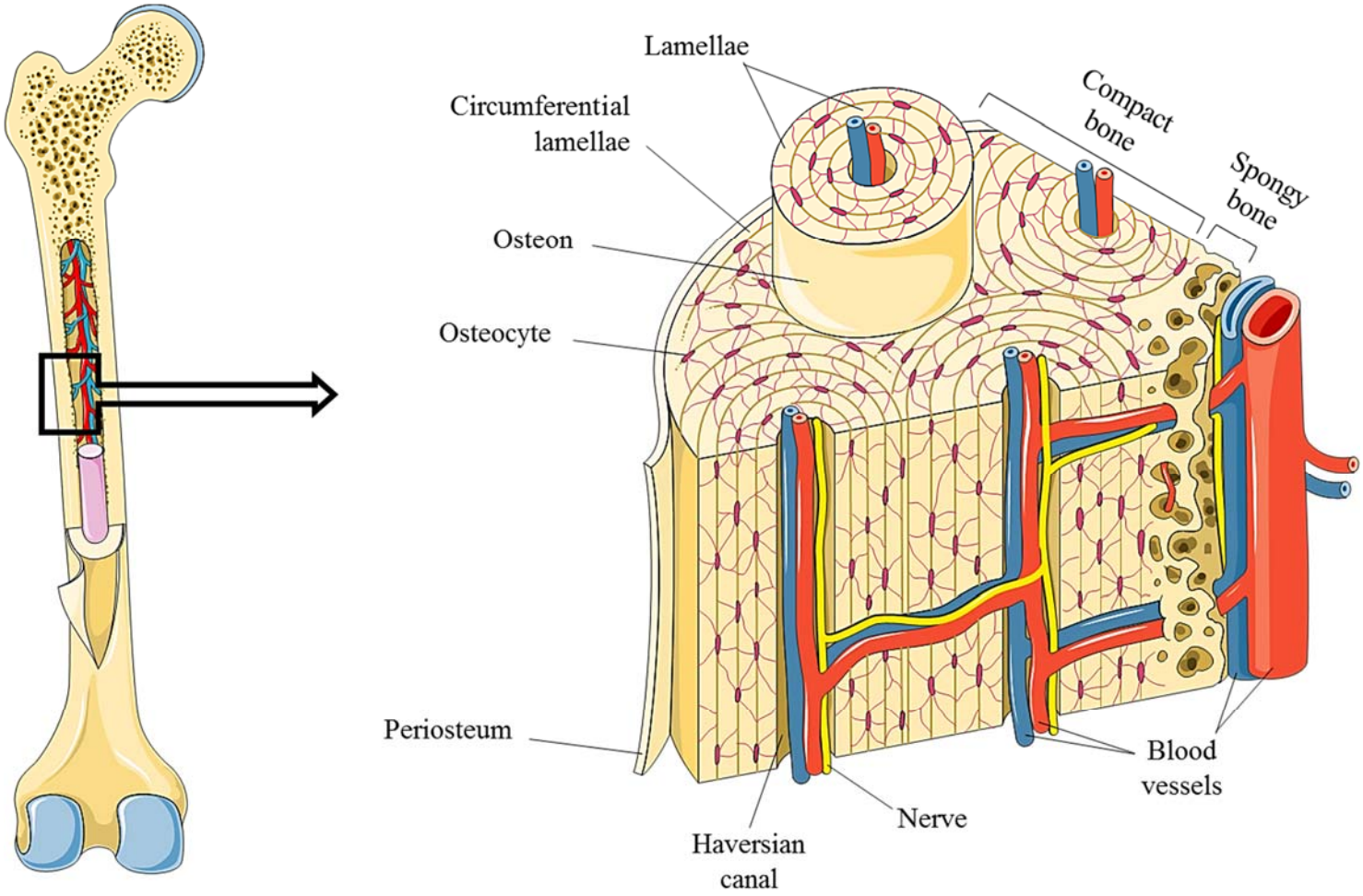

Figure 1.2: Schematic representation of an osteon structure in cortical bone.
Adapted using Servier medical art (Servier, 2017).

The organic matrix is mostly constituted of collagen type I (90%) which confers strength to the bone. Collagen fibrils are made of triple helixes of polypeptides chains, organised in a parallel fashion. Non-collagenous proteins and molecules are however also present (10%). Although some are of exogenous origin like albumin, most are synthesised by osteoblasts and are involved in the bone turnover process. Typical proteins would be alkaline phosphatase (ALP) involved in mineralization, osteonectin (OSN) involved in collagen organisation and bone formation, osteopontin (OPN) which is able to bind to cells and collagen, and may be involved in mineralization and cell proliferation, or osteocalcin (OCN, or bone GLA protein (BGP)) which may be involved in the regulation of osteoclast activity (Rosen, 2013).

Microscopically, bone appears in a woven or lamellar pattern. Lamellar bone is seen in the mature skeletons. It is found in cortical and trabecular bone and has, as its name implies, a lamellar organised appearance. Woven bone is observed during skeletal growth, but it can also be found in adult pathological bone with increased bone turnover. This includes fractures or Paget's disease of bone (PDB), which is a bone remodelling disorder with weak and disorganised bone (Section 1.2). Woven bone is characterized by a distinctive disorganised pattern and results in a significant reduction of mechanical strength (Clarke, 2008).

1.1.2 Bone cells

Osteoclasts and bone resorption

Osteoclasts are part of the monocyte macrophage family and are the only cell type responsible for the resorption of bone. They make up 1 to 2% of the total bone cells (Rosen, 2013).

Mononuclear precursor (pre-osteoclasts) proliferation and differentiation are under the control of the macrophage-colony stimulating factor (M-CSF, also called CSF1 for colony stimulating factor-1). These pre-osteoclasts then fuse into a polykaryon in response to the receptor activator of NFκB (RANK) stimulation, triggered by the pairing of RANK ligand (RANKL) to the RANK membrane receptor. This will result in the activation of the nuclear factor κB (NFκB) pathway, involved in osteoclastogenesis. Typical osteoclast genes such as tartrate-resistant acid phosphatase (*TRAP*) will also be activated (Figure 1.3) (Boyle et al, 2003).

RANKL is a member of the tumour necrosis factor super family (TNF), and is expressed in the bone microenvironment (Boyle et al, 2003). Knock out of RANK or RANKL in mice resulted in inhibition of osteoclast development and osteopetrosis which, in contrast with osteoporosis, leads to excess bone formation, denser and brittle bone (Dougall et al, 1999; Kong et al, 1999).

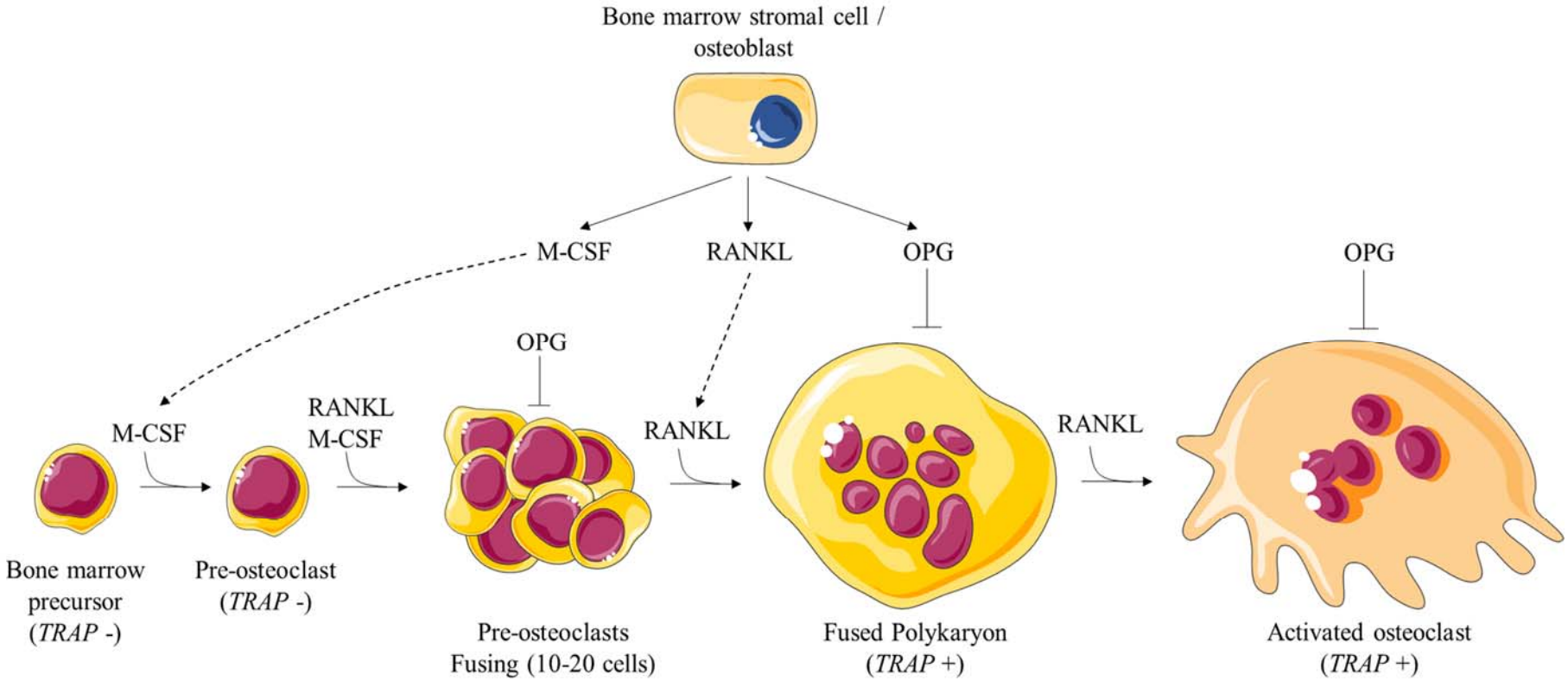

Figure 1.3: Schema of osteoclast differentiation (Boyle et al, 2003).

The M-CSF cytokine binds to the CSF1R receptor of the osteoclast precursor to induce proliferation and differentiation of the mononuclear cells. RANKL, produced by osteoblasts, interacts with RANK localised on the membrane of immature osteoclasts and of bone marrow stromal cells. This will result in the fusion of pre-osteoclasts into a polykaryon until full differentiation to become an active osteoclast capable of bone resorption. OPG, also produced by osteoblasts acts as a decoy of RANK, and regulates RANK activation to avoid over-activated bone resorption. RANKL also activates *TRAP* gene expression in the fused polykaryon and mature osteoclast. Adapted using Servier medical art (Servier, 2017).

M-CSF is also a key regulator for osteoclast survival, proliferation and differentiation of precursors by binding to the CSF1R receptor which is located on the osteoclast precursors membrane. CSF1R is encoded by *C-FMS*. As RANKL, it is produced by osteoblasts and stromal cells (Boyle et al, 2003). It was also shown that mutations in the M-CSF gene, *CSF1*, induces osteopetrosis in mice and that cell cultures from those were deficient in osteoclasts and mature macrophages (Yoshida et al, 1990).

In vitro osteoclasts can be obtained from M-CSF-stimulated bone marrow derived macrophages cells (BMDMs) with a combination of RANKL and M-CSF, or from peripheral blood mononuclear cell (PBMCs) (Rosen, 2013).

Osteoprotegerin (OPG) is produced by osteoblasts and has an inhibitory effect on the NFκB pathway. OPG has a strong affinity to RANKL and acts as a decoy receptor inhibiting resorption of the bone. As a result, the proportion of RANKL and OPG is a key regulatory factor for regulating bone resorption (Rosen, 2013). Mice lacking OPG show increased osteoclast activity, vascular calcification (Bucay et al, 1998) and osteoporosis (Mizuno et al, 1998).

The investigation of the pro-inflammatory cytokine interleukin 6 (IL-6) in bone resorption has led to complex outcomes and is not yet well understood. It was showed that a combination of soluble IL-6 receptor and IL-6 induces osteoclast formation in co-cultures of osteoblasts and bone marrow cells, with a resorption activity similar to control osteoclasts (Tamura et al, 1993). Osteoclast differentiation was promoted in the same way in human PBMC cultures, however a lower resorption activity was observed compared to control osteoclasts stimulated with RANKL and M-CSF (Kudo et al, 2003).

Some studies demonstrated that mice deficient in IL-6 showed more trabecular bone, a higher number of TRAP-positive osteoclasts and apoptotic osteoclasts, and a delayed bone remodelling compared to littermate controls (Liu et al, 2014). However, neutralization of the IL-6 receptor in mice resulted in a reduction of osteoclast differentiation and bone resorption activity (Axmann et al, 2009). It was also found that IL-6 could inhibit osteoclastogenesis by influencing the production of RANKL through osteoblasts (Duplomb et al, 2008).

Bone resorption starts by the creation of a space between the osteoclast and the bone surface, through the formation of actin sealing rings (Figure 1.4). Transmembrane integrins, particularly integrin $\alpha_v\beta_3$, allow the attachment of the cell to the bone by recognising the specific amino acid motif Arg-Gly-Asp of bone proteins, such as OPN (Rosen, 2013). Integrin $\alpha_v\beta_3$ is expressed in a similar way to *TRAP* during osteoclast differentiation and appears in osteoclasts stimulated by RANKL, while is absent in macrophages stimulated with M-CSF only (Teitelbaum, 2005). Specific ligands can also compete with integrin $\alpha_v\beta_3$ and inhibit bone resorption (Rosen, 2013).

Type I collagen (COL1A1) is then exposed from the inorganic mineral by the generation of an acidic environment. For this, the enzyme carbonic anhydrase II produces hydrogen and bicarbonate ions in the osteoclast. Bicarbonate ions are exchanged for chloride ions from the extracellular matrix in order to maintain normal intracellular pH. The protons and chloride ions are then brought to the bone-cell surface through the ATPase proton pump and a chloride channel (respectively) in order to lower the pH to 4.5 (Teitelbaum & Ross, 2003).

Enzymes, mainly cathepsin K and matrix metalloprotease 9 (MMP9), are then secreted in the resorptive microenvironment to start the degradation of the organic matrix of bone (Rosen, 2013).

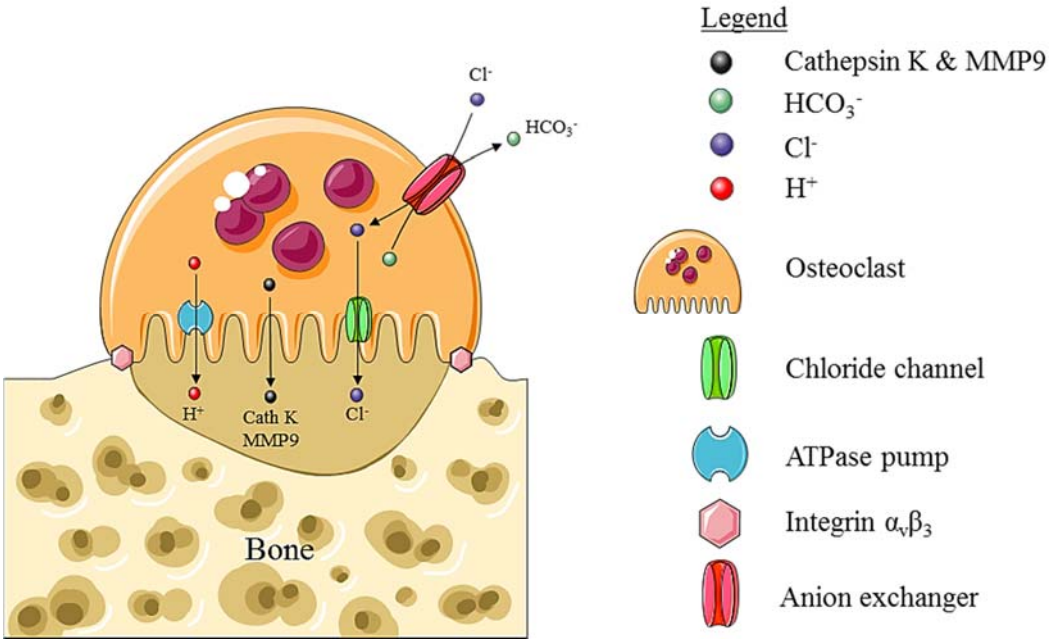

Figure 1.4: Summary of the osteoclastic resorption (Rosen, 2013).
The osteoclast seals to the bone to be resorbed by recognising the Arg-Gly-Asp motif found on bone proteins. Carbonic anhydrase II converts CO into hydrogen ions (H^+) and bicarbonate ions (HCO_3^-) in the intracellular compartment of the osteoclast. HCO_3^- is replaced by chloride ions (Cl^-) through an anion exchanger, to maintain the intracellular pH. The H^+ and Cl^- ions are then transferred to the bone/cell surface respectively by a proton pump and a chloride channel, which reduces the pH of the resorption zone down to 4.5 to degrades the non-organic matter of the bone. Collagenases such as cathepsin K and MMP9 can then degrade the organic proteins present in bone such as type I collagen. Adapted using Servier medical art (Servier, 2017).

Many components of this process have been associated with bone disorders. Firstly, mice deficient in the integrin $\alpha_v\beta_3$ show an increased bone mass (Rosen, 2013; McHugh et al, 2000). MMP9 deficient mice show delayed endochondral ossification, abnormal vascularisation and ossification in growth plates (Vu et al, 1998).

A lack of carbonic anhydrase II expression has been described in patients affected by osteopetrosis with renal tubular acidosis and cerebral calcification (Sly et al, 1983). Mutations in the a3 subunit of the proton pump were described in patients with human malignant osteopetrosis, where the osteoclasts were unable to form a resorptive microenvironment (Michigami et al, 2002). Mutations in the chloride channel are associated with osteopetrosis and resorption deficiency in osteoclasts (Kornak et al, 2001). Mutations in the cathepsin K enzyme have been detected in Pycnodysostosis patients, a hereditary form of osteopetrosis (Gelb et al, 1996). Cathepsin K inactivated in mice results in osteopetrosis where the osteoclasts were not able to degrade the collagen accumulated in the resorption environment (Saftig et al, 1998).

Osteoblasts

Osteoblasts are mononuclear bone cells differentiated from bone marrow mesenchymal stem cells (MSCs). They make up about 4-6% of the total bone cells (Rosen, 2013). Osteoblasts are responsible for the secretion of bone matrix constituents, such as OCN, OPN or COLIA1. They are also able to synthesise RANKL, M-CSF and OPG, key cytokines involved in osteoclast formation and bone resorption (Figure 1.3) (Rosen, 2013).

Osteoblast differentiation depends on many growth factors and cytokines. Flat quiescent osteoprogenitors are found lining on the outer surface of the trabecular bone (called endosteum) and under the periosteum of the cortical bone. Cell-cell adhesion is promoted by cadherins and desmosomes through the cell cytoskeletons (Rosen, 2013).

Upon osteoblast differentiation, the cell develops a very recognisable cubic shape. Active osteoblasts, able to synthesize bone structures such as collagen, show a large and round nuclei, enlarged organelles such as Golgi, and extensive endoplasmic reticulum (Rosen, 2013).

Although many pathways are known to be involved in osteogenesis, only the most important ones will be described here. The activation of the Runx2 transcription factor, also called core binding factor α subunit (CBFα1) or acute myeloid leukaemia 3 (AML3), is well established in osteoblast differentiation. The importance of Runx2 in osteoblast differentiation was described in knock out mice which died shortly after birth. The few mice which survived had no osteoblasts nor bone (Otto et al, 1997). Mutations in the *RUNX2* gene are also associated with Cleidocranial dysplasia, a congenital disorder with poorly developed bones (Mundlos, 1999). Runx2 is able to positively or negatively control the expression of key osteoblast genes, such as C*OL1A1*, *ALP*, *OPN*, *OSN*, or *OCN* (Rosen, 2013). The osteoblastic differentiation is pursued by the activation, through Runx2, of a transcription factor called Osterix. MSCs from mice lacking *Osx*, the gene encoding OSTERIX, are also not able to differentiate into osteoblasts (Nakashima et al, 2002).

Additional growth factors involved in bone formation are bone morphogenic proteins (BMPs). They are part of the transforming growth factor-β (TGF-β) superfamily and have an important role in fracture healing for which they are used therapeutically. BMP-2 is known to increase the expression of *Osx* (Rosen, 2013). TGF-β has different effects on bone remodelling depending on the environment and concentration.

In vitro investigations showed that it increases osteoblast activity in human MSC whereas it inhibits osteoblast differentiation at later stages (Alliston et al, 2001).

Osteogenesis from MSCs is also under the control of the canonical Wnt/β-catenin signalling pathway. Binding of Wnt to the Frizzled (Fzd) receptor, low-density lipoprotein receptor-related protein 5 (LRP5) and LRP6 co-receptors allows cytoplasmic accumulation of β-catenin which activates a downstream signalling leading to bone formation. Lack of β-catenin in limb and head osteoblast precursors inhibits osteoblast differentiation and shows abnormal skeletal development in mice (Hill et al, 2005). Increased bone mass disorders are also associated with *LRP5* mutations (Rosen, 2013).

The Indian hedgehog (Ihh) signalling is part of the Hedgehog family along with sonic and desert hedgehogs. The role of Ihh in osteogenesis has been showed in mice lacking *Ihh*, which prevented the development of osteoblasts in endochondral bone and formed abnormal long bones. Most pups died either during gestation or upon birth due to respiratory failure (St-Jacques et al, 1999).

It has also been shown that parathyroid (PTH) treatment controls bone formation in a time dependant manner. A continuous PTH treatment increases RANKL and M-CSF secretion by the osteoblasts favouring osteoclastic bone resorption, while intermittent treatment results in an increased bone resorption, but more significantly osteoblast differentiation and bone formation through the activation of Runx2 and Wnt/β-catenin pathway (O'Brien et al, 2008).

Additional factors mediating osteogenesis are insulin-like growth factor-1 (IGF-1), a protein mediating the osteoblast proliferation and function through the Ras-ERK MAPK pathway, and fibroblast growth factors (FGFs) which are involved in endochondral bone formation and osteoblast survival through the Ras-ERK MAPK and Runx2 pathways. NOTCH proteins also negatively affect osteoblast differentiation through Runx2 (Rosen, 2013).

Osteocytes

Osteocytes make up to 90-95% of the total bone cells. Osteocytes differentiate from osteoblasts following bone formation. They are located in the lacunae in the cortical bone. They have a dendritic shape with elongated processes traveling through canaliculi, forming a network which allows cellular contact with other osteocytes and lining osteoblasts (Rosen, 2013). The expression profile and function of the osteocytes are not yet as clear as for osteoblasts, however they are thought to be involved in the perception of mechanical loading of the bones through the canaliculi network. Osteocytes also have an important role in phosphate homeostasis by producing the hormone FGF23 (Feng et al, 2006; Rosen, 2013).

Typical osteocyte markers include E11/gp38, a mucin-like glycoprotein involved in mechanical strain and dendrite formation, fimbrin, involved in dendrite formation, CD44, associated with cytoskeleton, dentin matrix protein 1 (DMP1), involved in phosphate metabolism and sclerostin, shown to inhibit bone formation (Rosen, 2013). Sclerostin is encoded by the *SOST* gene, for which mutations were associated with patients affected by Sclerosteosis, where bone mass is increased (Balemans et al, 2001).

Chondrocytes

Chondrocytes have a crucial role in embryonic skeletal development and limb patterning, where they form a cartilage model for future ossification. They differentiate from MSCs. Typically, during embryogenesis, MSCs will condense to form either chondrocytes or osteoblasts through the expression Sox9 or Runx2 pathways. As described in the osteoblast section above, an increased Runx2 will trigger osteoblast differentiation by mediating the Wnt/β-catenin and the Ihh pathways. Once expressing high levels of Sox9 however, chondrocyte differentiation is prioritised. They are also present in adult cartilage at the end of long bones, which tempers mechanical loading and ease the movement of the articulations (Rosen, 2013).

1.1.3 Bone remodelling

Maintenance and repair of the skeleton occur in the process of bone remodelling. This process is performed by a coupled effort from osteoclasts and osteoblasts and involves the removal of the old bone to be replaced by new bone. This temporary arrangement is called basic multicellular unit (BMU). It has been estimated that 2 to 10% of the adult skeletal mass is being renewed every year (Fleisch, 2000).

The bone remodelling is organised in four steps: activation, resorption, reversal, and formation. This is summarised in Figure 1.5.

Activation

Firstly, mononuclear osteoclast precursors are recruited from the marrow to the area to be resorbed. Quiescent lining osteoblasts are activated and produce RANKL and M-CSF, leading to the fusion of osteoclast precursors into multinucleated polykaryons. Active osteoclasts attach to the bone through integrins like $\alpha_v\beta_3$, triggering re-polarization and structural re-organisation of the cell. Podosomes, made of the actin cytoskeleton of the cell, form a strong circular binding called actin ring, between the cell and the bone. It create the sealing zone which will contain the acidic environment. The cell membrane of the osteoclast broadens to the inside of the sealed zone and form the ruffled border responsible for protein and mineral exchanges (Figure 1.4). MMP9, cathepsin K, protons and chloride ions are synthesised by osteoclasts, and secreted in the cell/bone surface to create a low pH environment rich in proteases (Clarke, 2008).

Resorption

The bone is degraded in two ways. First, the acidic environment created by the accumulation of protons and chloride ions in the ruffled border via (respectively) the ATPase pumps and chloride channels, will dissolve the non-organic content of the bone. Proteases such as MMP9 and cathepsin K will then be responsible for the degradation of the newly exposed organic matter, such as type I collagen. The degraded molecules then undergo endocytosis and are transported in cellular vesicles where they will travel to the outer membrane of the cell and be released in the extracellular compartment. This will create a resorption pit in the bone. The osteoclast resorption is thought to take up to 4 weeks between each cycle and is done under the control of mediators like RANKL, OPG, M-CSF, or IL-6 (Clarke, 2008).

Reversal

Cavities formed in the bone by osteoclastic resorption will now be prepared for the addition of newly formed bone by osteoblasts. The transition, although not fully understood, is thought to be initiated by TGF-β which is released from the bone matrix during resorption and stimulates bone formation (Clarke, 2008).

Additional membrane bound factors called ephrins (ligands) and Ephs (receptors) act as mediators through inter-cellular contact. Although this is not well understood, such interactions result in the activation of bi-directional signalling in the Eph-cell (forward signalling) and the ephrin-cell (reverse signalling). Ephrin/Eph roles in osteoclast/osteoblast interactions and bone metabolism have been described for EphB4 and ephrinB2 (Brandi et al, 1995).

Forward signalling from the activation of osteoblast bearing-EphB4 by osteoclast bearing-ephrinB2 results in increased calvarial osteoblast differentiation through the Osx and Runx2 transcription factors. Reverse signalling, triggered by the binding of EphB4 with ephrinB2, was found to inhibit osteoclast differentiation from BMDMs (Brandi et al, 1995). Additionally, protein and mRNA levels of *EphrinB2* were detected in osteoblasts and osteocytes and a dose dependent increase of *EphrinB2* was established in calvarial osteoblasts following treatment with PTH (Allan et al, 2008). mRNA levels of *EphrinB2* were found to be constant during differentiation of Kusa 4b10 stromal osteoblastic cells (Allan et al, 2008). Although this has not yet been studied in the context of the BMU, the cellular proximity between osteoclasts and osteoblasts occurring during the reversal phase makes is a perfect environment for such interactions. Ephrin and Eph signalling have also been investigated in the context of PDB and are described in Section 1.5.4.

Formation

Bone formation is a process which takes up to 6 months. In addition to those present in the pit, mature osteoblasts are differentiated from recruited osteoblast precursors through activation of Runx2 and Osx as described in Section 1.1.2. This will induce the activation of osteoblast genes such as *OPN*, *OSN*, *OCN* or *ALP*. Extracellular matrix, mainly composed of type I collagen, is then synthesized to create an osteoid (Clarke, 2008).

Formation of hydroxyapatite crystals occurs within extracellular membrane-bound matrix vesicles (MVs) formed by osteoblast membrane blebbing. For this, calcium phosphate concentrates in MVs following phosphatase activity until precipitating. Once the vesicles are broken down, the newly formed hydroxyapatite crystals join the organic matrix and give strength to the bone. Calcium ions come in the MVs through Ca^{2+} ion channels, while inorganic phosphate (Pi) comes from the enzymatic degradation of inorganic pyrophosphate (PPi), a mineralisation inhibitor (Houston et al, 2004). The most described phosphatase is ALP (Narisawa et al, 2007), which binds to the outer face of MVs and controls the extracellular PPi/Pi ratio. Pi is thought to then enter the MVs through phosphate transporters (Roberts et al, 2004). PHOSPHO-1, located in the MVs, has also been showed to generate Pi by hydrolysing phosphoethanolamine and phosphocholine (Roberts et al, 2004). PHOSPHO-1 is a phosphohydrolase highly present in mineralised tissues and has an important role in endochondral ossification (Houston et al, 2004). Mice lacking PHOSPHO-1 showed fractures, long bone deformity, Osteomalacia and Scoliosis (Yadav et al, 2011).

It has been suggested that the *SOST* gene is associated with the cessation of osteoblast activity. Sclerostin has been shown to inhibit osteoblast activity and differentiation and decrease ALP expression in hMSC cell cultures. hMCS upon treatment with sclerostin also show an increased apoptotic phenotype (Sutherland et al, 2004).

Once the mineralisation is over, most of the osteoblasts undergo apoptosis (50-70%), while the others will be either buried in the newly formed bone to become osteocytes or differentiated into lining cells again (Clarke, 2008).

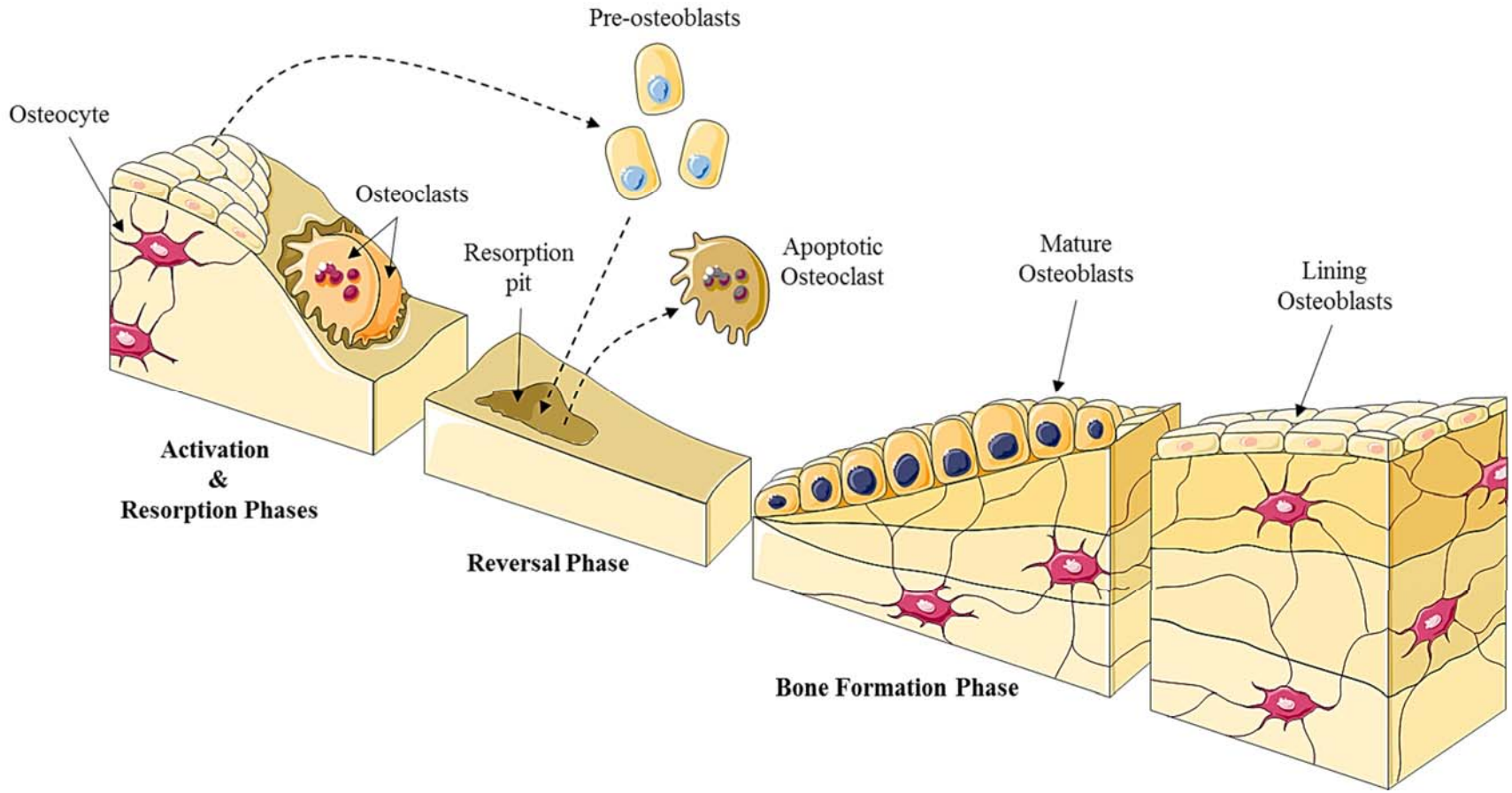

Figure 1.5: Schematic illustration of the bone remodelling.
Activated osteoclasts attach to bone to start the degradation process. Reversal phase involves removal of osteoclasts and recruitment of pre-osteoblasts found in the resorbed environment and from lining cells. Once differentiated into mature osteoblasts, they will start forming an osteoid, which will then be mineralised and becomes the new bone. The osteoblasts left will become either lining cells, or osteocytes if embedded with the newly formed bone until remodelling is needed again. Adapted using Servier medical art (Servier, 2017).

1.2 PAGET'S DISEASE OF BONE

1.2.1 Historical aspect

PDB was first described in 1877 by Sir James Paget, a highly respected English surgeon and pathologist. He then named it *Osteitis Deformans*, and suspected it to be an inflammatory bone disorder as described in his publication called "On a form of chronic inflammation of bones" (Paget, 1877).

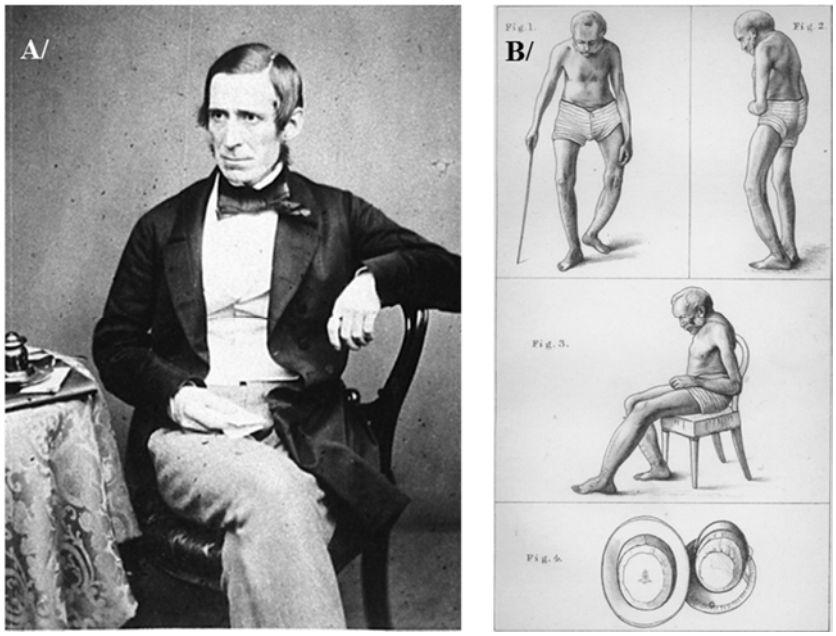

Figure 1.6: Sir James Paget and Paget's disease of bone.
A/ Photography of Sir James Paget (Paget's Association, 2017). B/ Illustrations drawn by Sir James Paget of his first *Osteitis Deformans* case (Paget, 1877).

We now know that PDB is a disorder of bone remodelling, and is today the second most common skeletal disorder after osteoporosis. It is a focal skeletal disorder, affects one or multiple sites at a time and is characterised by increased bone turnover. Although many patients are asymptomatic, the fragile and woven Pagetic bone can progress to cause significant bone pain, fractures and additional skeletal and neural complications (Ralston, 2008b).

Although the cause of PDB is not fully understood yet, segregation of the disease within family members led to genetic investigations. Mutations in the *SQSTM1* gene were detected in about 40% of familial cases and 10% of sporadic cases (Section 1.4.1). Additional candidate genes have been suggested and associated with PDB and PDB-like disorders, and are described in Section 1.4. Additional factors such as diet, pet ownership, repetitive mechanical loading and environmental toxins have also been considered to be involved in the development of PDB (Section 1.5.1), but the true role of these factors is still unclear (Ralston, 2008b).

1.2.2 Epidemiology

The incidence of PDB is quite low in younger subjects, but increases steeply in patients aged over 55. Overall prevalence in the UK is estimated around 8% in men and 5% of women over the age of 80 (Van Staa et al, 2002).

Great geographical differences in the prevalence of PDB have been observed. During the first epidemiological studies, a particularly high incidence was found in Lancashire, an industrial area from the North West of England (8.3%) (Barker et al, 1980). An archaeological study also reinforced the hypothesis of a Western European origin of the disease, as 94% of the European roman and medieval Pagetic samples examined were excavated in Britain (Mays, 2010).

PDB is also commonly found in countries with a high proportion of British migrants such as Australia and New Zealand (Gardner et al, 1978), North America (Altman et al, 2000) and South Africa (Guyer & Chamberlain, 1988).

Affected patients have also been reported in Northwest Europe such as France (up to 2.7%), Spain (up to 1.3%), Germany (up to 1.3%) and Italy (up to 1%) (Detheridge et al, 1982). More recent studies have shown high numbers of affected cases in rural areas of Italy (Merlotti et al, 2005) and Spain (Miron-Canelo et al, 1997). No difference of prevalence in PDB was reported between African Americans and Caucasian America, in contradiction to the low prevalence in Africa (Guyer & Chamberlain, 1980). The reasons are unclear, but are suspected to be due to genetic admixture in the US.

Although PDB is rarely observed in non-Caucasian populations, several recent cases of patients with Chinese (Wat et al, 2013), Indian (Bhadada et al, 2006), Japanese (Hashimoto et al, 2006) or Saudi Arabian (Alshaikh et al, 2011) descent have been reported and the prevalence in these countries may be underestimated.

A general decrease in prevalence of PDB has been noticed. A decline of about 40% has been described in the UK over the past two decades, with Lancashire keeping the highest prevalence in the country, estimated at 3.7% (Cooper et al, 1999). Additional reductions of prevalence have been recorded, with almost 50% in Australia (Cundy, 2006) and 30% in Minnesota (Tiegs et al, 2000).

1.2.3 Clinical features

Typical bone from Pagetic sites have an increased density with a disorganised and weak structure (Figure 1.7), and a loss of osteon organisation. This results in a loss of mechanical strength, although lamellar patterns may still be present (Meunier et al, 1980).

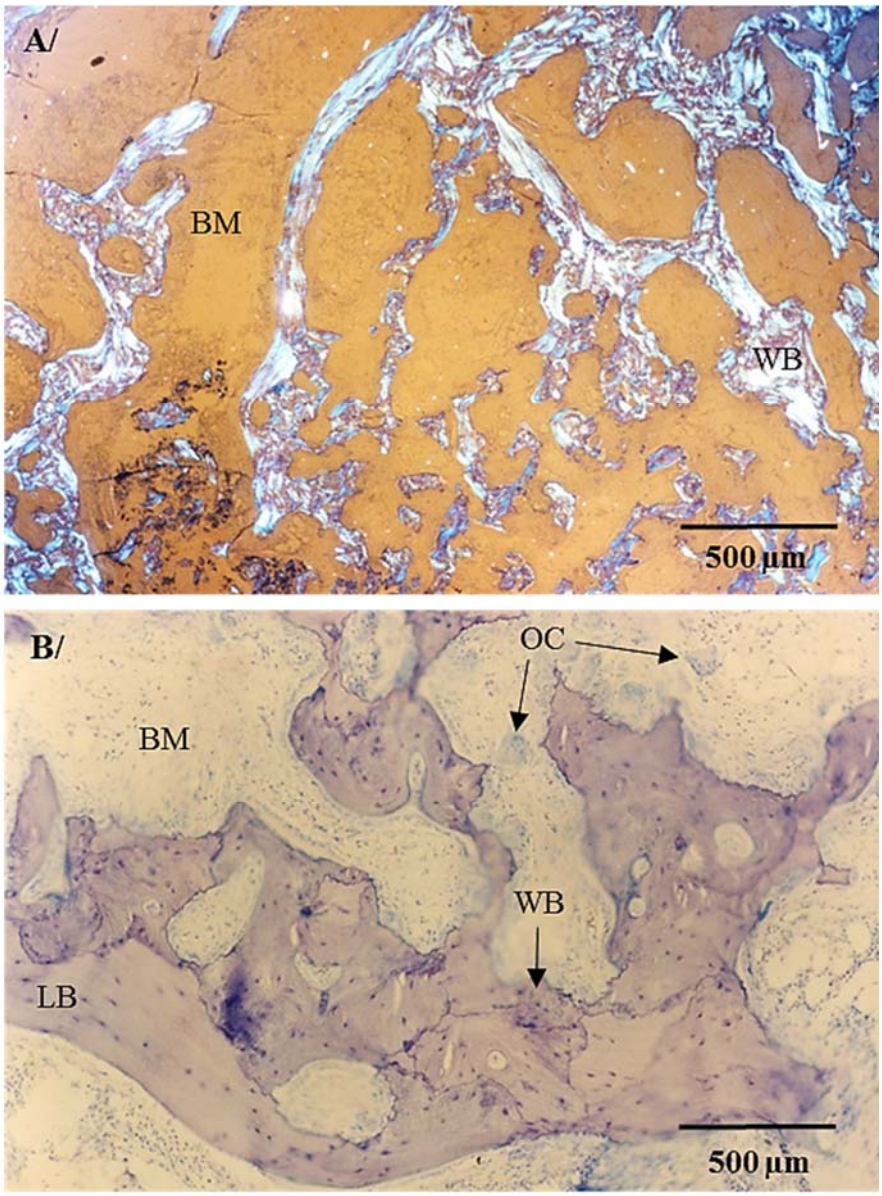

Figure 1.7: Trabecular biopsies of Pagetic bones.
WB = Woven bone; BM = Bone marrow; OC = Osteoclasts; LB = Lamellar bone. Courtesy of Prof Stuart H. Ralston. A/ Unstained section of bone visualised under polarised light. B/ Section of bone stained with toluidine blue.

PDB is a focal disorder which can be monostotic or polyostotic. It is observed on the axial skeleton with pelvis (67.4%), spine (39.2%), femur (33.3%), skull (24.6%) and tibia (19.0%) for the most common affected sites (Langston et al, 2007).

Although many patients are asymptomatic, musculoskeletal complications are frequently encountered in patients with bone pain reported in up to 15% of cases (Tan & Ralston, 2014). Bone deformity is also a common feature of PDB, which can lead to numerous disabling complications. Osteoarthritis can occur particularly near joints of the lower limbs (Siris, 1993) and nervous system damages can result from compression of the brain and cranial nerves (Seton et al, 2011). Hearing loss is commonly seen when the petrous temporal bone is affected (Monsell et al, 1999), but vision impairment and headaches can also be the result of an enlarged skull (Seton et al, 2011). Dental issues can occur when facial bones are affected (Seton et al, 2011).

Cardiovascular complications were also observed in severely affected patients, such as heart enlargement, arteriovenous malformation, aortic valves calcification or hypervascularisation (Hultgren, 1998; Parvizi et al, 2006). The latter could lead to excessive blood loss during bone fracture or surgery, making such interventions more challenging (Parvizi et al, 2006).

Osteosarcoma may occur but is uncommon, affecting less than 1% of the cases (Hansen et al, 2006). Rare GCT of bone can also be associated with PDB, and is usually seen in the already affected sites (Gebhart et al, 1998). Most GCT cases were reported on patients of Italian descent (Rendina et al, 2015).

1.2.4 Cellular abnormalities

Osteoclasts are abnormal in PDB. Their number, size, and number of nuclei are highly increased in Pagetic sites. As a result, a 7-fold increase of osteoclastic resorption surface has been reported in trabecular Pagetic iliac samples compared to controls (Meunier et al, 1980). The number of osteoclasts is also significantly increased in trabecular samples from active Pagetic biopsies compared to PDB samples from non-active biopsies (Meunier et al, 1980).

Changes in osteoblasts and increased bone formation in PDB cases are also reported, but are thought to be secondary to increased bone resorption. Osteoid surface has been reported to be about 4 times higher in Pagetic iliac samples compared to controls, and osteoid borders were shown to be thinner. Additionally, a 2-fold increase in mineralisation rate was also observed in Pagetic osteoblasts from the same samples compared to controls. This increase in bone formation was not found in the few lamellar areas from the sections analysed (Meunier et al, 1980).

1.3 MANAGEMENT OF PAGET'S DISEASE OF BONE

Guidelines are widely available for the diagnosis and treatment of PDB. The diagnosis is firstly assessed by the search of active turnover sites or lesions, using bone scintigraphy and X-ray analysis of the bone. High total serum ALP is as a marker of elevated bone turnover, although normal levels of ALP can occur in patients with limited disease. The diagnosis is usually made because of the apparition of bone pain, however many cases are reported during the investigation of another disorder (Selby et al, 2002).

1.3.1 Bisphosphonates

The most common treatment given for patients are bisphosphonates. They are structural analogues of inorganic pyrophosphate and have a strong affinity for the mineral part of the bone (Roelofs et al, 2006).

Two generations of bisphosphonates exist. The first one is represented by non-nitrogen-containing bisphosphonates such as Clodronate and Etidronate. Essentially, they induce apoptosis in osteoclasts by converting into methylene-containing ATP analogues and accumulating in the cell cytoplasm (Roelofs et al, 2006).

Nitrogen containing bisphosphonates such as Pamidronate, Ibandronate, Alendronate, Zoledronate, or Risedronate are more efficient in many ways including duration and method (oral or intravenous) of treatment. They are the second generation of bisphosphonates and are currently most widely used for the treatment of PDB. They inhibit farnesyl pyrophosphate (FPP) synthase, preventing the normal process of the mevalonate pathway (Roelofs et al, 2006).

This will block the post-translational modification of intracellular proteins such as small GTPases, which then accumulate in the cells. This leads to a disruption of the cellular trafficking and cellular apoptosis (Roelofs et al, 2006). Zoledronate offers a long duration of effect due to its strong inhibition with FPP synthase and high affinity for hydroxyapatite, and is therefore often the first treatment offered to Pagetic patients (Avramidis et al, 2008).

The administration of bisphosphonates for asymptomatic cases has shown some efficiency in regulation of the total serum levels of ALP but there is no evidence that it can prevent complications (Langston et al, 2010b).

The PRISM study (Paget's disease of bone: a randomized trial of intensive versus symptomatic management (Langston et al, 2010b)) investigated the effects of intensive bisphosphonate treatment on symptomatic patients, against a control group undergoing symptomatic therapy (anti-inflammatory or analgesics – bisphosphonates if needed). As a result, the patients of the intensive group showed a decrease in ALP serum levels compared to the symptomatic group, but there was no difference in their quality of life, numbers of clinical fractures or orthopaedic surgeries.

The ongoing ZiPP study (Zoledronate in the Prevention of Paget's, ISRCTN11616770) was initiated in 2009 and aims at investigating the prevention of focal bone lesions with Zoledronic acid treatment on patients with *SQSTM1*-mediated PDB. It also aims to evaluate the impact of the mutation screening on the quality of life on *SQSTM1* positive and negative PDB patients.

1.3.2 Other treatments

Other treatments can also be used for the therapy of PDB, while some others are still under investigation.

Denosumab is one of the most common alternative to bisphosphonates in osteoporosis. It is a human monoclonal antibody targeting RANKL and inhibits the NFκB pathway. Denosumab is beneficial for cancer-associated bone disease and post-menopausal osteoporosis (Romas, 2009). It is administrated subcutaneously. Recent case reports have shown its efficiency in reducing serum levels of ALP and bone turnover (Reid et al, 2016; Schwarz et al, 2012).

Non-steroidal anti-inflammatory drugs (NSAIDs) and analgesics can also help to manage bone pain. The PRISM study showed that 49.9% of the symptomatic group were administrated bisphosphonates, while 75.6% of the patients in the intensive group received it ($P < 0.001$). All patients from both groups received analgesic during the trial (Langston et al, 2010b).

Calcitonin treatment is a less commonly used alternative to bisphosphonates. It has a short duration of action and can cause nausea and flushing. It is now offered by physicians for short term use, only for Pagetic patients for whom all other alternative treatment were insufficient (Selby et al, 2002).

1.3.3 Non-pharmacologic treatments

Vitamin D and calcium supplements might be necessary during bisphosphonate treatment in order to reduce the risk of hypocalcaemia (Wat, 2014).

Acupuncture, hydrotherapy and physiotherapy can help improving muscle strength and maintaining joint flexibility. Occupational therapy, use of orthotics and walking devices for patients with affected lower limbs can also improve quality of life (Langston & Ralston, 2004).

1.3.4 Monitoring

As no definite cure exists for PDB, the follow-up of the disease activity and effect of treatments is a lifelong monitoring. The frequency of the monitoring essentially depends on the activity of the disease and symptoms.

Following a course of bisphosphonates, a significant reduction of serum ALP levels can be detected from the first 3 to 6 months. It is advised by the guidelines to check the level of serum ALP periodically thereafter (Selby et al, 2002).

1.3.5 Surgery

Surgery for PDB may be necessary in about 7% of the patients and can improve their quality of life significantly (Langston et al, 2010a). It is usually considered for the purpose of correcting orthopaedic complications such as osteoarthropathy, fracture management or spinal stenosis (Parvizi et al, 2006).

Surgery on PDB patients can be quite challenging. Delayed union from fractures has been observed in Pagetic bone, particularly in patients with active PDB (Kaplan, 1994).

The angular and irregular shapes of the affected bones complicate the surgeries (Kaplan, 1994). Hypervascularity also increases the risk of blood loss, and although the efficiency is still unclear, the administration of bisphosphonates before surgery is often given (Parvizi et al, 2006). Cochlear implantations for patients with affected temporal bone and suffering deafness were proven to be efficient, and surgeries were reported to have reversed hearing loss (Takano et al, 2014). Heart enlargement in patients with active PDB could lead to high output cardiac failure and must be monitored carefully (Parvizi et al, 2006).

1.4 GENETICS AND PAGET'S

As mentioned in Section 1.2.1, PDB has a strong genetic component which led to various pedigree and genetic studies. It was found that members from affected families have 7 times more chance to develop the disease compared to a patient without affected relatives (Siris, 1994). Although assessing family history can also be a difficult task considering that many patients are asymptomatic, pedigree studies concluded that PDB is inherited in an autosomal dominant fashion with high, but incomplete penetrance (Ralston & Albagha, 2014).

This part of the introduction focuses on the candidate and causing genes of PDB. PDB-like disorders, which share many clinical features with classic PDB, are also presented.

The loci described were found using linkage analyses in affected families. More specific investigations like genome wide association studies (GWAS), whole genome sequencing, whole exome sequencing or Sanger sequencing enabled the detection of several genes of interest.

1.4.1 Classical Paget's

The detail of genes associated with classic PDB is summarised in Table 1.1.

Table 1.1: Summary of genes associated with Paget's disease of Bone.

***Gene* (Protein)**	**Mutation(s)**	**Mechanism described**
SQSTM1 (p62)	28 mutations detected in PDB cases. p.P392L has the largest effect and is associated with more severe PDB.	Most mutations are located in UBA domain and reduce inhibition of NFκB signalling by affecting ubiquitin protein binding.
TNFRSF11A (RANK)	4 SNPs and 2 missense mutations have been detected in Pagetic cohorts.	Additional effect of p.V192A with p.P392L on increasing NFκB activity.
CSF1 (M-CSF)	3 SNPs have been detected in Pagetic cohorts.	M-CSF is involved in osteoclastogenesis but the role of the variants is still unknown in PDB.
GSTM4 (GSTM4)	1 SNP has been detected in Pagetic cohorts.	GSTM4 has an NRF-2 binding site. NRF-2 is a transcription factor involved in the regulation of cytoprotective genes and has been described in PDB: p.S349T mutation in *SQSTM1* impairs binding to Keap1, which controls NRF-2.
ZNF687 (ZNF687)	1 missense mutation has been associated with PDB.	p.S242I is associated with a younger age of onset and an increased number of Pagetic sites in patients.
TNRFSF11B (OPG)	1 SNP and 2 missense mutations were detected in Pagetic cases.	OPG levels are increased in serums of PDB patients. p.T950C and p.G1181C were associated with female cases. p.G1181C was suggested to affect OPG transport through the cytoplasm.
OPTN (OPTN)	2 SNPs were associated with PDB.	Silencing *Optn* increases osteoclastogenesis and NFκB signalling. OPTN also interacts with CYLD, which inhibits NFκB signalling.
TM7SF4 (DC-STAMP)	1 SNP and one missense mutation were detected in Pagetic patients.	An increased risk allele was associated with *DCSTAMP* and other genes. *DCSTAMP* has been associated with osteoclastogenesis.
NUP205 (NUP 205)	1 SNP was associated with PDB in patients carrying the p.P392L mutation in SQSTM1.	NUP 205 is involved in cellular trafficking, but its role in PDB is unknown.
CNOT4 (CNOT4)	1 SNP was associated with PDB.	CNOT4 is involved in ubiquitin mechanisms but its role in PDB is unknown.
VCP (VCP/p97)	1 SNP was detected in PDB patients.	The variant is located upstream of the gene and has been suggested to have an effect on the expression of VCP. Autophagy implications are also a possibility.
PML (PML)	1 coding variant was associated with PDB.	The mechanism of this variant is unknown but PML is involved in bone metabolism and regulates TGF-β signalling.

5q35 locus (SQSTM1)

p62 is a protein encoded by the gene Sequestosome 1 (*SQSTM1*). It is a scaffolding protein in the NFκB signalling pathway and is involved in osteoclast differentiation and activity, following RANK/RANKL activation (Chung & Van Hul, 2012). p62 has many motifs, such as (from the N-terminal to the C-terminal) a Src-Homology 2 (SH2) domain, an acidic interaction domain which binds to atypical PKCs (aPKCs), a ZZ finger which interacts with aPKCs recruiting receptor interaction proteins (RIP) (Sanz et al, 2000), a binding site for TNF receptor-associated factor 6 (TRAF6), and two PEST sequences rich in proline, glutamic acid, serine, and threonine amino acids (Geetha & Wooten, 2002). Finally, p62 has a LC3 Interacting region (LIR) and a ubiquitin-associated (UBA) domain (Chung & Van Hul, 2012).

It is thought that under normal conditions, p62 polyubiquitylates the TRAF6 protein, following binding of RANKL to the RANK receptor. This interaction is regulated by the UBA domain of p62. p62 then interacts with aPKC, a protein involved in cell survival, thereby activating the IKK (Iκβ kinase) complex, which in turn activates IkB (Inhibitor of NFκB). VCP-mediated degradation of Ikβ releases NFκB, which translocates to the nucleus and proceeds to the activation of osteoclast specific genes (Geetha & Wooten, 2002) (Figure 1.8). p62 is also part of a negative regulation of NFκB by recruiting the deubiquitinating CYLD protein. CYLD binds to TRAF6 to avoid over-ubiquitination of TRAF6. This results in a decrease of NFκB signalling and a reduced osteoclast activity (Jin et al, 2008) (Figure 1.8).

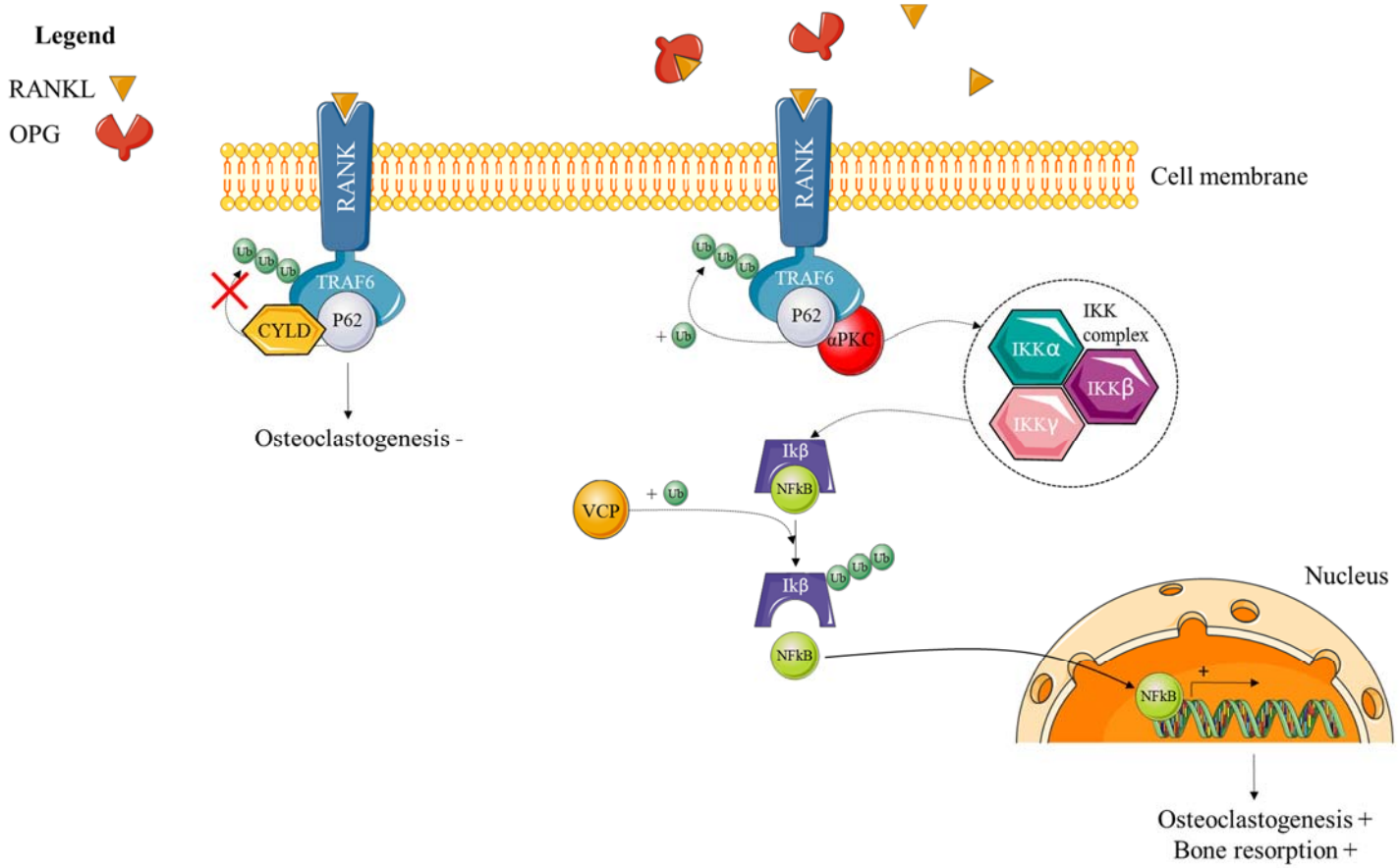

Figure 1.8: Regulation of the bone resorption activity through the NFκB pathway (Rea et al, 2013).

The first level of bone resorption regulation is at the cell membrane. RANKL can either bind to a decoy receptor called OPG, or to RANK. Once paired with the latter, a complex is formed with RANK, p62 and TRAF6, and TRAF6 is polyubiquitinated by p62. aPKC binds to this complex to then activate the IKK complex. This will result in the phosphorylation and VCP-mediated ubiquitination of Ikβ which will be degraded through a proteasome. NFκB is then released to translocate to the nucleus to process transcription of osteoclast activity promoting genes. Intervention of CYLD before the polyubiquitination results in the interruption of the downstream signalling. Adapted using Servier medical art (Servier, 2017).

The *SQSTM1* locus was associated with PDB by two linkage analyses and positional cloning performed on familial cases by two independent groups (Hocking et al, 2001; Laurin et al, 2001). Saturation mapping was then investigated in French Canadian families which refined the region of interest to a 300kb area, including the *SQSTM1* gene. Subsequent analyses of this gene revealed the presence of the p.P392L mutation in 46% of the members analysed from 24 families and 16% of the sporadic affected cases (Laurin et al, 2002). Since then, 27 additional mutations in the *SQSTM1* gene associated with PDB from worldwide cohorts were described. They are overall detected in 20-50% of the familial cases and in about 5-15% of the sporadic cases, with p.P392L being the most common mutation (Rea et al, 2013).

Most of the mutations related to PDB were detected in or around the UBA domain, which has a key role in the NFκB pathway and autophagy. It is involved in the transport of ubiquitinated proteins to autophagosomes through the binding of LC3 (Chung & Van Hul, 2012). Mutations in p62 are also thought to prevent the recruitment and binding to CYLD, thus reducing the inhibitory effect of p62 on the RANK/RANKL signalling pathway and increasing osteoclast activity (Rea et al, 2009). Additionally, *Cyld*$^{-/-}$ mice were found to develop osteoporosis by increasing osteoclast differentiation and activity, but no changes were observed in osteoblasts (Jin et al, 2008).

In mice, up to 95% of the homozygous p.P394L$^{+/+}$ (equivalent to the p.P392L mutation in human) showed a PDB phenotype by 12 months of age (Daroszewska et al, 2011). Contradictorily, an earlier study on p.P394L$^{+/+}$ mice aged up to 12 months showed no Pagetic bone phenotype (Hiruma et al, 2008).

This last study was however performed on the analysis of the first five lumbar vertebrae using histomorphometry, while Daroszewska and colleagues performed a more sensitive full microCT analysis on the lower limbs and the lumbar vertebrae and only 1 mouse out of 8 showed vertebrae abnormalities (Daroszewska et al, 2011).

Mutations in the *SQSTM1* gene have been associated with a more severe form of PDB, such as a significant younger age of diagnosis, a higher number of affected bones, and an increased need for orthopaedic surgeries and bisphosphonate treatments (Morissette et al, 2006; Visconti et al, 2010). This was particularly true in mutations leading to the truncation of the p62 as compared with missense mutations (Hocking et al, 2004).

Offspring of PDB patients carrying the p.P392L mutation have also been reported, where some were healthy and others had a delayed PDB (Cundy et al, 2015). This emphasises the incomplete penetrance of the disease, as well as the possibility of an additional genetic or environmental marker in the development of PDB.

18q21-22 locus (TNFRSF11A and BCL2)

Associations for rs663354, rs2980996, rs2957128 and rs3018362 in this locus were reported by a GWAS performed on a Pagetic cohort (Albagha et al, 2010). Borderline significance was described for the last two. These polymorphisms are also near recombination sites which are involved in genetic rearrangements of DNA segments. They are both located downstream the *TNFRSF11A* gene which encodes for RANK (Albagha et al, 2010), and were detected in a Dutch and British Pagetic cohorts (Chung et al, 2010).

A recent study has detected the coding variants p.H141Y and p.V192A in Italian subjects and confirmed an increase of the NFκB signalling in presence of p.192A, especially when co-transfected with p.P392L mutations compared to the p.192A mutated alone or the *SQSTM1* mutated alone (Gianfrancesco et al, 2012).

BCL2, in the same locus, was also considered as a gene candidate for PDB as it shows increased mRNA and protein levels in Pagetic individuals. Its promoter region has been sequenced on 20 patients but no variant has been associated with the disease. *BCL2* encodes an apoptosis suppressor, but has been not been well investigated and further work is necessary to understand its role in bone and PDB (Brandwood et al, 2003).

1p13 locus (CSF1)

In 2010, a GWAS showed strong signals for rs10494112, rs499345 and rs484959 in the locus 1p13 of PDB patients. This locus is localised upstream the *CSF1* gene. Independent associations were described for rs10494112 and rs484959, with a stronger signal for the latter (Albagha et al, 2010). Those three polymorphisms also reached GWAS significance in a British and Dutch study, with a stronger effect for rs484959 in the Belgium cohort (Chung et al, 2010). Allelic association in a French Canadian cohort has also revealed the polymorphisms rs499345 and rs10494112, with a stronger effect for rs499345 (Beauregard et al, 2014).

In the same locus, the variant rs650985 located in the *GSTM4* gene was also found in a French Canadian Pagetic cohort (Beauregard et al, 2014). The protein GSTM4 has a NRF-2 binding site. The Nrf2 transcription factor expression is involved in mediating gene response to cellular stress and has been recently associated with the p.S349T mutation in *SQSTM1*. The p.S349T variant is not present in the UBA domain of p62 but interferes with osteoclast activity by impairing the binding of p62 to Keap1, which binds to NRF-2 (Wright et al, 2013).

1q21.3 locus (ZNF687)

The locus 1q21.3 was associated with PDB using a genome-wide linkage analysis on a large affected Italian family (Gianfrancesco et al, 2013). p.S242I has been recently described in the *ZNF687* gene of the affected members using whole genome sequencing and was associated with an increased number of affected sites and decreased age of onset. *In silico* predictions suggests that the mutation is highly pathogenic (Divisato et al, 2016).

Very little is known about the role of ZNF687, but recent mass spectrometry based analyses showed that it is part of the Z3 transcriptional co-regulator complex, along with ZMYND8 and ZNF592. It has also been described to have C2H2 zinc fingers which interact with DNA (Malovannaya et al, 2011). ChIP-seq analysis on peripheral blood also revealed that ZNF687 is a downstream target of the NFκB pathway (Divisato et al, 2016).

8q24.2 locus (TNFRSF11B)

Shortly after the involvement of *TNFRSF11A* in FEO (Section 1.4.2), investigations of the *TNFRSF11B* gene were pursued for PDB. *TNRFSF11B* encodes the OPG protein. In Pagetic samples, OPG serum levels are increased (Alvarez et al, 2003). Several mutations were described in the *TNRFSF11B* gene of Pagetic individuals. Firstly, a 400 + 4 C>T intronic variation (intron 2) was more common in familial cases suggesting a potential allelic predisposition (Wuyts et al, 2001). PDB was associated with the more common variant p.G1181C (Daroszewska et al, 2004). Another study performed on a Belgian cohort investigated the gender specificity of variants in PDB and the polymorphisms p.T950C and p.G1181C were significantly associated with PDB in female cases only (P = 0.026 and 0.007, respectively). The same outcome was found in a UK cohort (Beyens et al, 2007). The variant p.G1181C was also showed to be in linkage disequilibrium (LD) with p.T950C and was suggested to affect the transport of OPG through the cell cytoplasm, however further work is necessary to prove such speculations (Daroszewska et al, 2004).

10p13 locus (OPTN)

The locus 10p13 was first described by genome wide search in Pagetic British families not mutated for *SQSTM1* (Lucas et al, 2008). Three GWAS confirmed the interest of this locus for PDB as rs1561570, a polymorphism within an intronic region of the Optineurin (*OPTN*) gene, showed a strong association with the disease (Albagha et al, 2010; Albagha et al, 2011; Chung et al, 2010). The rs825411 variant was also associated with PDB in a meta-analysis of two of those GWAS, combining British, Belgium and Dutch cohorts (Chung et al, 2010).

OPTN stands for optic neuropathy inducing. Mutations in this gene have been associated with glaucoma (Rezaie et al, 2002) and more recently, Amyotrophic lateral sclerosis (ALS) (Maruyama et al, 2010). It is a multifunctional protein, involved in membrane vesicle trafficking, signal transduction, autophagy, cell survival, Golgi ribbon formation and mitosis. Among many structural domains, OPTN has a ubiquitin-binding domain (UBD) and an NFκB essential modulator (NEMO)-like domain. NEMO participates in the activation of NFκB, by binding to the K63-linked polyubiquitinated chain of RIP, which interacts with p62. It was shown that these two domains confers OPTN the same ability in order to compete with NEMO, necessary to activate NFκB. Over-expression of *OPTN* in HEK293 cells has shown an inhibition of NFκB (Zhu et al, 2007). OPTN has an important role in autophagy regulation, by binding to ubiquitinated proteins and LC3 (Wong & Holzbaur, 2014).

A recent study showed that the silencing of *Optn* using shRNA enhances differentiation of osteoclasts from BMDMs and stimulates NFκB signalling. It was also showed that the mutation p.D477N (rs1561570) impairs binding between OPTN and CYLD (Obaid et al, 2015). RANKL, although involved in osteoclastogenesis, negatively regulates osteoclast activity by inducing IFNβ expression. This same study demonstrates that osteoclasts from $Optn^{D477N/D477N}$ mice have a lower increase in IFNβ compared to WT mice (Obaid et al, 2015).

8q22.3 locus (TM7SF4)

The locus 8q22 was initially associated with PDB by GWAS with the variant rs2458413, near the transmembrane 7 superfamily member 4 gene (*TM7SF4*) (Albagha et al, 2011). This polymorphism was also detected in a second GWAS, although of borderline significance, in a Belgian and Dutch study (Chung et al, 2010). However, when combined with the results of Albagha and colleagues' GWAS, rs2458413 reached significance. This last study also suggests that the cumulated risk alleles within *TM7SF4*, *CSF1*, *OPTN* and *TNFRSF11A* increase the risk of developing PDB by up to 67% (Chung et al, 2010).

The p.L397F missense (rs62620995) was also recently detected by sequencing on a French Canadian cohort (although of borderline significance) and categorised as probably damaging by *in situ* investigations (Beauregard et al, 2014). The *TM7SF4* gene encodes dendritic cells - specific transmembrane protein (DC-STAMP). It is preferentially, as its name indicates, expressed in dendritic cells (Hartgers et al, 2000) and is a strong candidate gene for PDB.

DC-STAMP was associated with increased osteoclastogenesis upon RANKL stimulation (Kukita et al, 2004) and higher bone mass and inhibition of osteoclast precursor's fusion were observed in mice lacking *Dcstamp* (Yagi et al, 2005).

7q33 locus (NUP 205 and CNOT4)

The locus 7q33 was firstly associated with PDB by GWAS, with a strong signal for the variant rs4294134, located in the 22nd intron of the Nucleoporin 205 gene (*NUP 205*) (Albagha et al, 2011). Although nominal, an allelic association was established between rs4294134 and PDB using genome sequencing study in patients carrying the p.P392L mutation (Beauregard et al, 2014). NUP 205 is involved in the regulation of macromolecules trafficking between the cytoplasm and nucleus via Nuclear Pore Complexes (NPC), which could be an interesting characteristic to consider knowing the importance of molecular traffic in osteoclasts during bone resorption (Section 1.1.2) (Grandi et al, 1997).

CNOT4, also present in this locus, produces a protein with an E3 ubiquitin ligase activity. The p.A7G change was detected in PDB patients, however was predicted to be benign. *CNOT4* could however be potentially relevant in the crucial ubiquitin mechanism observed in osteoclastogenesis (Beauregard et al, 2014). Further investigations are necessary to confirm such suggestions.

9p13.3-p12 locus (VCP)

The chromosomic locus 9p13.3-p12 includes the *VCP* gene, which encodes the VCP/p97 protein. VCP is a member of the type II ATPases associated with a variety of activities (AAA) proteins. As presented in Figure 1.8, it is involved in the activation of NFκB through ubiquitin mediated proteasome degradation of phosphorylated IκBα, an NFκB inhibitor (Lucas et al, 2006).

Although the first genetic screening study of PDB families revealed no association with VCP (Lucas et al, 2006), a second one performed on non-carriers of the *SQSTM1*/p.P392L mutation showed an allelic association with rs565070. This variant is however located 2kb downstream of *VCP*, and *in silico* prediction to excluded any damaging effect on the protein (Chung et al, 2011).

15q24.1 locus (PML)

The p.F645L variant (rs5742915), located in the promyelocytic leukemia *(PML)* gene, was significantly associated with PDB in a GWAS and is surrounded by two recombination hotspots (Albagha et al, 2011). An allelic association for PDB was also detected in a French Canadian cohort with p.F645L, particularly in patients carrying the *SQSTM1*/p.P392L mutation (Beauregard et al, 2014). PML was shown to be a regulator of TGF-β signalling. Although known to be involved in bone resorption and bone metabolism, the role of PML has not yet been established in the bone microenvironment (Lin et al, 2004).

14q32.12 locus (RIN3)

The 14q32 locus was initially associated with areal bone mineral density in healthy individuals, with a greater significance in men (Peacock et al, 2009). In the purpose of identifying new loci involved in the development of PDB, a GWAS was performed in our group in 2010 using 692 PDB cases of UK origin (597 from the PRISM study, others from UK and British migrant countries), against 1002 Scottish controls. The cases were not carrying *SQSTM1* mutations.

As a result, the variant rs10498635, located in the Rab and Ras interactor 3 gene (*RIN3*) was detected. It showed a borderline significance to PDB with a p-value of 9.69×10^{-8} (OR = 0.66); while the cut-off point was $P = 5 \times 10^{-8}$ (Albagha et al, 2010). In order to confirm those findings, another GWAS was performed in 2011 with a more appropriate control group from the British 1958 birth cohort, as the samples were collected from all over the UK. A total of 749 PDB individuals (692 previous cases and 57 newly recruited samples from the PRISM study) and 2930 controls were used. The rs10498635variant was detected again, and this time showed a strong association with the disease ($P = 2.55 \times 10^{-11}$; OR = 1.44) (Albagha et al, 2011). Recombination rates in the 14q32 locus were investigated using the European haplotype data from Hapmap as a reference (release 22), and recombination sites were found around the rs10498635 variant and throughout the *RIN3* gene (between exons 3 and 8), increasing the candidacy of *RIN3* in the context of PDB.

In the purpose of identifying additional rare variants in loci described from previous GWAS (Albagha et al, 2010; Albagha et al, 2011), Beauregard and colleagues sequenced candidate genes and genotyped previously described SNP in affected French-Canadian samples, along with healthy controls. The rs10498635 variant showed no association with PDB (Beauregard et al, 2014).

Protein expression of RIN3 was investigated in several human tissues and was found to be mostly expressed in peripheral blood cells. It was however also present in brain, muscle and colon (Kajiho et al, 2003). Another study showed that RIN3 is highly expressed in human mast cells. However, levels of expression in B cell, myeloblast, T cell, fibroblast and glioblastoma cell lines were found to be low (Janson et al, 2012).

RIN3 is part of the RIN family, along with RIN1 and RIN2. RIN3 is a guanine exchange factor (GEF) and is able to activate small GTPases. Small GTPases are divided in five families: Ras, Rho, Ran, Arf and Rab where Ras is currently the biggest and most described family (Itzstein et al, 2011). Small GTPases are activated when bound to a GTP, and inactivated when bound to a GDP. This inactivation is performed by GAP proteins (GTPase-activating proteins), which are enzymes responsible for hydrolysing a GTP molecule down to a GDP. Inactivated small GTPases can be activated again through a GEF protein such as RIN3, by binding to a GTP (Figure 1.9).

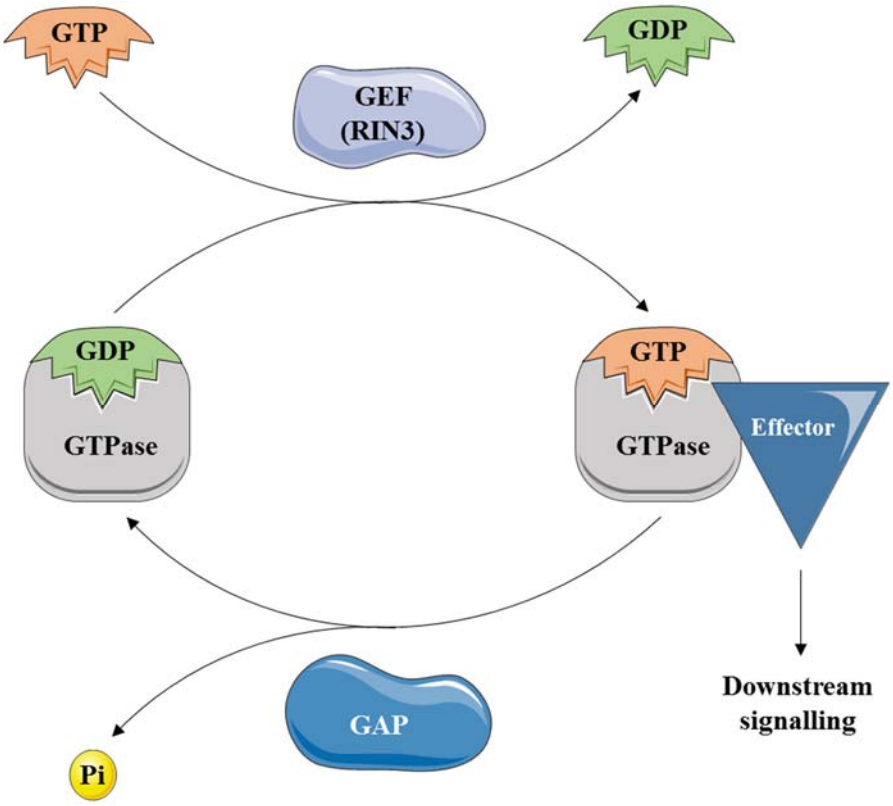

Figure 1.9: Schema of GTPase activation cycle (Nielsen et al, 2008).
The activation cycle of small GTPases is controlled by GEF proteins (guanine nucleotide exchange factor), through GTP binding. This results in the appropriate mediation of the cellular downstream signalling. Small GTPases are inactivated by GAP proteins (GTPase-activating protein), responsible for GTP hydrolyse into a GDP. Adapted using Servier medical art (Servier, 2017).

Small GTPases are involved in the mediation of downstream cellular signalling, controlled by their activation status (Itzstein et al, 2011). Their role in highly metabolically active osteoclasts is crucial and places *RIN3* as an interesting candidate gene for PDB. Small GTPases from the Arf and Rho families have been associated with many steps of the cytoskeletal polarisation during osteoclast activation. Rab small GTPases are involved in vesicular trafficking, which is crucial for the formation and function of the ruffled border of the osteoclast, receptor recycling, and transport of proteins and enzymes in and out the resorption environment (Itzstein et al, 2011). Rab, but most importantly Ras small GTPases have been associated with cell survival and have a key role in autophagy as described in Section 1.5.3 (Ao et al, 2014). Finally, activation of small GTPases was found to be inhibited under bisphosphonate treatment (Itzstein et al, 2011). Up to this date, RIN3 has been described to activates Rab5, which is involved in the fusion of early endosomes (Kajiho et al, 2003) and Rab31, a homolog of Rab5, thought to be involved in vesicular trafficking to late endosomes (Kajiho et al, 2011).

Little is known about the role of *RIN3* in the bone microenvironment. Protein levels of RIN3 are low in Saos-2 (human osteosarcoma cell line) (Janson et al, 2012). *RIN3* was recently associated with lower limb bone mineral density (LL-BMD) in children using a meta-analysis of GWAS on total-body DXA scans where rs754388 was associated with the phenotype (Kemp et al, 2014). In this same study, *RIN3* was found to be downregulated during osteoclast formation from human PBMCs, and expressed in primary calvarial osteoblast cultures. *RIN3* expression was also reduced in osteoporotic iliac biopsies compared to healthy postmenopausal controls (Kemp et al, 2014).

RIN3 is also involved in vesicular trafficking of proteins such as transferrin to early endosomes and interacts with Amphiphysin II, involved in the regulation of endocytosis. It was shown to have a cytoplasmic vesicular location in HeLa cells. (Kajiho et al, 2003). RIN3 has been showed to be involved in the internalisation of receptor tyrosine kinase KIT in human mast cells upon stem cell factor (SCF) stimulation (Janson et al, 2012).

From N-terminal to C-terminal, RIN3 has an SH2 domain, a proline rich region (PRR), a Ras-association (RA) domain, a vacuolar protein sorting 9 (VPS9) domain conferring its GEF activity, and a ubiquitin like domain (Geer et al, 2010). The latter increases interest, following the ubiquitin deficiency of *SQSTM1* in PDB (Kajiho et al, 2003). RIN3 also has an adaptor CD2-associated protein (CD2AP) interaction domain, recognised by the SH3 domain of CD2AP (Rouka et al, 2015).

RIN3 shares the SH2, VPS9 and RA domains with RIN1 and RIN2 (Bliss et al, 2006). As a result, the GEF activity for the Rab5 small GTPase has been detected in all three RIN members (Kajiho et al, 2011; Saito et al, 2002; Tall et al, 2001). Additionally, RIN1 is known for ABL tyrosin-protein kinase activation (Hu et al, 2005) and RIN2, like RIN3, interacts with Amphiphysin II (Kajiho et al, 2003).

In mice, four isoforms of RIN3 are predicted. The biggest one, of 980 amino acids (aa) is followed by an isoform of 900aa for which the first 80aa of RIN3 are missing, including the first 17aa of the SH2 domain. The other two isoforms are 198 and 127aa long, and share the first 176 and 122aa of the biggest isoform, respectively.

In human, five isoforms are described. The biggest isoform is made of 985aa, as shown in Figure 1.10. The next biggest isoform is 913aa long and lacks most of the PRR region of RIN3. The isoform of 420aa matches most of the C-terminal region of the 985aa isoform and starts from the end of the PRR region. Two smaller isoforms of 159 and 78aa are also predicted, and share the first 60 and 16aa of the biggest RIN3, respectively.

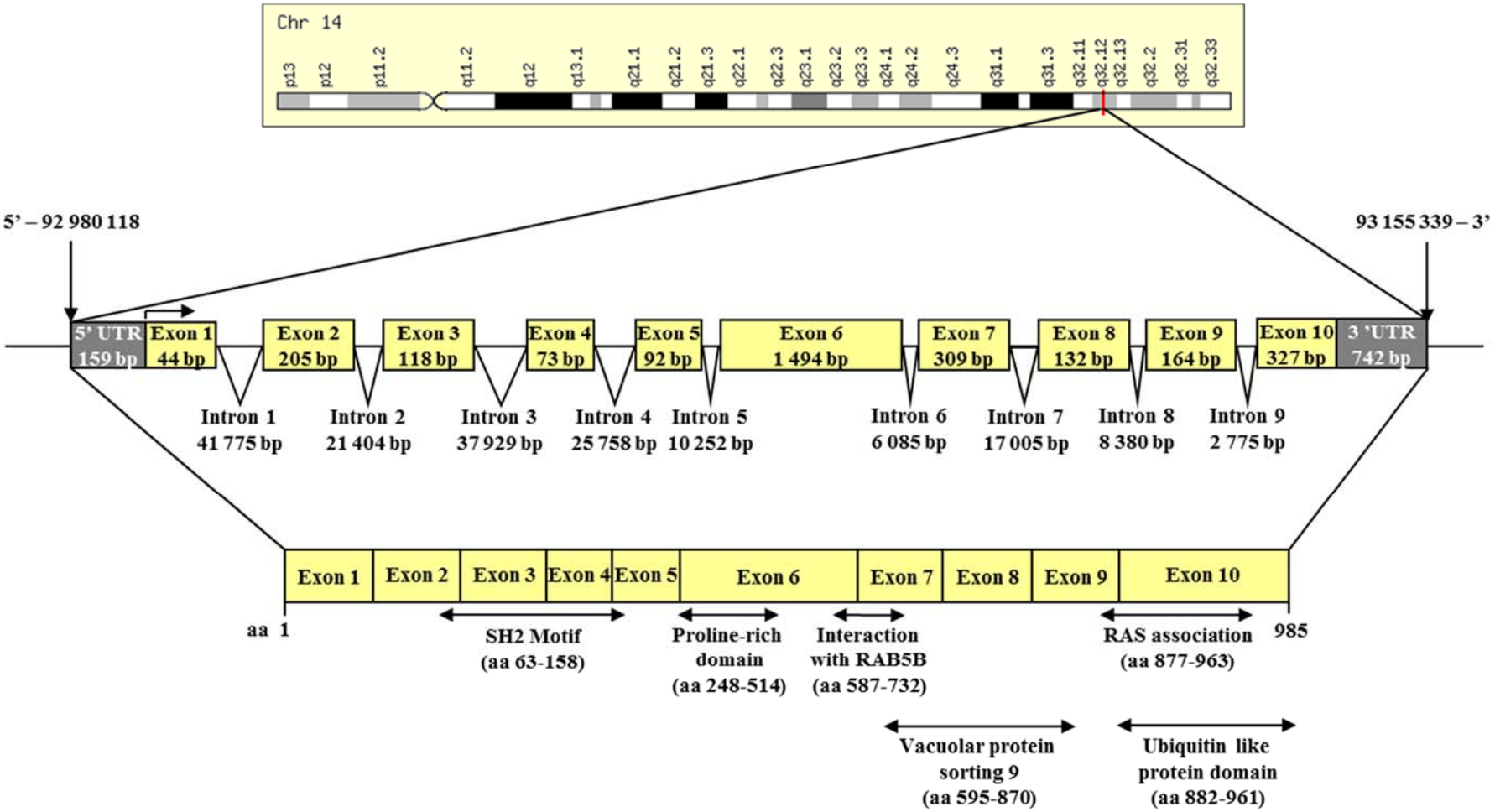

Figure 1.10: Schematic illustration of the human RIN3 gene and its domains.

The biggest isoform of *RIN3* in is made of 10 exons and has many domains such as the SH2 motif, a proline-rich region, a vacuolar protein sorting 9 domain, and a ubiquitin like protein domain (GRCh37).

1.4.2 Paget's disease-like disorders

Five rare inherited disorders with very similar clinical features to PDB have been described (Table 1.2).

Familial expansile osteolysis (FEO) (Hughes et al, 2000), early onset familial PDB (EoPDB) (Nakatsuka et al, 2003) and expansile skeletal hypophosphatasia (ESH) are caused by mutations in the *TNFRSF11A* gene (Whyte & Hughes, 2002). They typically show osteolytic lesions and/or sclerotic lesions, with earlier onset than in PDB. Different parts of the skeleton are usually affected and they show a strong penetrance (Ralston & Albagha, 2014).

Inclusion body myopathy, Paget's disease, and frontotemporal dementia (IBMPFD) has been associated with mutations in the *VCP* gene. IBMPFD is also inherited in an autosomal dominant manner and is described as a myopathy complicated in most cases by classic PDB. Dementia also appears later in life (Watts et al, 2004).

The last is the syndrome of Juvenile PDB (JDP), caused by mutations in the *TNFRSF11B* gene. Again its clinical features overlap with the classic PDB, but is developed during childhood. It is an inherited in a recessive fashion (Chong et al, 2003).

The genes associated with these five rare syndromes are presented in this section.

Table 1.2: Clinical features of rare inherited syndromes similar to Paget's disease of bone.

Syndrome	Main features	Inheritance	Mutation
Familial expansile osteolysis (FEO) (Ralston, 2008a).	Osteolytic lesions in long bones, and is less likely to be observed in the axial skeleton. Generalized and focal activity, bone pain, early-onset deafness and tooth loss. Overall more aggressive than classic PDB. Onset during childhood and young adulthood.	AD	Insertion mutations in *TNFRSF11A* - Gain of function
Expansile skeletal hyphosphatasia (ESH) (Ralston, 2008a).	Excessive bone growth which can be seen in the full skeleton but is more frequent in long bones and fingers. Early-onset deafness and tooth loss. Onset during childhood.	Highly penetrant AD	Insertion mutations in *TNFRSF11A* - Gain of function
Early onset PDB (EoPDB) (Ralston, 2008a).	Bone expansion and osteosclerotic lesions in the axial skeleton. Early-onset deafness and tooth loss. Onset during second to third decade of life.	AD	Insertion mutations in *TNFRSF11A* - Gain of function
Juvenile Paget (JPD) or idiopathic hyperphosphatasia (IHH) (Ralston, 2008a).	Bone expansion and osteosclerotic lesions in the axial skeleton. Early deformities, pathological fractures, progressive deafness and Protrusio Acetabuli. Onset during early infancy.	AR	Deletions, insertions and missense mutations in *TNFRSF11B* - Loss of function
Inclusion body myopathy, Paget's disease and frontotemporal dementia (IBMPFD) (Ralston, 2008a).	Affected muscles are mostly proximal and osteolytic lesions from PDB are seen in the axial skeleton. Asymmetric and patchy myopathy of muscles appear in the fourth decade of life, while dementia is found in the fifth decade. Death caused by respiratory and cardiac failure. Onset during fourth decade of life.	AD	Missense mutations in *VCP*- Loss of function
IBMPFD and amyotrophic lateral sclerosis (ALS) (Nalbandian et al, 2011) (Kim et al, 2013).	IBMDFP with muscle weakness and atrophy, dysarthria and dysphagia. Death from respiratory failure is seen 3 to 5 years after apparition of the symptoms. Onset during adulthood for ALS.	AD	Missense mutations in *HNRNPA1* – Loss of function
PDB with giant cell tumour (PDB-GCT) (Rendina et al, 2015).	Deformity of bones or extra-skeletal tissues. GCT increases the clinical severity of PDB and is mostly multifocal. GCT develops mostly in the already PDB affected sites. Onset during fifth decade of life.	AD	Missense mutations *ZNF687* – Unknown mechanism

AD = Autosomal Dominant; AR = Autosomal Recessive.

18q21-22 locus (TNFRSF11A)

The 18q locus was discovered by a genetic linkage analysis performed in 1994 on FEO (Hughes et al, 1994). This locus has then been refined to a 4.5Mb region, for which (at the time) no genes seemed to be good candidates for FEO (Hughes & Barr, 1996). Additional linkage analyses were undertaken in 1997 confirmed that FEO and PDB are both allelic disorders for that locus (Cody et al, 1997).Duplications in *TNFRSF11A* interfering with NFκB were additionally described for FEO (Hughes et al, 2000), ESH (Whyte & Hughes, 2002) and EoPDB (Nakatsuka et al, 2003).

Mutations in *TNFRSF11A* have also been described in patients affected by osteoclast-poor osteopetrosis with decreased gammaglobulin production (Guerrini et al, 2008).

1p13 locus (CSF1)

A missense mutation (p.L408P) was also found recently in the exon 6 of *CSF1* using next generation sequencing, in one sporadic JPD patient. However, this mutation (rs1058885) is quite common with a minor allele frequency (MAF) of 42.15% in 1000 Genome and is predicted as unlikely to be functional (Donath et al, 2015).

1q21.3 locus (ZNF687)

As presented in Section 1.4.1, genome-wide linkage analysis was performed on a large Italian family of 14 affected members. Four of those individuals were also affected by GCT, a disease associated with PDB in up to 1% of the cases (Gianfrancesco et al, 2013). The whole exome sequencing performed on this family revealed the missense p.P937R in the *ZNF687* gene of all affected members, including patients affected by GCT. Additional sequencing on 7 unrelated individuals confirmed the co-segregation of the p.P937R with GCT (Divisato et al, 2016).

In the bone microenvironment, *ZNF687* expression was showed to increase during differentiation of cultured PBMCs cultured osteoclasts obtained from PDB patients affected by GCT. The expression levels of *ZNF687* were also higher in PBMCs from affected patients compared controls (up to 3 fold), and even more (5-fold) from PBMCs of patients carrying the p.P937R missense. Additionally, osteoclasts cultured from individuals with the p.P937R mutation showed a higher number of nuclei and a larger size than control osteoclasts. p.P937R was also associated with p.S242I, in additional families severely affected by PDB (Section 1.4.1). *ZNF687* expression also increased during the differentiation of osteoblasts extracted from molar follicles, from healthy paediatric individuals (Divisato et al, 2016).

8q24.2 locus (TNFRSF11B)

Many mutations detected in the *TNFRSF11B* gene from worldwide cohorts were also found to cause JPD. Whyte and colleagues firstly presented two Navajo cases who showed no circulating OPG and carried a homologous 100kb deletion (Whyte et al, 2002). Additional deletions were then detected in the exon 3 of *TNFRSF11B* and resulted in a reduced affinity of OPG for RANKL (Chong et al, 2003; Cundy et al, 2002). A homozygous deletion/insertion was found in the exon 5 of the OPG gene of a JPD case, which leads to a frameshift and creates a stop codon. This results in the truncating of the last 76 amino acids of the OPG protein, also affecting greatly its ability to bind to RANKL (Janssens et al, 2005). The deletion of the Aspartate 182, located in one of the four cysteine rich domains constituting OPG, is thought to induce hyperglycosylation of OPG. This results in a reduced ability of OPG to bind to RANKL and therefore failure to inhibit osteoclastogenesis (Middleton-Hardie et al, 2006). Additional variants in the cysteine rich domains (Chong et al, 2003; Saki et al, 2013), disrupting the start codon of OPG (Grasemann et al, 2013) or in exon 2 (Chong et al, 2003) were also described.

Recently, the sequencing of two patients with JPD showed a deletion of exons 2 to 5 of *TNRFSF11B* in the most severely affected patients, and a novel missense mutation (p.T76P) in a mildly affected patient (Naot et al, 2014).

9p13.3-p12 locus (VCP)

The *VCP* gene was first associated with the syndrome of IBMPFD by genome wide scan (Kovach et al, 2001). Mutations described in *VCP* are localised in the N-terminal domain of the protein, and interfere with the binding of VCP to ubiquitinated proteins, similarly to p62 and PDB (Dai et al, 1998). The loss of VCP in U-2 OS cell line results in an accumulation of autophagosomes unable to continue the normal process of protein degradation (Ju et al, 2009).

The IBMPFD syndrome is characterised by muscle weakness, early onset PDB, and premature frontotemporal dementia (FTD). Six missense mutations (p.R95G, p.R155H, p.R155C, p.R155P, p.R191Q and p.A232E) were initially described in 13 affected IBMPFD families (61 individuals) by linkage analysis, followed by positional cloning. Ten of the 13 families had a change at codon 155 (Watts et al, 2004). Many additional missense mutations were then quickly detected by sequencing including p.R159H, in an Austrian family (Haubenberger et al, 2005), p.R93C in a French family (Guyant-Marechal et al, 2006), p.G157R in a German family (Djamshidian et al, 2009), p.P137L in a Finnish family (Palmio et al, 2011) and p.N387H and p.L198W, from two Polish and North American families (Watts et al, 2007).

VCP mutations were also associated with ALS by exome sequencing (Johnson et al, 2010).

7p15.2 and 12q13.13 loci (HNRNPs)

A recent study presents a family affected by IBMPFD/ALS which showed no mutation in the *VCP* gene (Kim et al, 2013). Additional exome sequencing and linkage analyses showed novel mutations in the heterogeneous nuclear ribonucleoprotein (*HNRNP*) A2B1 and A1 genes. They encode prion-like domain containing proteins, involved in the mediation of RNA metabolism and ribonucleoprotein granule accumulation through TDP-43 binding. Mutations in *HNRNPA2B1* and *HNRNPA1* increase the assembly of organelles into RNA granules, causing cellular toxicity in neurones and muscle cells (Kim et al, 2013).

Mutations in *hnRNPA1* were also detected in additional ALS families (Kim et al, 2013).

15q24.1 locus (GOLGA6A)

In the golgin A6 family member A gene (*GOLGA6A*) the mutations p.I40V and p.D52G were detected, although *in silico* investigations have not predicted a functional effect on the protein. GOLGA6A is a coiled-coil protein able to interact with the Golgi apparatus, which is involved in the transport of proteins and post-translational modifications. GOLGA6A is thought to participate in the membrane fusion and structural support of the cisternae, which forms the Golgi apparatus (Galson & Roodman, 2014). The role of GOLGA6A in bone is unknown, but studies have showed other members of the Golgin family carrying mutations causing lethal skeletal dysplasia (Smits et al, 2010) and severe form of osteoporosis (Hennies et al, 2008).

1.5 CANDIDATE PATHOPHYSIOLOGICAL MECHANISMS

Despite the aberrant NFκB signalling and genetic involvement of PDB (Section 1.4.1), the cause of the disease still remains unclear. Additional components such as environmental factors or autophagy dysfunction have been investigated, and this section focuses on the mechanisms thought to be involved in the development of PDB.

1.5.1 Environmental factors

The decreased prevalence over the recent years suggests a change in exposure of an environmental influence responsible for the evolution of PDB (Cooper et al, 1999).

Low calcium and vitamin D intake during childhood (Barker & Gardner, 1974; Siris, 1994), exposure to environmental toxins (Lever, 2002), repetitive mechanical stress onto affected bones (Gasper, 1979; Solomon, 1979), preponderance of cases in rural areas (Merlotti et al, 2005), dog exposure (O'Driscoll & Anderson, 1985), consumption of viscera or sick livestock of bovine cattle during childhood (Lopez-Abente et al, 1997) and chronic viral infections have been suggested to be associated with PDB.

The most widely studied possible trigger is viral infections. Microtubular inclusion bodies in the nuclei of Pagetic osteoclasts were first detected by Rebel et al., and were thought to be mRNA viruses from the Paramyxovirus family (Rebel et al, 1974). Several methods have been used to assess the specificity and frequency of their presence in Pagetic osteoclasts. Despite over 40 years of extensive investigations and conflicting results, this remains a debate.

Shortly after this publication, a study searched for the presence of nuclear inclusion bodies using electron microscopy. They were found in an average of 85% of osteoclasts per slide of embedded Pagetic biopsies, compared to controls. It was also suggested that the number of inclusions increased with the severity of the histological phenotype (Harvey et al, 1982).

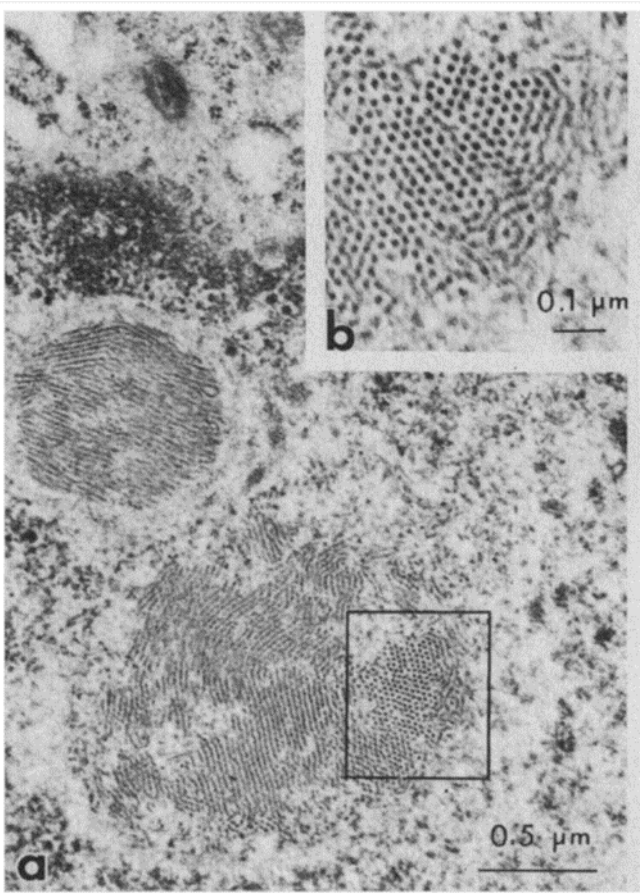

Figure 1.11: Electron microscopy photography of the nucleus of a Pagetic osteoclast (Mills & Singer, 1976).

A/ Photography of two nuclear inclusions at x21400 magnification showing paracrystalline structures. B/ Photography at higher magnification (x49400) showing cross section of filaments.

Another approach was to detect epitopes of viruses from the Paramyxovirus family using monoclonal antibodies. Measles virus (MV), simian virus 5, and human parainfluenza virus 3 were detected exclusively in osteoclasts from bone samples from Pagetic patients using immunohistochemistry. Respiratory syncytial virus (RSV), mumps, influenza and adenovirus type 5 were not detected in those samples (Basle et al, 1985).

An earlier study showed that RSV was detected by immunofluorescence on bone biopsies and cell cultures from Pagetic patients. In this same study, evidence of measles, mumps, herpes simplex, parainfluenza viruses, rubella, and influenza viruses were all absent (Mills et al, 1981).

Similarly, additional conflicting results were seen for measles. RNA was initially detected by *in situ* hybridization (Basle et al, 1986) and by PCR amplifications of the MV nucleocapsid protein (MVNP) on bone marrow samples of PDB patients (Friedrichs et al, 2002). Sequencing of the PCR products showed point mutations from the Edmonston strain MVNP, which varied amongst patients. This study asserts the validity of the results by the nature of their controls and the use of a PCR machine and room that has never been in contact with positive MVNP control samples (Friedrichs et al, 2002). Measle viruses were however not detected in other studies investigating cultured cells, bone marrow and bone samples from Pagetic patients using nested RT-PCR techniques, immunofluorescence, or *in situ* hybridisation. Here, cross contamination risks were overcame by analysing the samples and/or using samples from different cities (Helfrich et al, 2000; Matthews et al, 2008; Ralston et al, 2007).

Following the hypothesis suggesting that dog ownership was associated with PDB (O'Driscoll & Anderson, 1985), Canine Distemper Virus (CDV) was investigated and RNA was detected using techniques such as *in situ*-reverse transcriptase-polymerase chain reaction (Gordon et al, 1991; Mee et al, 1998). Here again, other studies have shown contradictory results in long term bone marrow cultures from Pagetic patients (Ooi et al, 2000). Osteoclastogenesis was also induced using CDV viral infection on human osteoclasts precursors (Selby et al, 2006).

All studies presented above were performed on limited number of patients and samples. To counter this, a recent case-control study used 463 Pagetic patients and 220 controls from the PRISM trial to investigate antibodies from measles, rubella, mumps, varicella zoster virus, RSV and CDV in serum. Mumps antibodies were significantly detected in Pagetic cases compared to controls. This study also suggested an association for the severity of PDB with antibody levels from clinical background, and no differences between the groups was detected (Visconti et al, 2017).

One study, despite not detecting the virus at a molecular level, observed nuclear inclusions in PDB samples (Helfrich et al, 2000). They confirmed a tight and parallel organisation observed by Rebel and al, but refuted the possibility of those being MV nucleocapsides. To support this, they analysed a brain sample extracted from a subacute sclerosing panencephalitis patient, a disease triggered by persistent measle infection. Those inclusions were smooth, diffused and spread within the cells. They suggested that Pagetic inclusions are more structurally similar to what is seen in multinuclear muscle skeletal cells from inclusion body myositis (Helfrich et al, 2000).

Similar nuclear inclusion bodies were also observed in osteoclasts from other bone disorders, such as primary oxalosis, osteopetrosis, osteoclastomas or pycnodysostosis (Bianco et al, 1992) which have a stronger genetic than environmental component.

Studies have also shown that human osteoclasts cultured from healthy donors display a Pagetic like phenotype after transduction of nucleocapsid genes construct of measles viruses. A higher sensitivity to 1,25-dihydroxyvitamin D_3 (also called $1,25(OH)_2D_3$), another typical feature of PDB presented below, was also detected (Kurihara et al, 2000).

The inconsistency of these data and the presence of inclusion bodies in other bone disorders only increases the speculations about the subject. It seems unlikely that these viral infections would be causing PDB. However it could be considered as an additional factor predisposing individuals to the disease, once associated with a genetic background or another environmental factor.

1.5.2 Osteoclastic factors of Paget's disease of bone

Osteoclastic hypersensitivity to RANKL and Vitamin D

Osteoclastic factors are essential for the differentiation and function of normal osteoclasts. In the Pagetic context, osteoclasts show increased sensitivity to several factors that stimulate osteoclast differentiation. As mentioned in Section 1.2.4, osteoclasts from Pagetic patients are bigger and more active at resorbing bone. This is thought to be partially due to a cellular hypersensitivity to RANKL (Menaa et al, 2000) and to $1,25(OH)_2D_3$ (Kukita et al, 1990), two critical factors involved in cellular differentiation and function of the cells. *TAFII-17*, a vitamin D binding receptor co-factor (Kurihara et al, 2004), and *TRAP* (Neale et al, 2000) expression are all increased in Pagetic osteoclasts.

A recent study has however detected a significant down regulation of six key osteoclastic genes, in cultured osteoclasts from PDB patients compared to healthy controls: *CASP3* (Caspase-3 gene) and *TNFRSF10A*, both involved in apoptosis, *TNFRSF11A*, *TRAP*, *CTSK* (Cathepsin K), and *MAPT* which encodes the Tau protein which interacts with tubulin and stabilises microtubules (Michou et al, 2010). Although these down-regulations can be contradictive to the increased osteoclastic activity seen in Pagetic lesions, more genes need to be investigated in order to understand the full molecular signature of Pagetic osteoclasts and have a better comprehension of the disease.

M-CSF

As presented in Sections 1.1.2 and 1.4.1, M-CSF is a key cytokine in osteoclastogenesis. Serum levels of M-CSF were shown to be significantly higher in PDB samples compared to controls and patients under treatment, suggesting a potential role in PDB (Neale et al, 2002).

Variation of M-CSF concentration in cultures of osteoclasts from Pagetic patients has however not shown any effect on bone resorption activity compared to controls (Neale et al, 2000).

Mice carrying the *op* mutation develop osteopetrosis, a disorder of osteoclastic dysfunction for which bone density is increased. The *op* mutation consists in the insertion of a thymidine in the *CSF1* gene, which leads to the inactivation of the gene and complete systemic absence of M-CSF in mice. Op/op mice were found to have low number of osteoclasts and macrophages, and a decrease in breeding performance and life expectancy. Osteopetrosis was rescued by administration of recombinant M-CSF (Wiktorjedrzejczak et al, 1990).

M-CSF plays a crucial role in osteoclast formation and is as a result an important factor of bone resorption. Although mutations in CSF1 were also associated with PDB, further investigations are needed to fully understand the precise role of M-CSF in the disease.

IL-6

IL-6 is an anti-inflammatory cytokine secreted by macrophages, osteoblasts and T-cells. Its role in osteoclastogenesis is not clearly understood since contradictory results were found from many studies (Section 1.1.2).

In the context of PDB, IL-6 and its receptor IL-6R were found to be more expressed in blood from patients compared to controls (Mossetti et al, 2005), as well as in long term osteoclasts cultures from Pagetic marrow samples (Roodman et al, 1992). Cultured osteoclasts precursors from mice carrying the p.P392L mutation and expressing MVNP showed a significant increase in IL-6 expression. Additionally, MVNP-expressing mice crossed with *Il-6*$^{-/-}$ mice showed reduced bone formation and mineralisation compared with MVNP overexpressing mice on a wild type background (Kurihara et al, 2011). Contradictory studies showed that mRNA levels of IL-6 from Pagetic bone biopsies were the same as in controls (Ralston et al, 1994). No increase in osteoclast formation nor bone resorption activity was also observed in an osteosarcoma cell line (UMR 106), co-cultured with mononuclear cells from peripheral blood of Pagetic patients, in the presence of IL-6 (Neale et al, 2000). The addition of a human anti-IL-6 antibody did not show any effect either and no significant differences of IL-6 levels were found in the conditioned media of these co-cultures compared to control co-cultures (Neale et al, 2000). Increased levels of IL-6 have also been associated with other bone disorders, such as postmenopausal osteoporosis (Girasole et al, 1992) or rheumatoid arthritis (Kotake et al, 1996).

Although it seems to have an effect on osteoclastogenesis, the role of IL-6 is still unknown in the pathogenesis of PDB and needs more work.

1.5.3 Autophagy

Autophagy is the process by which damaged proteins are degraded and recycled. As a result, it is responsible to the control of many cellular mechanisms such as cell differentiation, cell death, or response to cellular stress (Hocking et al, 2012). Autophagy is also essential for the regulation of bone signalling pathways such as Wnt/β-catenin and NFκB, thus influencing osteoblast and osteoclast function and differentiation, and playing an important role in the development of PDB (Shapiro et al, 2014).

Several proteins relevant to PDB have been correlated with autophagy. Firstly, p62 has been associated with accumulation of inclusion bodies in several neurodegenerative diseases such as Alzheimer's, Parkinson's diseases or ALS (Arai et al, 2003). p62 is thought to specifically bind to the autophagic marker LC3 and recruit protein clusters before their degradation in the autophagosome. This is performed by p62's ability to bind to polyubiquitinated proteins, using its UBA domain (Bjorkoy et al, 2005). Azzam and colleagues established three HEK293 cell lines expressing each one p62 mutation found in PDB patients (p.P392L, p.E396X and p.G425R), and the number of cells with nuclear inclusions was increased for p.P392L (+8%) and p.G425R (+4%) (Azzam et al, 2012). It has also been showed than *LC3* and *SQSTM1* expression levels are increased in osteoclasts precursors from p.P394L$^{+/+}$ mice, suggesting that the mutation impairs autophagy (Daroszewska et al, 2011).

As a result, the inclusion bodies described in osteoclasts (Section 1.5.1), were suggested to be protein aggregates, due to a dysfunction of the autophagy mechanism in Pagetic osteoclasts as in neurodegenerative disorders such as Parkinson's and Alzheimer's diseases (Daroszewska et al, 2011).

OPTN also acts as an autophagic receptor and is too, associated with the recruitment of ubiquitinated proteins to LC3. It was associated with mitophagy, process by which damaged mitochondria is sent to autophagosomes (Wong & Holzbaur, 2014), and autophagosome maturation (Tumbarello et al, 2012). It has also been found that phosphorylated OPTN enhances LC3 binding in *Salmonella* (Wild et al, 2011).

IBMPFD-causing mutations in the *VCP* gene have been described. VCP is thought to be involved in the maturation of autophagosomes, and the described mutations (Section 1.4.2) result in the accumulation of autophagic vesicles in the cells (Tresse et al, 2010). Similarly, loss of VCP in U2OS cell line leads to an accumulation of autophagosomes unable to continue the normal process of protein degradation (Ju et al, 2009). Such mechanisms can be considered similar to what is observed with p62 and could underline the importance of autophagy in the disease.

Small GTPases are involved in a variety of cellular process through mediation of cellular signalling. They are particularly known to be responsible for membrane trafficking and fusion of vesicles, key features of autophagy (Bento et al, 2013). The Rab proteins, part of the Ras GTPase superfamily, have been well described, especially Rab5 which interacts with RIN3 (Section 1.4.1) and is involved in early endocytic pathway (Kajiho et al, 2003).

Many Rab small GTPases are associated with different levels of autophagy such as autophagosome formation (Rab1, Rab5, Rab7, Rab9A, Rab11, Rab23, Rab32, Rab33B) or maturation (Rab7, Rab8B, Rab24) (Ao et al, 2014; Tresse et al, 2010). In association with the discovery of *RIN3* in the context of PDB, a disruption in the regulation of the small GTPases activation status and thus autophagy, is an important new mechanism to consider.

1.5.4 Ephrins

Following the suggestion of ephrin/Eph bearing cells interactions during the reversal phase of bone remodelling (Section 1.1.3), Teremachi and colleagues (2016) showed higher levels of ephrinB2 and EphB4 in osteoclasts and osteoblasts (respectively) in MVNP-expressing mice bone. Osteoclasts cultured from PDB patients expressing MVNP and the *SQSTM1*/p.P392L mutation were found to have increased protein levels of ephrinB2 compared to healthy donors and patients with the p.P392L mutation alone (Teramachi et al, 2016). Osteoblasts from MVNP expressing mice treated with EphB4-Fc (inducing reversal signalling) were found to have an increased osteoblastic differentiation and activity as well (Teramachi et al, 2016). This suggests an important additional coupling mechanism to further investigate for PDB.

1.6 AIMS OF THIS THESIS

PDB is a complex, but fascinating disorder. The encouraging and intense work of researchers and clinicians aims to improve the diagnosis and quality of life of patients. Although the last decades of research in PDB have offered great advances in the prevention and management of the disease in patients, its exact aetiology is yet to be understood. The incomplete penetrance observed in affected families and recent decrease of prevalence in many countries suggest that environmental factors play a role in the development of the disease. Diet, animal contact, viral infection and mechanical loading are considered. Although mutations in the *SQSTM1* gene have been associated with PDB, they account for less than half of the affected familial individuals and show a wide range of phenotype severity, stressing the need of finding additional causal genes. The purpose of this thesis is to investigate the role of *RIN3*, a gene described for PDB by GWAS. For this, genetic, functional and *in vivo* experiments were used to assess the effect of *RIN3* in osteoclasts and osteoblasts cells.

The aims of this study were the following:

- To investigate the possible presence of causal variants in *RIN3*, using a sequencing effort in Pagetic patients and controls
- To assess the expression pattern of *Rin3* in mouse tissues, measure RIN3 mRNA and protein levels in cells from the bone microenvironment, and investigate the subcellular location of RIN3 in human and mouse bone cells
- To evaluate the effect of the *Rin3* deletion on bone phenotype C57BL/6 x 129/OlaHsd mice at 8 weeks old
- To assess the functional role of *Rin3* in bone resorption and formation, using in vivo and in vitro techniques.

CHAPTER TWO

MATERIALS AND METHODS

2 MATERIALS AND METHODS

2.1 MUTATION SCREENING

The *RIN3* gene was sequenced using Sanger and next generation sequencings in order to identify new candidate variants for PDB. The samples used for this analysis were selected on their age of diagnosis and family history.

2.1.1 Sanger sequencing

The patient cohort

For Sanger sequencing, 101 Pagetic individuals were selected from the ZiPP study and an additional 24 cases from the PRISM study (Section 1.3.1). In both cohorts, the criteria of selection included that patients tested negative for *SQSTM1* mutations (exons 7 and 8), had a young age of diagnosis (average of 51.4 years old), and/or had family history (concerns 40% of the patients here).

DNA extraction

The DNA samples were extracted from blood using the Chemagen MSM I (Perkin-Elmer) or the Maxwell 16® (Promega) instruments according to the NHS Molecular Genetic laboratory instructions. The DNA concentrations were estimated using the Nanodrop ND-8000 (Thermoscientific) and the extraction quality was assessed using the A_{260}/A_{280} ratio.

Primer design

The coding regions, about 100bp of the intron/exon boundaries, the promoter region (2kb upstream the first exon), the 5'UTR and the 3'UTR of *RIN3* were sequenced.

The primers were designed using the NM_024832.3 sequence from Ensembl Genome Browser (www.ensembl.org). Detail of their sequences is summarised in Appendix 2.1. The primer properties used for their design included a GC content of about 40%, an annealing temperature of about 58°C, an absence of hairpin formation and 3' complementarity, and an absence of regions of self-annealing. These criteria were validated using the software OligoCalc (Kibbe, 2007). The primers also had a range of length varying between 18 to 25bp and were amplifying 400 to 550bp of the *RIN3* region of interest. Non-specific bindings against the chromosome 14 and the presence of SNPs were also excluded using SNPcheck (https://secure.ngrl.org.uk/SNPCheck/).

The sequencing reaction was performed using tag M13 as primers. These tags were added to the polymerase chain reaction (PCR) primers, on the 5' extremity for the forward primer and on the 3' for the reverse primer (Table 2.1).

Table 2.1: Sequences of the M13 primers used for sequencing PCR reactions.

	Sequence
Forward (5') primer tag	5'-GTAGCGCGACGGCCAGT-3'
Reverse (3') primer tag	5'-CAGGGCGCAGCGATGAC-3'

PCR Reactions

Amplifications were performed using the GeneAmp 9700 thermocyclers (Applied Biosystem). Two types of reactions were chosen depending on the quality of sequence that had to be amplified. The universal PCR mix was used for non-repetitive and low GC content sequences, while the multiplex PCR mix was used for repetitive and GC rich regions of *RIN3*. Both PCR reactions were set up by the Biomek NX robot (Beckman Coulter), on a 96 plate.

The Master mix used for universal PCR reactions was CM-102A 2X Reddymix custom (Thermo Scientific, Fermentas) (Table 2.2).

Table 2.2: Master mix used for universal PCR.

Reagents	Initial concentration	Final concentration	Amount for 1 reaction (µl)
Reddy mix custom PCR master mix	2X	1X	6
Primers (F+R)	5µM	0.83µM	2
DNA	20ng/µl	3.33ng/µl	2
Nuclease free H_2O			2
		Total	12µl

The thermal cycling protocol consisted of an initial incubation for 4 minutes at 94°C, followed by 30 cycles of 1 minute at 94°C, then 1 minute at 58°C and 1 minute at 72°C. There was a final incubation for 10 minutes at 72°C and the samples were kept at 15°C until further use.

The multiplex PCR mix (Qiagen) was used for sequences that were not amplified by the universal PCR mix, due to the presence of highly repetitive and/or GC rich regions (Table 2.3).

Table 2.3: Master mix used for GC rich PCR.

Reagents	Initial concentration	Final concentration	Amount for 1 reaction (µl)
Qiagen multiplex PCR master mix	2X	1X	6
Primers (F+R)	5µM	0.83µM	2
DNA	20ng/µl	3.33ng/µl	2
Qiagen Q solution	5X	0.83X	2
		Total	12µl

The thermal cycling protocol consisted of an initial incubation for 15 minutes at 94°C, followed by 35 cycles of 1 minute at 94°C, then 1 minute at 56°C and 1 minute at 72°C. There was a final incubation for 10 minutes at 72°C and the samples were kept at 15°C until further use. The type of PCR used for each exon is summarized in Table 2.4.

Table 2.4: PCR conditions used for each exon of the RIN3 gene.

Exon	Type of PCR	Exon	Type of PCR
RIN3_PROM_A_01	Universal PCR	RIN3_EX07_A_01	Universal PCR
RIN3_PROM_B_01	Universal PCR	RIN3_EX07_B_01	Universal PCR
RIN3_PROM_C_01	Universal PCR	RIN3_EX08_01	Universal PCR
RIN3_PROM_D_01	Universal PCR	RIN3_EX09_01	Universal PCR
RIN3_EX01_01	Universal PCR	RIN3_EX10_D_01	Universal PCR
RIN3_EX02_01	Universal PCR	RIN3_EX10_E_01	Universal PCR
RIN3_EX03_01	Universal PCR	RIN3_PROM_E_01	GC rich PCR
RIN3_EX04_01	Universal PCR	RIN3_PROM_F_04	GC rich PCR
RIN3_EX05_01	Universal PCR	RIN3_EX06_A_03	GC rich PCR
RIN3_EX06_B_01	Universal PCR	RIN3_EX10_A_01	GC rich PCR
RIN3_EX06_C_01	Universal PCR	RIN3_EX10_B_01	GC rich PCR
RIN3_EX06_D_01	Universal PCR	RIN3_EX10_C_01	GC rich PCR
RIN3_EX06_E_01	Universal PCR		

PROM = Promoter; EX = Exon.

Purification of the PCR product

The Agencourt AMPure XP purification system (Beckman Coulter) was used on PCR products to eliminate salt residues and other contaminants such as primers and dNTPs leftovers, which can interact with the sequencing PCR reaction.

The AMPure XP purification uses a magnetic bead-based technology, as shown in Figure 2.1. The AMPure reagent, containing magnetic beads, is added to the PCR products. The PCR amplicons bind to the beads and the plates are then placed on a rack, for which each well contains a magnetic ring. The beads are attracted to the magnets, allowing ethanol washes. The amplicons are then detached from the beads using an elution buffer, before being transferred to a new plate. This technique was robotised, using the Biomek NXP robot (Beckman Coulter).

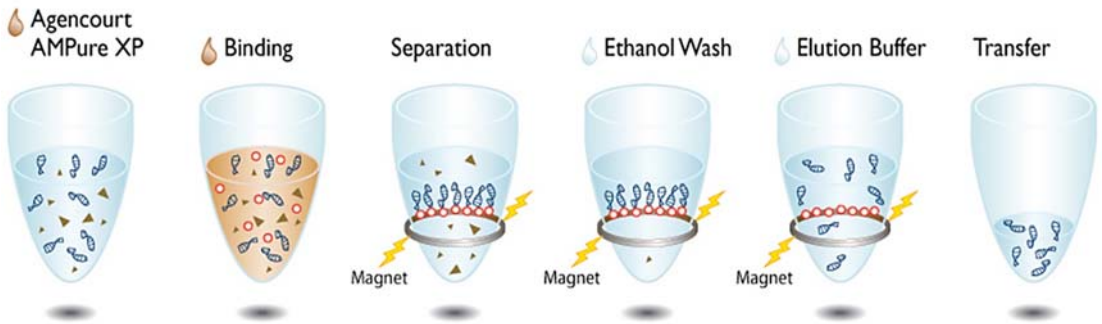

Figure 2.1: AMPure XP purification process (Beckman Coulter, 2017a).
PCR products (10µl) were purified from contaminants by adding 18µl of AMPure reagent, which contains magnetic beads. Once bound to the DNA, the beads are attracted to the outside of the well using a magnetic field, allowing ethanol washes and elution in 30µl of water. The program used was the Agencourt AMPure PCR Purification system, optimized by Beckman Coulter.

Sequencing PCR reaction

Following the AMPure XP purification, a sequencing master mix for 96 and 384 well plates was prepared as described in Table 2.5. The sequencing PCR reaction was performed using the M13 primer, mentioned previously (Section 2.1.1).

Table 2.5: Master mix composition for the sequencing reaction (96 and 384 well plates).

96 well plate		384 well plate	
Reagents	**Amount (µl)**	**Reagents**	**Amount (µl)**
Sequencing reaction mix	8	Sequencing reaction mix	3.5
DNA from the AMPure plate	2	DNA from the AMPure plate	1.5
Total	10µl	Total	5µl

The thermal cycling protocol consisted of an initial incubation for 1 minute and 15 seconds at 96°C, followed by 30 cycles of 15 seconds at 94°C, then 10 seconds at 50°C and 4 minutes at 60°C. There was a final incubation 15°C at which point the plate remained in the thermocycler until further use. The sequencing reaction mix composition is described in Table 2.6.

Table 2.6: Sequencing mix composition (96 and 384 well plates).

96 well plate		384 well plate	
Reagents	**Amount (µl)**	**Reagents**	**Amount (µl)**
Big dye v3.1	0.5	Big dye v3.1	0.25
Sequencing buffer (5X)	1.75	Sequencing buffer (5X)	0.875
M13 tag primers forward or reverse (3.2 µM)	1	M13 tag primers forward or reverse (3.2 µM)	0.5
dH_2O	4.75	dH_2O	1.875
Total	8µl	Total	3.5µl

Purification of the sequencing reaction products

The Agencourt CleanSEQ (Beckman Coulter) kit is also a magnetic bead-based sequencing purification system and was used for the elimination of contaminants from the sequencing PCR reaction products, such as primers and big dye leftovers which can interact with the sequence analysis. The different steps of the process are shown in Figure 2.2. This technique was also robotised using the Biomeck NXP robot (Beckman Coulter).

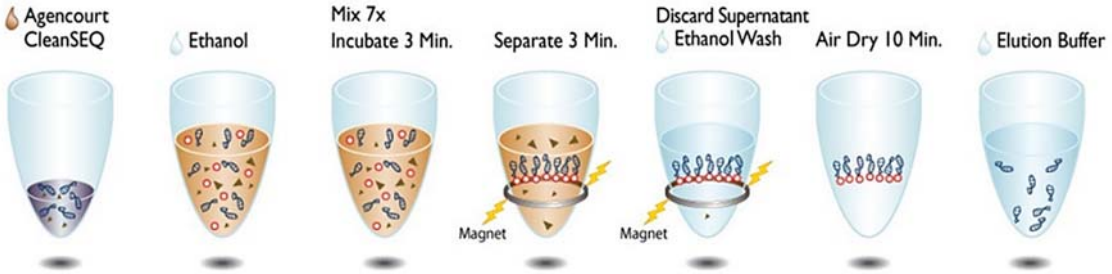

Figure 2.2: CleanSEQ purification process (Beckman Coulter, 2017b).
The sequencing reaction mix (10µl) was purified from contaminants by adding 10µl of CleanSeq reagent, which contains magnetic beads. Once bound to the DNA, the beads are attracted to the outside of the well using a magnetic field, allowing ethanol washes and elution in 80µl of EDTA. The program used was the Agencourt CleanSeq Dye Terminal Removal, optimized by Beckman Coulter.

Sequence analysis

CleanSEQ products were then analysed using the Sanger method (Sanger et al, 1977) and capillary electrophoresis (Kan et al, 2004) on the ABI 3130 and 3730 sequencers (Applied Biosystems). Each sequence was processed manually using the Mutation surveyor® V3.30 software (Softgenetics, US) and compared to the reference sequence NM_024832.3 of *RIN3* from Ensembl Genome Browser (www.ensembl.org). The severity of the DNA variations was analysed using the Alamut® Visual Version 2.1 software (Interactive Biosoftware, France).

Summary of the general process

Below is a schematic representation of the general process used from collection of blood to sequencing.

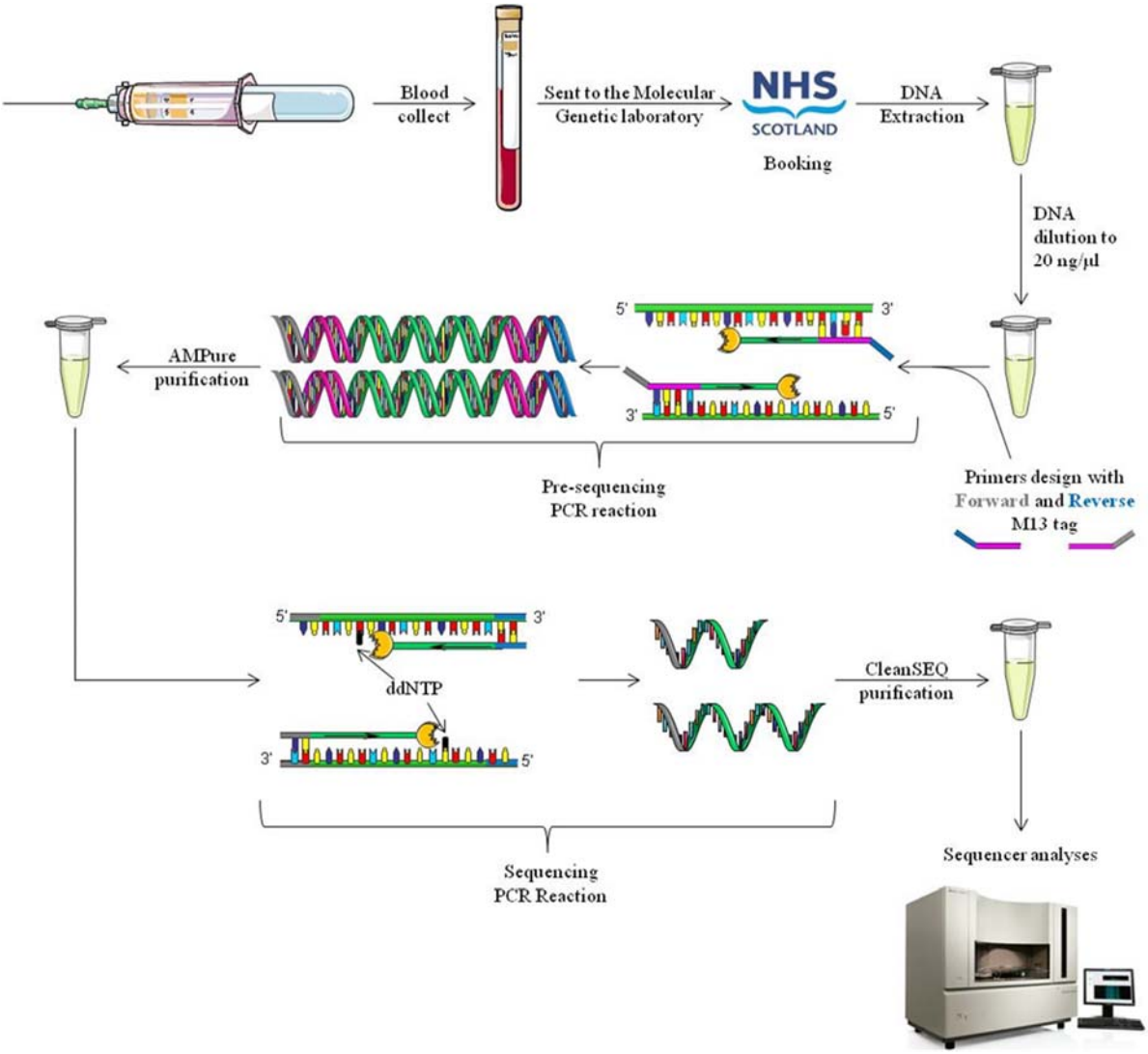

Figure 2.3: General process of sequencing reaction for RIN3.
Adapted using Servier medical art (Servier, 2017).

2.1.2 Next generation sequencing

Next generation sequencing was also performed to identify additional variants in the *RIN3* gene, and confirm results from the Sanger sequencing.

This work was supervised by Dr. Omar Albagha and Dr. Sachin Wani (Vallet et al, 2015).

The patient cohort

This mutation screening was performed on 121 Pagetic patients. 95 of those were obtained from the PRISM study, and the other 26 were familial cases. The criteria of selection included the absence of *SQSTM1* mutation and an age of diagnosis younger than 65 years old. 49 non-Pagetic controls were also investigated, where 40 were from the PRISM control cohort and 9 were unaffected members of familial cases.

The sequencing was performed using a Haloplex kit (Agilent technologies). The entire *RIN3* gene (175,211bp) and 20kb of flanking regions on either side were screened. The experiment was performed following the manufacturer instructions and an Illumina HiSeq2000 platform, available at the NHS Molecular Genetic laboratory, was used for the preparation and the labelling of the libraries.

Analysis

The sequences were analysed against the human genome version hg19/b37, using the Burrows-Wheeler Aligner software package (Li & Durbin, 2009).

The Picard command line tools (version 1.89, http://broadinstitute.github.io/picard/) was used to exclude duplicate reads. Local re-alignment around potential indel sites and base quality scores calibrations were adjusted using the genome analysis toolkit (version 1.6, GATK, https://software.broadinstitute.org/gatk/).

The unified genotyper (GATK) was used to analyse the different SNPs and indel with a quality score higher than 20 and coverage higher than x5.

2.1.3 Frequency analysis

The next generation sequencing data was combined with the Sanger sequencing results and analysed together.

Chi-square allelic test was used to investigate common variants while Fisher's exact test was chosen to perform a Burden test on rare variants (MAF < 1%) in cases and/or controls.

Frequencies were analysed against 379 European subjects from the 1000 Genomes (phase I version 3, www.1000genomes.org/) and 4300 European-American subjects from the NHLBI project (http://evs.gs.washington.edu/EVS/).

Finally, a haplotype analysis was performed using Haploview (Barrett et al, 2005).

2.1.4 Imputation

An imputation performed on Pagetic patients by Albagha and colleagues in 2011 revealed an association for a 60kb region of the *RIN3* gene. A conditional analysis performed on the top hit (rs10498635) confirmed the independency of the signal and recombination hotspots were also detected in and around the *RIN3* gene (Albagha et al, 2011). This imputation was performed using the Hapmap CEU dataset (release 22). Using the same European descent cohort of 741 PDB patients and 2,699 controls from the WTCCC, a second imputation was here carried out on the same locus (14q32) using Markov chain haplotyping (MACH) (Li et al, 2009). The 1000 Genomes European phased haplotype data (phase I version 3) (www.1000genomes.org/) was used as a reference, increasing the number of samples from 60 (Hapmap) to 379 (1000 Genomes).

Based on the estimated correlation between imputed and true genotypes ($r^2 < 0.3$), variants with low imputation quality as well as variants of MAF < 1% were excluded. The software ProbABEL (Aulchenko et al, 2010) was used to translate the allelic dosage of imputed variants into genotypes and identify a significant association between a variant and PDB, using a logistic regression analysis. The tool LocusZoom was used to generate regional association plots (Pruim et al, 2010). PLINK (version 1.07; http://pngu.mgh.harvard.edu/purcell/plink/) (Purcell et al, 2007) was used to perform a conditional analysis on the top hit variant described in the 2011 GWAS study (rs10498635), using logistic regression. LD was investigated using Haploview (Barrett et al, 2005).

2.1.5 In silico analysis of variant pathogenicity

Predicted regulatory regions in non-coding variant's locations were identified using Ensembl Genome Browser (www.ensembl.org) and ENCODE (https://www.genome.gov/encode/).

The nomenclature used for the description of sequence variants was using version 2.120831 of the human genome variation society (Den Dunnen & Antonarakis, 2000).

The pathogenicity level of each coding variants was estimated using six bioinformatic tools: SIFT (Kumar et al, 2009), PolyPhen-2 (Adzhubei et al, 2010), Condel (Gonzalez-Perez & Lopez-Bigas, 2011), MutationTaster (Schwarz et al, 2014; Schwarz et al, 2010), GERP conservation (Cooper et al, 2005), and Grantham scores (Grantham, 1974) obtained from the MutationTaster program. Severity scores were established by giving a point for each software considering the variant as damaging for the structure of RIN3. Mutations predicted as "damaging" by SIFT, "possibly or probably damaging" by PolyPhen-2, "deleterious" by Condel, "disease causing" by MutationTaster, had a GERP score higher than 2.0, or a Grantham score higher than 50 were given a point each. The final score ranges from 0 (low estimated functional/structural effect) to 6 (high estimated functional/structural effect).

Additional *in silico* analyses of the coding variants were performed with the help of Dr. Dinesh Soares to further assess their impact on the RIN3 protein structure. For this, the SH2 and VPS9 domains of RIN3 were modelled using Modeller 9v12 (Sali & Blundell, 1993). Structure stability modifications between the mutated and wild type RIN3 were investigated using FoldX (Schymkowitz et al, 2005), by measuring their differences of delta delta Gibbs free energy ($\Delta\Delta G$).

Prediction of intrinsic disorder in the full RIN3 protein was assessed using two meta servers, MetaPrDOS (Ishida & Kinoshita, 2008) and MetaDisorder (Kozlowski & Bujnicki, 2012). Finally, the evaluation of order/disorder changes translated in PONDR score were undertaken using PONDR VL-XT (Li et al, 1999) for each coding variant located in the PRR of RIN3.

2.2 GENOTYPING FOR ALLELIC ASSOCIATION

Most of the variants analysed from the previous sequencing data (Section 2.1) were of rare frequency and were detected using a cohort with patients diagnosed at a young age and/or family history. In order to confirm those findings and investigate in more depth the effect of the rare variants, those SNPs were genotyped using a bigger cohort with different levels of severity of PDB. A disease severity association was also performed.

2.2.1 Cohort

For this study, 974 UK samples (712 cases and 262 controls) from the PRISM cohort were genotyped for *RIN3* variants, in relation to disease activity. All samples were analysed on genomic DNA extracted from peripheral blood using standard procedure.

2.2.2 Variants analysed

The details of the 16 variants genotyped, selected from the mutation screening presented in Section 2.1 are summarised in Table 2.7.

Four coding variants (p.T425M, p.R427Q, p.P447S, and p.G613A) were located in repetitive areas making the genotyping assay technically impossible to design. In an attempt to find alternative assays, an LD analysis was carried out using Haploview version 4.2 (Barrett et al, 2005). SNPs in strong LD with the four coding variants will offer similar genomic patterns and can be used as alternative SNPs. This LD was performed on the results obtained from the 101 ZiPP samples sequenced by Sanger (Section 2.1.1), and only variants in association with a $r^2 > 0.8$ were considered. The alternative variants are described in Table 2.7.

Table 2.7: Summary of genotyped variants in RIN3.

Genotyped variants				In LD with the following alternative variants:				
Variant ID	**Protein change**	**Position (GRCh37 /hg19)**	**Gene region**	**Variant ID**	**Protein change**	**Position (GRCh37 /hg19)**	**Location**	**r^2**
N/A	c.[1-926A>G];[=]	92979351	Promoter	—	—	—	—	—
rs368389701	c.-21C>A	92980256	5'UTR	—	—	—	—	—
N/A	c.[422C>T], p.A141V	93081806	Exon 4	—	—	—	—	—
rs8022440	c.[440+74G>T];[=]	93081898	Intron 4	rs74074812	c.[1429C>T];[=], p.P477S	93118823	Exon 6	1
rs113876303	c.[441-103A>C];[=]	93107480	Intron 4	rs12434929	c.[1838G>C];[=], p.G613A	93119232	Exon 6	1
N/A	c.[691C>T];[=], p.R231C	93118085	Exon 6	—	—	—	—	—
rs147329151	c.[751C>A];[=], p.Q251K	93118145	Exon 6	—	—	—	—	—
rs3814830	c.[804C>T];[=]	93118198	Exon 6	rs3742717	c.[1274C>T];[=], p.T425M	93118668	Exon 6	0.891
N/A	c.[866T>C] ;[=], p.L289P	93118260	Exon 6	—	—	—	—	—
N/A	c.[874T>C] ;[=], p.C292R	93118268	Exon 6	—	—	—	—	—
N/A	c.[880C>T];[=], p.P294S	93118274	Exon 6	—	—	—	—	—
N/A	c.[916G>C] ;[=], p.A306T	93118310	Exon 6	—	—	—	—	—
rs201271121	c.[1156C>T];[=], p.P386S	93118550	Exon 6	—	—	—	—	—
rs3818321	c.[2013C>T];[=]	93119407	Exon 6	rs74074811	c.[1280G>A];[=], p.R427Q	93118674	Exon 6	1
rs145292991	c.[2311G>A] ;[=], p.D771N	93125790	Exon 7	—	—	—	—	—
rs147042536	c.[2377T>C];[=], p.Y793H	93142861	Exon 8	—	—	—	—	—

N/A = Indicates that the SNP does not have an rs number.

A Taqman® SNP genotyping (Thermo Fisher Scientific) reaction was performed using a QuantStudio 12K Flex Real Time PCR System (Thermo Fisher Scientific) at the Wellcome Trust Clinical Research facility Genetic Core, Edinburgh. Allelic discrimination was performed using a PCR, where 2 types of probes recognising either allele were added. Each probe was associated with a different fluorochrome which was freed during the polymerisation step. This generated a signal, read by the QuantStudio. This procedure is summarised in Figure 2.4.

2.2.3 Analysis

The samples were analysed on a Taqman® Genotyper Software (version 1.3, Thermo Fisher Scientific) at the Genetic core facility. Variants with a call rate < 97% were not analysed. All statistical analyses were then performed on SPSS Version 22 (SPSS Ltd, UK).

Frequencies within each cohort were established first. A case/control analysis was then performed with Fisher's exact test on rare variants (MAF < 1%), or one-way ANOVA for common variants (MAF > 1%). A Burden test was also performed on rare variants with Fisher's exact test.

Haplotypes were estimated using the Phase software (version 2.1.1) for the cases compared to controls (Stephens & Scheet, 2005; Stephens et al, 2001). A 90% imputation accuracy was used, while a frequency threshold of 0.0001 was chosen. The data was run 5 times to get the best estimated haplotypes, as advised by the user's instructions.

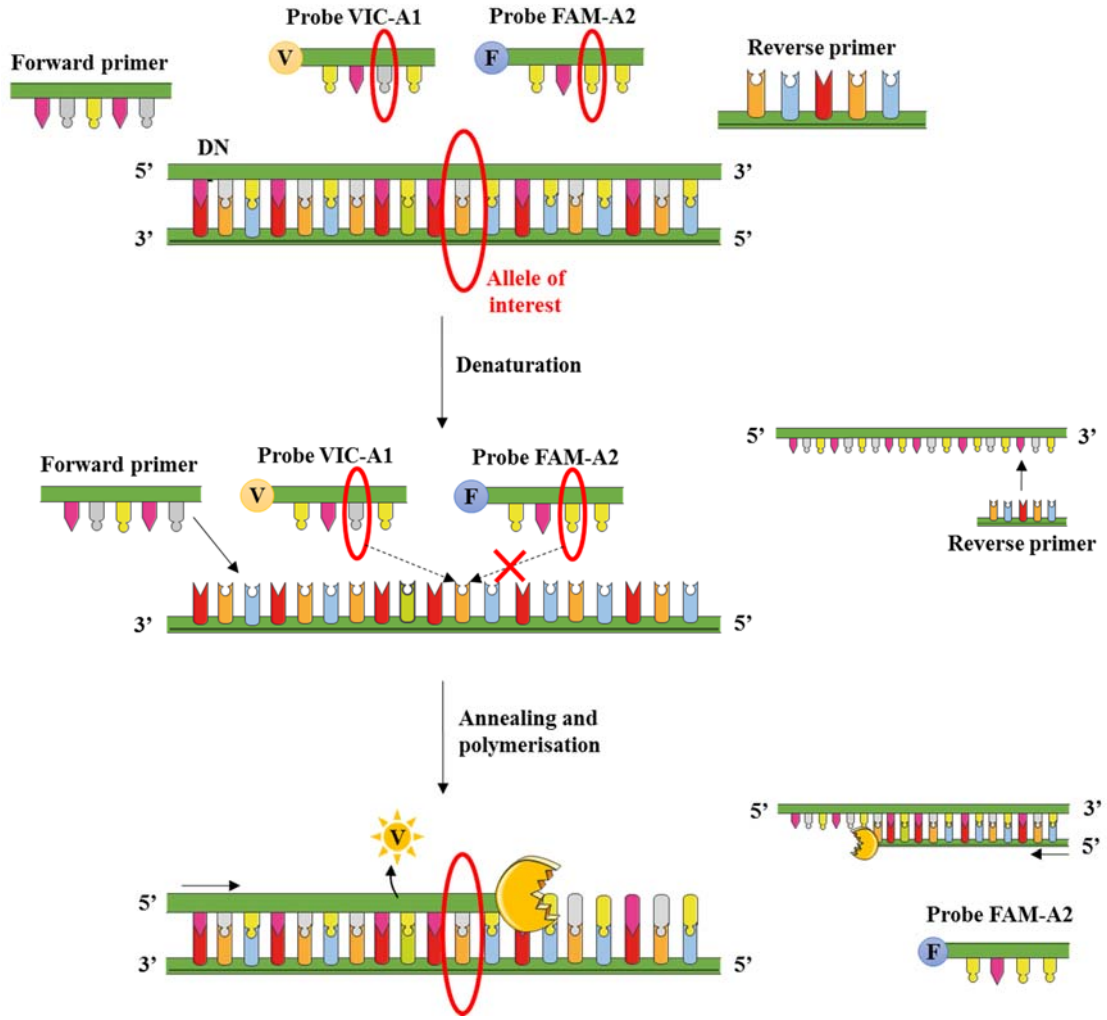

Figure 2.4: Summary of the Taqman SNP Genotyping assay (Life Technologies, 2011). The template DNA is initially prepared with classic polymerase chain reaction reagents. After denaturation of the DNA, two probes are added to the reaction. Each recognise specifically one of the possible allele (A1 or A2) of the variant to analyse and are attached to a different fluorochrome (here VIC or FAM). The corresponding probe will then recognise the allele of interest following the annealing step and the fluorochrome will be released during polymerisation. The fluorochrome is measured by the system and the allele is deducted from the VIC or FAM fluorescence. Adapted using Servier medical art (Servier, 2017).

A severity analysis using clinical information was additionally performed on the PRISM cases. For this, data was collected from Pagetic patients for relevant clinical variable including gender, number of bisphosphonates previously received, presence of family history of PDB, age at diagnosis, age at which the patient has joined the trial (age at recruitment), the number of affected bones, whether the patient had orthopaedic surgery, fractures (associated with PDB or not), skull involvement and use of a hearing aid. Bone pain was also assessed, and clinicians evaluated if it was caused by PDB (Table 2.8). A clinical deformity score was assessed by the physician, for which 0 corresponds to no deformity; 1 corresponds to mild deformity; 2 corresponds to moderate deformity; and 3 corresponds to severe deformities. An overall PDB severity score was deducted from those observations. For this, the number of affected bones was added to the presence of bone pain (yes = 1; no = 0; unsure 3), previous fractures (yes = 1; no = 0), previous surgeries (yes = 1; no = 0), the severity of bone deformities for which the score of the severity was cumulated for each affected bone (range 0-7), and the use of hearing aids if the skull of the patient is affected (yes = 1; no = 0) (Visconti et al, 2010).

Data from the allelic dosage of the p.R279C variant was imported from a GWAS performed by Albagha and colleagues (Albagha et al, 2011). A first association study was performed on the genotyping data for each common variant (p.R279C and p.T425M; No-mutation, heterozygote mutation or homozygote mutation) and all rare variants grouped together (no mutation or at least one rare variant mutated). This was investigated in all Pagetic cases (PRISM), in cases who were positively mutated for *SQSTM1* (PRISM/SQSTM1+), as well as in the cases who were not mutated for *SQSTM1* (PRISM/SQSTM1-).

The clinical phenotypes investigated are summarised in the Table 2.8, as well as the type of statistical test performed on SPSS Version 22 (SPSS Ltd, UK).

Table 2.8: Clinical phenotypes investigated in presence of RIN3 mutations (Visconti et al, 2010).

Analysis	Description	Test
Gender	Female/Male	Chi square
Family history of PDB	Presence or not of family history for the patient	Chi square
Orthopaedic surgery	Whether the patient had surgery or not	Chi square
Any fractures	Whether the patient had fractures or not	Chi square
Skull disease and hearing aid	Whether the patient has PDB located in his or her skull and wears hearing aid	Chi square
Bone pain	Whether the patient has bone pain or not	Chi square
Fracture in Pagetic bone	Whether the fractures were due to PDB	Chi square
Bisphosphonates	Number of bisphosphonates the patient has received	Anova
Age at diagnosis	Age at which the patient was diagnosed with PDB	Anova
Age at recruitment	Age at which the patient joined the trial	Anova
Number of bones affected	Number of affected bones the patient has	Anova
Pagetic pain	Confirmation from the clinician that the bone pain felt by the patient is associated to PDB	Anova
Deformity score	Severity of deformities the patient has	Anova
Paget Severity score	Overall severity of PDB based on the other phenotypes	Anova

A second association for disease severity was performed on the most common haplotypes of those 16 variants (including p.R279C), which were obtained from the cases by using Phase (version 2.1.1) (Stephens & Scheet, 2005; Stephens et al, 2001). The settings used were the same as those presented above. As the Phase software estimates haplotypes from the genotyping data by imputing missing information, numbers detected in this last analysis will differ slightly from the association performed on true genotypes.

2.3 TISSUE CULTURE

All experimental protocols were approved by the Ethics Committee at the University of Edinburgh and were conducted in accordance with the UK Animals (Scientific Procedures) Act 1986 (project licence number PPL 70/7964).

2.3.1 Osteoclast cell culture

Bone marrow was isolated from the hind limbs (tibias and femurs) of C57BL/6 x 129/OlaHsd female mice aged between 9 and 14 weeks old, sacrificed by cervical dislocation according to Schedule 1 of the Animals (Scientific Procedures) Act. The bone marrow was kept in PBS buffer at room temperature and were processed within 30 minutes of collection.

All steps described below were performed in a sterile environment using a laminar flow hood. Before use, the hood was cleaned with Trigene, Mycoplasma off, and 70% (v/v) ethanol and UV sterilisation (including all inert material) was applied for 10 minutes.

Bone marrows were flushed out of the long bones using a 25-gauge (G) needle and using non glutamax α-minimum essential medium (αMEM, Invitrogen) supplemented with 1% L-Glutamine, 100U/ml penicillin and 100μg/ml streptomycin and 10% foetal calf serum (Hyclone). The bone marrow was then broken down to a cell suspension by passing successively through decreased size needles (19G – 25G). The cells were isolated by a 3 minute centrifugation at 300g and the pellet was resuspended in αMEM supplemented with 100ng/ml of M-CSF (Prospec) to be plated in a 10cm petri dish. The plates were then incubated at 37ºC, with 5% CO_2, 95% air in a humidified atmosphere.

After two days of incubation, adhered cells enriched in macrophages (Zhang et al, 2008) were scraped off using dissociation buffer (Gibco cell dissociation buffer) for 3 minutes at 37ºC and a soft rubber scraper. The macrophages were plated in 12 well plates at $1.5x10^5$ cells per well in 1ml of standard αMEM supplemented with 100ng/ml of human RANKL and 25ng/ml of M-CSF to initiate osteoclast differentiation. The plates were incubated at 37ºC, 5% CO_2 for 72 hours when the media was changed, keeping the same conditions. The plates were incubated for 24 hours before terminating the cultures. A summary of the bone marrow cell procedure is shown in Figure 2.5.

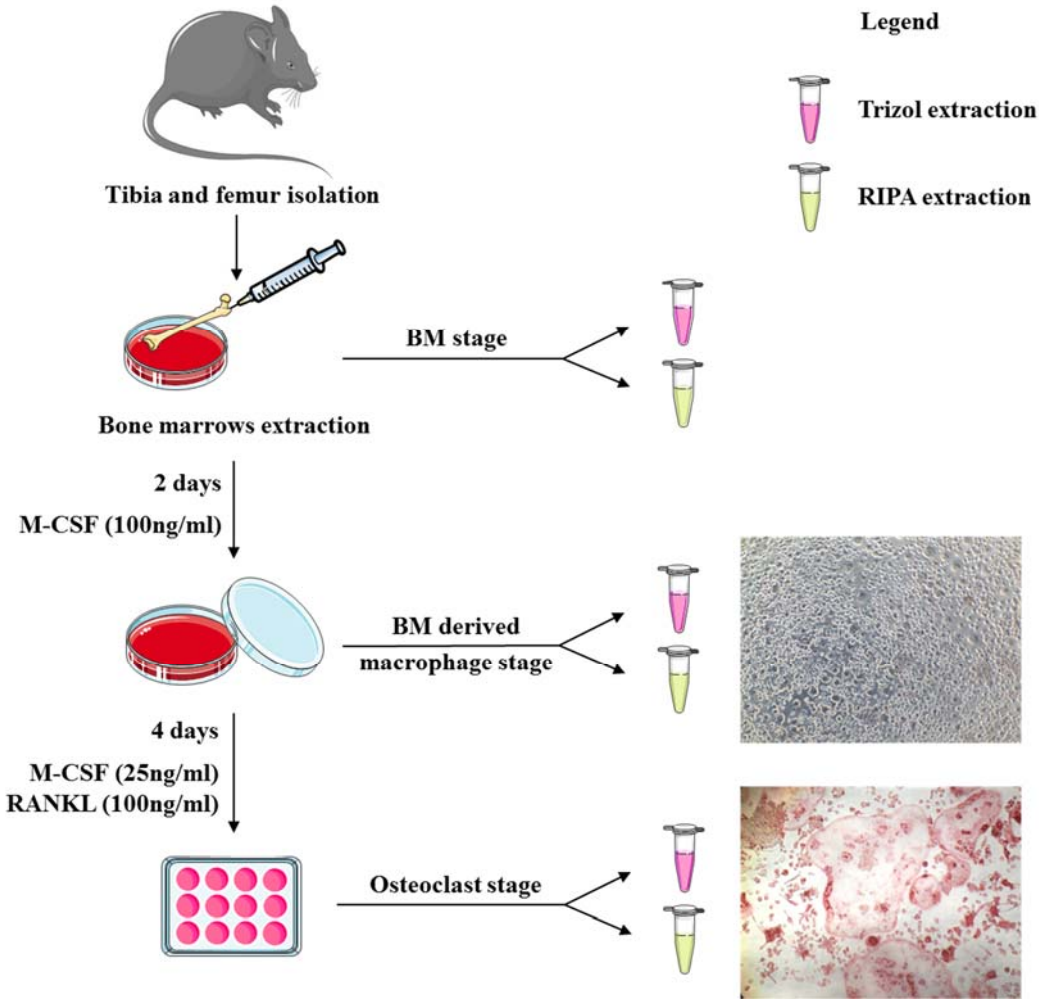

Figure 2.5: Summary of bone marrow osteoclast culture.
BM = Bone marrow. Adapted using Servier medical art (Servier, 2017).

For the investigation of survival of osteoclasts, 25ng/ml of human RANKL was used for the differentiation of the cells. The RANKL cytokine was then removed from the media, and the cells were cultured for an additional three days. Cultures were terminated at 0h, 4h, 8h, 24h, 48h, and 72h.

Tartrate-resistant Acid Phosphatase staining

Tartrate-resistant acid phosphatase (TRAcP) staining was performed on osteoclast like cells. For this, the cultures were terminated by removing the medium from the cells and washing them in PBS buffer twice. The cells were then fixed in 4% (v/v) formaldehyde in PBS for 15 to 20 minutes at room temperature. They were then rinsed in PBS twice, and stored in fresh PBS at 4^{o}C until future use.

A TRAcP staining solution was freshly prepared, all in sterile clean glass tubes as shown in Appendix 2.2. First, solution A was made of veronal buffer, acetate buffer, acetate buffer with tartrate, Naphthol-AS-BI-phosphate in dimethylformamide. Aside, solution B was prepared, including pararosanilin, and sodium nitrite.

The detailed concentrations used for solution A and B can be found in Appendix 2.2. The two solutions were mixed, and filtered through a 0.45μM filter.

The cells were rinsed in PBS twice, and the TRAcP staining solution was added to cover all wells. Plates were incubated at 37^{o}C for one hour until red staining developed. The staining solution was removed and the cells were rinsed twice with PBS. The cells were kept in 70% (v/v) ethanol and stored at 4^{o}C. Red cells with at least 3 nuclei were counted using a Zeiss Axiovert light microscope (Carl Zeiss Ltd., UK) under a magnification x10.

2.3.2 Osteoblast cell culture

Osteoblasts were obtained from isolated calvarial from 2 days old pups, which were decapitated according to Schedule 1 of the Animals (Scientific Procedures) Act. All pups from each litter were used for each experiment. The number of pups varied from 5 to 9 for each litter.

The calvaria was carefully removed using scissors and tweezers before being washed in Hank's balanced salt solution (HBSS) to remove any unwanted tissue. The samples were then moved into a tube containing 2ml of collagenase type I at 1 mg/ml in HBSS, and were left at 37ºC for 10 minutes. The tube was shaken every 2 minutes to help the enzymatic digestion. The supernatant was discarded, and 4ml of collagenase type I at 1mg/ml in HBSS was added. After 30 min of incubation at 37ºC and regular shaking, the supernatant was transferred to a tube containing 6ml of standard αMEM for future use. The samples were washed carefully in PBS, and 4ml of EDTA at 4mM were then added for 10 minutes at 37ºC under regular shaking. The supernatant was then transferred to a tube containing 6ml of standard αMEM for future use. The samples were washed carefully in PBS, and 4ml of collagenase type I at 1mg/ml in HBSS were then added for 20 minutes at 37ºC under regular shaking. Finally, the supernatant was transferred to a tube containing 6ml of standard αMEM for future use. The three supernatants kept aside during the digestion were centrifuged at 300g for 3 minutes and the pellets were resuspended together in standard αMEM. The final cell suspension was plated in a $75cm^2$ and incubated at 37ºC, 5% CO_2 for 24 hours. The media was then refreshed to remove non-adherent cells every two days until cellular confluence was reached, about 4 to 5 days after isolation.

Once the osteoblasts reached 95-100% confluence, the adherent cells were carefully rinsed with PBS before adding 4ml of trypsin. The flask was incubated at 37ºC, 5% CO_2 for 3 minutes. Full cell dissociation was assessed by microscopic observation, and once confirmed, 8ml of standard αMEM were added to the flask to inactivate the trypsin. The suspension was then centrifuged for 3 minutes at 300g and the pellet was resuspended in standard αMEM. The cell number was estimated using a Neubauer haemocytometer. Osteoblasts were plated at $8x10^3$ cells/well in 150µl of standard αMEM in a 96 well plate, or $1x10^5$ cells/well in 1ml standard αMEM in a 12 well plate. The cells in the 96 well plate were used for measuring ALP activity (described below, in this section) while the cells in the 12 well plates were used for the Alizarin red/bone nodule assay (described below, in this section). The plates were incubated for 48h, at 37ºC, 5% CO_2.

The media of the 12 well plate was replaced by standard αMEM supplemented with 50µg/ml vitamin C and 3mM beta-glycerophosphate (β–GP) called osteogenic medium, for 48h at 37ºC, 5% CO_2. The cells were kept in those conditions until cell viability was assessed using AlamarBlue® (10% v/v) (Thermo Fisher Scientific) at weeks 1, 2 and 3. AlamarBlue® is a blue non-toxic reagent, which becomes red fluorescent once metabolised by viable cells. The fluorescence is directly proportional to the amount of viable cells present in the media.

The plate was incubated for 1 hour before being measured on a plate reader at an excitation wavelength of 540nm and an emission wavelength of 590nm. The measured fluorescence was corrected against blanks without cells, which were added on the last day the media was changed from the cells before test. The cells were then washed once in PBS and fixed in 70% ethanol (v/v). The cells were kept at 4 degrees until future analyses.

Osteoblasts cultured in a 96 well plate were used for the ALP activity assay. For this experiment media of the 96 well plate was refreshed using standard αMEM, and the cells were incubated for an additional 24h, at 37ºC, 5% CO_2. Cell viability was assessed using AlamarBlue® for 2 hours, before being washed in PBS once. Cells were then incubated in 150µl of ALP lysis buffer (Appendix 2.3) for 15 minutes at room temperature before successive pipetting. The cells were stored in the plate at -20ºC until future use.

The procedure of osteoblast culture is summarised in Figure 2.6.

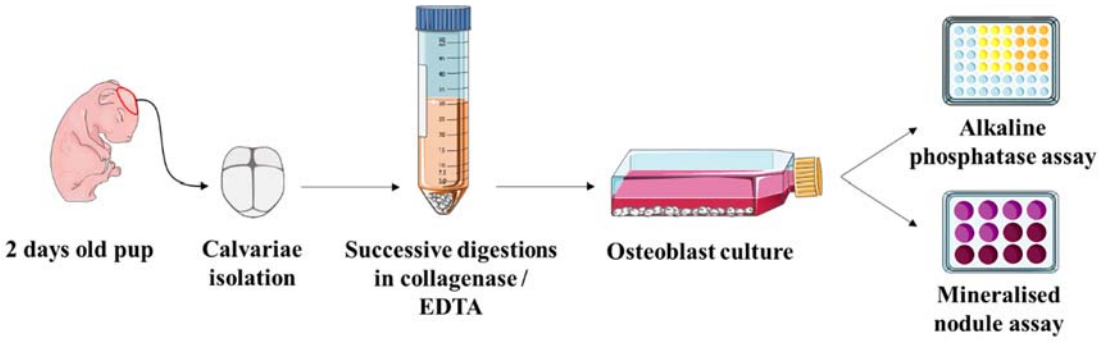

Figure 2.6: Summary of calvarial osteoblast culture.
Adapted using Servier medical art (Servier, 2017).

Alizarin Red staining and quantification

Alizarin red staining is a biochemical assay used to quantify calcium deposits produced by osteoblast cultures, in presence of osteogenic media. The staining process induces the chelation of calcium with Alizarin red and results in a dark red colour. Free calcium ions also precipitate with Alizarin red to form red deposits. The coloured complexes are then dissolved in a destaining solution and measured at 562nm.

For this, Alizarin red was initially dissolved in distilled water to a final concentration of 40mM, and adjusted to a pH of 4.1 to 4.3 using 10% (v/v) ammonium hydroxide. The fixed osteoblasts were carefully rinsed 4 times in distilled water to remove all traces of 70% (v/v) ethanol. 800µl of Alizarin red solution was added to each well and the plates were then left on a shaker for 20 minutes at room temperature to stain all calcium nodules. The staining solution was then removed and the wells were rinsed at least 5 times with water until leftovers of the staining solution were completely removed. Plates were then left to air-dry overnight at room temperature and mineralized nodules were imaged the following day by scanning the plates. A destaining solution was prepared by adding 10% (w/v) cetylpyridinium chloride solution to 10mM sodium phosphate (pH 7.0). The pH was adjusted to 4.1 to 4.3 with concentrated hydrochloric acid. 800µl of the destaining solution was added to each well and the plates were left on a shaker overnight at room temperature. The Alizarin red was quantified in duplicates at 562nm on a Bio-Tek Synergy HT, along with a standard curve prepared in the same destaining solution (0 to 10mM). The amount of Alizarin red (mM) from the samples was then deducted using the standard curve and once corrected over cell viability, was compared between both groups.

Alkaline phosphatase assay

The ALP assay is used as a biochemical marker for osteoblast differentiation. Its activity is measured by colorimetric assay, through the conversion of p-nitrophenyl phosphate (no colour) to p-nitrophenol (yellow).

The monolayer of osteoblasts previously resuspended in lysis buffer (Section 2.3.2) was measured by colorimetric assay. A standard curve made of serial dilutions of p-nitrophenol (0 to 30nM) was measured against each sample, in duplicates. The plate was then analysed on a Bio-Tek Synergy HT at 405nm at 2 minute of intervals for 20 minutes. ALP activity was determined from the slope of the linear part of the kinetics curve and was corrected over cell number.

2.4 RNA RELATED INVESTIGATIONS

The expression of mRNA for *Rin3* has been quantified at different stages of osteoclast differentiation from primary BMDMs to assess its level and variation of expression, as well as in primary osteoblast cells. It was also quantified in mouse tissues, such as brain, kidney, liver, lung and total crushed bone.

2.4.1 TRizol® sample collection

Total RNA isolation was performed using TRizol® reagent (Invitrogen). Flushed out bone marrows were centrifuged at 1200rpm for 3 minutes, and the medium was carefully removed. The cells were washed at least once in PBS. The cells were centrifuged again at 1200rpm for 3 minutes, and the pellet was resuspended in TRizol® (Thermo Fisher Scientific). For plated cells, the media was removed from wells, and two PBS washes were done. TRizol® was added in excess and the cells were lysed by pipetting up and down thoroughly. The amount of TRizol® used varied depending on the number of wells (50µl per well in a 12 well plate) and size of tissue (1ml TRizol® per 50-100mg of tissue). Tissues were homogenised for about 20 seconds in TRizol® using the OMNI general laboratory homogeniser (OMNI GLH). The homogeniser was washed before and after each sample in nuclease and protease free Hyclone ultrapure water, followed by a wash in DNAse out, then in RNAse out, and two final washes in Hyclone ultrapure water. Each lasted at least 5 seconds, except for the RNAse out wash (10-20 seconds).

After lysis, the TRizol® samples were incubated in ice for 10 min before being stored at -80^{o}C.

2.4.2 RNA isolation

All RNA isolation and qPCR steps were performed using diethyl pyrocarbonate (DEPC) – treated 1.5ml eppendorf tubes.

The RNA was separated from the DNA and proteins using 200µl of chloroform per millilitre of TRizol® used and by vortexing for 15 seconds. After 3 minutes of incubation at room temperature, the samples were centrifuged for 15 minutes at 12000g, at 4ºC. The aqueous phase containing exclusively the RNA was precipitated in isopropyl alcohol in order to remove the TRizol® left in the samples. After 10 minutes of incubation at room temperature, the samples were centrifuged for 10 minutes at 12000g, at 4ºC. The pellets were then washed twice with 1ml of 75% (v/v) cold ethanol, followed by a centrifugation at 7500g for 5 minutes at 4ºC. Once dried, the pellets were dissolved on ice in DEPC - treated water depending on the size of the pellet (about 20µl). Once done, the samples were heated at 65ºC for 5 minutes before being homogenised by pipetting up and down. The samples were kept at -80ºC until further use.

The concentration and quality of RNA samples was also measured using a Nanodrop ND-8000 (Thermoscientific).

2.4.3 Reverse transcription

The RNA was then transcribed into cDNA by reverse transcription. After diluting the RNA to the same concentration across all samples in a final volume of 11µl, the following reaction was added to each sample:

1µl of oligo(dt)20 at 50µM

1µl of 10mM dNTP mix

1µl of DEPC-treated H_2O

The negative controls had 11µl of DEPC water instead of diluted RNA.

The plate was heated for 5 minutes at 65ºC and incubated on ice for 1 minute. After briefly spinning down the samples by centrifugation, the following reagents were added in each well:

4µl of 5X first-strand buffer

1µl of DTT at 0.1M

1µl of RNaseOut Recombinant RNase Inhibitor at 40U/µl

1µl of SuperScript III Reverse Transcriptase at 200U/µl

The plate was incubated in an MJ Research cycler firstly at 50ºC for 60 minutes, then at 70ºC for 15 minutes.

The samples were then stored at -20ºC until further use.

2.4.4 Quantitative real-time PCR

Quantitative real-time PCRs (qPCRs) were performed on cDNA to investigate the level of *Rin3* mRNA expression in the bone microenvironment.

The primers were designed manually using the mouse sequence NM_024832.3 from Ensembl Genome Browser (www.ensembl.org). The forward primer overlaps between exon 1 and 2, while the reverse primer is at the beginning of exon 4, yielding a size of 357bp. This results in the specific amplification of the heaviest isoform (980aa) of *Rin3*, as the 900aa isoform starts from the last 9 nucleotides of exon 2. A probe located in this region was also used (Roche, Probe #13).

This amplification was performed on mRNA measured from cells and tissues from WT mice. Details of primer sequences are shown in Table 2.9.

The PCR reaction master mix was set up for each reaction as shown below:

10µl of 2X Sensifast probe no-ROX mix

0.8µl of Forward primer at 10µM

0.8µl of Reverse primer at 10µM

0.2µl of Probe at 10µM

4.2µl of DEPC-treated H_2O

Table 2.9: qPCR primers of Rin3 and probe library number and sequence.

Primer	Primer sequence	Annealing temperature (ºC)	GC content (%)	Probe number	Probe sequence
Forward	5'-GCCGGTCCTATTCCAGATG-3'	59.5	58	13	AGGCAGAG
Reverse	5'-AAGAACTGAGCCTTCCAGGTA-3'	59.5	48		

4µl of template was added to each well of a 96 well microplate, followed by 16µl of the master mix described above. The plate was then read in the Chromo 4 Real Time PTC-200 PCR thermocycler (MJ Research) after a brief centrifugation.

The thermal cycling protocol consisted of an initial incubation for 10 minutes at 95°C, followed by 35 cycles of 15 seconds at 95°C, 30 seconds at 61.9°C, and 15 seconds at 72°C. Each sample was run in duplicate, except for the tissues which were run in triplicates.

Successive ten-fold dilutions of a *Rin3* standard were run in parallel to samples. The standard was made from a qPCR product with strong signal, purified using the QIAquick PCR Purification Kit. The product was then loaded on an agarose gel to validate its specificity and purity (data not shown). The concentrations and quality were measured using the Nanodrop ND-8000 (Thermoscientific).

The number of molecules per reaction was assessed from the standard dilutions using these two formulas:

$$\text{Copy Number} = \frac{\text{Amplicon size (bp) x (330 Da x 2 Nucleotides/bp)}}{6.022 \times 10^{23}}$$

$$\text{Number of Molecules/µl} = \frac{\text{Concentration of the product (g/µl)}}{\text{Copy Number}}$$

The Opticon Monitor software v3.1 (Genetic Research Instrumentation Ltd, UK) was used to translate each curve of the standard into a linear plot of the logarithmic amount of DNA against the cycle number ($C_{(t)}$ cycle).

The intensity of fluorescence from each sample, within range of the ones from the standard, could then be measured and translated into a number of molecules. A negative control was also added to each experiment performed to avoid amplification from contaminants (Figure 2.7).

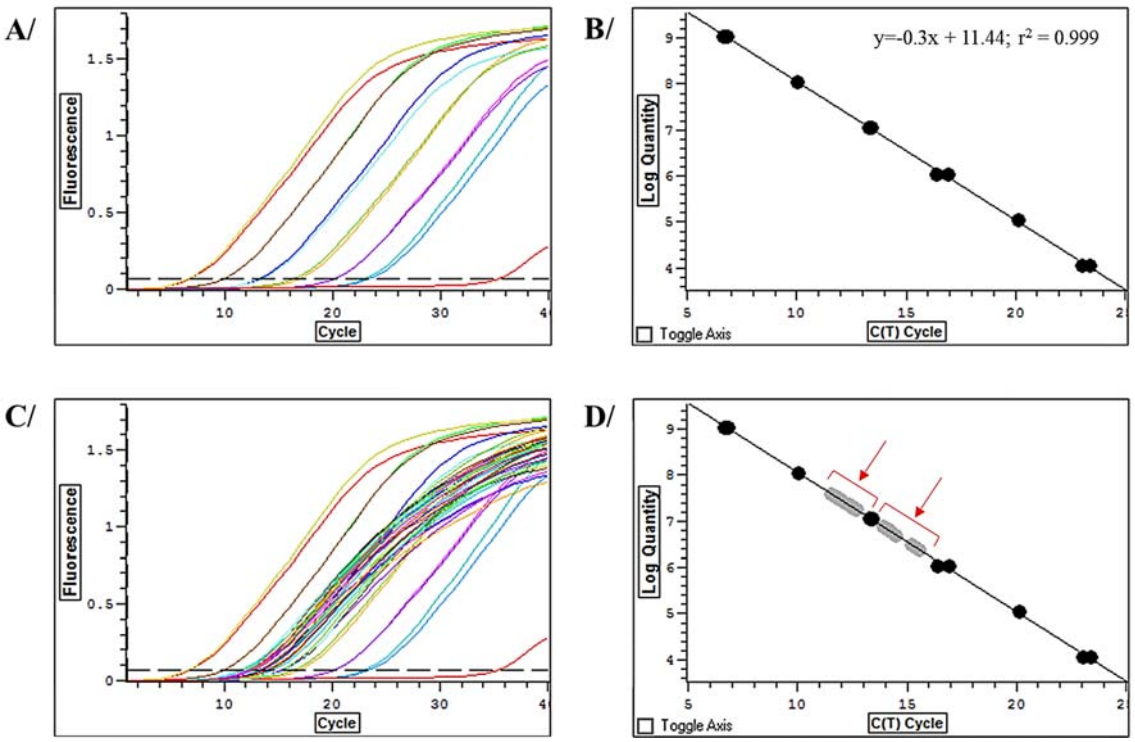

Figure 2.7: Screenshots of the Opticon Monitor 3.1 quantification curves.

A/ Amplification curves from the standard successive dilutions, where fluorescence is plotted against the $C_{(t)}$, or number of cycles. The negative control has the highest $C_{(t)}$ value. B/ Linear plot of standard where the logarithmic number of molecules is against the $C_{(t)}$ cycle. This is adjusted by manual threshold adjustment until reaching an equation offering an r^2 value as close as possible to 1. C/Amplification graph of the standard and samples. D/ Linear plot with addition of the samples (red arrows) values.

The copy number values were normalised against the housekeeping gene Eukaryotic 18S ribosomal RNA (rRNA) measured alongside the *Rin3* gene in ten-fold dilutions.

The 18S endogenous control master mix was set up as shown below, for each reaction:

10µl of 2X Sensifast probe no-ROX mix

1.5µl of TaqMan® Gene Expression Assay Mix for 18S ribosomal RNA

4.5µl of DEPC-treated H_2O

4µl of template was aliquoted in the microplate per sample tested before adding the master mix described above.

The thermal cycling protocol consisted of an initial incubation for 10 minutes at 95°C, followed by 40 cycles of 15 seconds at 95°C, then 10 seconds at 60°C and 15 seconds at 72°C.

The estimation of number of molecules for each sample was determined using the formula described in page 105, as for the *Rin3* reaction. Each test was amplified in duplicate except for the mouse tissues which were done in triplicate.

The specificity of the housekeeping gene and *RIN3* amplifications were confirmed by running the qPCR products on an agarose gel (data not shown).

2.5 PROTEIN RELATED INVESTIGATION

Protein expression of RIN3 was measured during osteoclast differentiation cultured from BMDMs. The same experiment was performed as a time course following the RANKL stimulation where cells were lysed on a daily basis from the first day of RANKL stimulation up to four days after.

2.5.1 Protein isolation

The protein extraction was performed on cell lysates from cultured cells washed in cold PBS and scraped in cold RIPA lysis buffer (Appendix 2.4) supplemented with 20mM sodium fluoride, 1mM of EDTA, 0.4% (v/v) phosphatase and 2% (v/v) protease inhibitor cocktails (Sigma). Flushed out bone marrows were centrifuged at 1200rpm for 3 minutes, the pellets were resuspended in cold PBS, centrifuged again and finally resuspended in RIPA buffer. The samples were left on ice for 15 minutes before being centrifuged for 15 minutes at 13000 rpm (4°C). The supernatants were kept at -20°C until further use.

2.5.2 Protein quantification

The protein concentration was then quantified from the cell lysates against a bovine serum albumin standard pre-diluted set (Thermo Fisher Scientific), using the copper (II) sulphate-bicinchoninic acid (Sigma) method. Once incubated at 37°C for 15 minutes, the plate was read at 562nm using the BioTek™ SynergyHT plate reader and the values were obtained with the Gen5™ software (Appendix 2.5). 14µg of protein lysate was loaded per sample.

2.5.3 Gel electrophoresis

Western blots were performed in 12% Criterion™ XT Bis-Tris pre-cast gels (Bio-Rad), held in a vertical tank filled with XT MOPS (Bio-Rad) electrophoresis buffer diluted twenty times in H_2O (Appendix 2.5).

Protein lysates were denaturated for 3 minutes at 100°C in loading buffer (Appendix 2.5). The samples were then loaded along with MagicMark XP western protein standard (Invitrogen) and Kaleidoscope pre-stained standard (Bio-Rad) ladders, at 200V for 45 minutes.

2.5.4 Electrophoretic transfer

Proteins were then transferred on a methanol-activated polyvinylidene difluoride (PVDF) Hybond-P membrane (GE Healthcare Life Sciences), using a semi-dry technique. A blotting sandwich of pre-soaked blot paper, membrane, polyacrylamide gel and pre-soaked blot paper was carefully prepared on the transfer tank to allowed the negatively charges protein to transfer from the gel to the membrane. The sandwich was topped with 1X transfer buffer (Appendix 2.5), and the tank was programmed at 90mA for 2 hours and 30 minutes.

2.5.5 Immunostaining and antibody detection

Once the transfer finished, the membrane was saturated in 5% non-fat dry milk (Marvel) diluted in 0.1% TBST (Tris-Buffered Saline and Tween 20; Appendix 2.5) for an hour at room temperature before being washed in 0.1% TBST every 5 minutes for 30 minutes, at room temperature.

The membrane was then incubated overnight at 4ºC under slow agitation in the primary antibody (anti-RIN3 from Proteintech or anti-β-actin from Sigma) diluted at 1:1000 in 3% BSA, in 0.1% TBST. After being washed with 0.1% TBST every 10 minutes for one hour, the membrane was incubated with the second antibody (Peroxidase-AffiniPure donkey anti-rabbit IgG [H+L], Jackson Immunoresearch) at a dilution of 1:5000 in 5% milk made in 0.1% TBST at room temperature for 1 hour.

The membranes were washed again with 0.1% TBST every 10 minutes for one hour before being visualised using the Clarity western ECL substrate (Bio-Rad) on a Syngene GeneGnome bio imaging system. The intensities of the bands were quantified using the GeneSnap software from Syngene.

Stripping was necessary for the membranes that were previously incubated with a RIN3 antibody, before being probed with β-actin. To do this, the membranes were incubated in stripping buffer (Appendix 2.5) supplemented with DTT at 50°C until the ECL substrate did not detect any band. The stripped membranes were then blocked in milk again, probed and visualised as described above.

2.6 IMMUNOFLUORESCENCE

The localisation of RIN3 was also investigated using immunostaining on RANKL-induced osteoclasts, from mouse bone marrow.

The cells were obtained as described in Section 2.3.1. After 2 days of incubation in M-CSF, the macrophages were then plated in a 96 well plate at $2x10^4$ cells per well. After four days of culture in RANKL, the cells were fixed for 10 minutes in 4% paraformaldehyde in PBS, at room temperature. The cells were carefully washed in PBS three times, to remove all traces of formaldehyde. Cell permeabilisation was performed using cold 0.5% (v/v) Triton X-100 in 10% milk in PBS, for 10 minutes at room temperature. After three washes in PBS, the cells were incubated at room temperature with a primary anti-RIN3 antibody (Proteintech) diluted 20 times in 10% FCS in PBS for 1 hour, at room temperature. Negative controls were incubated in 10% FCS in PBS. Cells were washed three times in PBS again, and were incubated one hour at room temperature in Alexa Fluor® 488 goat anti-rabbit IgG (H+L) secondary antibody (Life technologies), diluted 500 times in 10% FCS in PBS. The cells were washed 3 times in PBS and a 10 minutes Hoechst staining (DAPI) was performed. The cells were finally washed three times in PBS and an anti-fading agent (DABCO, Sigma) was added before imaging. Pictures were taken using Zeiss Axiovert light microscope (Carl Zeiss Ltd., UK) at x20 magnification.

2.7 IMMUNOHISTOCHEMISTRY

Immunohistochemistry was performed to investigate the cellular location of RIN3 in human bone samples. The tissues selected for this experiment included frozen sections of osteosarcoma and formalin-fixed paraffin-embedded (FFPE) sections of osteoclastoma, patients affected with PDB, GCT and healthy controls. The negative controls used included osteosarcoma and lung samples, while positive controls were performed on lung tissue where RIN3 is highly expressed (http://www.proteinatlas.org).

Samples prepared in FFPE were fixed in formalin overnight. A decalcification treatment with Decalcifier II (Leica) was performed. The tissue was then processed through a series of graded alcohol, xylene and wax using the Excelsior AS tissue processor (Thermos). The tissue was then embedded in molten wax using the Leica embedding centre and wax was then allowed to set. The sections were cut at 3-4µm using the Leica microtome and were placed in a flotation bath to flatten them before being transferred to glass slides. The glass slides were then dried overnight at 37°C, or at 60°C for smaller sections, which detach easily.

The frozen samples were embedded in Optimal Cutting Temperature compound (CellPath, UK) medium on dry ice, onto cryostat chucks and was left to harden. Using a Leica cryostat (CM1850), the blocks were sectioned at a thickness of 3-4µm. The sections were then transferred onto glass slides, and were fixed with acetone for 5 minutes.

The envision immuno protocol was performed, using Heat Induced Epitope Retrieval (HIER) technique on FFPE sections only. For this, the sections were dewaxed in 3 successive batches of xylene for 5 minutes each, before being hydrated through batches of graded alcohol (2x100%, then 80%, then 50%) for two minutes each. After being washed briefly with tap water, the antigen retrieval was performed on slides placed in a microwavable pressure cooker, containing a solution of warm 0.1M sodium citrate and 0.1M citric acid at pH6. The cooker was heated up for 5 min in a microwave. Once cooled, the slides were washed in PBS-Tween (0.1%) for 5 minutes under slow agitation. Endogenous peroxidase activity was inactivated with a solution of 3% hydrogen peroxide in water for 10 minutes. The slides were then washed in PBS-Tween (0.1%) for 5 minutes before being loaded in a carefully sealed Sequenza rack. Non-specific binding was prevented using Dako total protein blocking solution (Agilent) for 10 minutes. 120µl of the primary antibody diluted 100 times (Or Dako antibody diluent for the negative controls) were prepared in Dako antibody diluent (Agilent), and incubated on the slides for 1 hour at room temperature or overnight at 4ºC. The antibody used for detecting human RIN3 was produced in rabbit (Sigma). After 2 washes in PBS-Tween (0.1%), the sections were incubated in secondary antibody Dako Envision labelled polymer (Agilent) for 30 minutes. After 2 washes in PBS-Tween (0.1%), 120µl of H_2O_2-containing DAB substrate diluted fifty times in DAB buffer were added for 5-20 minutes (usually 10 minutes) until colour develops.

After one wash in PBS-Tween (0.1%) and a two minutes wash in tap water, the sections were counterstained with Haematoxylin for 10 minutes. They were then washed successively in water, Scotts tap water solution and water again for 10 seconds each. Sections were dehydrated through graded alcohol (50%, then 80% for 30 seconds each, followed by 2 batches at 100% for 2 minutes each) before being incubated in 3 successive batches of xylene for 5 minutes each.

Sections were mounted with a cover slide covered in DPX mounting medium (Sigma) and analysed on an Olympus BX51 microscope (Olympus, UK).

2.8 MICE EXPERIMENTATION

2.8.1 Mice

Rin3$^{-/-}$ mice were obtained from the Jackson Laboratory which used embryonic stem cells provided by the International Mouse Phenotyping Consortium. A deletion was performed by inserting a Velocigene cassette (ZEN-Ub1) follow by a Cre-mediated excision of the neomycin cassette. 29,890bp were removed from the *Rin3* gene, corresponding to the amino acids 2 to 101 (end of exon 1, all exon 2 most of exon 3) of the protein where the SH2 domain is localised (Figure 2.8). The knock out status of the mice was assessed by qPCR, using the primer set described in Section 2.4.4. This set targets the deleted area of *Rin3*, and a complete knock out was confirmed (data not shown).

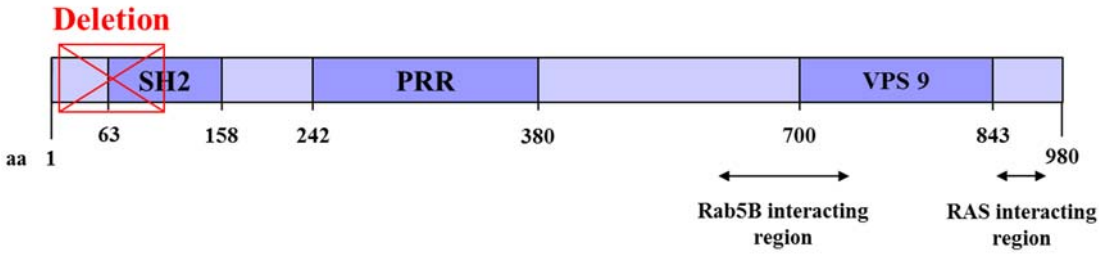

Figure 2.8: Area deleted of Rin3 by the Internal Mouse Phenotyping Consortium.
The amino acids (aa) 2 to 101 of *Rin3* were deleted.

All experiments were performed on *Rin3*$^{-/-}$ and wild type (WT) mice generated from mating heterozygous breeding pairs. To generate those, a *Rin3*$^{-/-}$ female C57BL/6NJ was crossed with a WT 129/OlaHsd male mouse to create a mixed background C57BL/6NJ and 129/OlaHsd line. All mice were housed in a designated animal facility in pathogen-free rooms maintained at constant temperature, with 12 hours light/12 hours dark cycles. They had free access to water and pelleted standard commercial diet (SDS, Special Diets Service). Genetic status were assessed by genotyping as described in Section 2.8.2.

Hind legs and spines were isolated for micro computed tomography (microCT) analysis (Section 2.8.3). Hind legs were selected for histomorphometry, and osteoclast cell cultures (Section 2.8.4). All were collected at 8 weeks old. Calvarial osteoblast cultures were performed on 2 days old pups, that were generated from *Rin3*$^{-/-}$ or WT parents (Section 2.3.2).

Intraperitoneal injections of 200µl of calcein at 2g/L were given 6 and 2 days prior to collection of samples for histomorphometry analyses.

The sample size for the *in vivo* experiment was chosen to provide at least 80% power to detect a 1.3 standard deviation difference in BV/TV between *Rin3*$^{-/-}$ and WT mice. Power calculations were performed using G*Power software, version 3.1.9.2 (Heinrich Heine University Düsseldorf, Germany).

2.8.2 Genotyping methods

The knock out status was assessed by extracting genomic DNA from ear notches. The DNA was extracted using the Invisorb® Spin Tissue Mini Kit following the manufacturer's instructions. The product was either stored at -20ºC until further use, or analysed directly by PCR amplification.

For this, two sets of primers were designed and used for each PCR reaction (Table 2.10). The first set specifically targeted WT genotypes by amplifying a region of 275bp, located in the intron 2 of *Rin3*. As this amplicon is completely absent in mutated mice, this product will not be amplified in *Rin3*$^{-/-}$ samples.

The second set of primers however, revealed *Rin3*$^{-/-}$ mice genotypes. The forward primer targets a sequence located in the Velocigene cassette, present in case of successful knock out only. The reverse primer amplifies a region located at the 5' extremity of the third intron of *Rin3*. The result of this reaction showed a product of 513bp. *Rin3*$^{-/-}$ samples showed a band at 513bp while the *Rin3*$^{+/-}$ ones showed both amplicons (Table 2.9).

All PCR reactions were performed as below, for a total volume of 25µl:

Water: 15.8µl

5X Kapa 2G HS buffer: 5µl (final 1X – with 0.3mM $MgCl_2$)

10mM dNTP KAPA: 0.5µl (final 0.2mM)

10µM Forward *Rin3* primer: 0.4µl (final 0.33µM)

10µM Reverse *Rin3* primer: 0.4µl (final 0.33µM)

10µM Forward WT primer: 0.4µl (final 0.33µM)

10µM Reverse WT primer: 0.4µl (final 0.33µM)

5U/µl Kapa 2G HS taq: 0.1µl (final 0.02U/µl)

DNA: 2µl

Amplification of both fragments was performed in a MJ Research thermocycler. The thermal cycling protocol consisted of an initial incubation for 2 minutes at 94ºC, followed by 35 cycles of 20 seconds at 94ºC, 15 seconds at 61.4ºC and 7 seconds at 72ºC. A final extension step at 72ºC for 2 minutes in the last cycle (Figure 2.9).

Table 2.10: Sets of primers used for the determination of the mice genotypes.

Primer set	Forward	Location	Reverse	Location	Amplicon size
Wild Type	5'-CTGTGCCAACAACAGCATCT-3'	Intron 2	5'-CTCCTCTTGTCCCAGCACTC-3'	Intron 2	275bp
Rin3$^{-/-}$	5'-CGGTCGCTACCATTACCAGT-3'	Velocigene cassette	5'-CTGTGGGGAGCATTCTGAGT-3'	Intron 3	513bp

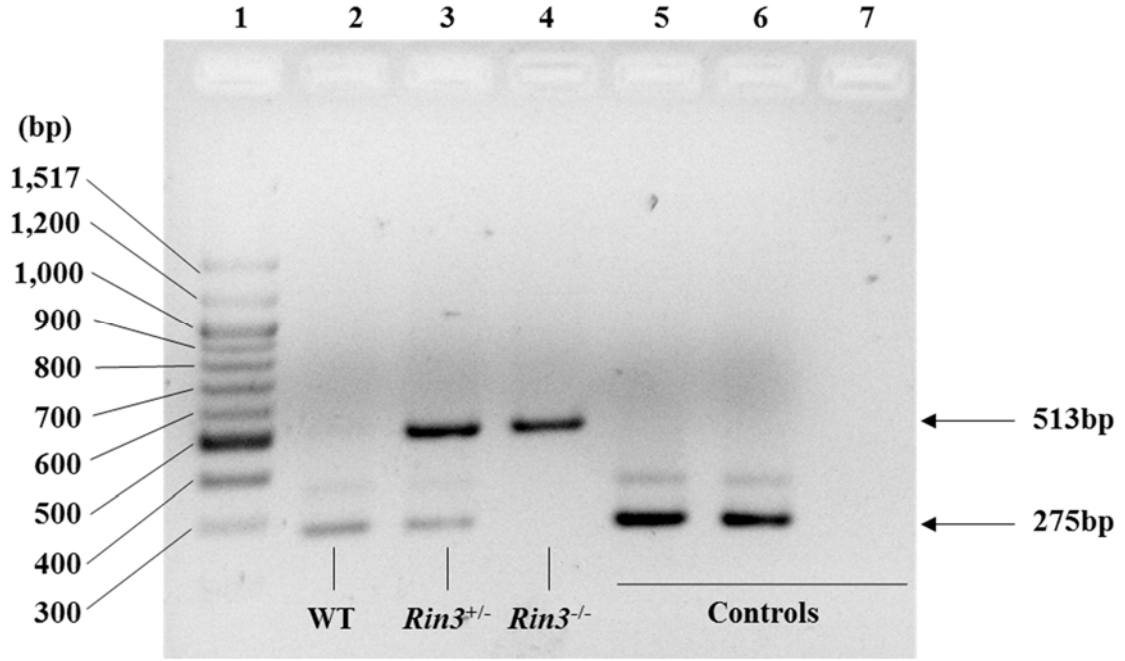

Figure 2.9: DNA gel electrophoresis to determine Rin3 mice genotype.

Lane 1: 100bp DNA ladder; Lane 2: Wild Type; Lane 3: Heterozygote for the *Rin3* mutation; Lane 4: Homozygote for the *Rin3* mutation; Lane 5: Wild Type control; Lane 6: Wild Type control; Lane 7: Negative control.

A non-specific band was observed just below 400bp. This was also present in the genotyping guidelines provided by Jackson lab, and seems to be amplified for the WT genotype, as it is also seen in heterozygote genotypes but not in the homozygote one. This band was present in all gels including positive controls.

2.8.3 Micro computed tomography

Female mice aged 8 weeks were sacrificed by cervical dislocation and the hind legs and spine were isolated. They were initially fixed in 4% (v/v) paraformaldehyde in PBS overnight, before being carefully washed twice in PBS and stored in 70% (v/v) ethanol at 4^{o}C until further use.

Both legs were scanned as well as the L6 vertebra of the spine was also analysed. The microCT sample preparation consisted in carefully removing the muscle tissue around the bones with a scalpel. The muscle was cut around the spine using small scissors. Each bone was tightly wrapped in stretched parafilm in order to assure a straight upright position during the scan, to avoid dehydration and allow it to fit properly in the respective holder (Figure 2.10). The cortical analyses were performed on the femoral diaphysis while trabecular analyses were done on both femoral and tibial metaphysis using a SkyScan 1172 scanner (Bruker, Belgium).

The scanner settings chosen included an X-ray radiation source of 60kV and 167μA, a 0.5mm aluminium filter, and a pixel size of 5μm, an average of 2 images per level and a rotation step of 0.6 degrees of the samples.

Figure 2.10: Holders used for the microCT analyses.
The left tube was used for spines, while the right tube, longer and narrower was used for legs. The tweezers are used for size comparison.

Once the scans were finished, the cross-section images were reconstructed using the Skyscan N-recon software (Bruker, Belgium). The reconstruction allows a better stack of all the images, through reduction of noise, rectification of low energy X-ray not absorbed by the aluminium filter on the outside of the sample, and amelioration of pixel artefacts. The different settings are summarised in Table 2.11.

Table 2.11: NRecon software parameters for reconstruction (Campbell & Sophocleous, 2014).

Parameter	Description	Setting
Smoothing	Smoothes images and removes noise	Width; 1 pixel
Beam Hardening factor correction	Corrects for the absorption of lower energy x-ray on the outside of specimen	0.09
Ring correction level	Corrects for the non-linear behaviour of pixels causing ring artefacts	3

The stack of images was then straightened using Dataviewer (Bruker, Belgium).

The transaxial view of the 3D reconstructed model was then analysed to measure trabecular and cortical bone, using the CTAn software (Bruker, Belgium). For the analysis of the limbs, the end of the growth plate was used as a reference point.

The trabecular bone was first measured on the proximal femoral metaphysis by selecting a set of 450 slices, located 150 slices distally from the end of the growth plate. Each slice has a thickness of 5µm. It was then analysed at the distal tibial metaphysis for 200 slices, located 100 slices distally from the end of the growth plate. The cortical bone was assessed using 200 slices proximally from the midpoint of the femur, evaluated at 1000 slices. Finally, the trabecular bone was measure on the lumbar vertebrae 6 and the frame showing the transverse process connecting with the vertebral axe was used as a reference. The analysis was then performed 50 slices from this baseline, for 200 slices distally from the secondary spongiosa. All regions of interest are summarised in Figure 2.11.

The CTAn software (Bruker, Belgium) uses a free hand tracing of the region of interest (ROI). The trabecular bone was drawn excluding the endocortical surface of the bone, while the cortical analysis included cortex surface and trabecular bone. The total volume of interest (VOI) is then deducted by the software after auto-interpolation of the ROI traced levels. The VOI goes through a process of amelioration, such as reduction of background noise or closing pores (Table 2.12).

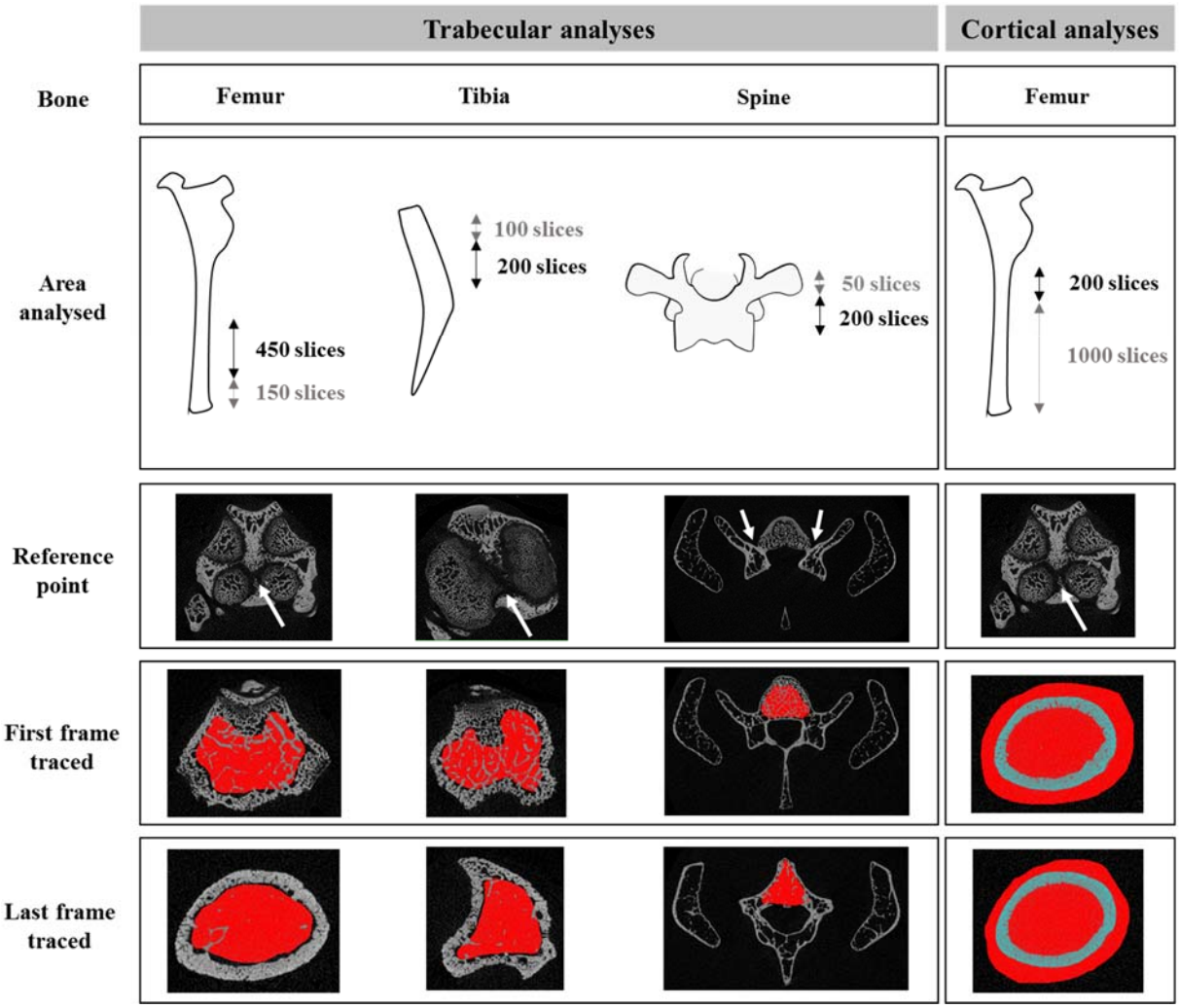

Figure 2.11: Summary of the area traced from bone for microCT analysis.

Area analysed: All bones illustrated here are presented in an upright position. Each picture analysed corresponds to a transversal slice of the bone, taken every 5µm by the microCT scanner. The number of slices written in light grey correspond to the distance between the reference point (growth pate) until the area analysed, written in black.

Reference point: This row shows examples of reference points used with the CtAn software (Bruker, Belgium). For the long bones, this corresponds to the picture for which at least two growth plates touched each other, from the knee. For the spine, this corresponds to the first picture (from the secondary spongiosa) where the transverse process connects with the vertebral axe on both sides. The growth plates connection points are showed by white arrows.

First frame traced: This row shows the region traced (in red) on the first transversal picture, from the reference point.

Last frame traced: This row shows the region traced (in red) on the last transversal picture.

Once performed on all samples, the VOI goes through a specific trabecular or cortical task list, in order to measure the following parameters: trabecular bone volume corrected by total volume (BV/TV, %), trabecular thickness (μm), trabecular separation (μm), trabecular number (1/mm), cortical bone volume (mm^3), cortical thickness (μm), medullary cavity diameter (μm), and cortical diameter (μm).

3D modelling of the scans was also performed using CTVol (Bruker, Belgium) on each region investigated to visually observe changes in the bones and confirm the results from the CTAn analysis.

Table 2.12: CTAn software parameters outcome (Campbell & Sophocleous, 2014).

Parameter	Description	Setting
Smoothing	Smoothes images and removes noise	Median filter; 2D space, radius 1
Threshold	Segments the foreground from background to binary images	Global; low level 100, high level 255
Despeckle	Removes speckles from binary images	Image; remove white speckles < 150 voxels
3D-Model	Creates a 3D surface from binary images	Adaptive rendering; file saved as .p3g
3D-Analysis	Calculates 3D parameters of binary images	Requested for basic values, trabecular thickness, number and separation

2.8.4 Bone histomorphometric analysis

Sample embedding

Once all samples were scanned, the femurs were embedded in plastic blocks for further histomorphometry analyses.

As the legs were scanned as whole, the first step was to carefully separate the tibia from the femur by cutting all ligaments around the knee. The samples were then dissected using an electric saw to remove the area not analysed and to keep the size of the sample as small as possible (Figure 2.12).

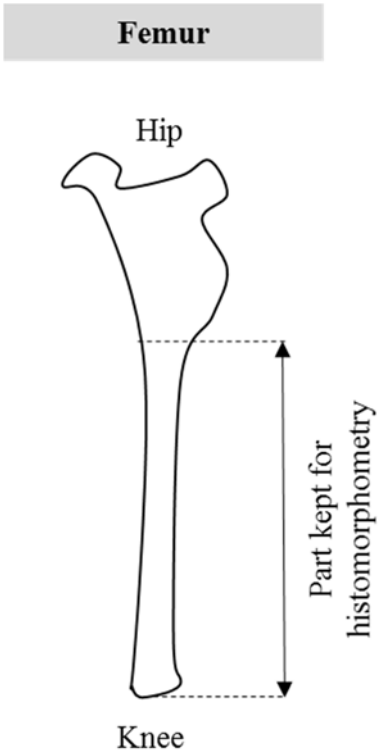

Figure 2.12: Site of dissection of femur for plastic embedding and histomorphometry. The knee, metaphysis and most of the diaphysis were kept for histomorphometry, as shown within the double arrow.

Once isolated, the samples were placed in disposable baskets divided in four parts, which were then placed in a Leica automatic tissue processor in a solution of 70% ethanol.

The femurs were taken through a program lasting 23h30, through which they were dehydrated and defatted in xylene as shown in Table 2.13.

Table 2.13: Embedding process program used with the Leica tissue processor.

Step	Reagent	Duration	Temperature
Dehydration			
1	70% Ethanol	30 min	Room temperature
2	80% Ethanol	2h	Room temperature
3	96% Ethanol	2h	Room temperature
4	100% Ethanol	3h	Room temperature
5	100% Ethanol	3h	Room temperature
Defatting			
6	Xylene I	1h	Room temperature
7	Xylene II	12h	Room temperature

The samples were then transferred into a freshly made 2-methoxyethyl acetate (MEA) solution prepared as shown below (Table 2.14), and were kept into a vacuum desiccator for 7 days at 4^{o}C to be infiltrated. The samples were then ready for embedding into blocks.

Table 2.14: Composition of the methoxyethyl acetate infiltration solution.

	Quantities to prepare 100ml
Methyl Methocrylate (MMA)	89ml
Di-butyl-phtalate	10ml
Perkadox 16	1g
Novoscave	0.01g

For this, the samples were delicately placed in moulds in an orientation favouring coronal sectioning. They were immersed in one week old MEA and tightly closed by metal lids screwed on top of the sample. The samples were then incubated in a waterbath pre-warmed at 30°C for 48 to 72 hours until polymerisation. The blocks were then completed by adding a resin made of 2 parts of dibenzoylperoxide for 1 part of N,N-dimethyl-p-toluidine in an embedding ring placed tightly above the samples. Following an overnight incubation at room temperature, the blocks were removed from the moulds and stored at room temperature.

The blocks were then loaded on a Leica microtome and were trimmed automatically at a speed not exceeding 5mm/sec until reaching the sample. The sections were then cut at a thickness of 5µm, using a diamond knife. The block was moisturised with 90% ethanol during this process. The sections were carefully placed and straightened on a saline coated microscope slide and covered in Kisol foil.

The excess ethanol was removed with a filter paper. The slides were then kept under mechanical pressure in a 37°C oven, and left to dry for 3 days.

Once dried, the Kisol foil was carefully removed and the slides were stored in hermetic boxes at room temperature until further use.

Tartrate-resistant-acid-phosphatase staining

The sections underwent TRAcP staining, a coloration allowing the identification of multinucleated osteoclasts by turning them red. The MEA resin was removed from the sections using an auto-stainer, which incubated the slides in a succession of MEA, xylene, and series of ethanol solutions with decreasing concentration as shown in Table 2.15.

Table 2.15: MEA resin removal steps in preparation of TRAcP staining.

Solution	Incubation time
Fresh MEA	20 minutes
Fresh MEA	20 minutes
Fresh MEA	20 minutes
Fresh Xylene	10 minutes
Fresh Xylene	10 minutes
100% Ethanol	2 minutes
100% Ethanol	2 minutes
80% Ethanol	2 minutes
70% Ethanol	2 minutes
50% Ethanol	2 minutes
Distilled water	2 minutes
Distilled water	2 minutes

The slides were then placed in a TRAcP staining solution (Table 2.16) for 2 hours at 37^{o}C, until the red staining developed. The samples were then washed four times in distilled water.

Table 2.16: Tartrate-resistant-acid-phosphatase staining solution composition for histomorphometry.

Reagent	Amounts to prepare 100ml
Napthol AS-TR phosphate	140mg
N-N Dimethyl formamide	500µl
0.2M Sodium acetate anhydrous buffer, pH5.2 (pre-warmed at 37^{o}C)	100ml
Sodium tartrate dihydrate	230mg
Fast red salt TR	140mg

Every physical transfer of the slides was done with high care, as without the resin, the sample can move easily from the slide and float, or detach completely from the slide. Once drained, the slides were counterstained in Aniline blue, prepared at a final concentration of 0.332g/L with phosphotungstic acid at 6g/L in water. The samples were incubated at room temperature for 5 minutes, before being washed in water four times.

The slides were quickly mounted using apathy syrup (Appendix 2.6) and were left to air dry for 1 hour before being imaged. Each sample was imaged within the same day of staining, to avoid Aniline blue fading.

The microscope used for imaging at magnification x10 was a confocal Zeiss LSM800 (Carl Zeiss Ltd., UK). The trabecular analysis was performed using TrapHisto (Van't Hof et al, 2017), allowing semi-automatic recognition and measuring of bone (blue) and osteoclast (red) parameters using the colour discrimination (Figure 2.13). Information such as osteoclast resorption surface, number of osteoclasts, bone surface and bone volume could be determined (Table 2.17).

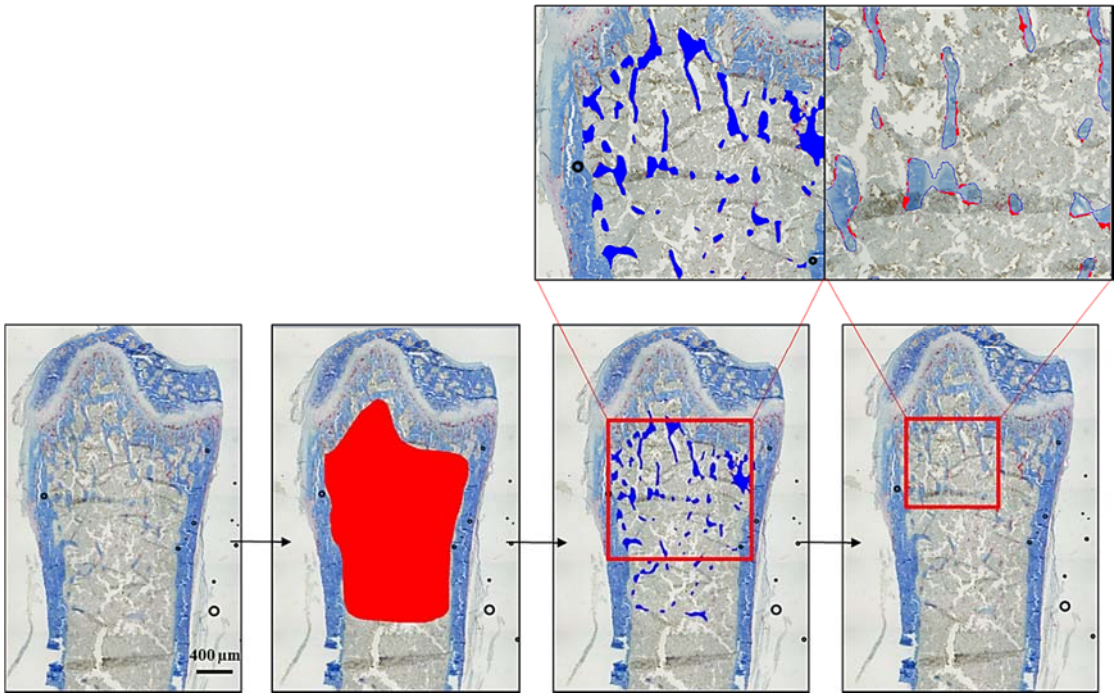

Figure 2.13: Process of the TrapHisto software to identify and measure bone and osteoclast parameters.

The red area is traced to define the region to analyse, and the software automatically identifies bone (blue) from osteoclasts (in red) due to the TRAcP and Aniline blue counterstaining. Manual edition was then used to refine the tracing.

Table 2.17: TrapHisto software outcome data.

Parameter	Abbreviation	Unit
Bone area	B.Ar	μm^2
Bone perimeter	B.Pm	µm
Osteoclast surface per bone surface	Oc.S/BS	%
Osteoclast number per bone surface	Oc.N/BS	mm^{-1}

Calcein staining

Calcein blue is a calcium chelating fluorochrome, used to evaluate bone growth.

Calcein labelled bone sections (Section 2.8.1) were incubated in a calcein blue solution at 0.1% in water (pH 8) solution for 3 minutes. They were then washed three times in distilled water and were transferred to an auto-stainer Leica ST5020. The specimen were then dehydrated through a series of decreasing concentrated ethanol solutions.

They were incubated in xylene for three minutes and mounted using a Leica CV5030 cover-slipper in xylene, using Eukitt® Quick-hardening mounting medium.

The slides were left to air dry in a fume hood with low lightening for an hour before being imaged. The slides from this point on were stored in a hermetic box.

Imaging of the sections was performed using a confocal Zeiss LSM800 (Carl Zeiss Ltd., UK), at magnification x20. The mineralised bone was analysed by using a DAPI fluorescent filter and appeared in blue, while the calcein labelling appeared green under FITC fluorescent filter. The distance between the two calcein labels was reflective of bone growth within the four days of interval between injections.

The trabecular analysis was performed using the CalceinHisto software (Van't Hof et al, 2017). As for the TRAcP analysis, the differences in colours were recognised automatically, and were used to measure bone and label parameters (Figure 2.14). Manual adjustment was then performed to refine the label tracing. Information such as label width, bone volume/total volume, minimum acquisition rate, mineralised surface, bone formation rate and bone surface were then determined (Table 2.18).

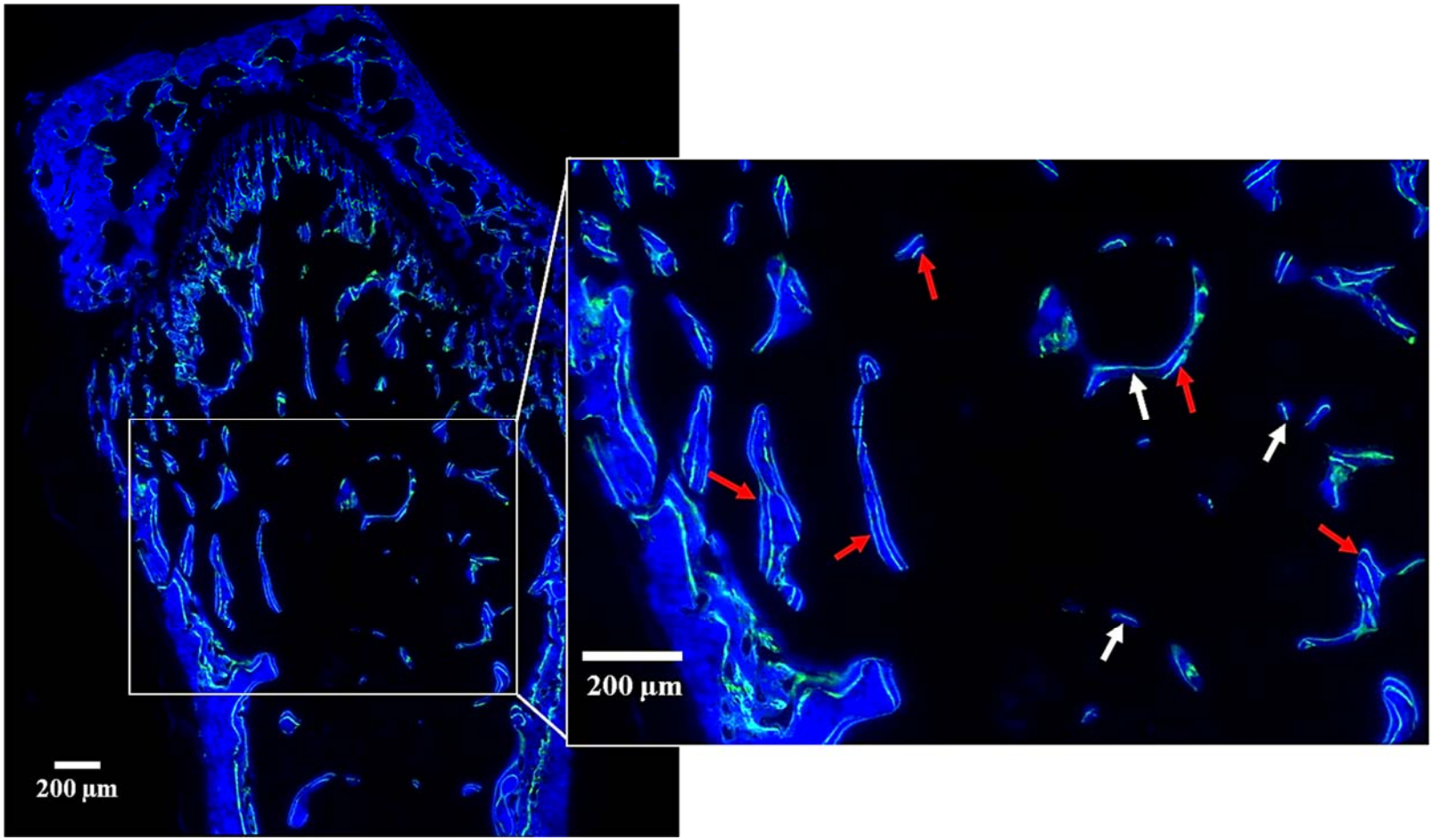

Figure 2.14: Images of the calcein labelling analysed by the CalceinHisto software.
The mineralized bone appears in blue, while the calcein labelling appears in green. The space between the 2 labels corresponds to 4 days of bone formation. Double labelling is pointed by red arrows while single labelling is pointed by white arrows.

Table 2.18: CalceinHisto software outcome data.

Parameters	Abbreviation	Expression	Significance
Single labelled perimeter	sLS	µm	Measure of the length of single labels through the ROI
Double labelled surface perimeter	dLS	µm	Measure of the length of double labels through the ROI
Labelled width	L.Wi	µm	Interlabel distance through the ROI
Bone volume per total volume	BV/TV	%	Bone volume through the ROI
Mineral acquisition rate	MAR	µm/day	Rate of mineral formation per day through the ROI
Mineralising surface per bone surface	MS/BS	%	Translates the percentage of labelled surface relative to the total bone surface through the ROI
Bone formation rate per bone surface	BFR/BS	$\mu m^3/\mu m^2$/day	Translates how much mineralised bone is formed per day, relative the bone surface of the ROI
Bone formation rate per bone volume	BFR/BV	%/day	Translates how much mineralised bone is formed per day, relative to the bone volume of the ROI

ROI = Region of interest.

2.8.5 Data analysis

Mean values were calculated using SPSS Version 22 (SPSS Ltd, UK). Statistical significances within groups were analysed using independent-samples *t* test, on SPSS. P-values were considered significant when lower than 0.05. A generalized linear models (GLM) analysis was performed on mineralised nodule assay, for time, genotype and staining using Minitab Version 12 (Minitab Inc., UK).

CHAPTER THREE
TARGETED SEQUENCING OF THE PAGET'S DISEASE ASSOCIATED 14Q32 LOCUS IDENTIFIES SEVERAL MISSENSE CODING VARIANTS IN *RIN3* THAT PREDISPOSE TO PAGET'S DISEASE OF BONE

3 TARGETED SEQUENCING OF THE PAGET'S DISEASE ASSOCIATED 14Q32 LOCUS

3.1 SUMMARY

The candidacy of the 14q32 locus in PDB was initiated by a GWAS performed in 2011 on a Pagetic cohort, which revealed the rs10498635 variant located in the *RIN3* gene (Albagha et al, 2011). The rs754388 variant, also located in *RIN3*, was associated with an increased lower limb bone mineral density DXA scans in children (Kemp et al, 2014). Here, *RIN3* was sequenced in order to identify new PDB associated variants.

An imputation was performed based on the one described in the 2011 GWAS, which used Hapmap SNP database for reference. The same cohort of 741 PDB patients and 2699 controls was used, but the 1000 Genomes database was chosen as a reference to increase the sample size. It confirmed the independent signal of rs10498635. Frequencies of the 18 *RIN3* variants detected by sequencing 295 affected individuals were compared to public databases, and an association was found for p.R279C (OR = 0.64; $P = 1.4 \times 10^{-9}$). *In silico* analysis of p.R279C showed no predicted functional effect. p.R279C and rs10498635 are in LD and share the same risk haplotype, which was over-represented in cases (81.2%; OR = 1.48; $P = 2.8 \times 10^{-6}$). Many rare variants were also described and an association was found for those once combined (OR = 3.72; $P = 8.9 \times 10^{-10}$). Most were on the same haplotype as p.R279C's risk haplotype.

Functional work is still needed for the p.R279C variant despite the *in silico* prediction. Indeed, previous experience has shown that the *SQSTM1/*p.P392L change was predicted to be benign when in fact is disease causing (Hocking et al, 2004). Nevertheless, these results still confirm an association between *RIN3* with PDB.

3.2 INTRODUCTION

PDB is a skeletal disorder with high bone turnover. Although the origin of the disease is yet to be understood, an inherited component has been described as PDB can be passed onto family members in an autosomal dominant manner (Ralston & Albagha, 2014). A total of 28 mutations in the *SQSTM1* gene are described to be associated with PDB. Most are located in the UBA domain of the protein, and result in a loss of function or truncation of the protein. They are detected in about 20-50% of familial cases, and 5-15% of the sporadic cases, and the most reported mutation is the p.P392L variant (Rea et al, 2013). Although mutations in the *SQSTM1* gene have greatly helped in the diagnosis of PDB and the understanding of its molecular signature, additional loci need to be investigated. To this end, and as described in Section 1.4.1 (14q32.12 locus (*RIN3*)), a GWAS performed in our group identified the *RIN3* gene by using PDB cases which did not carry *SQSTM1* mutations (Albagha et al, 2011). The strong signal came from the rs10498635 intronic variant ($P = 2.55x10^{-11}$; OR = 1.44), which was also surrounded by genetic recombination sites. Such genetic results place *RIN3* as a great candidate gene for the investigation of PDB, however the role of *RIN3* in bone has not been investigated much. Only one study so far has showed that *RIN3* is associated with higher bone density in lower limbs from children and that it is expressed in osteoclast and osteoblast mouse primary cells (Kemp et al, 2014). Additionally, RIN3 was found to have a role in endocytosis (Kajiho et al, 2003), kinase receptor recycling (Janson et al, 2012) and activating small GTPases such as Rab5 and Rab31 through its GEF activity. This chapter aims to further investigate the association between PDB and the *RIN3* gene, by identify new potentially pathogenic variants using next-generation and Sanger sequencings, and *in silico* analyses.

3.3 METHODS

Here, the *RIN3* gene was sequenced to identify new variants which could be involved in PDB and bone metabolism. For this, Sanger sequencing was performed in 101 cases from the ZiPP study and 24 cases from the PRISM study on all 10 exons of *RIN3* as well as the promoter and UTRs (Section 2.1.1). Next generation sequencing was also performed in 95 PRISM cases and 26 familial cases using the Haloplex kit (Agilent technologies), on the *RIN3* gene and 20kb surrounding areas on either side (Section 2.1.2). All patients were selected on a young age of diagnosis basis and/or family history.

The variants discovered from both techniques were categorised in groups of rare (MAF < 1%) or common incidence (MAF > 1%). Frequencies were compared to 379 European subjects from the 1000 Genomes (www.1000genomes.org/) and 4300 European-American subjects from the NHLBI project (http://evs.gs.washington.edu/EVS/) as controls. The combined effect of rare variants was investigated using a Burden test, by Fisher's exact test (Section 2.1.2). An imputation, based on the one performed in the 2011 GWAS (Albagha et al, 2011) which highlighted *RIN3*, was performed using MACH (Section 2.1.4) (Li et al, 2009). The same cohort of 741 PDB patients and 2699 controls from the WTCCC (Wellcome Trust Case Control, 2007) was used. The 1000 Genomes European phased haplotype data (phase I version 3) (www.1000genomes.org/) was used as a reference. An LD and a haplotype analysis were performed on Haploview (Barrett et al, 2005) (Section 2.1.3).

In silico analysis of those variants was performed by using bioinformatic tools (SIFT, PolyPhen-2, Condel, MutationTaster, GERP conservation score and Grantham score). One point was given for each bioinformatic program predicting the effect of the mutation to be "damaging" by SIFT (Kumar et al, 2009), "possibly or probably damaging" by PolyPhen-2 (Adzhubei et al, 2010), "deleterious" by Condel (Gonzalez-Perez & Lopez-Bigas, 2011), "disease causing" by MutationTaster (Schwarz et al, 2014; Schwarz et al, 2010), have a GERP score higher than 2.0 (Cooper et al, 2005), or to have a Grantham score higher than 50 (Grantham, 1974).

3D modelling was also performed to validate such predictions. For this, stability energy calculations of the mean ΔΔG were determined to investigate the destabilising effect of variants in ordered regions of RIN3. Structural changes were established for coding variants located in the PRR of RIN3 by using PONDR scores (Section 2.1.5).

3.4 RESULTS

3.4.1 Imputation of the 14q32 locus

The imputation performed here was used to confirm the effect of the intronic polymorphism rs10498635 previously described (Albagha et al, 2011). European haplotype data from the 1000 Genomes project was used in order to increase power, compared to the imputation performed in the GWAS study in 2011 (Albagha et al, 2011).

Although not predicted to be structurally damaging for RIN3, rs10498635 was detected in this repeated analysis with an association signal of about $1x10^{-5}$ (Figure 3.1, plot A). Conditional analysis for the rs10498635 variant excluded additional signals in the area which indicates that the association was driven by rs10498635, or by variants in LD with rs10498635 (Figure 3.1, plot B).

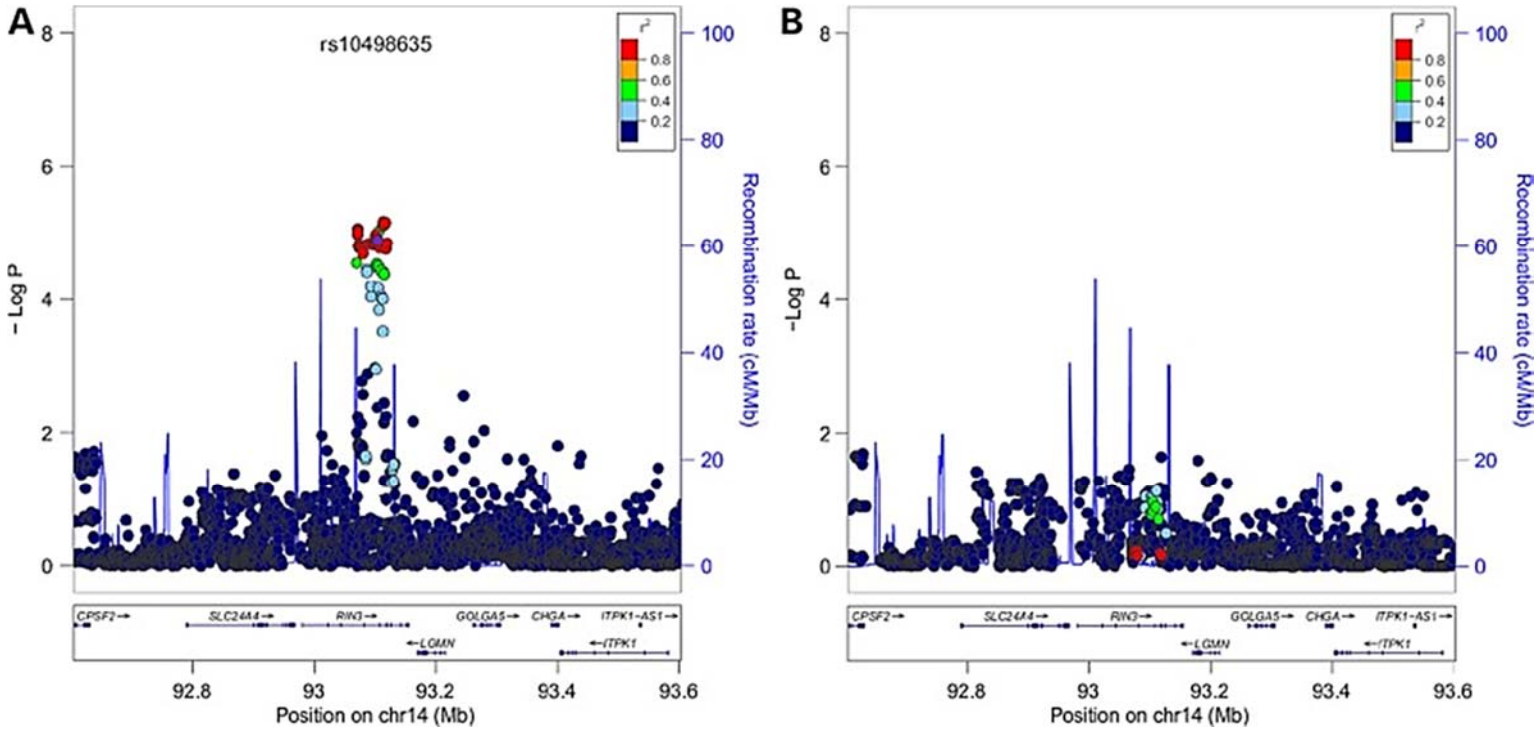

Figure 3.1: Association plots for the 14q32 locus and conditional analysis for rs10498635.

The X axis corresponds to the chromosomic position, the left Y axis corresponds to the -Log10 P-value, and the right Y axis shows the recombination rate (cM/Mb) from Hapmap (release 22, CEU population). Vertical lines represent the recombination rate. On the plots, the GWAS hit rs10498635 which is represented as diamond purple. Each circle corresponds to a SNP either genotyped or imputed, and a colour code translating the r^2 value of LD against (red = strong LD; blue = weak LD). The plot A shows regional association for the 14q32 locus, and the plot B shows the same following conditional analysis for the rs10498635.

3.4.2 Detection of variants in RIN3

In order to investigate additional variants which were either missed by the GWAS or not described by the 1000 Genomes project, deep sequencing of the *RIN3* gene was carried out. For this, Haloplex (Agilent technologies) and Sanger sequencing were carried out as described in Sections 2.1.1 and 2.1.2.

A total of 18 variants were detected, 7 of those were not previously described in public databases such as 1000 Genomes or NHLBI. 15 variants were of rare frequency (MAF < 1%) and detected only in patients. Statistical analysis for those variants is shown in Table 3.1, and representative location of the coding variants within the RIN3 protein is summarised in Figure 3.2.

Frequencies in cases from both sequencing techniques were analysed against European subjects from the 1000 Genomes and the NHLBI project as controls. A strong association was observed for the p.R279C variant (rs117068593) once analysed against 1000 Genomes (OR = 0.60; 95% CI = 0.43 to 0.84; $P = 3.1\text{x}10^{-3}$), or NHLBI (OR = 0.50; 95% CI = 0.38 to 0.67; $P = 2.0\text{x}10^{-6}$). When combined, a p-value of $1.4\text{x}10^{-9}$ was detected (OR = 0.64; 95% CI = 0.55 to 0.74). Subsequently, imputed data for p.R279C was extracted from the GWAS analysis and confirmed such significance (OR = 0.68; 95% CI = 0.58 to 0.81; Imputed $P = 5.7\text{x}10^{-6}$). p.R279C was also in strong LD with the GWAS hit rs10498635 ($r^2 = 0.96$, $D' = 0.98$), as shown in Figure 3.3.

Table 3.1: Statistical analysis of frequencies from potential pathogenic variants detected by sequencing in RIN3.

Variant ID	Position (hg19)	Reference allele	Sample allele	Gene region	Protein variant	AF cases[a] (%)	AF 1000G[b] (%)	P-value	AF NHLBI[d] (%)	P-value[e]	Prediction score[f]
N/A[g]	92979351	A	G	Promoter	—	2/492 (0.41)	0 (0.0)	0.15	—	—	NFE2L1/MafG
rs368389701[h]	92980256	C	A	5′UTR	—	1/492 (0.20)	0 (0.0)	0.39	—	—	TFBS (TAF1; POLR2A)
N/A[g]	93081806	C	T	Exon 4	p.A141V	1/492 (0.20)	0 (0.0)	0.39	0 (0.0)	0.05	5
rs3829947[g,h]	93118038	A	G	Exon 6	p.H215R	257/492 (52.2)	427 (56.3)	0.15	4902 (57.0)	0.04	0
N/A[g]	93118085	C	T	Exon 6	p.R231C	1/492 (0.20)	0 (0.0)	0.39	0 (0.0)	0.05	4
rs147329151[g]	93118145	C	A	Exon 6	p.Q251K	2/492 (0.41)	0 (0.0)	0.15	2 (0.02)	0.02	1
rs117068593[g,h]	**93118229**	**C**	**T**	**Exon 6**	**p.R279C**	**54/492 (10.97)**	**129 (17.0)**	**$3.1x10^{-3}$**	**1687 (19.6)**	**$2.0x10^{-6}$**	**4**
N/A[g]	93118260	T	C	Exon 6	p.L289P	1/492 (0.20)	0 (0.0)	0.39	0 (0.0)	0.05	1
N/A[g]	93118268	T	C	Exon 6	p.C292R	1/492 (0.20)	0 (0.0)	0.39	0 (0.0)	0.05	2
N/A[g]	93118274	C	T	Exon 6	p.P294S	1/492 (0.20)	0 (0.0)	0.39	0 (0.0)	0.05	1
N/A[h]	93118310	G	A	Exon 6	p.A306T	1/492 (0.20)	0 (0.0)	0.39	0 (0.0)	0.05	0
rs201271121[g]	93118550	C	T	Exon 6	p.P386S	1/492 (0.20)	0 (0.0)	0.39	0 (0.0)	0.05	4
rs3742717[g,h]	93118668	C	T	Exon 6	p.T425M	77/492 (15.65)	165 (21.8)	$7.5x10^{-3}$	1458 (16.9)	0.45	1
rs74074811[g]	93118674	G	A	Exon 6	p.R427Q	2/492 (0.41)	0 (0.0)	0.15	10 (0.12)	0.11	0
rs74074812[g]	93118823	C	T	Exon 6	p.P477S	1/492 (0.20)	0 (0.0)	0.39	2 (0.02)	0.14	3
rs12434929[g,h]	93119232	G	C	Exon 6	p.G613A	4/492 (0.81)	7 (0.92)	0.24	57 (0.66)	0.19	1
rs145292991[g]	93125790	G	A	Exon 7	p.D771N	1/492 (0.20)	0 (0.0)	0.39	2 (0.02)	0.14	3
rs147042536[g]	93142861	T	C	Exon 8	p.Y793H	5/492 (1.02)	5 (0.66)	0.19	54 (0.63)	0.11	6

[a]Allele frequency (AF) shown as number of alleles observed/total number of alleles. [b]Allele frequency in European subjects from 1000 Genomes (n = 379). [c]P-value from testing sequenced cases (n = 246) and European subjects from 1000 Genome. [d]Allele frequency in European-American subjects in NHLBI data set (n = 4300). [e]P-value from testing sequenced cases (n = 246) and European-American subjects from NHLBI data set. [f]For missense variants, as assessed by SIFT, PolyPhen-2, Condel, MutationTaster, GERP conservation score and Grantham score. [g]Variant detected in sporadic cases. [h]Variant detected in familial cases. N/A = Indicates that the SNP does not have an rs number.

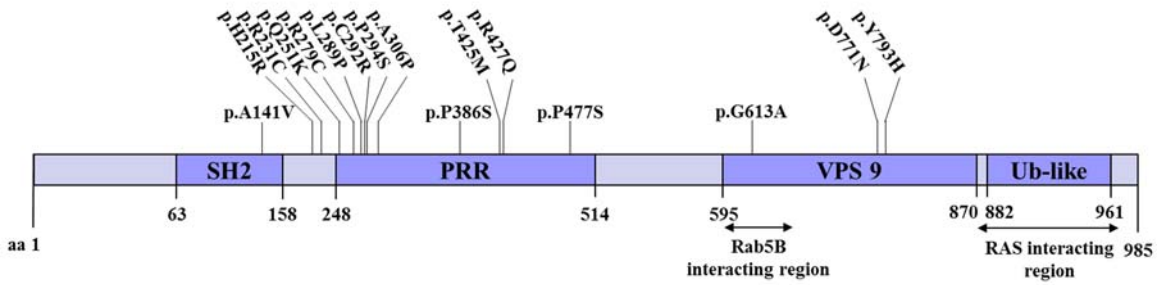

Figure 3.2: Schematic illustration of missenses on the RIN3 protein sequence.
Most of the coding variants detected by Sanger and next generation sequencing were located or around the PRR or *RIN3*. One was located in the SH2 domain, and another 3 were in the VPS9 domain of RIN3.

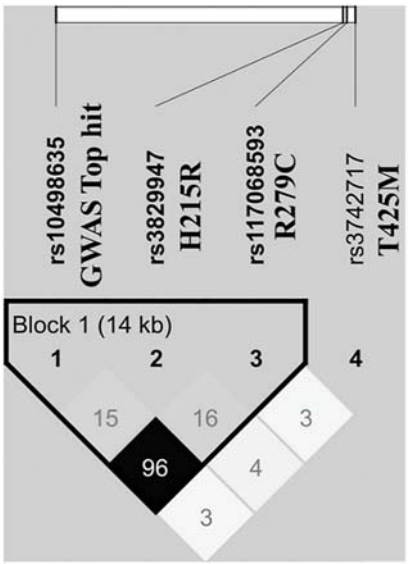

Figure 3.3: Screenshot of the Hapmap LD analysis for the GWAS hit against common variants detected in RIN3 by fine-mapping.
Out of the three common variants detected in this study, the p.R279C variant shows a strong LD for the GWAS hit rs10498635 ($r^2 = 0.96$, $D' = 0.98$).

To look for any statistical association amongst the variants detected, a haplotype analysis was performed on the GWAS cohort. Due to the rare frequency of most polymorphisms analysed, only two common haplotypes were found for the p.R279C and the GWAS hit rs10498635 (both polymorphisms changing from a C allele to a T). The risk allele rs10498635C–rs117068593C was over-represented in the GWAS cases with a frequency of 86.4%, against 81.2% in the controls (OR = 1.48; 95% CI = 1.25 to 1.74; $P = 2.8 \times 10^{-6}$). The other haplotype (T alleles) was found with a frequency of 18.2% in the GWAS controls. Additional haplotypes detected had frequencies lower than 0.2%. Although not significant, the risk allele rs117068593C was found to be more present in familial cases ($n = 9$; 17.3%) than in sporadic Pagetic patients ($n = 45$; 10.3%).

Two additional common variants, p.T425M and p.H215R, were also detected. None showed association for the disease whether they were compared to control subjects from 1000 Genomes or from the NHLBI. This was confirmed in the GWAS cohort as well. Finally, they did not show to be in LD with the GWAS top hit, as shown in Figure 3.3.

The 15 rare variants (MAF < 1%) were also investigated. Most were found to be near the p.R279C missense, on exon 6. Although all but p.D771N showed a higher frequency in cases than controls, none reached statistical significance. A combining effect of those rare variants was found to be strongly associated with PDB (OR = 3.72; 95% CI = 2.38 to 5.82; $P = 8.9 \times 10^{-10}$). Amongst those 15 rare polymorphisms, two were detected in familial cases, one in both sporadic and familial cases and 12 in sporadic cases (Table 3.1).

The three variants found in families (rs368389701, p.A306T, p.G613A) were additionally genotyped in related members of the proband tested here, to investigate the inheritance pattern of the variant. In one family the missense p.G613A was found in father and daughter, both affected by PDB. Similar investigations for the additional p.A306T or the rs368389701 variant were not possible as the DNA was only available from the probands. Additionally, most rare variants (n = 24; 96%) occurred on the rs10498635C–rs117068593C risk haplotype described above.

3.4.3 In silico analysis of RIN3 mutations

The noncoding variants located in the promoter and UTRs regions of *RIN3* were analysed using the ENCODE database. Two variants, one located in the promoter (no rs number) and one in the 5'UTR (rs368389701), were found to be of interest (Table 3.1). The variant located in the promoter is thought to interfere with the MafG transcription factor motif (also called V-maf musculoaponeurotic fibrosarcoma oncogene homologue G), which is part of the small Maf family of proteins involved in repression of transcriptional regulation. rs368389701 is located at the binding site of the transcription initiation factor TFIID subunit 1 (TAF1) for the lymphoblastoid, human embryonic stem cells and neuroblastoma cell lines. TAF1, or TATA box binding protein associated factor, plays a crucial transcriptional role as part of the RNA polymerase IID (TFIID) transcription factor complex.

The predicted pathogenicity of the coding variants was investigated by assigning a score, deducted from six *in silico* prediction tools (Section 2.1.5). p.A141V, p.R279C, p.R231C, p.P386S, and p.Y793H showed the highest scores (4 or higher). p.A141V is located in the SH2 domain of RIN3, p.Y793H is in the VPS9 domain, and p.R279C, p.R231C and p.P386S are located in the PRR of RIN3 as shown on Figure 3.2. The p.R279C variant also lies in a PXXP protein-binding motif, able to interact with domains such as SH2 and SH3 (Kay et al, 2000; Rouka et al, 2015).

Recent *in silico* studies have shown that proline is the most "disorder promoting" amino acid, therefore categorising the PRR of RIN3 to be an intrinsically disordered protein regions (IDPRs) (Theillet F-X., 2013). Tools mentioned above, used to establish a prediction score, investigate the functional effect of the variant by detecting changes in structures and conservation of amino acid which result in a loss of accuracy for variants located in IDPRs (Vacic & Iakoucheva, 2012). To counter this, meta-server consensus disorder predictor programs (MetaPrDOS (Ishida & Kinoshita, 2008) and MetaDisorder (Kozlowski & Bujnicki, 2012)) were used to assess and model the disordered regions of RIN3 before incorporating each missense from the PRR region.

The analysis was performed using PONDR VL-XT (Li et al, 1999), to detect a loss or a gain of disorder within the protein (Figure 3.4). A slight disorder-to-order shift was observed for p.R279C, p.P386S and p.P477S, while a more perceptible order-to-disorder transition shift was seen in p.R427Q. No effect was predicted for the other variants lying in this area.

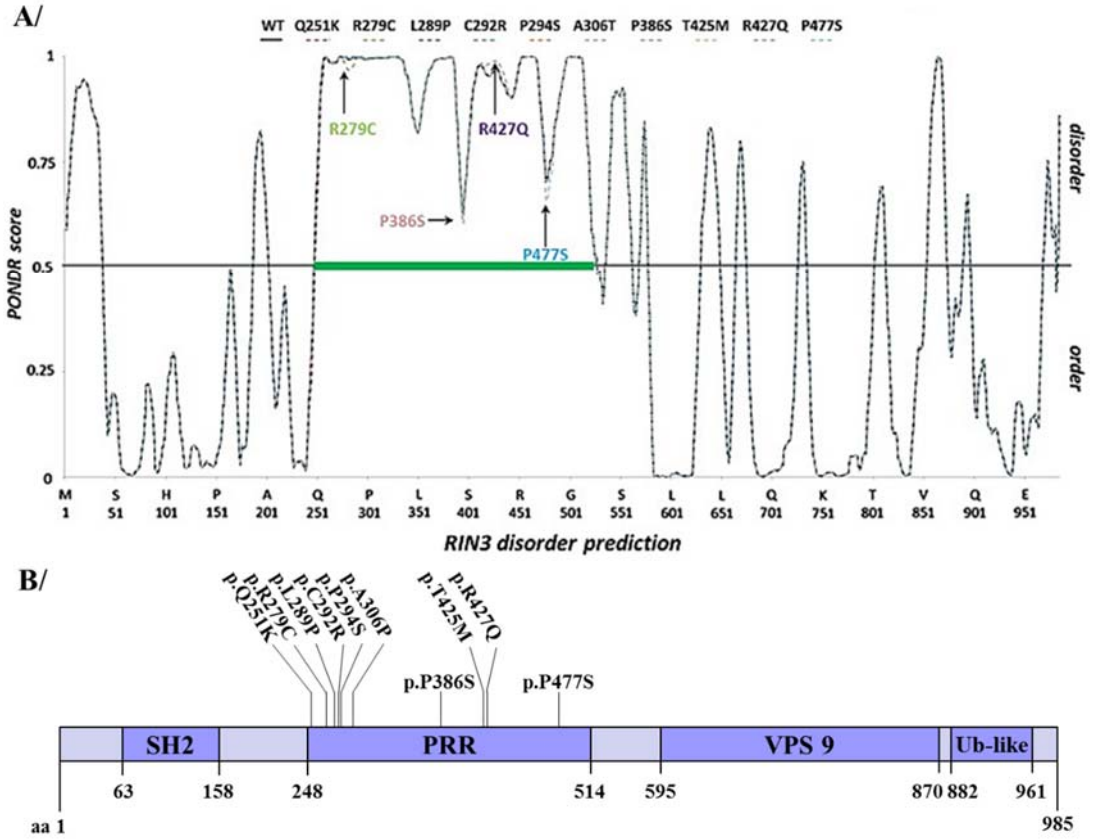

Figure 3.4: PONDR VL-XT disorder predictions of the coding variants locating in the PRR region of RIN3.

PONDR score was used to investigate the effect of mutations on the disordered regions of RIN3, symbolised in green on the PONDR plot (A), on scale with the protein sequence showed in the panel B. PONDR scored < 0.5 were considered to go towards an ordered structure, while values > 0.5 tend to predict a disordered effect on the protein. Disordered effect generated by the variants (dotted lines) were assessed against the WT sequence (full line). The mutated alleles of p.R279C, p.P386S and p.P477S show a minor drop of the PONDR score suggesting an ordering effect. p.R427Q shows a higher score than the WT sequence however, predicting an increased in disorder effect of the variant.

To analyse the coding variants located in alternative domains, protein stability between the WT and mutated RIN3 was measured by FoldX (Schymkowitz et al, 2005). For this, the SH2 domain, in which p.A141V was detected, and the VPS9 domain, where p.G613A, p.D771N and p.Y793H were found, were modelled using Modeller 9v12 (Sali & Blundell, 1993) (Figure 3.5).

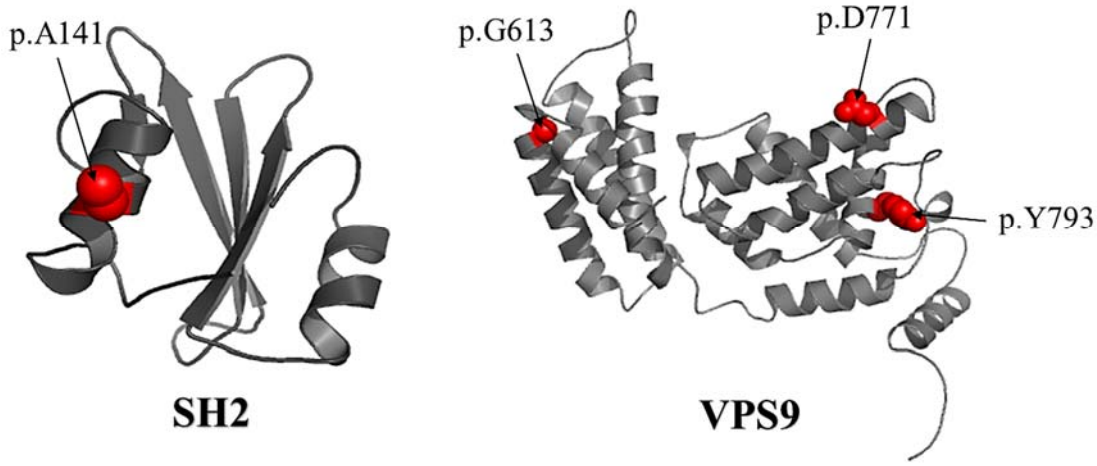

Figure 3.5: 3D Homology model of the SH2 and VPS9 domains.
p.A141V is located in the SH2 domain but is showed to be poorly conserved, as for p.D771N located in the VPS9 domain. They are both exposed on the surface of the protein. p.G613A is also poorly conserved. p.Y793H is however conserved, and largely buried in RIN3.

p.A141V which had a predicted score of 5 and p.D771N, with a score of 3, were both solvent exposed and were thus unlikely to impact the structure of RIN3. p.G613A was predicted to be unlikely functional by previous tools (score of 1) and here shows similar results due to low amino acid conservation, as for p.A141V and p.D771N. Confidence in the model was performed using MetaMQAPII, and p.G613A was in a low confidence area (Figure 3.6) (Pawlowski et al, 2008). The p.Y793H variant however is located in a more defined region of the modelled VPS9 domain.

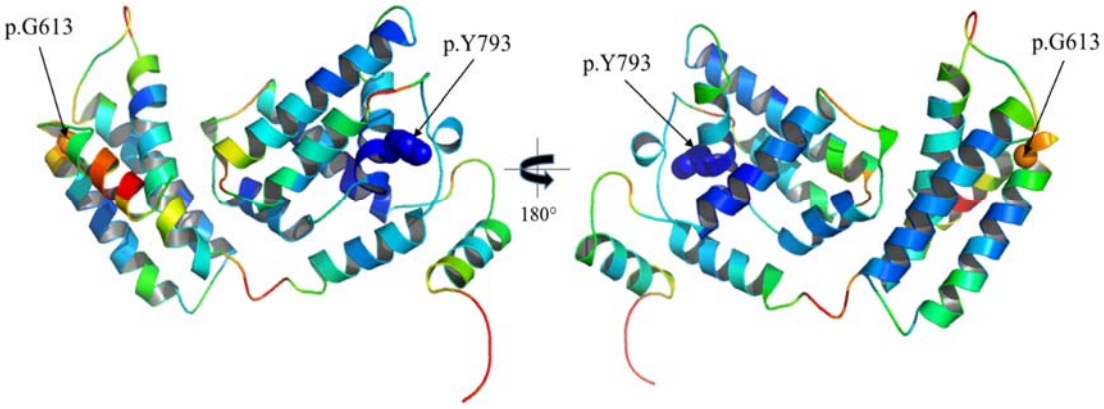

Figure 3.6: Evaluation of the 3D Homology model of the VPS9 domain using MetaMQAPII.

A coloured spectrum extending from blue (correct) to red (incorrect) was used to easily visualize the confidence and accuracy of the model. p.G613A is located in a region of low confidence in the model.

p.Y793H was the only missense with the prediction score of 6, and the WT tyrosine is predicted to be structurally buried within RIN3 which could subsequently have a bigger effect on the 3D structure of the protein (Figure 3.7).

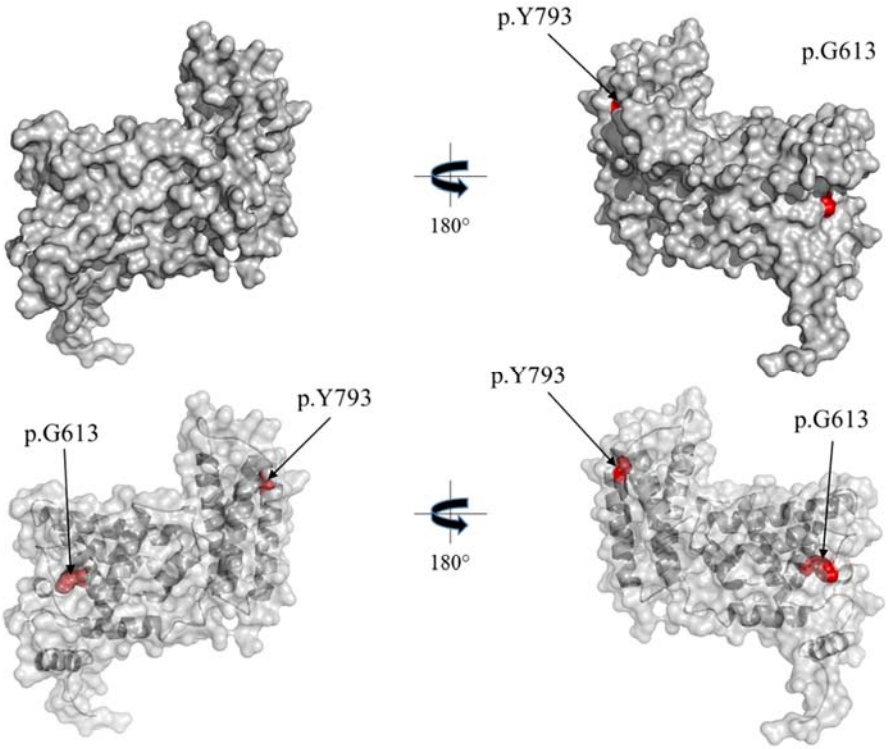

Figure 3.7: Assessment of the exposition of p.G613A and p.Y793H in the VPS9 domain.

Amino acid concerned by the mutations are red. The top two pictures show the outer-shell of RIN3, for which the tyrosine at 793 is predicted to largely buried, with the exception of its hydroxyl group.

The VPS9 domain is made of a succession of helices conferring overall stability of RIN3. Particularly, two helices called αV4 and αV6 form a hydrophobic indentation responsible for protein interactions and overall structure of the domain (Figure 3.8, A). p.Y793H is located within the αV4 helix of the VPS9 domain (Figure 3.8, B) and induces a loss of hydrophobic interactions with 4 amino acids compared to the wild type RIN3 (Figure 3.8, C). FoldX predicts a delta delta Gibbs (ΔΔG) of 2.02kcal/mol for the mutant RIN3, which is considered to be destabilising (> 1.6kcal/mol). ΔΔG translates the free energy between folded and unfolded states of the protein. This was constantly observed in equivalent amino acid changes from the templates used for modelling this domain (Table 3.2).

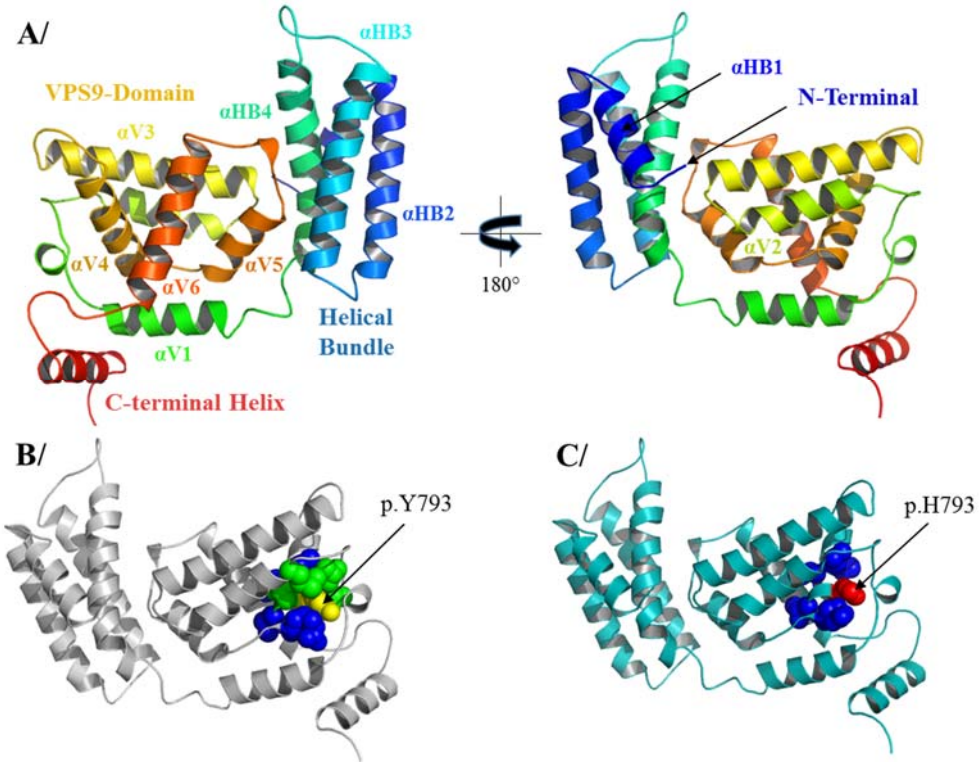

Figure 3.8: Importance of helical structures in the VPS9.
In the WT RIN3 (A), helices αV4 and αV6 for a V-shape creating a hydrophobic environment, indispensable for protein interactions and overall structure of the domain. The tyrosine amino acid located at position 793 makes hydrophobic interactions with p.L727, p.V729, p.M739 and p.V794 (shown in green), and hydrogen interactions with p.P789, p.V790, p.L791, p.L795, p.A796, p.R797 (shown in blue) (B). Upon mutation (C), all hydrophobic interactions are lost while hydrogen bonds remain.

Table 3.2: FoldX stability calculations for equivalent residues in template structures.

Mutation (Protein)	Stability energy calculation on mutant VPS9 domain structure (Mean ΔΔG)
p.Y793H in human RIN3-VPS9 domain homology model	2.02kcal/mol
p.Y193H in *Arabidopsis* VPS9A domain (2.08 Å crystal structure; PDB ID: 2EFE_A)	2.32kcal/mol
p.Y321H in human RABX5 domain (2.1 Å crystal structure; PDB ID: 2OT3_A)	2.06kcal/mol
p.Y321H in human RABX5 domain (2.35 Å crystal structure; PDB ID: 1TXU_A)	2.91kcal/mol

ΔΔG was measured between WT and mutated RIN3 on the model which was used for this project, as well as on each template used for its creation. Values > 1.6kcal/mol are considered destabilising for the protein.

3.5 DISCUSSION

As described in Section 1.4.1 (14q32.12 locus (*RIN3*)), the *RIN3* gene has been suggested as a candidate for PDB as the rs10498635 intronic variant was tagged by a GWAS performed in 2011 (Albagha et al, 2011). This chapter focused on confirming such findings, and investigates variants in the *RIN3* gene which could be associated with PDB.

The repeated imputation, based on the one performed during the GWAS study of 2011, was performed using 1000 Genomes database to increase the power of the analysis.This database offers 379 European individuals while the original imputation, which used the Hapmap database (release 22), had 60 (Albagha et al, 2011). As for the imputation from the 2011 study, a conditional analysis for the GWAS top hit rs10498635 showed that it was the only signal for the 14q32 locus. This suggests that the rs10498635 variant, or a variant in strong LD with it would be a good candidate variant for PDB.

Knowing the genetic component of the disease (Section 1.4), screening for pathogenic mutations in *RIN3* was the first logical step of the project. The combining effort of next generation and Sanger sequencings led to the finding of 18 mutations, 7 of which were not present in controls nor described in public databases. To look at the significance of their incidence in the cases, frequencies were compared to controls from the NHLBI and 1000 Genomes databases. One common variant, rs117068593 (p.R279C), showed statistical association for PDB ($P = 1.4x10^{-9}$; OR = 0.64; 95% CI = 0.55 to 0.74). This SNP is a C>T change, thus the odd ratio suggests that the minor rs117068593T (p.279C) allele is more present in controls than in cases.

It could then be suggested that the rs117068593T (p.279C) allele would have a protective effect over the disease for the patient. Other mutations have been described to have a similar effect, such as the ε2 allele in the *APOE* gene, which encodes a cholesterol carrier. Indeed, the ε2 allele has a protective effect against Alzheimer disease with an incidence of 8.4% in Caucasian, compared to the ε3 (77.9%) or ε4 alleles (13.7%) (Liu et al, 2013). Further analysis of the rs117068593 variant revealed that is in strong LD with the GWAS hit rs10498635. Following the results from the conditional analysis presented in section 3.4.1, this places rs117068593 as a good candidate for PDB. Furthermore, haplotype analysis also showed that this variant was on the same allele than the GWAS hit (rs10498635C–rs117068593C).

Kemp and al. recently reported an association for the intronic rs754388 variant located in *RIN3* with an increased BMD in lower limbs, using DXA scans. They performed fine mapping by imputing variants from the 1000 Genomes database, which detected the p.R279C variant. Both rs754388 and p.R279C are in strong LD ($r^2 = 0.96$). They also found that p.R279 was associated with increased lower limb BMD, as well as total-body less head in children (Kemp et al, 2014). In the context of PDB, bones are enlarged and osteosclerosic lesions can lead to an increased BMD. This has however not been investigated at a large scale and only a few isolated cases have been described for increased BMD of the spine (Vasireddy & Halsey, 2001). This has also not been reported in lower limbs. Our analysis suggests that the p.R279 allele predisposes to PDB but it is difficult to predict an association with BMD. Kemp and colleagues has also analysed samples from children with growing bones while PDB is a late onset disease. Additionally, their discovery of p.R279C resulted from imputation, which is not as reliable as the Sanger sequencing we used.

The two other common variants (p.H215R and p.T425M) showed no statistical association in this cohort, and were not in LD with the top hit, thus unlikely to be involved in PDB. The other variants detected were of rare frequency. All but one were more commonly present in cases than controls. Taken individually, they did not show any association with the disease. However, a strong p-value was detected once their incidence was put together and as a result, a combined effect could be suggested here. Additionally, 96% of the rare variants were sharing the rs10498635C–rs117068593C haplotype described above.

In silico analyses were performed on coding variants. Firstly, six bioinformatic tools investigating structural effect and amino acid conservation changes were used to deduct a predicted functionality score. p.A141V, p.R231C, p.R279C, p.P386S and p.Y793H showed the highest scores (4 or higher out of 6). Prediction tools like the ones used here have however been showed to have limited performance and studies have reported than most common programs offer an accuracy lower than 82% (Walters-Sen et al, 2015). Although they can be useful for well conserved variants inducing a big structural change in proteins, such predictions are to be considered carefully. Similarly, the p.P392L variant in the *SQSMT1* gene was initially predicted to be benign by *in silico* tools but is now known to be disease causing (Hocking et al, 2004). In order to try and reinforced the reliability of the prediction scores, two additional and more complex analyses were performed, depending on the location of the variants in the RIN3 protein. For this, variants located in the intrinsic disordered regions of RIN3 were analysed using PONDR scores. As mentioned above, bioinformatics tools such as SIFT or Polyphen-2 use amino acid alignments and/or conservation to evaluate the effect of the missense.

Such tests have been found to be irrelevant to disordered regions like PRR, as they are prone to low phylogenetical conservation and do not have a fixed 3D structure like variants in ordered regions would display resulting (Vacic et al, 2012). To counter this, PONDR scores are used to investigate the impact of variants by searching for "ordering shifts", meaning that the introduction of a variant brings "order" to a "disordered" region. Studies have shown that about 20% of disease mutations in such disordered regions cause local disorder-to-order transitions (Vacic & Iakoucheva, 2012; Vacic et al, 2012). As a result, only four missense mutations p.R279C, p.P386S, p.R427Q and p.P477S lead to order shifting. Here, p.R279C, p.P386S, and p.P477S induced such transition, while p.R427Q was found to enhance disorder. All were however minor, as none shifted the PONDR score from > 0.5 to < 0.5. This suggests that they are predicted to be unlikely pathogenic.

Finally, the four variants located in ordered regions of the protein (p.A141V, p.G613A, p.D771N and p.Y793H) were analysed using 3D homology of RIN3, before and after introduction of the coding variant. Only p.Y793H was shown to have a pathogenic effect on the structure. This variant is located in the VPS9 domain of RIN3, which confers the GEF activity of the protein. p.793H triggers a loss of crucial hydrophobic interactions in the helical hydrophobic bundle formed in the VPS9 domain. A previous study has shown that mutations in the helical bundle of RIN3 amino acid impairs the GEF activity for Rab31 (Kajiho et al, 2011). Although p.Y793H was not investigated in this study, they induced a p.P789A/p.D785A change in RIN3. p.P789 was found in our analysis to interact with p.Y793 via hydrogen binding, which was not lost upon the introduction of p.793H.

Although p.Y793H could be a good candidate from this *in silico* analysis, no association with PDB was found by looking an incidence of the mutation in cases compared to controls.

It is not clear yet if the genetic association of *RIN3* with PDB is due to an effect of the rare variants combined, common variants or a mixture of both and sequencing additional patients is needed to answer this question. However, looking at the frequency, LD and haplotype analyses, the p.R279C variant seems to be a good candidate for PDB. Although the *in silico* analysis predicts that it is unlikely to be functional, it is important to notice that arginine to cysteine changes are predicted to be amongst the most "order-enhancing" mutations in regions such as PRR and thus should not be excluded (Vacic & Iakoucheva, 2012; Vacic et al, 2012). Additional functional analyses are necessary to confirm the involvement of p.R279C.

CHAPTER FOUR
RIN3 VARIANTS AND DISEASE SEVERITY IN PDB

4 *RIN3* VARIANTS AND DISEASE SEVERITY IN PDB

4.1 SUMMARY

The analysis presented in Chapter 3 places p.R279C as a good candidate for PDB. Additionally, many rare variants were over-represented in the cases and a combined effect was detected. Here, a genotyping and a severity association were performed on those variants using a bigger Pagetic cohort (PRISM) in order to confirm previous results and understand their clinical effect.

Taqman® SNP genotyping (Thermo Fisher Scientific) was performed on p.T425M and all rare variants previously detected, in 712 Pagetic cases and 262 controls from the PRISM study. The frequencies were compared between cases and controls and confirmed that most rare variants were over-represented in the cases, although this was not significant. The rare variant p.R427Q detected at a frequency of 0.41% in chapter 3 was detected here at a frequency of 2.1%. No combined effect was observed for the rare variants, however haplotype analysis confirmed that the common allele of all variants analysed (i.e. reference allele) were more present in cases than controls (82.31%; OR = 1.25; P = 0.008). The severity association showed that patients carrying the variant (rs117068593T) had a younger age of diagnosis (P = 0.034).

Although a younger age of diagnosis for the p.279C change opposes the findings from Chapter 3, the association was nominal and lost once corrected over the number of clinical features investigated and is unlikely to be a true effect. Such findings suggests however that the association with PDB is unlikely to be driven by a large effect from common and rare variants combined, but could be of a more modest effect from the p.R279C variant.

4.2 INTRODUCTION

The previous chapter identified 18 variants in *RIN3* using next generation and Sanger sequencing, including 16 missense mutations and 7 novel variants.

The analysis of the common variant p.R279C (rs117068593) is suggestive of a strong association with PDB, as it is in LD with the GWAS hit described by Albagha and colleagues (rs10498635) (Albagha et al, 2011), and both share the same risk haplotype (rs10498635C–rs117068593C) associated with PDB.

Fifteen out of the 18 variants were of rare frequency (MAF < 1%) and most were clustering in the exon 6, a PRR. Such regions are categorised as "disordered", have important cellular roles and have been associated with diseases (Theillet F-X., 2013). All but one rare variant were more frequent in cases than controls, and although none showed individual statistical significance for PDB, a combined effect was found to have a strong association with PDB. Finally, 96% of those variants were on the same rs10498635C–rs117068593C haplotype described above. Although no variant with an association for PDB was predicted to be functional using bioinformatic tools, it is important to keep in mind that such programs need to be supported by functional analyses.

This chapter aims to repeat the analysis performed in Chapter 3, using a bigger cohort from the PRISM trial, to evaluate the effect that these rare and/or common variants have on PDB, including a combined effect with variants such as p.P392L from *SQSTM1* or p.R279C from *RIN3*. This chapter will also investigate the clinical effect of the variants using Pagetic information from each patient. This includes features like bone pain, deformity of clinical fractures.

4.3 METHODS

The rare coding variants and p.T425M described in Table 2.7 were genotyped using a Taqman® SNP genotyping (Thermo Fisher Scientific) in 712 Pagetic cases and 262 controls from the PRISM study. Only variants with a call rate > 97% were analysed. Frequency differences between cases and controls were investigated by Fisher's exact test for the rare variants (MAF < 1%) and Anova for the common variants using SPSS Version 22 (SPSS Ltd, UK) (Section 2.2.3). The overall effect of the rare variants was assessed using a Fisher's Burden test, and a haplotype analysis was performed using Phase version 2.1.1 (Section 2.2.3) to confirm previous data reported in Chapter 3 (Stephens & Scheet, 2005; Stephens et al, 2001).

Associations between the variants and clinical Pagetic features were investigated. For this, a severity analysis was performed on the PRISM cases (Section 2.2.3). The following parameters were considered as shown in Table 2.8: gender, family history, if the patient had an orthopaedic surgery, fractures (and if they were Pagetic), bone pain (and if it was related to PDB or not), if the patient has a Pagetic skull and wears a hearing aid, how many bisphosphonate treatments the patient received, the age at diagnosis and at recruitment for the trial, the number of bones affected, bone deformities and an overall severity score deducted from this data (Visconti et al, 2010). The effect of the p.R279C variant was also analysed, using the GWAS hit rs10498635 data as a surrogate. Indeed, both variants are in strong LD ($r^2 = 0.96$) thus will show a similar genetic pattern. As data was already available for the rs10498635 variant from the 2011 GWAS the p.R279C was not genotyped (Albagha et al, 2011).

The analysis was performed on all cases PRISM (noted PRISM) and two subgroups: patients not carrying *SQSTM1* mutation (noted PRISM/SQSTM1-), and patients carrying at least one mutation in the *SQSTM1* gene (noted PRISM/SQSTM1+). The genotypes used from those 3 cohorts were the following: common variants (p.R279C and p.T425M) were investigated for "no mutation", "heterozygote mutation", or "homozygote mutation", while the rare variants were combined, and analysed for "no mutation", or "at least one of the rare variants is mutated" (Section 2.2.3).

Another association study was performed on the most common haplotypes found in the PRISM/SQSTM1- cases, estimated by Phase version 2.1.1 (Stephens & Scheet, 2005; Stephens et al, 2001). For both, an ANOVA was performed on quantitative traits while a Chi square test was used for the others using SPSS Version 22 (SPSS Ltd, UK).

Genotyping of the variant p.L289P resulted in no amplification and was not interpretable. The variants p.T425M, p.R427Q, p.P447S, and p.G613A were located in regions of *RIN3* for which the assay was not designable. Alternative variants which were in LD ($r^2 > 0.8$) with those were genotyped instead, using data from Sanger sequencing as described in Table 2.7.

4.4 RESULTS

4.4.1 Case and control investigations

The three rare variants p.C292R, p.A306P and p.P386S were not detected in controls nor cases. Out of the 10 rare variants previously described, 7 were found in this study to be more common in the cases. The p.R427Q missense mutation, detected as a rare variant in the previous investigation (0.41%), was found with a frequency of 2.1% in the cases here.

A nominal significance was reached for p.T425M with PDB (OR = 0.72; 95% CI = 0.55 to 0.95; $P = 0.021$), however once corrected the association was lost. Overall, no statistical difference between the two cohorts was observed. The results can be found in Table 4.1.

An aggregative Burden test was then performed on the same cohort, but there was not association for PDB (OR = 0.98; 95% CI = 0.50 to 1.93; $P = 0.45$). Results are shown in Table 4.2.

Table 4.1: Burden test analysis on rare variants genotyped in RIN3.

# of minor allele observed in all rare variants	AF in controls[a]	AF in cases[a]	p-value
≥ 1	12/262 (4.58%)	32/712 (4.49%)	0.45

[a]Allele frequency (AF) shown as number of observed patients/total patient count.

Table 4.2: Statistical analysis of frequencies from rare variants genotyped in RIN3.

Variant ID	DNA change	Protein change	Reference allele	Sample allele	AF controls[a] (%) *n* = 262	AF cases[a] (%) *n* = 712	p-value
N/A	c.[1-926A>G];[=]	-	A	G	0/518 (0)	2/1378 (0.15)	1
N/A	c.-21C>A	-	C	A	5/494 (1.01)	5/1420 (0.35)	0.137
N/A	c.[422C>T] ;[=]	p.A141V	C	T	0/522 (0)	1/1416 (0.07)	1
N/A	c.[691C>T];[=]	p.R231C	C	T	0/510 (0)	1/1414 (0.07)	1
rs147329151	c.[751C>A];[=]	p.Q251K	C	A	0/504 (0)	3/1420 (0.21)	0.571
N/A	c.[874T>C] ;[=]	p.C292R	T	C	0/520 (0)	0/1420 (0)	-
N/A	c.[880C>T];[=]	p.P294S	C	T	1/506 (0.20)	1/1394 (0.07)	0.462
N/A	c.[916G>C] ;[=]	p.A306T	G	C	0/522 (0)	0/1390 (0)	-
rs201271121	c.[1156C>T];[=]	p.P386S	C	T	0/512 (0)	0/1416 (0)	-
rs3742717	**c.[1274C>T];[=]**	**p.T425M**	**C**	**T**	**93/512 (18.16)**	**189/1366 (13.84)**	**0.021**
rs74074811	c.[1280G>A];[=]	p.R427Q	G	A	5/516 (0.97)	30/1418 (2.12)	0.12
rs74074812	c.[1429C>T];[=]	p.P477S	C	T	0/514 (0)	1/1408 (0.07)	1
rs12434929	c.[1838G>C];[=]	p.G613A	G	C	3/516 (0.58)	13/1416 (0.92)	0.58
rs145292991	c.[2311G>A] ;[=]	p.D771N	G	A	0/510 (0)	1/1380 (0.07)	1
rs147042536	c.[2377T>C];[=]	p.Y793H	T	C	3/520 (0.58)	6/1378 (0.44)	0.712

[a]Allele frequency (AF) shown as number of minor alleles observed/total number of alleles. N/A = Indicates that the SNP does not have an rs number.

A haplotype analysis was also performed on the PRISM cases and controls using Phase (Appendix 4.1). Because of the rarity of most variants, only two common haplotypes were detected by the software (Appendix 4.2). The most common haplotype (Haplotype 1), which corresponds to the major alleles of all 15 variants, was more frequent in cases (82.31%) than in controls (78.97%). This was statistically significant (OR = 1.25; 95% CI = 0.98 to 1.61; $P = 0.008$). The second most common haplotype (Haplotype 6 containing p.T425M) corresponds to a change for the p.425M missense only, and was also over-represented in the controls at 17.73%, while found at 13.22% in the cases. This was also statistically significant (OR = 0.7; 95% CI = 0.53 to 0.91; $P = 0.001$). All others 12 haplotypes showed a frequency < 1.55%.

4.4.2 Association study with disease activity

From Genotyping data

An association study was performed on the genotyping results of PRISM cases, to investigate any effect of the variants on the severity of the disease.

Each clinical feature was investigated against allele dosage of p.R279C (+/+, +/-, -/-), p.T425M (+/+, +/-, -/-) and all other variants combined (no mutation or at least one mutation). The data is summarised in Appendices 4.3 to 4.11. Nominal significance was achieved for the age of diagnosis of the PRISM and the PRISM/SQSTM1+ cohorts carrying the p.425M allele ($P = 0.002$ and $P = 0.003$ respectively) (Appendices 4.3 and 4.5).

Age at recruitment, which corresponds to the age at which the patient has joined the trial, was also significant for all three cohorts tested (PRISM P = 0.001; PRISM/SQSTM1- P = 0.019; PRISM/SQSTM1+ P = 0.047) for patients carrying the p.425M allele (Appendices 4.3 to 4.5). Nominal significance was additionally achieved for the age at diagnosis in the PRISM/SQSTM1- subgroup, for patients carrying the p.279C change (P = 0.034) (Appendix 4.7). This was not detected in the whole cohort or PRISM/SQSTM1+ subgroup.

From haplotype data

A second haplotype analysis was performed on all PRISM cases after importing information from the GWAS top hit rs10498635C, to represent p.R279C changes (Appendix 4.1). All haplotypes detected are presented in Appendix 4.12. Three common haplotypes were detected. The first two were similar to the previous haplotype data: the most common haplotype corresponding to the major allele of all 16 polymorphisms was found in 69% of the PRISM cases (haplotype 1). The second most common haplotype, for which only the minor allele p.425M was detected, was present in 13% of the PRISM cases (haplotype 7 containing p.425M). Finally, the third and new haplotype found corresponds to patients carrying only the p.279C allele and was detected in 12% of the PRISM cases (haplotype 18 containing p.279C). Other haplotypes were detected at frequencies of < 1.8%. The effect of those haplotypes on PDB severity markers was investigated for haplotypes 1,7 and 18 on the PRISM/SQSTM1- patients. The results are summarised in Tables 4.3 to 4.5. Nominal significance (P = 0.026) was achieved for the age of diagnosis in patients carrying the haplotype 18 (containing p.279C). The other variables did not show significance.

Table 4.3: Statistical analysis of the severity association on haplotype 1 from PRISM/SQSTM1- cases.

Haplotype 1				
Variable	**-/- (*n* = 61)**	**+/- (*n* = 258)**	**+/+ (*n* = 308)**	**p-value**
Gender (Male)	36/61 (59.02%)	137/258 (53.10%)	170/308 (55.19%)	0.685
Family history of PDB	2/61 (3.28%)	29/258 (11.24%)	41/307 (13.36%)	0.078
Orthopaedic surgery	10/61 (16.39%)	49/258 (18.99%)	39/308 (12.66%)	0.117
Any fracture	23/61 (37.70%)	105/258 (40.70%)	126/308 (40.92%)	0.894
Skull disease and hearing aid	5/61 (8.20%)	14/258 (5.43%)	24/308 (7.79%)	0.492
Bone pain	44/59 (74.58%)	170/242 (70.25%)	221/298 (74.16%)	0.561
Fracture in Pagetic bone	4/23 (17.39%)	26/105 (24.76%)	28/126 (22.22%)	0.728
Bisphosphonates	1.20 ± 1.33	1.21 ± 1.04	1.26 ± 1.05	0.821
Age at diagnosis	62.69 ± 10.78	65.98 ± 9.84	64.70 ± 10.79	0.064
Age at recruitment	72.16 ± 8.82	73.93 ± 7.92	72.99 ± 7.81	0.194
Number of bones affected	1.48 ± 0.79	1.76 ± 1.04	1.77 ± 1.02	0.102
Pagetic pain	1.64 ± 0.89	2.00 ± 7.52	1.42 ± 0.69	0.487
Deformity score	0.50 ± 0.85	0.56 ± 0.96	0.56 ± 0.93	0.888
Paget severity score	5.27 ± 2.06	5.59 ± 2.45	5.64 ± 2.39	0.539

Values are allele frequency shown as number of alleles observed/total number of alleles, or mean ± SD.

Table 4.4: Statistical analysis of the severity association on haplotype 7 containing p.T425M from PRISM/SQSTM1– cases.

Haplotype 7 containing p.T425M				
Variable	**-/- (*n* = 481)**	**+/- (*n* = 135)**	**+/+ (*n* = 11)**	**p-value**
Gender (Male)	258/481 (53.64%)	77/135 (57.04%)	8/11 (72.73%)	0.375
Family history of PDB	59/480 (12.29%)	13/135 (9.63%)	0/11 (0%)	0.335
Orthopaedic surgery	71/481 (14.76%)	25/135 (18.52%)	2/11 (18.18%)	0.553
Any fracture	193/481 (40.12%)	56/135 (41.48%)	5/11 (45.45%)	0.908
Skull disease and hearing aid	35/481 (7.28%)	8/135 (5.93%)	0/11 (0%)	0.57
Bone pain	333/461 (72.23%)	94/127 (74.02%)	8/11 (72.73%)	0.924
Fracture in Pagetic bone	42/193 (21.76%)	16/56 (28.57%)	0/5 (0%)	0.266
Bisphosphonates	1.25 ± 1.05	1.19 ± 1.14	1.18 ± 1.40	0.85
Age at diagnosis	65.31 ± 10.45	64.26 ± 10.60	62.27 ± 7.43	0.399
Age at recruitment	79.38 ± 7.84	73.26 ± 8.58	70.36 ± 5.07	0.463
Number of bones affected	1.74 ± 1.01	1.77 ± 1.00	1.36 ± 0.81	0.437
Pagetic pain	1.44 ± 0.71	2.50 ± 10.09	1.50 ± 0.76	0.157
Deformity score	0.57 ± 0.97	0.54 ± 1.04	0.36 ± 0.67	0.753
Paget severity score	5.58 ± 2.34	5.66 ± 2.58	4.73 ± 1.49	0.458

Values are allele frequency shown as number of alleles observed/total number of alleles, or mean ± SD.

Table 4.5: Statistical analysis of the severity association on haplotype 18 containing p.R279C from PRISM/SQSTM1– cases.

Haplotype 18 containing p.R279C				
Variable	**-/- (*n* = 471)**	**+/- (*n* = 144)**	**+/+ (*n* = 12)**	**p-value**
Gender (Male)	264/471 (56.05%)	72/144 (50%)	7/12 (58.33%)	0.429
Family history of PDB	60/470 (12.77%)	12/144 (8.33%)	0/12 (0%)	0.156
Orthopaedic surgery	69/471 (14.65%)	28/144 (19.44%)	1/12 (8.33%)	0.299
Any fracture	194/471 (41.19%)	54/144 (37.5%)	6/12 (50%)	0.583
Skull disease and hearing aid	31/471 (6.58%)	11/144 (7.64%)	1/12 (8.33%)	0.889
Bone pain	334/450 (74.22%)	91/138 (65.94%)	10/11 (90.91%)	0.063
Fracture in Pagetic bone	43/194 (22.16%)	15/54 (27.78%)	0/6 (0%)	0.276
Bisphosphonates	1.25 ± 1.06	1.16 ± 1.08	1.58 ± 1.51	0.354
Age at diagnosis	**64.68 ± 10.63**	**66.64 ± 9.15**	**59.50 ± 14.65**	**0.026**
Age at recruitment	73.03 ± 7.91	74.17 ± 7.98	73.50 ± 9.91	0.317
Number of bones affected	1.77 ± 1.02	1.66 ± 0.99	1.42 ± 0.52	0.284
Pagetic pain	1.73 ± 5.38	1.51 ± 0.78	1.20 ± 0.63	0.879
Deformity score	0.55 ± 0.95	0.53 ± 0.88	1.08 ± 0.99	0.138
Paget severity score	5.63 ± 2.43	5.38 ± 2.26	6.25 ± 1.91	0.328

Values are allele frequency shown as number of alleles observed/total number of alleles, or mean ± SD.

4.5 DISCUSSION

Chapter 3 led to the identification of new *RIN3* mutations for PDB. Most were of rare frequency but one common variant (p.R279C) showed a strong association for PDB. The GWAS hit rs10498635, which was confirmed to be the only independent signal in this locus (Section 3.4.1), is in strong LD with p.R279C. Both also share the same risk haplotype, placing p.R279C as good candidate for PDB. The many rare variants detected were found to be over-represented in cases and although no individual association for the disease was found for those, a combined effect was observed. Most (96%) were found on the same risk haplotype as the GWAS hit and p.R279C.

It is not yet understood if the rare variants have a combined effect with common variants (such as p.P392L from *SQSTM1* or p.R279C from *RIN3*), or if a common variant has an independent effect. To answer this question, 712 Pagetic cases and 262 controls from the PRISM study were genotyped here, for the variants described in Chapter 3. Allele and haplotype frequencies between both groups were compared and a clinical severity association was performed on genotyped data, as well as on haplotype results.

Some differences were found in this analysis in comparison to the previous one. The p.C292R, p.A306P and p.P386S rare variants were not detected in cases nor controls. The p.P386S variant was, in the previous chapter, observed in the ZiPP cohort by Sanger sequencing but not in PRISM samples analysed by next generation sequencing. From this PRISM group, only 95 samples overlap with the genotyping cohort. Similarly, the p.A306T and p.C292R mutations previously detected in familial and sporadic cases (respectively), were not analysed here.

The p.R427Q variant, which was found at a rare frequency in the previous chapter was detected at 2.1% of the cases by genotyping. Here, 27 cases showed a mutation for p.427Q (allele count of 30), and only 4 were also sequenced in the previous chapter. Finally, although most of the rare variants (7/10) were also over-represented in cases here and no individual association was found, the combined effect from the rare variants was not confirmed (OR = 0.98; 95% CI = 0.50 to 1.93; $P = 0.45$). Although there are differences in the samples used in the analysis, such changes in the frequencies were not expected. This can be due to a chance factor, but also to the type of cohort used. Indeed, the previous analysis focused on a cohort that was selected on stricter PDB criteria (no SQSTM1 mutation, young age of diagnosis and/or family history), while the PRISM cohort used here have an important range of disease severity. It is also important to note that the previous analysis used two public datasets for controls (379 European subjects from 1000 Genomes and 4300 from European-American subjects in NHLBI study), while only 262 PRISM controls were used here.

A nominal association for PDB was achieved for p.T425M, where p.425M was more present in controls (OR = 0.72; CI = 0.55 to 0.95; $P = 0.021$) suggestive of a protective effect over PDB (similarly to p.279C). However, this association was lost once corrected, making these results consistent with Chapter 3.

The haplotype analysis performed on the PRISM cases and controls showed two common haplotypes. The most frequent one, as described in Chapter 3, represents all SNPs on their major allele and was significantly more present in cases (OR = 1.25; 95% CI = 0.98-1.61; $P = 0.008$).

The second most common haplotype corresponds to a change for p.425M only, which as for the genotyping analysis, was more present in controls than cases (OR = 0.7; 95% CI = 0.53 to 0.91; $P = 0.001$).

The clinical effect of those variants was also investigated, after important data for the rs10498635 variant from the GWAS. The common allele p.425M showed nominal associations with age of diagnosis and age recruitment for all PRISM and PRISM/SQSTM1+ patients, while PRISM/SQSTM1- negative patients showed an association for age at recruitment only. The interpretation is however uncertain, as the statistics seem stronger in patients carrying *SQSTM1* mutations. Additionally patients carrying *SQSTM1* mutations were over-represented in the PRISM cohort affected by a homozygote mutation of p.425M (26.32%). This suggests that the *SQSTM1* gene is driving this association.

Patients carrying the p.279C allele but no *SQSTM1* mutation had a younger age of diagnosis ($P = 0.034$) than patients without any of those two mutations, or with both. This is contradictory to the previous findings. Indeed, sequencing of *RIN3* showed that the p.279C was more present in controls and was thought to have a protective effect over PDB. This was also found in haplotype analyses detailed in Chapter 3 and this chapter, as the major alleles are significantly over-represented in cases.

There are several reason why this association is unlikely to be reliable. Firstly, this is only a nominal association, lost once corrected over the number of clinical features investigated. Secondly, when compared to a similar study performed on mutations from the *SQSMT1* gene (Visconti et al, 2010), additional phenotypic associations such as deformity, bone pain, or numbers of fractures would have made this finding more credible. Additionally, the age of diagnosis can be a subjective feature to investigate on its own, as many other factors can impact its reliability such as patients being asymptomatic. Finally, looking at the detail of p.R279C allelic dosage in patients not carrying *SQSTM1* mutations (Appendix 4.7), it seems that the association is driven by the C/C genotype as the mean age is 59.5 years old, compared to 64.26 for the R/R genotype and 66.45 years old for the R/C genotype. There is an inconsistency in the allele dosage as the mean age is the highest in the heterozygote genotype. The small size of the C/C subgroup (12 individuals) is also not comparable to the size of the other genotypes (467 for the R/R, and 145 for the R/C). This would need to be analysed in a cohort with a higher number of patients affected by the C/C genotype.

A second haplotype analysis was performed on all PRISM cases, this time with the addition of the p.R279C variant. This resulted in haplotypes of similar frequencies than the ones described above, with the addition of one common haplotype containing a change for the p.279C allele only. A severity study was performed on those haplotypes (not mutated, mutated for p.425M only, mutated for p.279C only) in the PRISM/SQSTM1- patients only in order to eliminate the association to be driven by mutations from the *SQSTM1* gene.

Here too, a nominal significance (P = 0.026) was reached for patients carrying the p.279C variant, for which the age of diagnosis was younger. Similar ages and C/C group size were found as in the association discussed above, confirming this result unlikely to be a true match.

As an overall result, it would seem that the association with PDB is more likely to be driven by the common variant p.R279C with a modest effect size rather than by the rare variants. This is opposite to the effect of mutations from the *SQSTM1* gene, for which rare variants have a large and cumulative effect associated with PDB (Albagha et al, 2013). Although disease severity association was found for the variants that were investigated, an adding effect on other markers of PDB such as environmental factors stays a possibility, and were not available from the PRISM trial data. Functional analyses are necessary to investigate the effect of those mutations on bone microenvironment, as well as to understand the mechanism of *RIN3* in bone metabolism.

CHAPTER FIVE
EXPRESSION OF *RIN3* IN BONE AND BONE CELLS

5 EXPRESSION OF *RIN3* IN BONE AND BONE CELLS

5.1 SUMMARY

Genetic investigations have shown that *RIN3* is a good candidate gene for PDB. In the context of bone metabolism, little is known about this gene. *RIN3* expression was found to decrease during differentiation of osteoclasts from PBMCs and was detected in calvarial osteoblasts (Kemp et al, 2014). High levels of RIN3 were reported in human mast cells (Janson et al, 2012) and peripheral blood cells (Kajiho et al, 2003). Here, I sought to investigate the expression pattern and localisation of *RIN3*.

Rin3 mRNA was investigated in mouse tissues and was highly expressed in lung and total crushed bone, while present at lower levels in brain and muscles. During osteoclast differentiation from BMDMs, *Rin3* mRNA decreased during macrophage differentiation before increasing during osteoclast formation to a level similar than found in bone marrow. *Rin3* mRNA expression in calvarial osteoblasts was 8.5 times lower than in osteoclasts. Protein levels of the 98kDa isoform of RIN3 tend to decrease gradually during osteoclast differentiation, while the 108kDa isoform seems to follow the mRNA pattern described above. This however needs to be repeated in additional experiments. Using a time course experiment, RIN3 protein levels of the 98kDa isoform dropped during the first 24h of RANKL stimulation, and remained as such for the next 72h. RIN3 was detected throughout the cytoplasm of osteoclasts from BMDMs and bone sections from Pagetic patients and controls.

In conclusion, I confirmed that RIN3 is expressed in bone, especially in osteoclast cells where it is diffusely expressed in the cytoplasm. Variation of *RIN3* during osteoclast differentiation was also assessed for mRNA and protein expression in mice.

5.2 INTRODUCTION

The previous genetic investigations highlighted a potential role for *RIN3* in PDB. However, the current knowledge about *RIN3*'s role in bone metabolism is very limited.

RIN3 is a GEF involved in the activation of small GTPases, proteins responsible for normal downstream signalling in the cell. More specifically, RIN3 is known to interact with Rab5 and Rab31, involved in vesicular trafficking and fusion of early endosomes (Kajiho et al, 2003; Kajiho et al, 2011). This could place RIN3 as a good candidate protein for PDB. Indeed, the role of small GTPases is well characterised in osteoclasts function, especially Rab proteins and their role in vesicular trafficking near the ruffled border, crucial for bone resorption and the transport of molecules and protein, from and to the resorption area (Itzstein et al, 2011). RIN3 is also involved in endocytosis, and binds to Amphiphysin II, a protein involved in the mediation of receptor-induced endocytosis (Kajiho et al, 2003). RIN3 was additionally shown to be involved in the internalization of the receptor tyrosine kinase KIT after SCF stimulation of mast cells (Janson et al, 2012).

RIN3 is highly expressed in human mast cells, but not in B cells, myeloblasts, T cells, fibroblasts and glioblastoma cell lines (Janson et al, 2012). RIN3 was also detected in human peripheral blood cells in high amount, but showed lower levels in brain and muscle (Kajiho et al, 2003). In the bone microenvironment, *RIN3* expression was found to decrease during the first 3 days of osteoclast differentiation from PBMCs, and was detected in calvarial osteoblasts (Kemp et al, 2014).

The aim of this chapter was to establish the expression pattern of *RIN3* in the bone microenvironment and its cellular location in both human and murine osteoclast cells.

5.3 METHODS

The expression of mRNA *Rin3* was measured in the following mouse tissues: lung, total crushed bone, liver, kidney, brain and muscle. For this, cDNA was obtained by reverse transcription, was used for quantitative real time PCR as described in Section 2.4. mRNA and protein levels (Section 2.5) were assessed by qPCR and western blot on the three key stages of osteoclast differentiation from primary BMDMs: bone marrow, upon tissue collection, macrophages, which have been stimulated in M-CSF for two days, and osteoclasts, differentiated after 4 days of RANKL and M-CSF stimulation from those macrophages (Section 2.3.1). RIN3 protein levels were also investigated through a daily time course, during the four day-RANKL stimulation of osteoclasts (Section 2.5). Expression of mRNA *Rin3* in calvarial osteoblasts was also analysed (Section 2.3.2).

Localisation of RIN3 was assessed using immunostaining as described in Section 2.6, for which the protein of interest was labelled by green fluorescence in cultured osteoclasts differentiated from BMDMs. Nuclei were counterstained using DAPI.

Immunohistochemistry was performed as described in Section 2.7, on human bone samples from Pagetic, GCT, osteosarcoma and osteoclastoma affected patients. Non-Pagetic controls were also verified. Lung was used as positive and negative controls, and osteosarcoma sections were used as negative control.

5.4 RESULTS

5.4.1 Expression of Rin3 in mouse tissues

mRNA levels of *Rin3* were quantified in different tissues. The expression was found to be the highest in lung and gradually lowers in decreasing order from total crushed whole bone, to liver, kidney, brain and muscle as shown in Figure 5.1. Variations of the housekeeping gene were observed, where muscle showed the highest expression of ribosomal 18S RNA, followed by bone and the other tissues (data not shown).

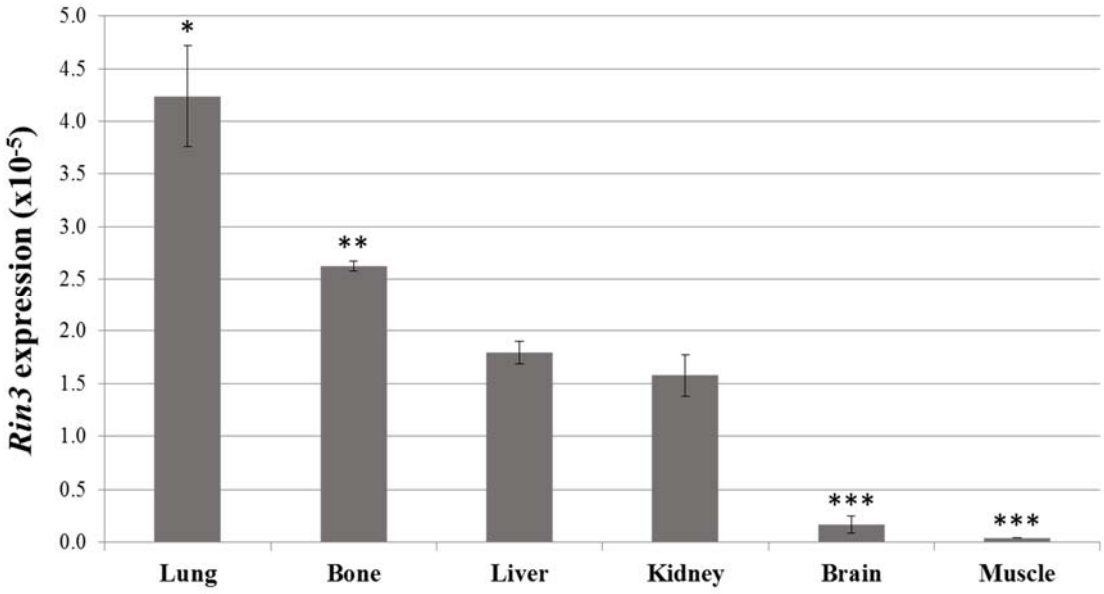

Figure 5.1: Expression of mRNA Rin3 in mouse tissues.
mRNA levels were measured in lung, total crushed bone, liver, kidney, brain and muscle from mice. The expression of *Rin3* was normalised with 18S rRNA. Values are presented as mean ± SEM from one independent experiment in triplicates for all. *$p<0.05$ from all, ** $p<0.05$ from all but liver. ***$p<0.05$ from all but brain and muscle.

5.4.2 Rin3 mRNA is expressed in cells of the bone micro environment

The expression of *Rin3* was then measured during osteoclast differentiation from M-CSF and RANKL stimulated osteoclasts. mRNA *Rin3* expression levels were also compared to calvarial osteoblasts and murine total crushed bone (Figure 5.2).

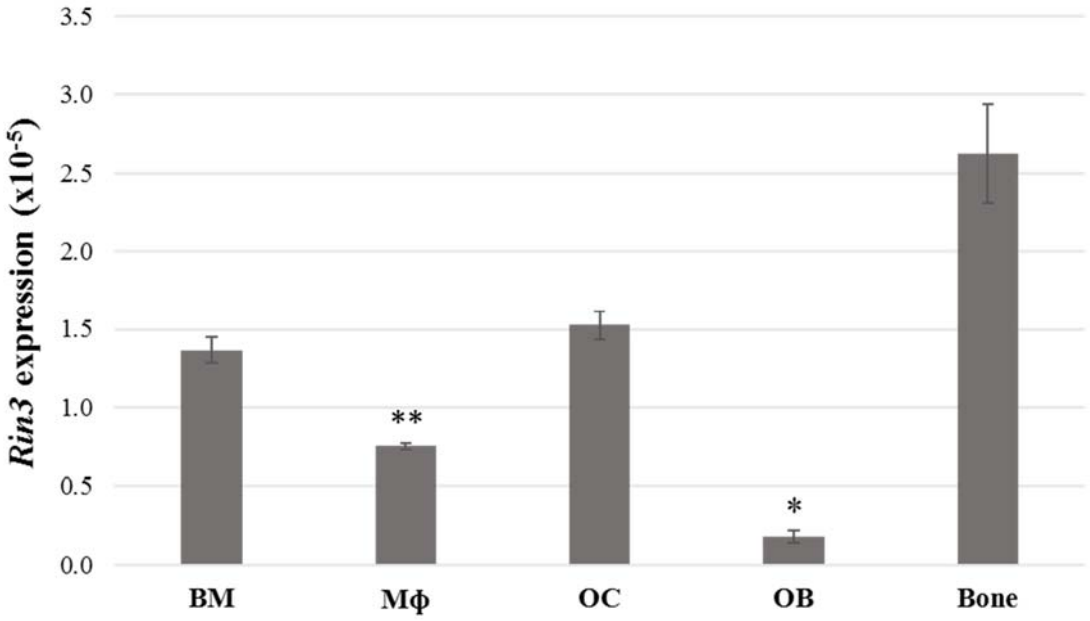

Figure 5.2: mRNA expression of Rin3 in the bone microenvironment.
mRNA levels of *Rin3* in bone marrow (BM), M-CSF-stimulated macrophages (Mϕ), M-CSF and RANKL-stimulated osteoclasts (OC), total crushed bone from mice and calvarial osteoblasts (OB). The expression of *Rin3* was normalised with 18S rRNA. Values are presented as mean ± SEM from three independent experiments in duplicates for all but OB and bone (one experiment in triplicates). *$p<0.05$ from all, **$p<0.05$ from BM and OC.

Rin3 expression was found to significantly vary at each steps of osteoclast differentiation. The mRNA levels decrease after macrophage differentiation, before increasing again during OC differentiation to a similar level than originally found in bone marrow samples. Expression in osteoclasts is found to be about 8.5 times more abundant than in osteoblasts, while total crushed bone seems to be expressing *Rin3* the most from these samples.

5.4.3 RIN3 protein is expressed in the murine bone micro environment

Protein expression of RIN3 was also assessed during osteoclast differentiation from BMDMs. Two bands were observed around the expected size of interest (108KDa). One, slightly below 100kDa corresponds to the 98KDa isoform of RIN3. The second band, slightly below 120kDa is likely to correspond to the biggest isoform of RIN3 (108kDa). This was the size expected to be found by the manufacturer's instructions. Figure 5.3 shows the deduced levels of RIN3 (panel A) for each band, corrected by β-actin (panel B). For the lightest isoform (98kDa), RIN3 gradually decreases during osteoclast differentiation (panel C). For the 108kDa isoform, the bands were particularly faint and although a similar pattern to the one found by mRNA could be suggested, no significant variation of expression was observed (panel D).

The expression of RIN3 was then investigated in more detail during osteoclast differentiation, from M-CSF derived macrophages. Proteins were extracted first on M-CSF differentiated macrophages (d0) and this was repeated daily until full osteoclast formation under RANKL and M-CSF stimulation (d1, d2, d3, d4). The results are showed in Figure 5.4, and were measured again for each band (panels A and B). The isoform at 98kDa shows a significant drop of the RIN3 protein expression during the first 24h of RANKL addition in the cell medium (panel C). The low levels did not vary from day one until termination of the culture. For the isoform of 108kDa, no significant variation could be observed. However, in agreement with Figure 5.3, it seems that RIN3 tends to increase during osteoclast differentiation (panel D).

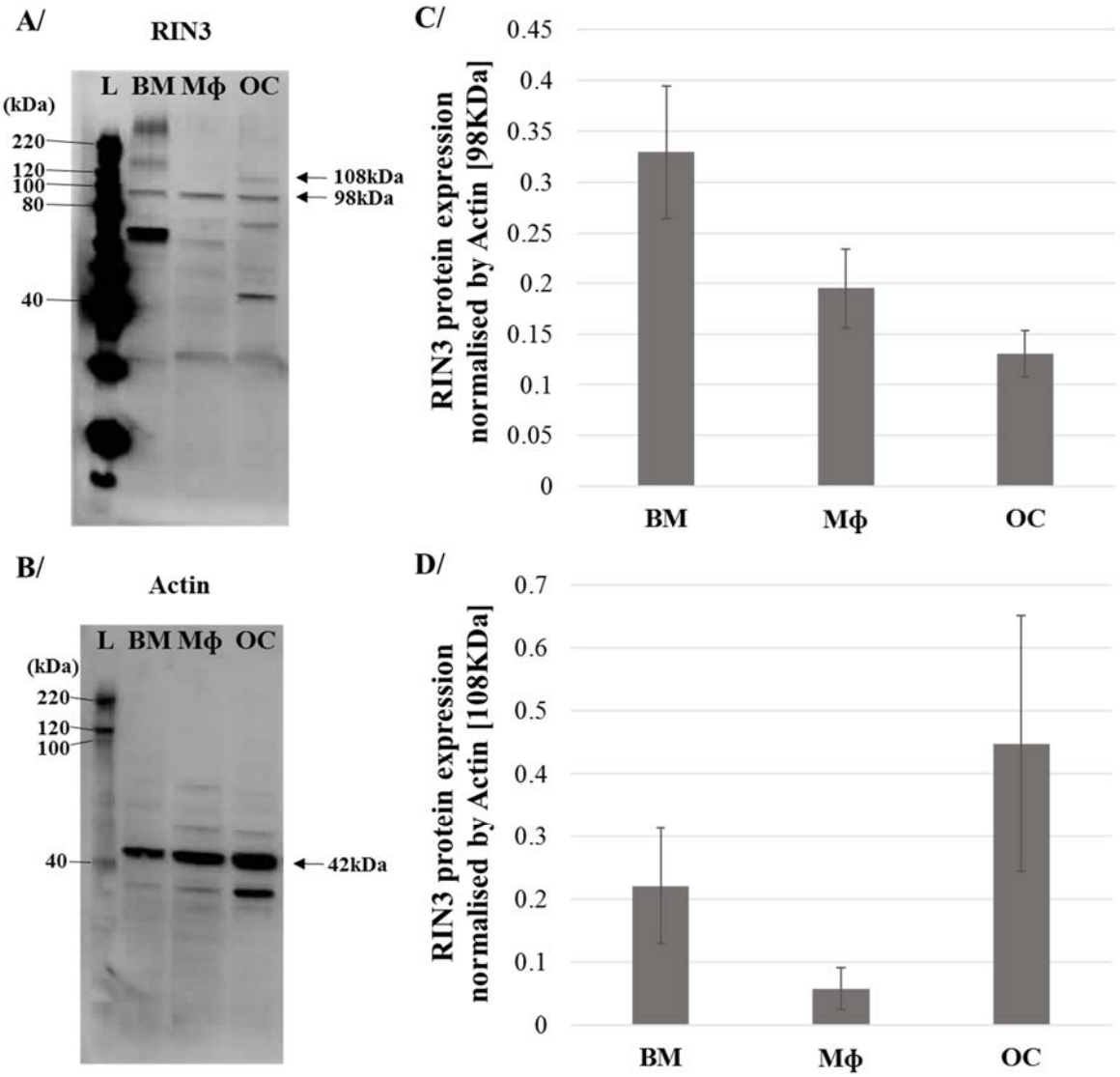

Figure 5.3: Expression of protein RIN3 in BM, Mϕ and OC under RANKL stimulation. RIN3 shows two bands at 98kDa and 108kDa (A) while Actin is expected at 42kDa (B). Protein levels of the 98KDa and 108kDa isoforms of RIN3 were quantified in bone marrow (BM), M-CSF-stimulated macrophages (Mϕ), M-CSF and RANKL-stimulated osteoclasts (OC). Both 98kDa (C) and 108kDa (D) isoforms of RIN3 were normalised by Actin. Values are presented as mean ± SEM from four independent experiments.

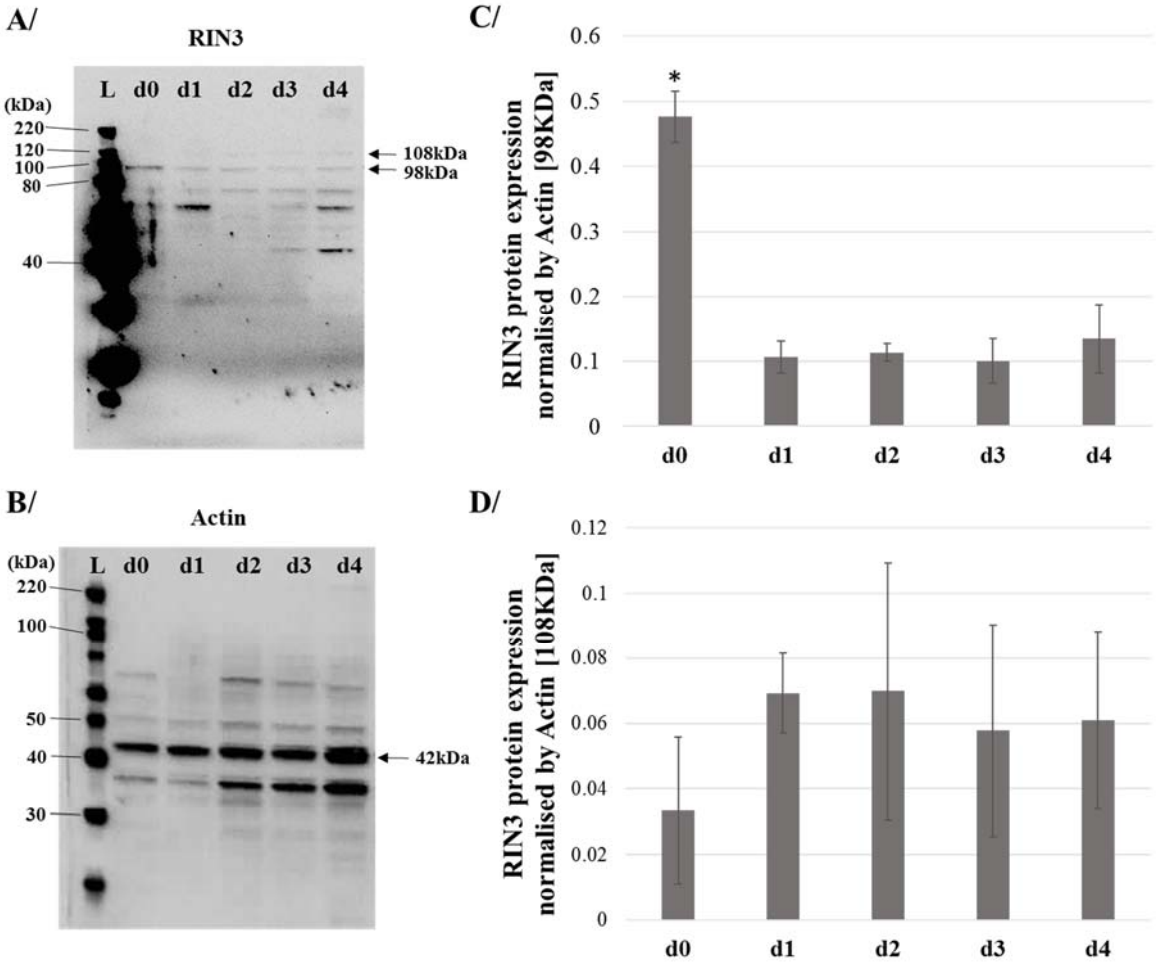

Figure 5.4: Expression of protein RIN3 during osteoclast differentiation under RANKL stimulation.

RIN3 shows two bands at 98kDa and 108kDa (A) while Actin is expected at 42kDa (B). Protein expression was measured during RANKL stimulation (d0), every day for 4 days (d1, d2, d3, d4) until development of osteoclasts from primary BMDMs. Both 98kDa (C) and 108kDa (D) isoforms of RIN3 were normalised by Actin. Values are presented as mean ± SEM from three independent experiments. *$p<0.05$ from all.

5.4.4 RIN3 is expressed through the cytoplasm of osteoclasts cultured from mice

The cellular localisation of RIN3 was investigated on osteoclasts stimulated with M-CSF and RANKL for 4 days, obtained from mouse BMDMs. The cells were studied using immunofluorescence as described in Section 2.6. RIN3 was stained using Alexa Fluor® labelled antibodies. The pictures were captured using inverted microscopy and green fluorescence is observed thorough the cytoplasm of the osteoclasts (Figure 5.5, panel D). A stronger signal can be observed near the plasma membrane (blue arrows, panel D) and stronger specks can be see through the cytoplasm (red arrows, panel D).

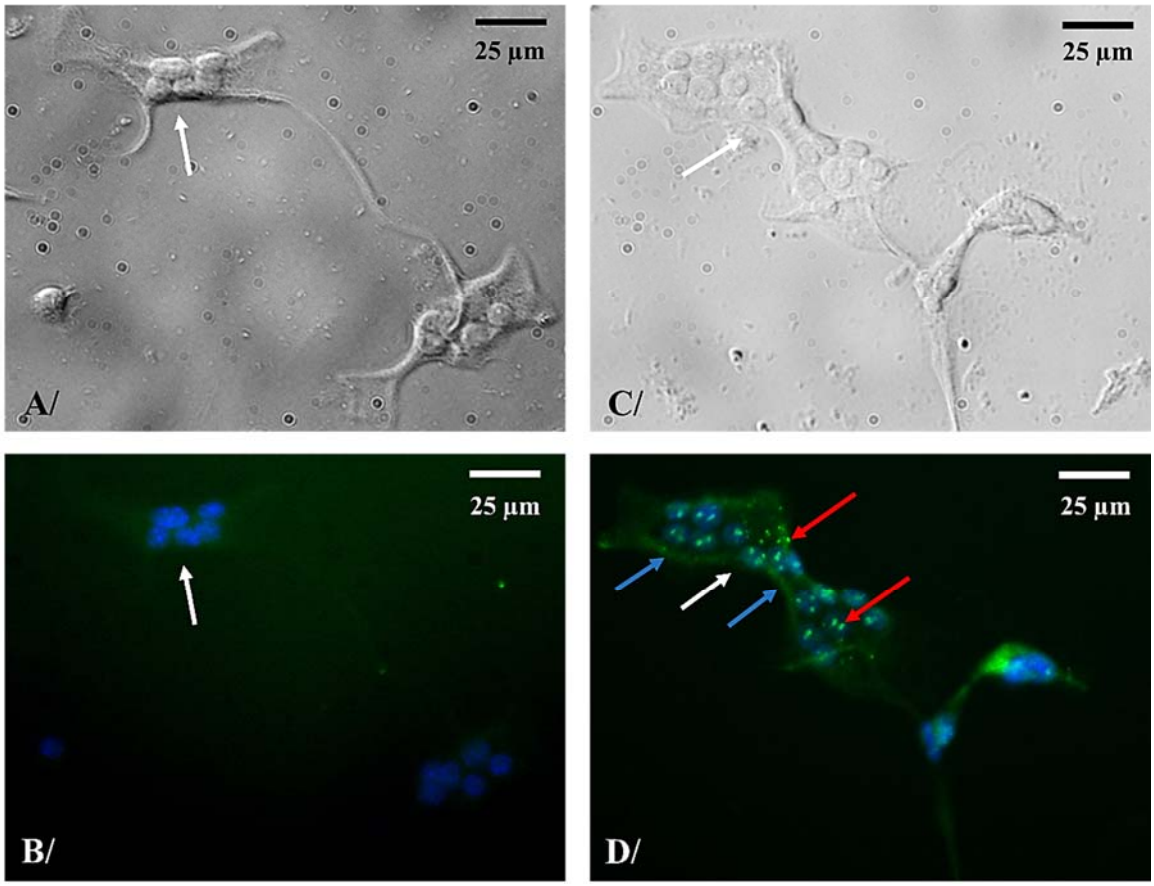

Figure 5.5: Pictures of cultured M-CSF and RANKL stimulated mouse bone marrow derived-osteoclasts stained by immunofluorescence for RIN3.

Panels A (phase) and B (merged) show the negative control where the primary anti-RIN3 antibody was replaced by the diluent. Panels C (phase) and D (merged) show the osteoclasts labelled with RIN3. Cultured osteoclasts are pointed by white arrows, specks by red arrows and concentrated staining by blue arrows. RIN3 is green-fluorescent and nuclei are dyed in blue by DAPI counterstaining. The pictures were merged using ImageJ. Magnification x40.

5.4.5 RIN3 is highly expressed through the cytoplasm of human osteoclasts

Finally, the expression of RIN3 was investigated in human bone samples using antigen retrieval immunohistochemistry (Section 2.7). Osteosarcoma was used as a negative control (Figure 5.6, panel A) and human lung was used as a negative (Figure 5.6, panel B) and positive control (Figure 5.6, panel C). Bone samples from Pagetic (Figure 5.6, panel D), non-Pagetic (Figure 5.6, panel E), osteoclastoma (Figure 5.6, panel F), GCT (Figure 5.6, panel G), and osteosarcoma (Figure 5.6, panel H) patients were investigated. All osteoclasts showed a strong and specific staining for RIN3 (black arrows).

Although RIN3 is expressed diffusely in the cytoplasm of the cells for all samples analysed here, a stronger staining can be seen near the membrane of the osteoclasts, particularly in the Pagetic and GCT samples (red arrows).

Osteoblasts and osteocytes were however not expressing RIN3 in those samples (data not shown).

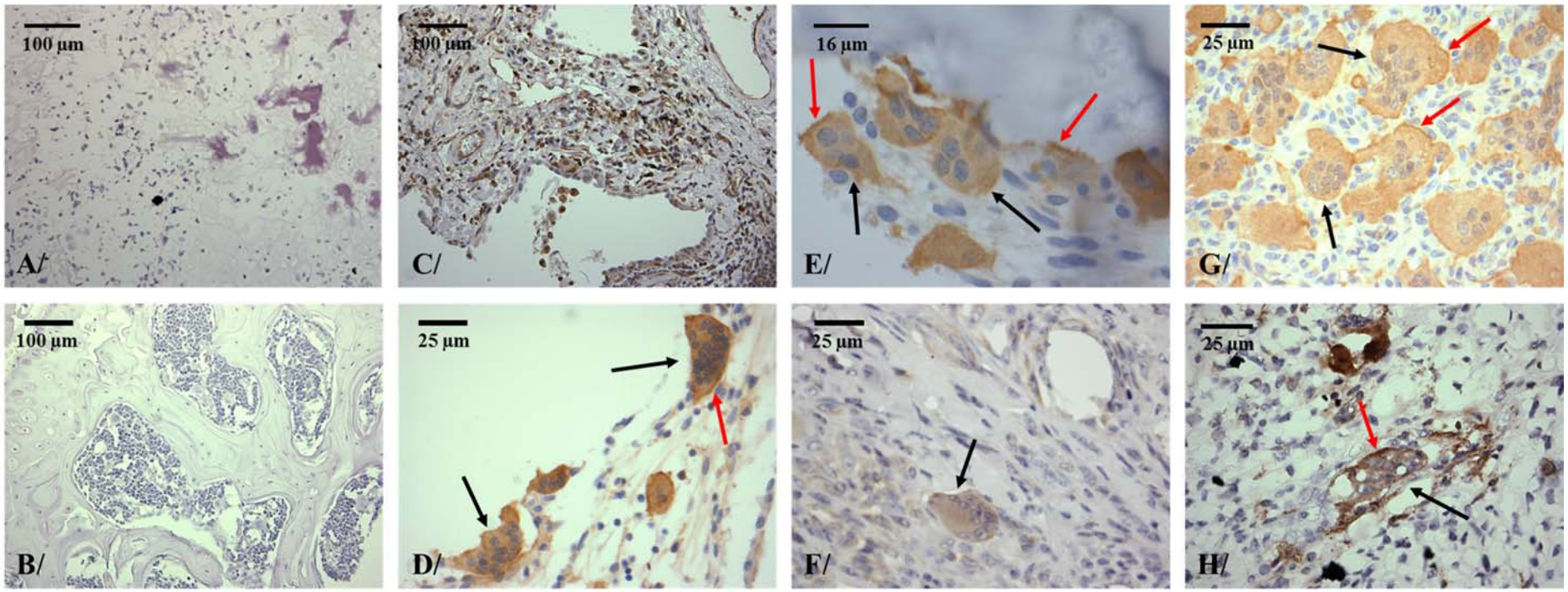

Figure 5.6: Pictures of tissue sections stained by immunohistochemistry for RIN3.

Sections of osteosarcoma (A) used as negative control, and of human lung used as negative (B) and positive (C) controls against Pagetic sample (D), non-Pagetic sample (E), osteoclastoma (F), GCT sample (G), and osteosarcoma sample stained for RIN3 (H). All at magnification x40 but controls (x10) and non-Pagetic sample (x60). Example of stained osteoclasts are pointed by black arrows, and enhanced staining are pointed by red arrows.

5.5 DISCUSSION

Previous studies showed that *RIN3* was highly expressed in human mast cells, compared to B cells, myeloblasts, T cells, fibroblasts, glioblastoma cell lines and osteosarcoma cell lines showed a low expression of *RIN3* (Janson et al, 2012). *RIN3* was detected in calvarial osteoblasts and is down-regulated during human PBMCs osteoclasts. *RIN3* expression is also decreased in osteoporotic iliac biopsies compared to healthy postmenopausal controls, suggestive of a role in bone metabolism (Kemp et al, 2014).

Here, *Rin3* was measured in six tissues extracted from mice, using qPCR. Total crushed bone had the second highest relative level of mRNA *Rin3*, and was significantly different from all tissues except from liver. Lung was found to have the highest amount of *Rin3*, which was 1.6 times greater than in bone. This was expected as mast cells were found to be abundant in investigations reported by Janson and colleagues (2012). The lowest levels of *Rin3* were found in muscle and brain and were 100 and a 25 times fold respectively, lower than in lung. Similar findings were reported in human tissues as described by Kajiho and colleagues (Kajiho et al, 2003). The mRNA for *Rin3* was also quantified during osteoclast differentiation from M-CSF and RANKL stimulated osteoclasts from BMDMs. For this, cells were analysed upon bone marrow flushing, after 2 days of M-CSF stimulation (macrophages), and after 4 days of M-CSF and RANKL stimulation (osteoclasts).

Rin3 was shown to significantly vary during osteoclast differentiation, suggestive of a role in osteoclastogenesis. Indeed, the *Rin3* mRNA expression decreased almost by half after macrophage differentiation and proliferation, before increasing in osteoclasts to a level similar than initially found in bone marrow. A similar trend was detected in osteoclasts from PBMCs by Kemp and colleagues (2014). A pattern of expression showing a down-regulation of *RIN3* during early differentiation phase (up to day 3), before modestly increasing again and stabilising during late differentiation phase (day 7 to day 21) (Kemp et al, 2014). Although this final increase was not as significant as in osteoclasts derived from murine BMDMs, there was a similar pattern of expression between the two studies. Calvarial osteoblasts were also investigated here and showed a low expression of mRNA. In comparison to osteoclasts, the level of *Rin3* was about 8.5 times lower. The RNA expression of *RIN3* was also investigated during calvarial osteoblast differentiation by Kemp and colleagues, but there was no comparison between the *Rin3* mRNA levels of expression in osteoclasts and osteoblasts (Kemp et al, 2014). Total crushed bone showed a trend towards a higher level of mRNA *Rin3,* once compared to bone marrow, macrophages, osteoclasts and osteoblasts.

As for the mRNA, the protein levels of RIN3 were assessed on bone marrow, macrophages and osteoclasts samples from BMDMs. It is likely that two isoforms of RIN3 were detected. The most predominant one corresponded to the isoform of 98kDa, and showed a band at the expected size. Unexpectedly, this isoform of RIN3 showed a trend towards a decrease from bone marrow to macrophage, and further decrease from macrophages to osteoclasts. Correlations between mRNA and protein levels have not always been clear.

Differences of expression pattern between *Rin3* mRNA and protein detected here could be explained by variations in the stability of mRNA, post-transcriptional mechanisms, or a short protein half-life, although this is not clear yet (Greenbaum et al, 2003).

Another isoform was seen and most likely corresponds to the heaviest isoform of RIN3, expected at 108kDa. According to the manufacturer's instructions, this was the expected band. Analysis of this isoform during osteoclast differentiation revealed a similar trend of expression than the mRNA one, for which the probe was targeted in a region only found in the 108kDa isoform only. Indeed, a trend where RIN3 decreases during macrophage differentiation and increases again during osteoclast differentiation to a level similar than initially observed in bone marrow was observed. This was however not significant, probably due to the faintness of the bands, and additional experiments with a higher amount of protein loading are needed to confirm this expression pattern. The other two known isoforms of RIN3 are of small sizes (22 and 14kDa) and were not seen on the western blots.

To further investigate the decrease of RIN3 protein levels during osteoclast formation, a time course was performed on M-CSF derived macrophages. Cells were collected daily, until full osteoclasts differentiation. The protein expression of the lightest isoform of RIN3 (98kDa) was corrected by β-actin and interestingly showed a significant decrease of a 4.5-fold during the first 24 hours of RANKL stimulation and stayed low for the next 72 hours.

The heaviest isoform (108kDa) did not show significant variation of expression, however a slight increase of RIN3 can be suggested during the first 48h, before slightly decreasing. As explained previous this is probably due to the faintness of the bands and additional experiments with a higher protein concentration is needed to confirm such trend.

Overall, the expression of *RIN3* is in accordance with what is published in the literature, whether it is for expression pattern in different generic tissues, during BMDMs differentiation or in calvarial osteoblasts. Within my investigation, it seems that protein and mRNA levels of the 108KDa are following similar trends (although this needs to be pursued for confirmation by additional western blot analyses), and one explanation comes to mind as *RIN3* expression seems to oppose M-CSF stimulations in BMDM cultures. Knowing the role of *RIN3* in the recycling of tyrosine kinase receptors (Janson et al, 2012), it could be involved in the downregulation of CSF1R. It is not clear however as to why the lighter isoform, which is the most abundant, is downregulated during osteoclast expression.

Localisation of RIN3 in cultured osteoclasts was assessed by immunofluorescence. RIN3 was expressed diffusely in the cytoplasm of those cells, and showed a stronger staining by the border of the cell. This would be justified by the GEF activity of RIN3 for Rab5 and Rab31, both involved in membrane trafficking to early and late endosomes respectively, as described by Kajiho and colleagues (Kajiho et al, 2003). Specks were also detected through the cells and could correspond to a vesicular location of RIN3, as described by the same group in HeLa transfected cells (Kajiho et al, 2003).

Finally, immunohistochemistry was used to assess the levels of RIN3 in human bone samples. For this, Pagetic bone, non-Pagetic control, GCT, osteoclastoma and osteosarcoma were stained, and all showed a strong staining for RIN3 in osteoclasts. Similarly to the immunofluorescence, the control and GCT show a stronger staining by the border of the cells, in accordance with the immunofluorescence result.

Interestingly, the reported protein expression of RIN3 in the Saos-2 osteosarcoma cell line was quite low, especially compared to HMC1 and LAD2 cell lines (Janson et al, 2012). An explanation could be that osteoclasts make up a small percentage of the total bone cells (up to 2 % in a normal bone environment, see Section 1.1.2) and as my immunocytochemistry suggest, osteoblasts and osteocytes do not express much RIN3. The Saos-2 cell line is used as osteoblastic model, and is unlikely to see great amount of RIN3 (Pautke et al, 2004). It also is in accordance with the small quantities that were seen in western blots here, despite loading sufficient amount of protein lysate. No specks were seen by immunohistochemistry in the osteoclasts, however this is probably due to the sensitivity of the assay, compared to immunofluorescence.

In conclusion, the work found in the literature is in accordance with what was detected here. *RIN3* is expressed in the human and mouse bone microenvironment, and significantly fluctuates during osteoclast differentiation from BMDMs, suggestive of a role in the bone metabolism.

CHAPTER SIX
PHENOTYPE ANALYSIS OF *Rin3* DEFICIENT MICE

6 PHENOTYPE ANALYSIS OF *Rin3* DEFICIENT MICE

6.1 SUMMARY

RIN3 expression pattern was established in mice for the first time in the previous chapter. It is highly expressed in total crushed bone and varies significantly during osteoclast differentiation. RIN3 is localised through the cytoplasm of osteoclasts, especially by the border of the cells. *Rin3* was also detected at low levels in calvarial osteoblasts.

In order to further understand the role of *RIN3* in bone metabolism, skeletal and cellular changes were investigated in young female mice lacking the *Rin3* gene (*Rin3*$^{-/-}$) and were compared to wild type mice (WT). MicroCT analyses showed that *Rin3*$^{-/-}$ mice had an increased bone mass and trabecular number in both tibia and femur. Histomorphometric analyses of trabecular femur showed that *Rin3*$^{-/-}$ mice had an increased trabecular bone surface and a decreased resorption surface, which is occupied by active osteoclasts. Calvarial osteoblasts cultured from *Rin3*$^{-/-}$ mice show a trend towards increased differentiation level and mineralised nodule formation, however additional experiments are necessary to confirm this. Osteoclasts differentiated from mice bone marrow showed no difference in number, formation or survival patterns between the two groups.

In conclusion, *RIN3* was proven to play a role in bone in young mice and could have a positive effect on osteoclast activity. Additional *in vitro* and *ex vivo* experiments on bone resorption need to be repeated to confirm such suggestions.

6.2 INTRODUCTION

The role of *RIN3* in bone metabolism has been poorly studied so far. RIN3 has been detected at low levels in the osteosarcoma Saos-2 cell line (Janson et al, 2012) and calvarial osteoblasts (Kemp et al, 2014). *RIN3* has been also analysed in osteoclasts from PBMCs and was found to decrease in the first 3 days of differentiation before increasing again and stabilising until the end of the 21 days culture (Kemp et al, 2014).

The functional work presented in Chapter 5 place as a strong candidate for PDB. Total crushed bone from mice showed a high level of *Rin3* mRNA, and mRNA and protein levels were established during osteoclast differentiation. The 98kDa isoform of RIN3 was found to drop drastically from the addition of RANKL to the cells used for osteoclast differentiation, and stayed low until termination of the culture. The 108kDa isoform of RIN3 however, as for its mRNA, showed a decrease during macrophage proliferation and an increase during RANKL stimulation. Low levels of mRNA were detected in calvarial osteoblasts, and were about 8.5 times lower than found in cultured osteoclasts. RIN3 was found to be expressed diffusely through the cytoplasm of osteoclasts in human bone and cultured osteoclast from BMDMs, and a stronger concentration of RIN3 was noticeable by the border of the cells. Although RIN3 was not detected in osteoblasts or osteocytes in human bone samples, RIN3's expression in osteoclasts places it as a good candidate in the context of PDB where osteoclasts are over-active (Meunier et al, 1980).

The main role of RIN3 is the activation of small GTPases, through its GEF function. Small GTPases are known to have a crucial role in osteoclast resorption function, as they act as switches of molecular signalling pathways. As a result they are involved in many cellular mechanisms, including autophagy or cytoskeletal re-organisation, crucial for osteoclast activation during bone resorption (Itzstein et al, 2011). RIN3 interacts with Rab5, which is the most described small GTPase (Kajiho et al, 2003), as well as Rab31 (Kajiho et al, 2011). Both are involved in molecular trafficking in early and late (respectively) endosomes, which are key features of the osteoclastic bone resorption. Another mechanism in which RIN3 can be relevant is tyrosine kinase receptor recycling (Janson et al, 2012). Indeed, as mentioned in Section 1.1.2, the differentiation of osteoclasts is mediated by cytokines like RANKL and M-CSF which bind to receptors located on the membrane of the cells. CSF1R is recognised by M-CSF for differentiation of macrophages from osteoclast progenitors is a key tyrosine kinase receptor of osteoclastogenesis and a potential target for RIN3. Small GTPases are also involved in autophagy as described in Section 1.5.3 (Ao et al, 2014). Autophagy-related proteins have been reported in PDB and PDB-like diseases (p62, OPTN, VCP - Section 1.4) and is a mechanism to consider for RIN3's role in PDB.

The aim of this chapter was to investigate *Rin3*-deficient young mice on a mixed C57BL/6 x 129/OlaHsd background, to confirm a functional role for *RIN3* in bone metabolism on an *in vivo* scale. Skeletal phenotypes were investigated using microCT scanning and cellular changes in bone sections were assessed by histomorphometry in metaphysis of the femur. Osteoblast differentiation and mineralisation rate were measured on cultured calvarial osteoblasts and calcein stained bone sections, while formation and survival pattern were assessed in osteoclasts cultured from BMDMs.

6.3 METHODS

Bone phenotypes were investigated in 8 week old C57BL/6 crossed with 129/OlaHsd *Rin3*$^{-/-}$mice, and WT littermates were used as controls. Mice used for calvarial osteoblast cultures were from 2 days old pups, generated from *Rin3*$^{-/-}$ or WT parents (Section 2.3.2). Changes in trabecular bone were analysed in femurs, tibias and spines by microCT, while cortical bones were investigated in femurs as described in Section 2.8.3. This was performed on 14 *Rin3*$^{-/-}$ and 11 WT 8 weeks old female mice. Cellular changes were assessed by histomorphometric studies on the proximal metaphysis of the right femurs as described in Section 2.8.4. Osteoclast phenotypes were investigated by TRAcP staining on 13 *Rin3*$^{-/-}$ and 10 WT mice. Osteoblast phenotypes and bone mineralisation rates were analysed by calcein staining of 9 *Rin3*$^{-/-}$ and 10 WT femurs. Changes in cultured osteoclasts and osteoblasts from *Rin3*$^{-/-}$ and WT were investigated (Sections 2.3.1 and 2.3.2). Once M-CSF and RANKL-generated, TRAcP-positive osteoclasts with 3 or more nuclei were manually counted, and a second count was performed on large osteoclasts with at least 10 nuclei. A survival assay was also carried out. For this, BMDMs-generated osteoclasts were counted at 0h, 4h, 8h, 24h, 48h, and 72h after RANKL being removed from the media. Mineralised nodule formation was also investigated in cultured osteoblasts. For this, the cells were stimulated using osteogenic medium (50μg/ml vitamin C and 3mM β-GP) for up to three weeks. The cultures were then fixed at the end of one week, two weeks and three weeks of incubation, and nodules were stained using Alizarin red staining. Once dried, the deposits were destained and absorbance was measured at 562nm against a standard curve. Differentiation levels in osteoblasts were also assessed by measuring the activity of ALP in cell lysates.

6.4 RESULTS

6.4.1 Rin3 deficient mice have a normal body weight

Body weight was investigated in *Rin3*$^{-/-}$ mice before tissue collection. They were of similar size and weight compared to WT littermates, and were generally healthy (Figure 6.1).

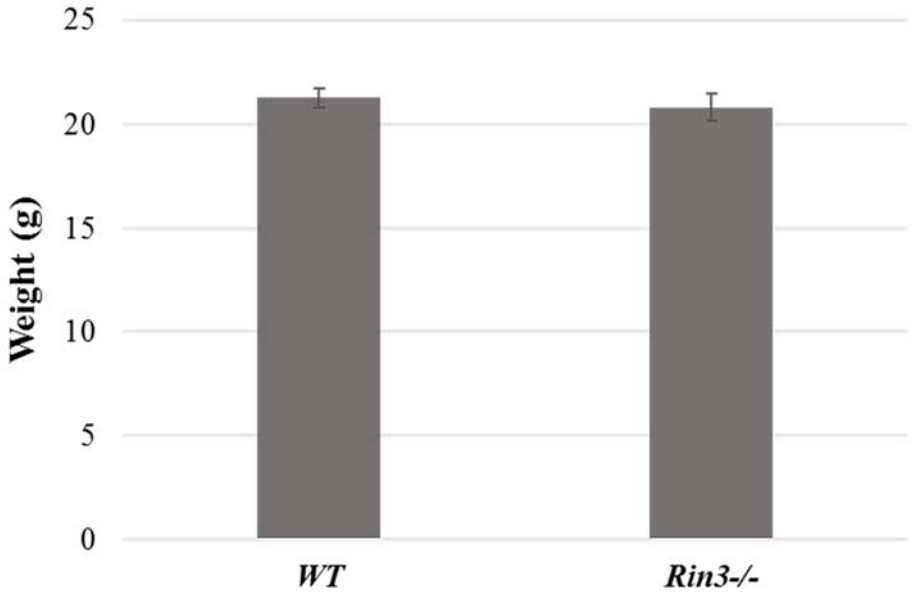

Figure 6.1: Body weight of Rin3$^{-/-}$ female mice at age 8 weeks.
Values are mean ± SEM from 14 *Rin3*$^{-/-}$ mice and 11 WT mice.

6.4.2 Rin3 deficient mice have an increased bone mass and trabecular number

Skeletal phenotypes in young female mice lacking the *Rin3* gene were investigated using microCT analysis. Trabecular bone was investigated in femur, tibia and spine, and cortical bone was studied in femur. Results are summarized in Figures 6.2 to 6.5 and Table 6.1.

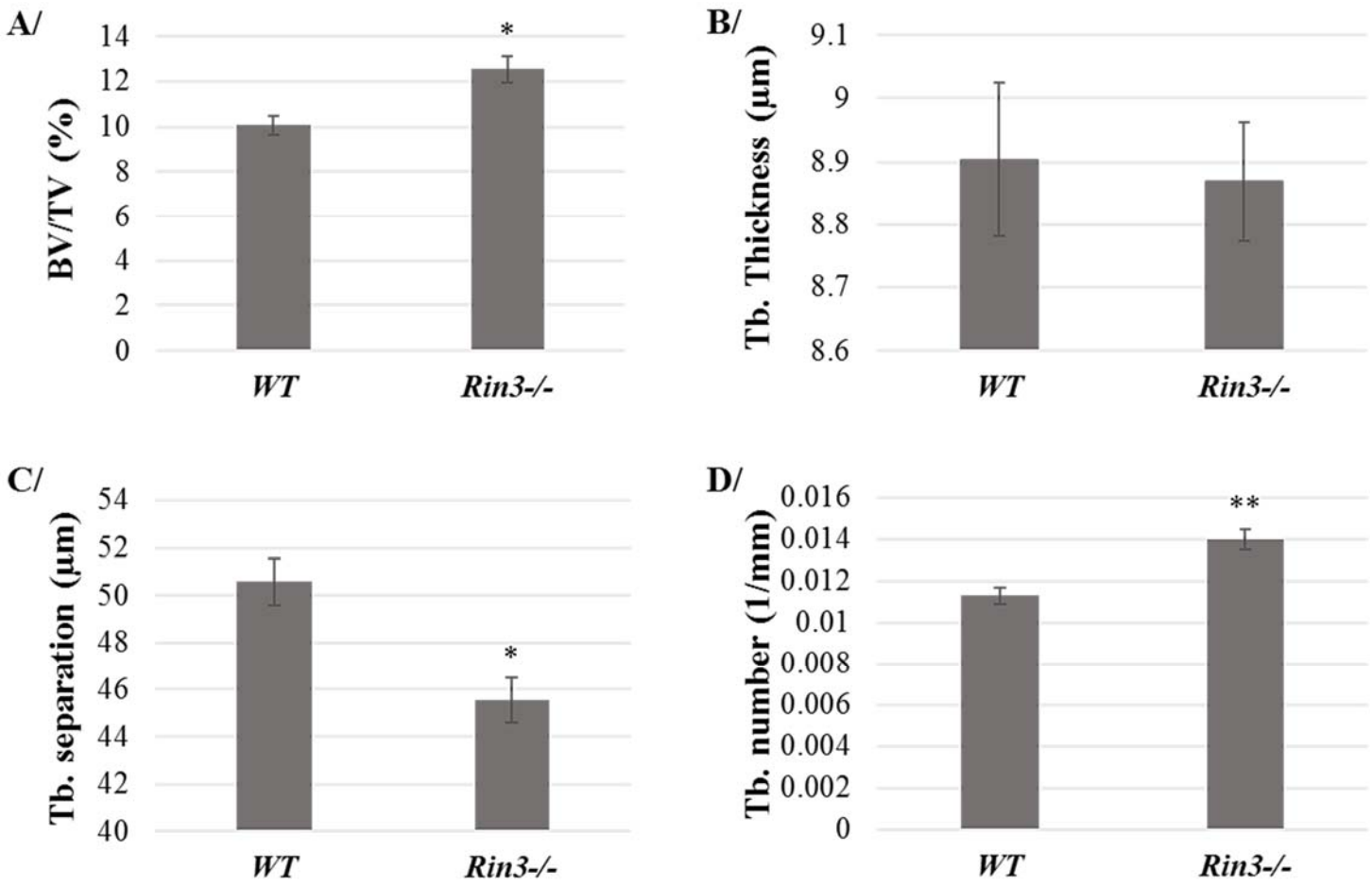

Figure 6.2: MicroCT results on the Rin3$^{-/-}$ mice and WT controls, for the femoral trabecular bone.

Young *Rin3*$^{-/-}$ and WT female mice were analysed for trabecular phenotypes in metaphysis of both left and right femurs. The following parameters were investigated: A/ Trabecular bone volume (BV/TV); B/ Trabecular thickness (Tb. Thickness); C/ Trabecular separation (Tb. Separation); D/ Trabecular number (Tb. Number). Values are mean ± SEM of 14 *Rin3*$^{-/-}$ mice and 11 WT mice. *$p<0.05$ and **$p<0.001$ from WT controls.

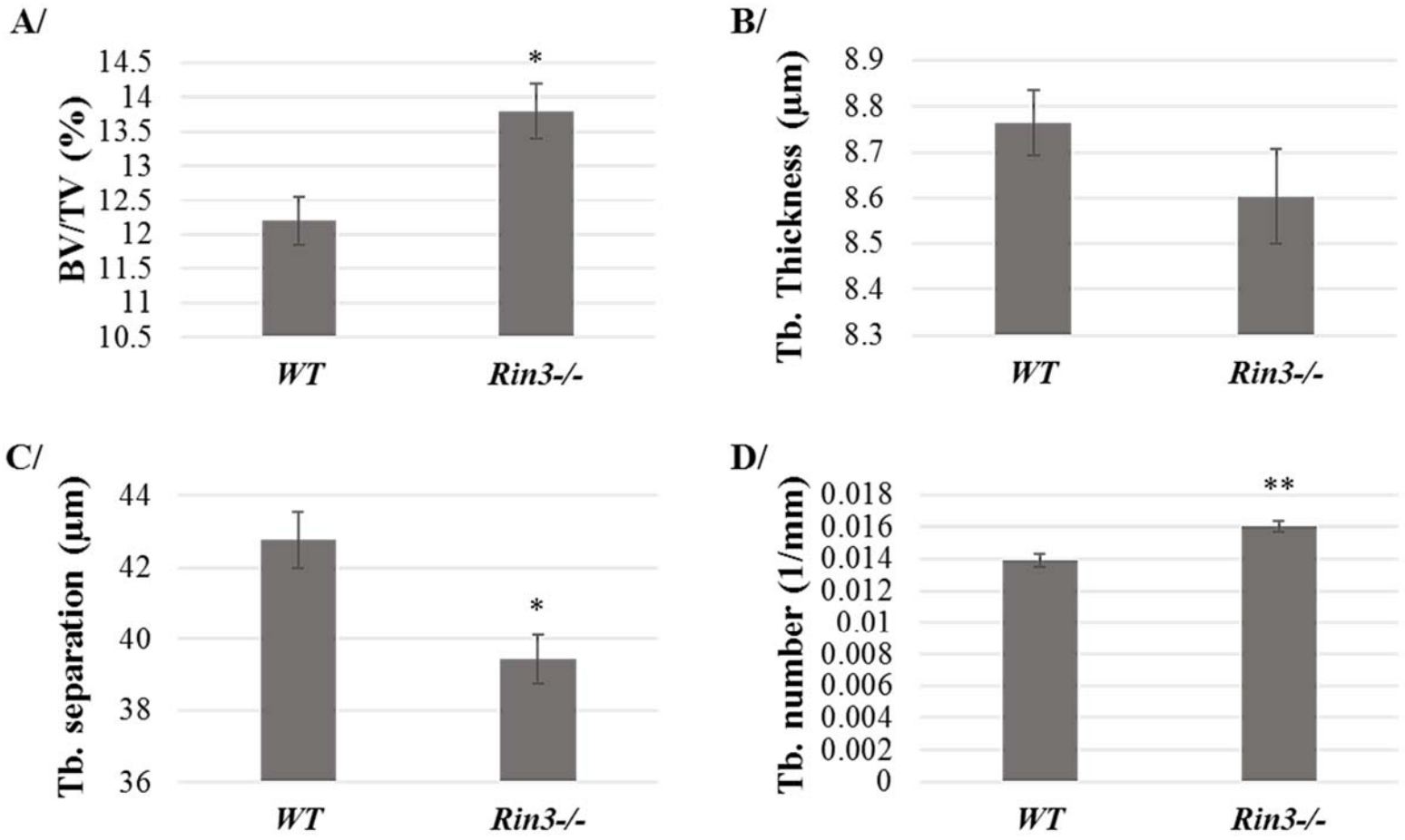

Figure 6.3: MicroCT results on the Rin3$^{-/-}$ mice and WT controls, for the tibial trabecular bone.

Young *Rin3*$^{-/-}$ and WT female mice were analysed for trabecular phenotypes in metaphysis of both left and right tibias. The following parameters were investigated: A/ Trabecular bone volume (BV/TV); B/ Trabecular thickness (Tb. Thickness); C/ Trabecular separation (Tb. Separation); D/ Trabecular number (Tb. Number). Values are mean ± SEM of 14 *Rin3*$^{-/-}$ mice and 11 WT mice. *p<0.01, **p<0.001 from WT controls.

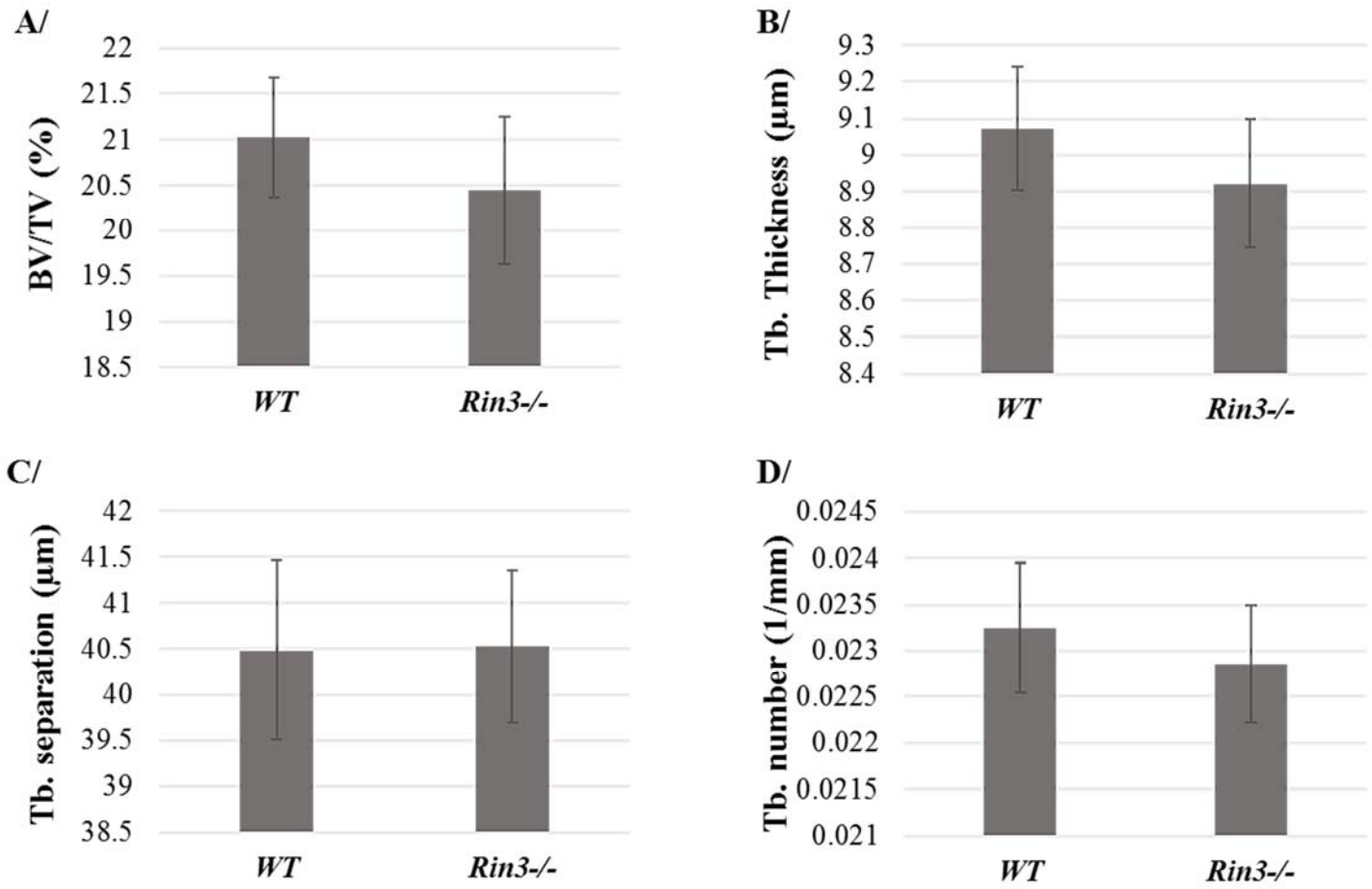

Figure 6.4: MicroCT results on the Rin3$^{-/-}$ mice and WT controls, for the trabecular bone of the spine.

Young *Rin3*$^{-/-}$ and WT female mice were analysed for trabecular phenotypes in spines. The following parameters were investigated: A/ Trabecular bone volume (BV/TV); B/ Trabecular thickness (Tb. Thickness); C/ Trabecular separation (Tb. Separation); D/ Trabecular number (Tb. Number). Values are mean ± SEM of 14 *Rin3*$^{-/-}$ mice and 11 WT mice.

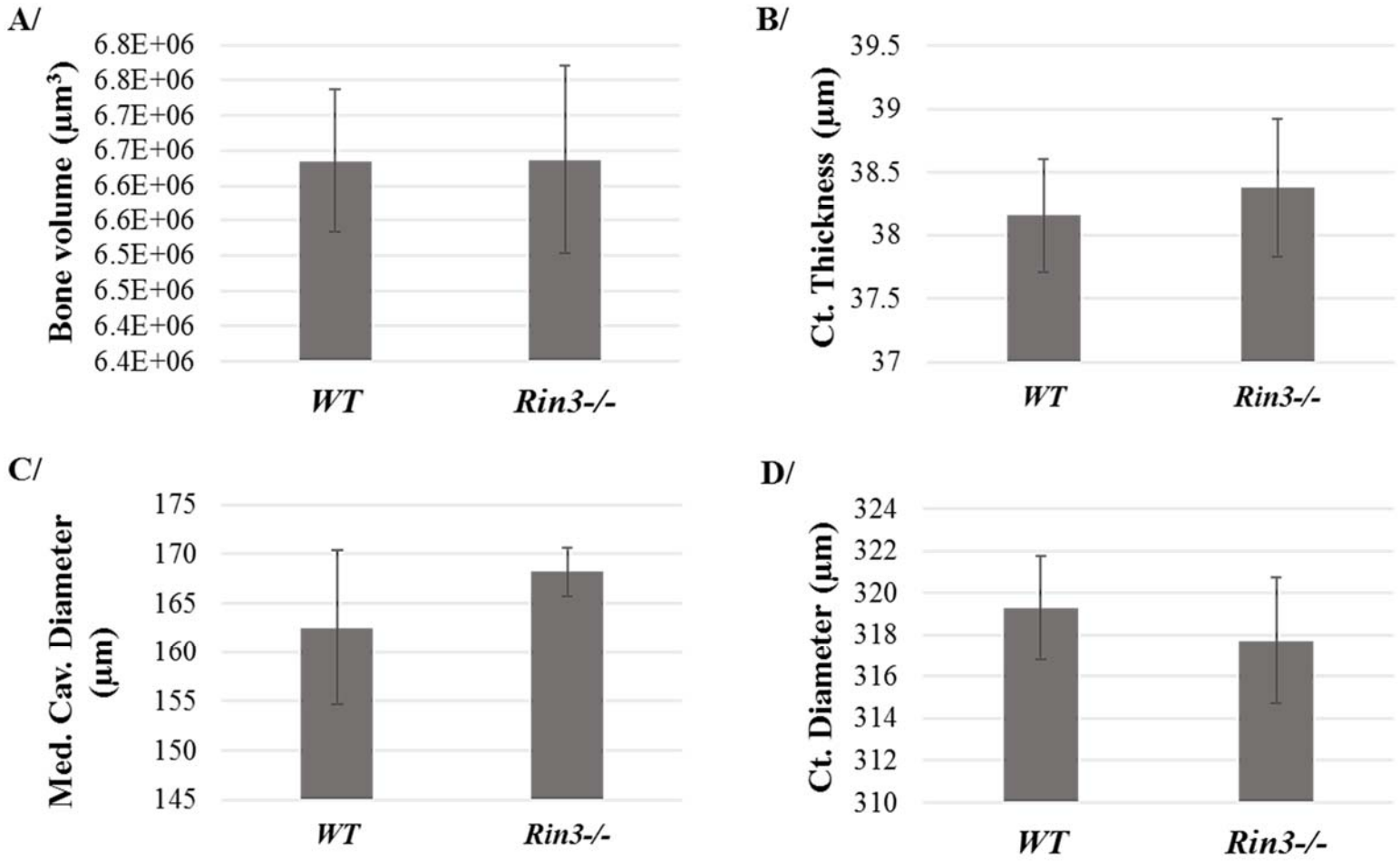

Figure 6.5: MicroCT results on the Rin3$^{-/-}$ mice and WT controls, for the femoral cortical bone.

Young *Rin3*$^{-/-}$ and WT female mice were analysed for cortical phenotypes in both left and right femurs. The following parameters were investigated: A/ Bone Volume; B/ Cortical thickness (Ct. Thickness); C/ Med. Cav. Diameter (Medullar Cavity Diameter); D/ Cortical Diameter (Ct. Diameter). Values are mean ± SEM of 14 *Rin3*$^{-/-}$ mice and 11 WT mice.

Table 6.1: Summary of statistical analyses of the microCT scanning results on the Rin3$^{-/-}$ mice and WT controls.

		WT	*Rin3*$^{-/-}$	95% CI	p-value (T-test)
Femur	BV/TV	10.08 ± 0.42	12.53 ± 0.58	-3.90 to -0.99	0.001
	Tb separation (µm)	50.57 ± 0.99	45.54 ± 0.95	2.23 to 7.83	0.001
	Tb number (1/mm)	0.011 ± <0.01	0.014 ± <0.01	-0.01 to -0.005	<0.001
Tibia	BV/TV	12.20 ± 0.36	13.80 ± 0.40	-2.70 to -0.50	0.005
	Tb separation (µm)	42.77 ± 0.77	39.43 ± 0.69	1.27 to 5.42	0.002
	Tb number (1/mm)	0.014 ± <0.001	0.016 ± <0.001	-0.003 to -0.001	<0.001

Tb = Trabecular; BV/TV = Bone volume/Total volume. Values are mean ± SEM of 14 *Rin3*$^{-/-}$ mice and 11 WT mice.

Rin3$^{-/-}$ mice showed similar results for femur and tibia. Indeed, microCT analysis has shown that long bones from both legs of *Rin3*$^{-/-}$ mice have a significantly increased trabecular bone volume (BV/TV; Figures 6.2 and 6.3, A) (Femur +24.29%, 95% CI = -3.90 to -0.99, P = 0.001; Tibia +13.12%, 95% CI = -2.70 to -0.50, P = 0.005) and trabecular number (Femur +23.86%, 95% CI = -0.01 to -0.005, P = <0.001; Tibia +14.81%, 95% CI = -0.003 to -0.001, P = <0.001) (Figures 6.2 and 6.3, D). As a result, trabecular separation in *Rin3*$^{-/-}$ mice was significantly decreased (Femur -9.95%, 95% CI = 2.23 to 7.83, P = 0.001; Tibia -7.81%, 95% CI = 1.27 to 5.42, P = 0.002) (Figures 6.2 and 6.3, C).

No differences between WT and *Rin3*$^{-/-}$ mice in the trabecular bone of the spine, or the cortical bone of the femur were detected (Figures 6.4 and 6.5).

3D modelling pictures from the scans were generated using the CTVol (Bruker, Belgium) (Figure 6.6). Increased bone volume and trabecular number described above can be seen in the trabecular bone of the tibia and femur between WT and *Rin3*$^{-/-}$.

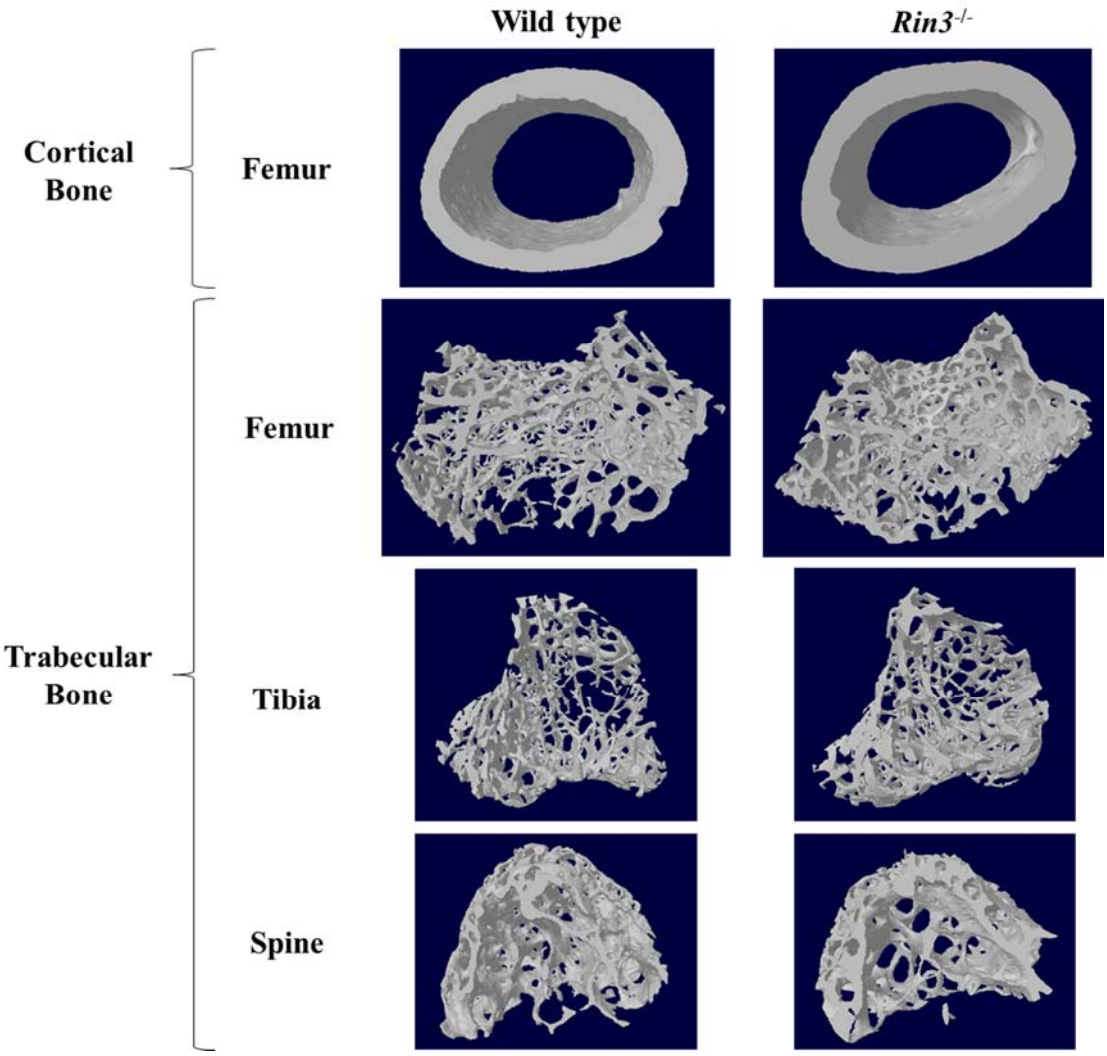

Figure 6.6: 3D remodelling pictures of the scanned bones in Rin3$^{-/-}$ and WT controls. These reconstructions were performed with the CTVol program and show either trabecular or cortical bone, in femur, tibia and spine.

6.4.3 Rin3 deficient mice show an osteoclastic phenotype

Metaphyses of the right femurs were analysed using histomorphometry in WT and *Rin3*$^{-/-}$ mice to investigate cellular changes due to the *Rin3* deletion (Figures 6.8 and 6.10).

Bone sections showed a significantly increased bone area and perimeter in *Rin3*$^{-/-}$ mice compared to WT (Figure 6.7, A and B). In particular, TRAcP staining showed an overall significant decrease in osteoclast active resorption surface (surface occupied by red osteoclasts corrected over trabecular bone surface) in *Rin3*$^{-/-}$ mice compared to WT mice (Figure 6.7, C).

Calcein staining and labelling were additionally performed to investigate mineralisation rate and osteoblast activity. Increased single label perimeter was seen in *Rin3*$^{-/-}$ mice (Figure 6.9, A), but this significance was lost once bone formation parameters were investigated. Bone volume was suggested to increase in *Rin3*$^{-/-}$ mice, which would be in agreement with the more sensitive microCT analysis, however this was not statistically significant (Figure 6.9, D).

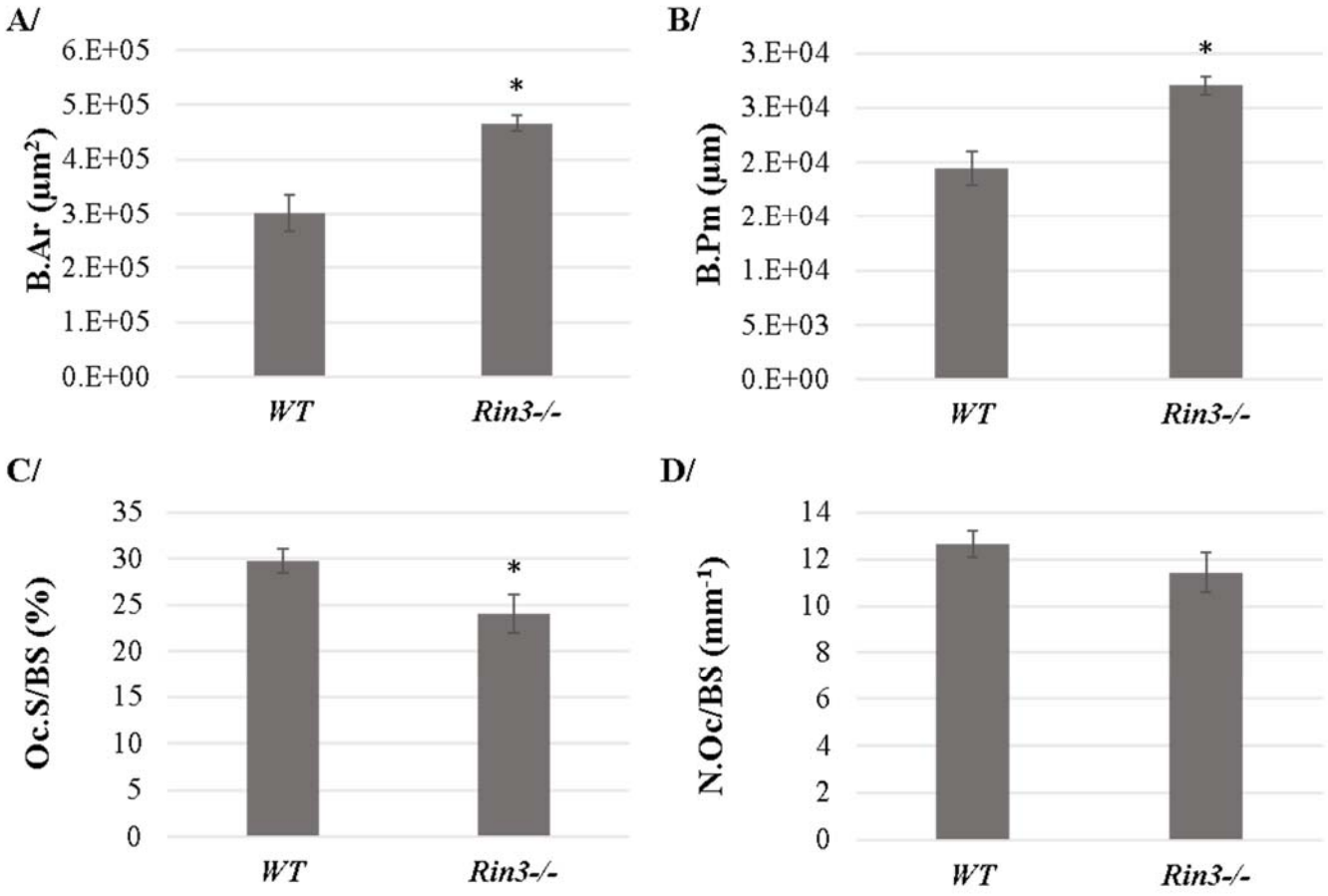

Figure 6.7: Histomorphometric results on the Rin3$^{-/-}$ mice and WT controls for TRAcP staining and osteoclast analysis.

This investigation was performed on the metaphysis of the right femurs. A/ B.Ar = Bone area; B/ B.Pm = Bone perimeter; C/ Oc.S/BS = Surface occupied by osteoclasts per bone perimeter; D/ N.Oc/BS = Number of osteoclasts per bone surface. Values are mean ± SEM of 13 *Rin3*$^{-/-}$ mice and 10 WT mice. *$p < 0.05$ from WT controls.

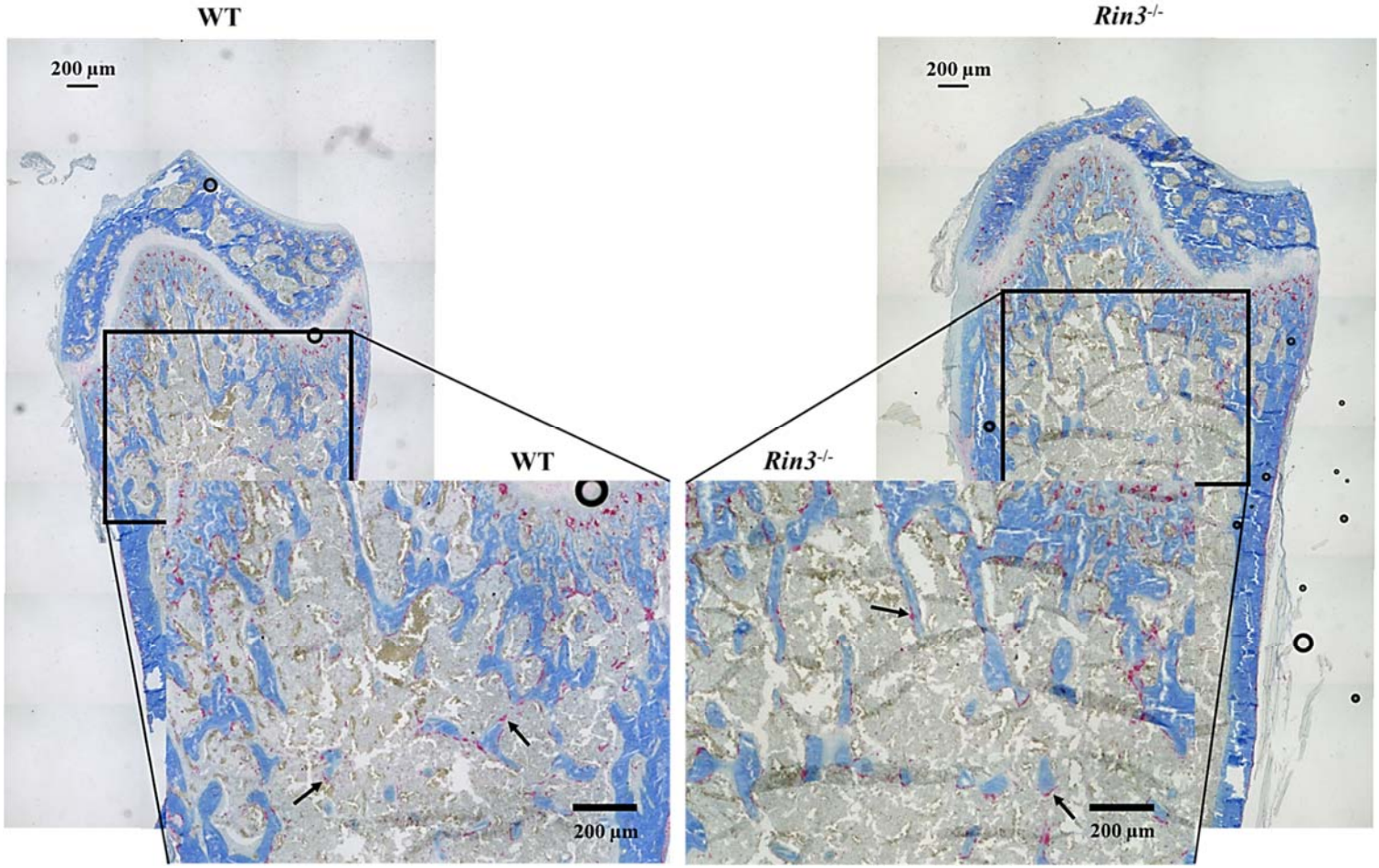

Figure 6.8: Representative sections of the WT and Rin3$^{-/-}$ mice after TRAcP staining.

The bone is stained using Aniline blue while osteoclasts are red (arrows) from TRAcP staining. Trabecular bone is increased in *Rin3*$^{-/-}$ mice compared to WT and the number of active osteoclasts (laying on the trabecular bone surface) is reduced in *Rin3*$^{-/-}$ mice once corrected over bone surface. Analysis was done using the TrapHisto (Van't Hof et al, 2017) program by using colour thresholding and manual editing. Bubbles (black circles) were also removed during the analysis by excluding the colour black.

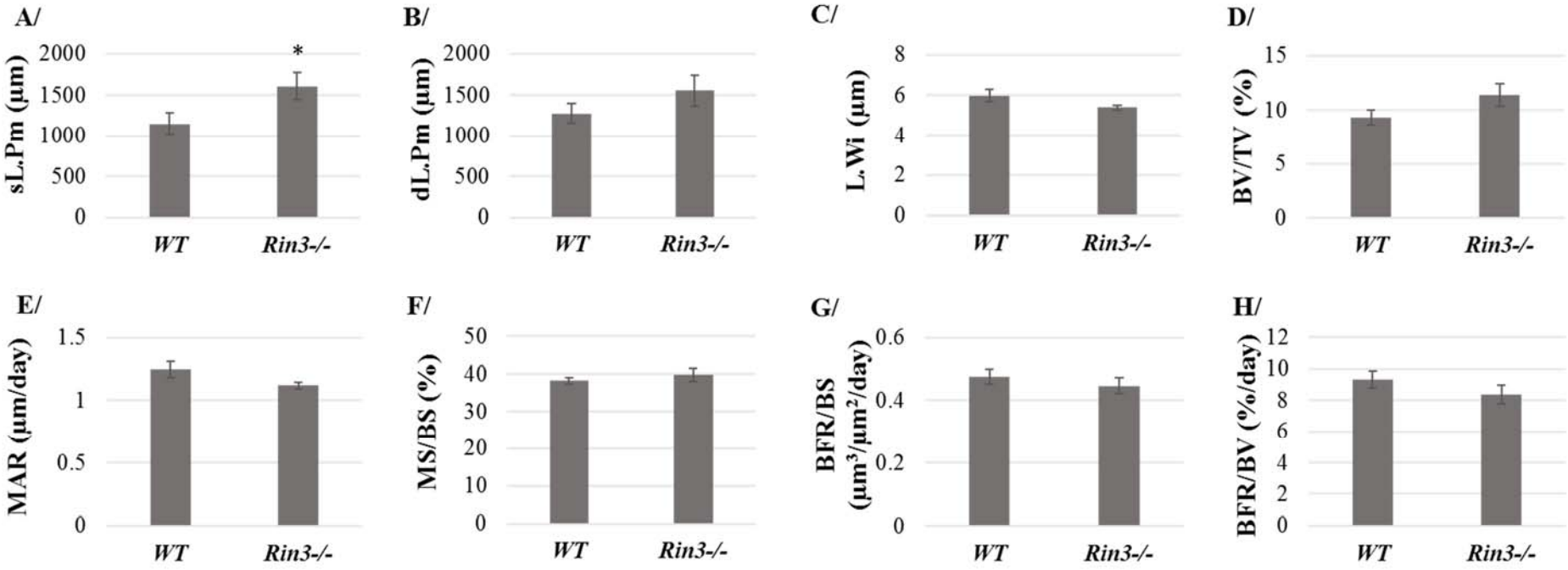

Figure 6.9: Dynamic histomorphometric analysis from calcein labelling on Rin3$^{-/-}$ mice and WT controls.

This investigation was performed on the metaphysis of the right femurs. A/ Single label Perimeter = sL.Pm; B/ Double label Perimeter = dL.Pm; C/ Label width = L.Wi; D/ Bone volume over total volume = BV/TV; E/ Minimum Acquisition rate = MAR; F/ Mineralised surface over bone surface = MS/BS; G/ Bone formation rate over bone surface = BFR/BS; H/ Bone formation rate over bone volume = BFR/BV. Values are mean ± SEM of 9 *Rin3*$^{-/-}$ mice and 10 WT mice. *$p < 0.05$ from WT controls.

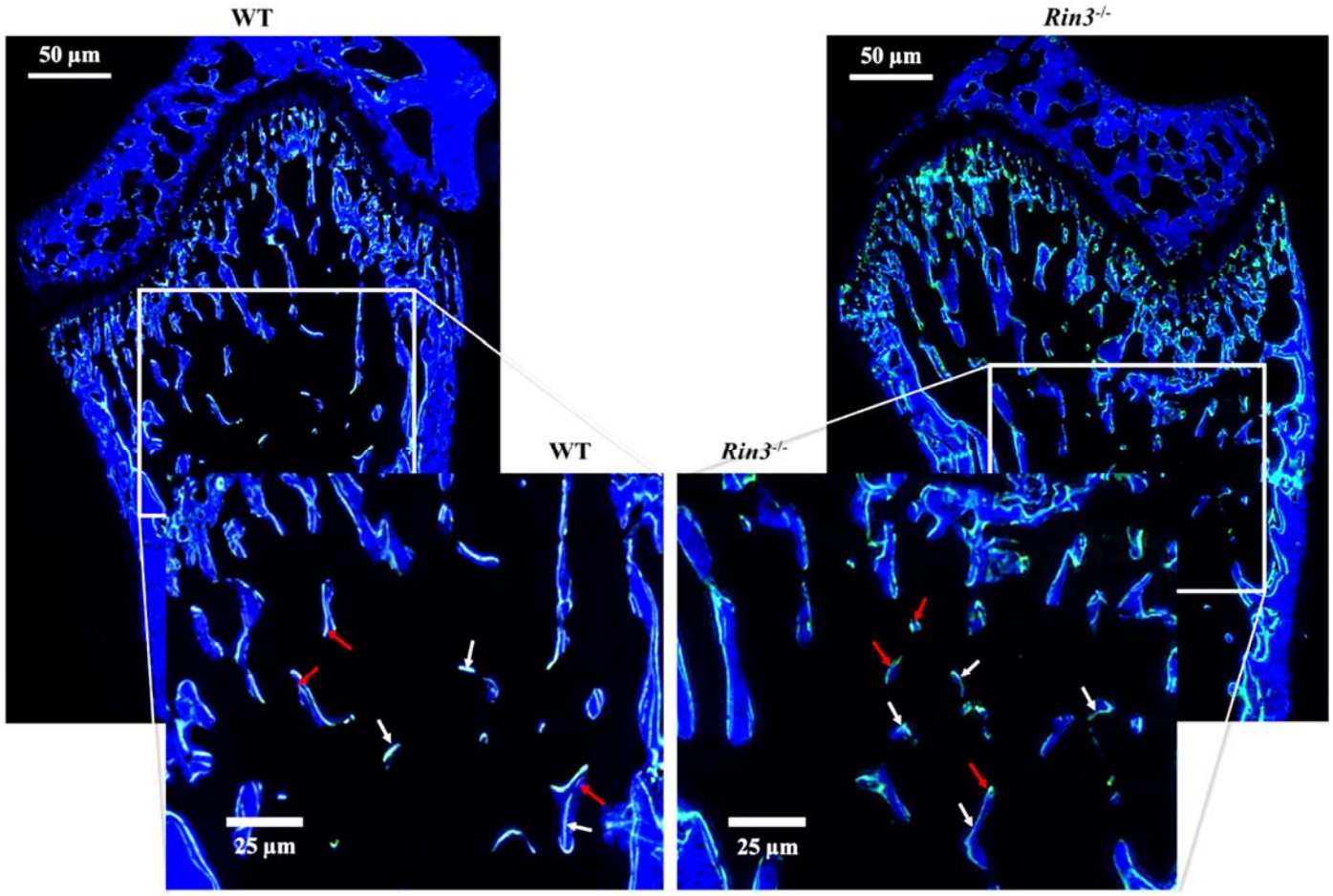

Figure 6.10: Representative sections of the WT and Rin3$^{-/-}$ double calcein labelling staining.

The bone is stained with calcein blue, and is detected using a blue fluorescent filter. Single calcein labelling (white arrows) and double calcein labelling (red arrows) are showed using green fluorescence, from injections performed at 6 and 2 days before collection. The CalceinHisto program (Van't Hof et al, 2017) detected the trabecular bone and calcein labelling using colour thresholding and manual editing. More single labelling was detected in the *Rin3*$^{-/-}$ mice, while double labelling and mineralisation rate were similar between the two genotypes.

6.4.4 Osteoblasts cultured from Rin3 deficient mice

To investigate the impact of the *Rin3* deletion on the function of isolated osteoblasts, calvarial osteoblast differentiation levels in *Rin3*$^{-/-}$ and WT mice were measured by quantifying ALP activity. Values were normalised by cell number. A modest trend towards increased ALP activity can be suggested in osteoblasts from *Rin3*$^{-/-}$ mice compared to WT mice, but this did not reach statistical significance (Figure 6.11).

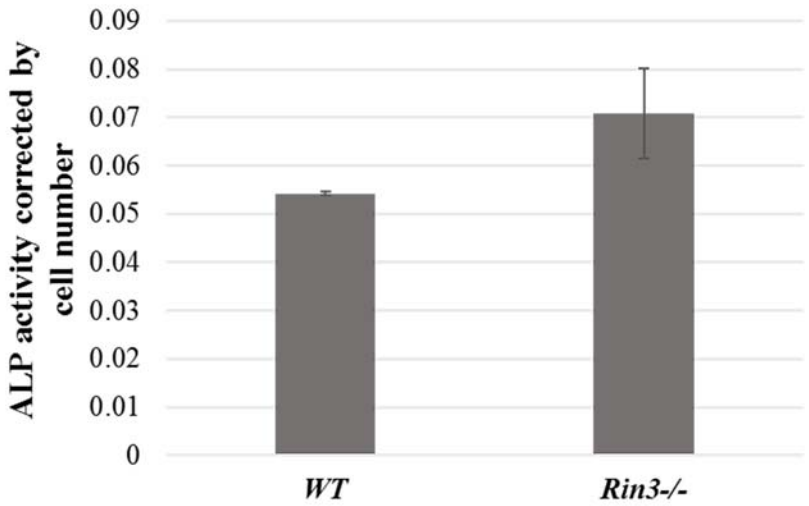

Figure 6.11: Calvarial osteoblasts ALP activity levels from Rin3$^{-/-}$ mice and WT controls. ALP levels were normalised to cell number. Values are mean ± SEM of three experiments with 10 replicates for each.

The results of Alizarin red staining are shown in Figure 6.12. The absorbance measured was normalised to cell number. The amount of Alizarin red varied significantly red over time ($P < 0.001$) and between experiments ($P = 0.012$). No differences in Alizarin red was however detected between the *Rin3*$^{-/-}$ and WT cultures, although a slight increase is noticeable in *Rin3*$^{-/-}$ mice. Taken individually, all three experiments showed more staining in the *Rin3*$^{-/-}$ cultures, however only two out were statistically significant, at both week 2 and week 3 (data not shown). This significance was lost once all three experiments were put together ($P = 0.091$) (Figure 6.12, B).

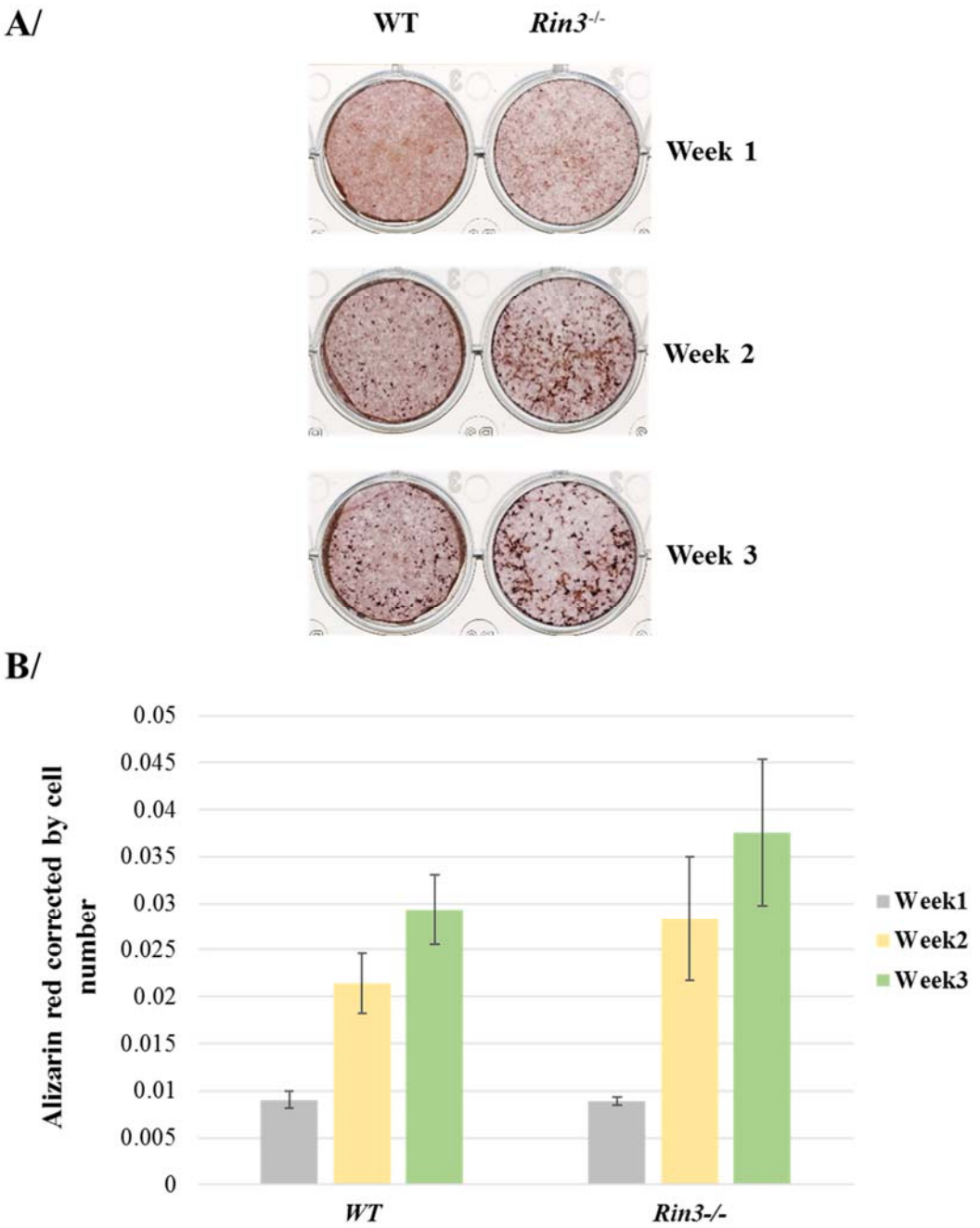

Figure 6.12: Alizarin red staining of mineralised nodules from Rin3$^{-/-}$ mice and WT calvarial osteoblasts.

A/ Photomicrographs of mineralised nodules stained with Alizarin red from *Rin3*$^{-/-}$ and WT mice over the period of three weeks analysed. B/ Quantification of Alizarin red from nodules in A by measuring absorbance at 562nm. Values are mean corrected by cell number ± SEM of three experiments with 6 replicates for each.

6.4.5 Osteoclasts cultured from Rin3 deficient mice show the same formation and survival pattern than wild type mice

To investigate the role of *RIN3* on osteoclast formation *in vitro*, M-CSF and RANKL generated osteoclasts from *Rin3*$^{-/-}$ and WT mice were cultured and TRAcP-stained. TRAcP positive cells with a nuclei number higher than 3 and higher than 10 were counted for each time point.

Although there was a trend towards a reduced total osteoclast number (Figure 6.13, A) and large osteoclast number (Figure 6.13, B) in cultures from *Rin3*$^{-/-}$ mice compared to WT, this did not reach statistical significance.

The survival of osteoclasts from BMDMs was also assessed at different time points in the absence of RANKL. As showed in Figure 6.14, the amount of osteoclasts drastically falls following 8h in the absence of RANKL for both groups, and no difference in cell survival was observed between *Rin3*$^{-/-}$ and WT mice.

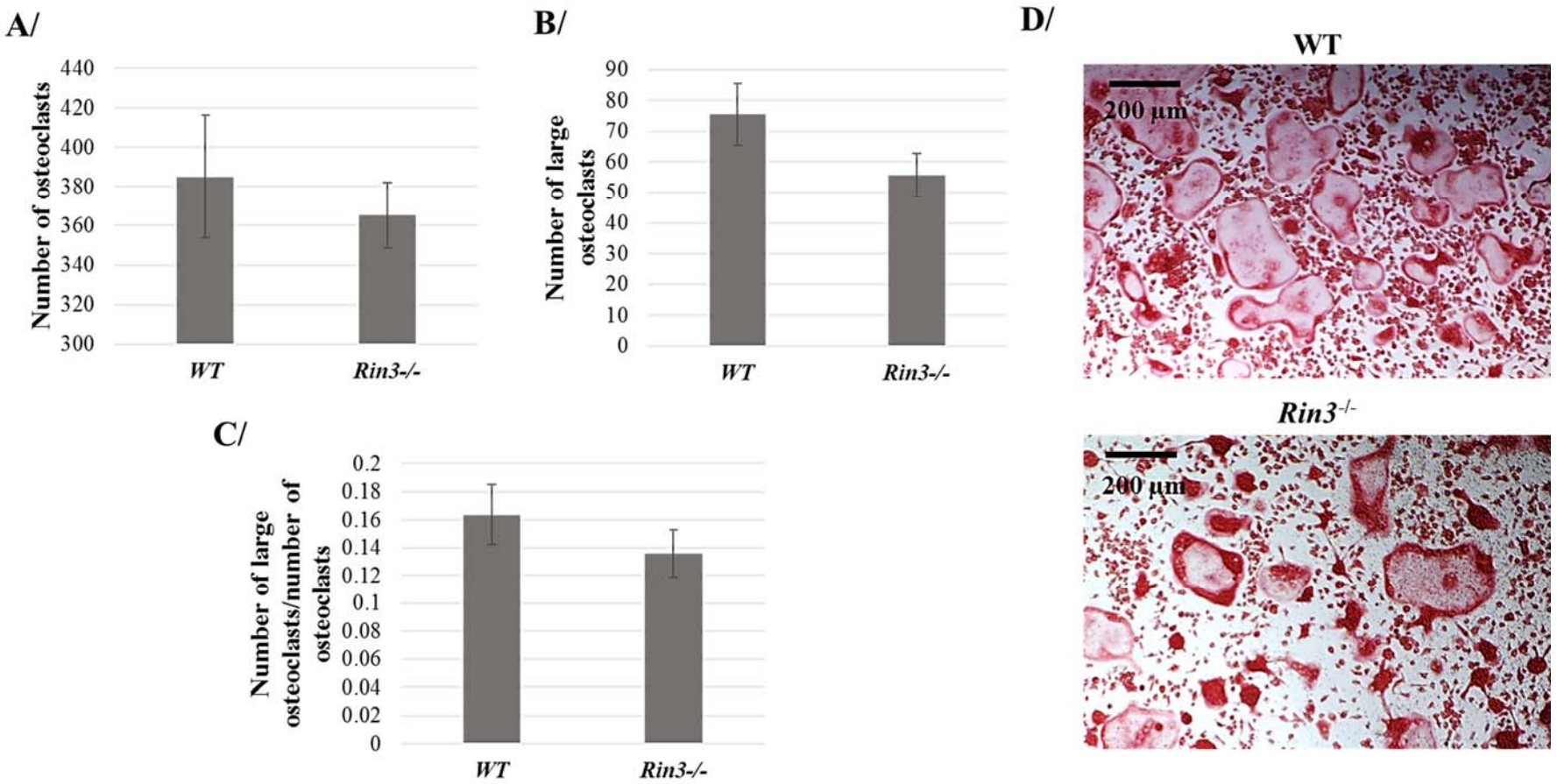

Figure 6.13: Osteoclast numbers from RANKL and M-CSF stimulated osteoclast cultures, from Rin3$^{-/-}$ and WT control mice.

A/ Number of TRAcP positive osteoclasts with at least 3 nuclei from *Rin3*$^{-/-}$ and WT cultures. B/ Number of large TRAcP positive osteoclasts with at least 10 nuclei from *Rin3*$^{-/-}$ and WT cultures. C/ Ratio of large osteoclasts over all osteoclasts between WT and *Rin3*$^{-/-}$ cultures. D/ TRAcP staining of osteoclasts cultures for WT and *Rin3*$^{-/-}$ mice. Magnification x5. Values are mean ± SEM of three experiments with 10 replicates each.

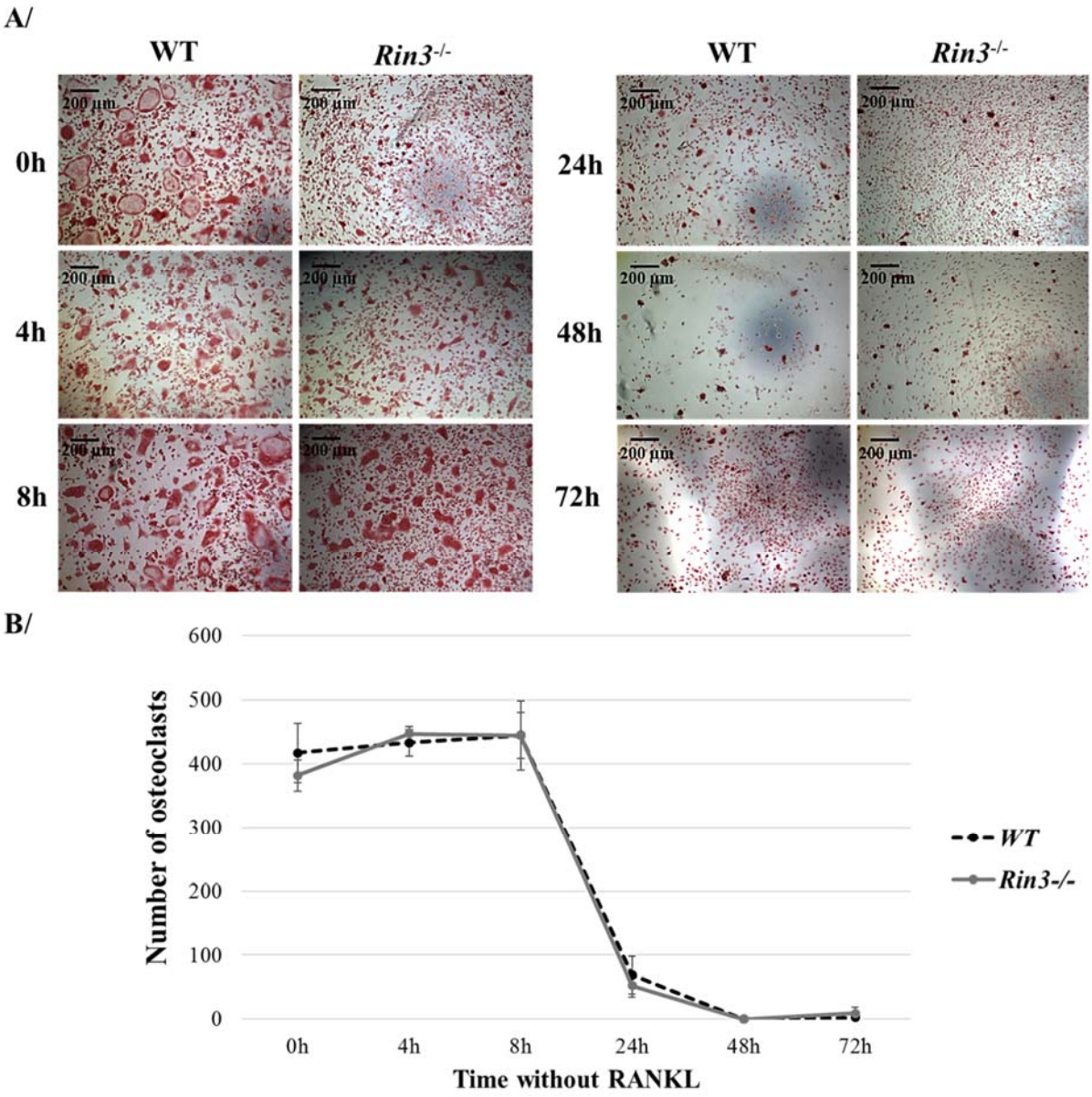

Figure 6.14: Survival assay in RANKL and M-CSF stimulated osteoclasts from Rin3$^{-/-}$ and WT control mice.

A/ TRAcP staining of osteoclast cultures for each time point. Magnification x5. B/ Number of TRAcP positive osteoclasts with at least 3 nuclei from WT and *Rin3*$^{-/-}$ cultures. Values are mean ± SEM of three experiments with at least 5 replicates each.

6.5 DISCUSSION

Although the role of *RIN3* in bone is not yet established, a genetic association has been made between *RIN3* and PDB in 2011 and variants were detected in this study (Albagha et al, 2011). Kemp and colleagues showed that *RIN3* levels were found to decrease during the first stages of PBMCs osteoclast differentiation before increasing again (Kemp et al, 2014). Similar results were found in Chapter 5, for protein and mRNA levels of *RIN3* (isoform 108kDa) in BMDMs. Kemp and colleagues also detected *RIN3* in osteoblasts, which was confirmed here too (Kemp et al, 2014). I also showed that RIN3 is expressed through the cytoplasm of osteoclasts with a stronger concentration by the borders of the cells. This could be expected as RIN3 is able to interact with small GTPases, involved in molecular trafficking of early and late endosomes. Immunofluorescence also showed that RIN3 could be expressed in vesicles through the cytoplasm of the cell, in accordance with the study from Kajiho and colleagues for which *RIN3* was over expressed in HeLa cells (Kajiho et al, 2003). These recent findings, in combination with the ones described here place the *RIN3* gene as a good candidate as a regulator of bone metabolism.

To answer this, this chapter investigates skeletal and cellular changes in mice lacking the *Rin3* gene. The full knock out status of the mice was confirmed by qPCR (Section 2.8.1) however it is necessary to validate the complete absence of RIN3 at a functional level and will be done in the near future as no previous *Rin3* knock out mouse model have been presented in the literature. The antibody used throughout this study recognises the last 349aa of RIN3 (C-terminal end), carried by both main isoforms and would then be an ideal choice to use in a western blot analysis of $Rin3^{-/-}$ mice samples.

Measuring a downregulation in RIN3's function would also be another way to confirm the full knock out status of the mice. This can be investigated by monitoring the release of [^{3}H]GDP from Rab5 activation (Hama et al, 1999) or the migration of mast cell towards SCF (Janson et al, 2012).

The two other isoforms seen in mice are of 198aa and 127aa. Following the deletion, the 198aa isoform becomes 97aa long, while the 127aa isoform becomes 26aa long. None will be recognised by the antibody as they are from the N-terminal part of the protein, but if the deletion was confirmed in the 900 and 980aa isoforms, the effect of these smaller isoforms could be negligible.

Phenotype effects of the deletion of the *RIN3* gene was performed in age-matched (8 weeks old) WT and *Rin3*$^{-/-}$ female mice on a mixed C57BL/6 x 129/OlaHsd background. Considering the late onset of PDB, it would have been more ideal to look into an older model, however time constraints led me to use young adult mice. The microCT analysis showed that *Rin3*$^{-/-}$ mice have a significantly increased bone mass and trabecular number, and a significant decreased trabecular separation once compared to controls. This suggests that the higher bone volume is due to an extended pattern of the trabecular network rather than an increased thickness of it. Similar results were also described in the MVNP mice, although they also reported an increased trabecular thickness (Kurihara et al, 2006). Quantitative histomorphometric analyses in Pagetic individuals are actually difficult to find, however Seitz and colleagues investigated a total of 247 Pagetic samples from iliac crest biopsies of German patients. They reported an increased bone volume, trabecular number, but not increased trabecular thickness (Seitz et al, 2009).

No differences between the *Rin3*$^{-/-}$ and WT groups were seen in trabecular bone from the spine. Although it is also commonly involved in Pagetic patients (Langston et al, 2007), such outcome can be expected considering the bone anatomy of the mice and the differences in weight bearing on the spine with human (Bagi et al, 2011). Similarly, lesion in lower limbs from mice carrying the p.P394L mutation were more frequent than in spines (Daroszewska et al, 2011). No differences were also found in the cortical bone between the two groups.

To further investigate the origin of those changes, histomorphometry was performed in the metaphysis of the right femurs previously scanned. This showed that *Rin3*$^{-/-}$ mice had a significantly higher trabecular bone area and perimeter in accordance with the microCT results. The surface occupied by TRAcP-positive osteoclasts, relative to the total surface of the trabecular bone was significantly reduced in *Rin3*$^{-/-}$ mice. This could suggest that the *Rin3*$^{-/-}$ mice have less osteoclasts, or less active osteoclasts. The number of osteoclast in the trabecular bone was however not reduced in those sections analysed. RIN3 could then impact either osteoclastogenesis or osteoclast resorption activity. To confirm this, osteoclasts were cultured from *Rin3*$^{-/-}$ mice and WT bone marrows, and osteoclasts were counted after 4 days of RANKL-stimulation. Accordingly to the histomorphometry analysis, no differences in osteoclasts numbers was detected between the two experimental groups, although a trend was noticed towards a smaller number of osteoclasts as well as larger osteoclasts in *Rin3*$^{-/-}$ mice. This could imply that the increased bone mass is due to a decreased bone resorption from the osteoclasts and not from osteoclast formation or number. However, there is still the possibility that the decreased trend seen in the number of BMDMs is simply not significant because of the power of the assay.

Indeed, the counting of the cells is was performed manually, and only three experiments were done because of time constraints. Additional experiments are necessary to confirm the validity of this result, and the implication of *RIN3* in osteoclast formation and activity. Additionally, considering that overall osteoclast activity is increased and that their survival has been suggested to be increased in Pagetic conditions (Chamoux et al, 2009; Roodman & Windle, 2005), the survival of RANKL and M-CSF stimulated osteoclasts from *Rin3*$^{-/-}$ and WT mice was also investigated. Interestingly, no changes in survival was observed.

Osteoblast phenotypes were also investigated. Osteoblast activity was assessed by histomorphometry and only showed an increase of single calcein labelling in the *Rin3*$^{-/-}$ mice. Overall, no increased bone formation was overall detected. The increased single label parameter can be due to the fact that calcein does not fix to the calcium while osteoblasts are actively forming bone. A way to know if the increase in single labelling is from the first or second injection would have been to use two different fluorochromes such as Alizarin red, or demeclocycline (Erben et al, 1997). Using one fluorochrome for both injections is however common to evaluate mineralisation and bone formation rates, when the marker interval is chosen carefully (Erben & Glosmann, 2012). Overall, increased number of single labelling can still suggest a mild increase in osteoblast activity. Bone mass was also found to be higher in *Rin3*$^{-/-}$ samples although this was not statistically significant. This is not as obvious as what was observed by microCT analysis, but it can be expected considering that histomorphometry is not as sensitive as it does not consider the totality of the bone but two sections.

Maturation levels and function of primary calvarial osteoblasts were also investigated and no major differences between the two groups were observed. Osteoblasts from *Rin3*$^{-/-}$ mice show a trend towards increased mineralised nodule formation. Two of the three experiments showed a significant increased nodule formation, however this was lost once put together. Additional experiments are necessary to confirm such results, as it would be in accordance with the increase of single calcein labelling seen by histomorphometry. *Rin3*$^{-/-}$ calvarial osteoblasts also seem to have increased ALP activity, a marker of osteoblast differentiation. This was however not statistically significant. Here too, additional experiments might be necessary considering that significance was achieved for one out of the 3 experiments performed.

Such variations between the *in vivo* and *in vitro* analyses can suggest that the bone phenotype would actually be due to a coupled osteoblast/osteoclast effect, which would have been missed from the osteoclasts and osteoblast cultures. It would be analysed by investigating co-cultures of stromal cells with non-adherent cells obtained from the bone marrow (Cao et al, 2005). Another explanation would be that osteoblasts could also have a focal effect which cannot be seen by histomorphometry. The use of factors which would enhance osteoblast differentiation, such as PTH (Sophocleous et al, 2011), could be more indicative whether *Rin3*$^{-/-}$ osteoblasts are lagging in cell differentiation and whether this was due to resistance to such factors. Moreover, the impact of *Rin3*$^{-/-}$ deficiency on osteoblast differentiation and function would need to be investigated in bone marrow-derived osteoblasts, which are portrayed as early-stage differentiated osteoblasts compared to calvarial osteoblasts (Rosales-Rocabado et al, 2014).

PDB being a late onset disease (Van Staa et al, 2002), additional work on older mice would be necessary to confirm those findings and maybe reveal more obvious phenotypes or a focal abnormality missed here. Nevertheless, this chapter indicates that *RIN3* clearly has a role in bone metabolism and suggests a positive effect on osteoclast resorption as its deletion induces an increase in bone mass, and a reduction in osteoclast active surface with a possible effect on osteoblast differentiation.

CHAPTER SEVEN
DISCUSSION AND CONCLUSIONS

7 DISCUSSION AND CONCLUSIONS

PDB is a disease of bone remodelling, for which osteoclasts are abnormal and over-active. They are characterised by a bigger size, an increased number of nuclei and increased bone resorption activity compared to healthy osteoclasts (Meunier et al, 1980). Osteoblasts also show an increased activity in bone mineralization, however this is thought to be in response to the osteoclastic phenotype (Meunier et al, 1980). As a result, the bone formed is woven and fragile, leading to many orthopaedic complications such as clinical fractures, deformities, or bone pain. Deformities can lead to nerve and artery compressions, while an affected skull can also result in brain pressure and hearing loss (Langston et al, 2007).

Although the origin of the disease is yet to be fully understood, PDB has a strong genetic component and is distributed in families in an autosomal dominant fashion. Causing variants have been described for PDB and PDB-like disorders (Ralston & Albagha, 2014). The p.P392L mutation in the *SQSTM1* gene was showed to have the largest effect in Pagetic cohorts, and is found in 20-50% of the familial cases and in 5-15% of the sporadic cases (Rea et al, 2013). Patients affected by p.P392L show a more severe phenotype, including an earlier age of diagnosis, higher number of affected bones, and an increased need for surgeries and treatments (Visconti et al, 2010). Additional mutations were described in the *SQSTM1* gene and most (including p.P392L) result in the loss of ubiquitin binding of p62 which is necessary for protein ubiquitination and autophagy function. This leads to an over-activation of the NFκB pathway which controls osteoclasts resorption (Chung & Van Hul, 2012).

In order to identify additional genes associated with PDB, a GWAS was performed in our group on PDB patients and rs10498635 was detected in the *RIN3* gene. Subsequently, rs10498635 was found to be surrounded by genetic recombination hotspots and to be the only independent signal, increasing our interest in this gene (Albagha et al, 2011). The aim of this study is to investigate the genetic and functional involvement of *RIN3* in PDB and bone metabolism.

In order to confirm the findings of this GWAS and further investigate *RIN3* in the context of PDB, Sanger and next generation sequencings were performed in affected patients. A total of 18 variants, including 7 novel ones were described. 15 rare variants were associated with PDB once their effect was combined (OR = 3.72; $P = 8.9 \times 10^{-10}$), but the common variant p.R279C (rs117068593) is the most likely candidate for PDB. First, it showed a strong association for PDB (OR = 0.64; $P = 1.4 \times 10^{-9}$) where the p.279C allele is likely to be protective of the disease. Second, this missense mutation was found to be in strong LD with the GWAS hit previously described (rs10498635). Third, both variants share the same risk haplotype rs10498635C–rs117068593C which was over-represented in the cases, and most rare variants share this same haplotype. The effect of the rare variants combined was also lost on the PRISM cohort. Finally, the rs754388 variant detected by Kemp et al., which associates RIN3 with lower BMD in children was found to be in strong LD with p.R279C (Kemp et al, 2014).

Severity associations showed that patients carrying the p.279C allele but carried no mutations in the *SQSTM1* gene had a younger age of diagnosis. This association was however nominal and the significance was lost once corrected over the number of phenotypes investigated. Although it would be important to confirm such findings in a bigger cohort, this result is for now contradicting the hypothesis that the p.279C allele would have a protective effect of the disease and seems unlikely to be a true association. Both analyses (sequencings and genotyping) were performed on different cohort. The sequenced individuals were selected on the basis that they had a young age of diagnosis and/or family history, while the genotyped cohort includes patients with different levels of severity of PDB. Additionally, the control cohort from the sequencing analysis was also including public databases (379 European subjects from 1000 Genomes and 4300 European-American subjects from NHLBI) and offered a higher power in that respect. These findings all point to p.R279C being likely involved in PDB, with an effect more subtle than mutations detected in the *SQSTM1* gene. A cumulative allelic effect can however be another mechanism to consider, as susceptibility loci (including 14q32.12) were described from GWAS data in patients who do not carry *SQSTM1* mutations (Albagha et al, 2011). Although the rare variants might not be as relevant, the p.R279C could be used for genetic profiling and could, speculatively, be a potential therapeutic target for the disease.

I then sought to investigate the expression pattern of *Rin3* in mouse tissues and primary bone cells. In the literature, protein levels of RIN3 were reported to be high in human peripheral blood cells and mast cells, but lower in brain, muscle, colon and cell lines such as the osteosarcoma Saos-2 line, B cell, myeloblast, T cell, fibroblast and glioblastoma (Janson et al, 2012; Kajiho et al, 2003).

Accordingly in this study, the mRNA expression of the 980aa (108kDa) isoform of *Rin3* was low in brain and muscle and high in lung. I also report that *Rin3* is highly expressed in total crushed bone and varies significantly during osteoclast differentiation from murine BMDMs. This suggests that RIN3 could have a role in the generation of osteoclasts. Janson and colleagues showed that RIN3 is involved in the recycling of receptor tyrosine kinase KIT in human mast cell line, upon SCF cell stimulation (Janson et al, 2012). As discussed in Section 5.5, it can be speculated that RIN3 could have a similar mediation role in the regulation of CSF1R recycling, another tyrosine kinase receptor. Indeed, looking at the mRNA expression pattern of *Rin3*, it is less expressed during macrophage proliferation where the M-CSF/CSF1R binding is crucial, and expressed again during osteoclast formation to a level similar to what was originally seen in bone marrow. During this phase, the M-CSF/CSF1R gives priority to the RANKL/RANK binding to promote osteoclast formation (Boyle et al, 2003). Similar trends of expression were found for protein investigations of RIN3 and its larger isoform (108kDa/980aa), however this needs to be repeated with higher protein loading concentrations as the RIN3 bands were particularly faint and generated graphs with high values of standard error of mean. This could however be in accordance with the low protein levels detected in the osteosarcoma Saos-2 line by Janson and colleagues (Janson et al, 2012). The smaller isoform of RIN3 (98kDa/900aa) showed stronger bands and was more predominant than the heavier isoform. It was found to be constantly downregulated during BMDM differentiation, and particularly once RANKL was added in the media to promote osteoclast formation.

The protein expression suggests that this isoform is unlikely to be involved in this process however there is still the possibility for it to indirectly impact key signalling pathways, or to be downregulated to allow the expression of the heavier isoform. This requires additional work. I have also reported that *Rin3* is expressed at low levels in calvarial osteoblasts. Total RNA was investigated in such cells by Kemp and colleagues and although *Rin3* was also detected, it was not compared to the levels in osteoclasts (Kemp et al, 2014).

I additionally established the cellular location of RIN3 in osteoclasts derived from mouse BMDMs, human bone samples of non-Pagetic subjects and patients affected by Paget's, osteosarcoma, osteoclastoma, and GCT. RIN3 is expressed through the cytoplasm of the osteoclasts, and is more concentrated by the borders of the cells. This can be expected considering the GEF activity of RIN3, which activates small GTPases such as Rab5 and Rab31, crucial for vesicular trafficking of molecules to early endosomes (Kajiho et al, 2003). Additionally, strong specks of fluorescence were detected in osteoclasts from BMDMs, which could be in accordance with previous work published by Kajiho and colleagues, where RIN3 was over-expressed in HeLa cells and was found to be sitting in vesicles in the cell cytoplasm (Kajiho et al, 2003).

Finally, the role of RIN3 in bone metabolism was investigated using an *in vivo* mouse model. Young female mice lacking the *Rin3* gene (*Rin3*$^{-/-}$) were analysed for bone phenotypes using microCT and for cellular changes in the bone microenvironment using histomorphometric assays. *Rin3*$^{-/-}$ mice showed an increased trabecular bone volume and trabecular number in tibias and femurs, suggesting that RIN3 would negatively regulate bone formation.

No changes were observed in the trabecular bone of the spine and cortical bone of the femur, probably due to differences in genetic determinants (Paternoster et al, 2013). As discussed in Section 6.5, similar findings were reported by Daroszewska and colleagues who investigated p.P394L$^{+/+}$ mice, and very few lesions were found in lumbar vertebrae compared to the long bones (Daroszewska et al, 2011). This can be expected when taking into account the anatomy of the mouse compared to human, and how much less weight is put on their spine. Although mice are an established *in vivo* model, it is important to take such differences into consideration when extrapolating the results (Bagi et al, 2011). In our case nevertheless, a clear bone phenotype is reported in both tibia and femur, confirming a definite role for *RIN3* in bone metabolism. Additional work is however necessary to prove that the knock out of the three first crucial exons of the gene is affecting all isoforms of *Rin3,* as it is a multi-domain protein and although unlikely, remaining functional activity is still a possibility. Such findings cannot however be compared to the suggested Pagetic effect of p.R279C mentioned above, as this is a point mutation. Similarly, introduction of the p.P394L missense in mice models leads to the development of PDB (Daroszewska et al, 2011) while a full knock out of the *SQSTM1* gene is associated with mature-onset obesity (Rodriguez et al, 2006).

Using histomorphometry, the trabecular bone area was also found to be significantly increased in mice lacking *Rin3*, confirming the microCT analysis. A reduction of resorption surface occupied by active osteoclasts was also detected in *Rin3*$^{-/-}$ mice while only an increase in single calcein labelling was detected when investigating osteoblast phenotypes. This, along with the expression pattern discussed above, suggests that RIN3 could act on osteoclasts rather than osteoblasts.

Although the number of osteoclasts in the trabecular bone was the same between both groups, it does not exclude the possibility that the deletion resulted in generating less osteoclasts. For this, BMDM cultures have been considered. RIN3 can also affect the function of the osteoclasts, and knowing its role in vesicle trafficking, an effect in the formation of the ruffled border can be speculated.

To evaluate the role of RIN3 in the formation of osteoclasts, BMDMs were cultured from the *Rin3*$^{-/-}$ and WT mice. Although less osteoclasts seem to be formed from the *Rin3*$^{-/-}$ mice, this was not significant. Similarly, the osteoclasts lifespan was the same between the two genotypes. It is important to bear in mind that such results are only analysed from three experiments. Since then, three additional BMDM cultures have been performed and confirmed that no differences in osteoclast number was observed (data not shown). This suggests that the reduction of active resorption surface in *Rin3*$^{-/-}$ mice is unlikely to be due to the formation of osteoclasts. Such result was also confirmed from the histomorphometry analysis.

Calvarial osteoblasts were also cultured from both groups and although they showed a trend towards being more differentiated and forming more mineralised nodules, no significant difference was observed.

Again, additional work is necessary as this was obtained from three experiments only. The osteoblastic phenotypes analysed from those cultures could be more likely to result into true significance, particularly for the Alizarin red assay. Indeed, two of the three experiments performed showed significant increased mineralised nodule formation in the *Rin3*$^{-/-}$ mice. The appearance of the nodules was also different in all cultures, somehow bigger in the *Rin3*$^{-/-}$ mice (Figure 6.12, panel A).

Since then, one additional experiment has been performed indicating a clear difference between the two genotypes. Such findings would also reflects the increased single calcein labelling found by histomorphometry, and offer the possibility that the reduction in active resorption surface is due to a communication effect between osteoclast and osteoblasts.

Future studies

In order to confirm the trends observed in osteoblast for ALP activity and Alizarin red staining, two additional calvarial osteoblast cultures are currently undergoing. Additional experiments could also be performed using PTH to enhance the subtle phenotypes seen in the calvarial cultures as mentioned in Section 6.5 (Sophocleous et al, 2011).

Following the suggestion that the decreased resorption surface in the trabecular bone is due to an interference with the osteoclast/osteoblasts coupling effect, which would have been missed by individuals osteoclasts cultures, an *ex vivo* model has since been optimised using co-cultures of murine bone marrow osteoblasts with bone marrow cells. At this stage however, co-cultures with *Rin3*$^{-/-}$ mice have not been performed. Osteoclasts formed at the end of the culture will be counted using TRAcP staining and differences between both genotypes will be analysed according to the protocol used by Cao and colleagues (Cao et al, 2005).

In the same context, it would be interesting to investigate the involvement of RIN3 in the mediation of Eph tyrosine kinase receptors (Section 1.1.3 and 1.5.4), which are important in bi-directional signalling and involved in osteoclast/osteoblast cellular communication (Brandi et al, 1995).

If no differences are observed in the *ex vivo* model, RIN3 is then more likely to affect the function of osteoclasts, rather than their formation. In that case, it would be interesting to investigate differences in osteoclast resorption. For this, osteoclasts will be cultured on dentine slices using a low pH to simulate *in vivo* conditions. Osteoclasts will then counted following TRAcP staining, and resorption pits will be visualized using light microscopy (Van't Hof et al, 2004).

Knowing the importance of Rab proteins in vesicular trafficking, disruption in the osteoclast ruffled border function and formation could be assessed using electronic microscopy (DeSelm et al, 2011). Similarly, investigating the role of RIN3 in autophagy could be another interesting path to follow, particularly in autophagosome formation in which Rab5 plays an important role. This could be performed using electron microscopy, or fluorescence (Ao et al, 2014).

In order to increase our insight on *RIN3* in the context of bone signalling pathways, an RNA-sequencing is also currently under investigation on calvarial osteoblasts and osteoclasts cultured from BMDMs.

Environmental factors could also be investigated. By looking at the literature, most of the evidence considering such lines of work are quite dated (most are from the 1980/1990's) except for viral infections, which by now, do not seem the way forward for PDB. Indeed, as discussed in Section 1.5.1, there is a lot of inconsistency in the data. The appearance of the inclusion bodies as has also been refuted once they were compared to the density and organisation pattern of other measles infection caused-disorders (Helfrich et al, 2000).

Finally, studies have shown that MVNP expressing osteoclasts are thought to show a Pagetic phenotype, it is likely not representative of PDB, but of any infected cell for which their machinery has been enhanced by viruses and in the case of osteoclasts, their bone resorption activity (Ruddle et al, 1993). However, the impact of the diet on the disease has not been investigated much. Somehow, older studies which have associated PDB to diet such as vitamin D and calcium intake (Barker & Gardner, 1974; Siris, 1994) have been slightly overlooked. Recently, a lot of research has been focusing on the understanding of the intestinal microbiome, following a change in dietary consumption in the general population over the last few decades. In the context of bone, the term osteo-microbiology was introduced in 2015 reporting that changes in diet and microbiome was associated with bone phenotypes (Ohlsson & Sjogren, 2015). Our increased overall knowledge in this field might be an opportunity to investigate this further, and could be interesting to consider in the context of *RIN3* and PDB.

The introduction of the p.R279C mutation in osteoclasts using site directed mutagenesis is also another experiment to perform, hoping it will lead to typical PDB phenotypes such as increased number, size and number of nuclei in osteoclasts.

Lastly, the mice selected for this thesis were of a young age due to time restrictions. However, as PDB is a late onset disease, *Rin3*$^{-/-}$ mice are currently being aged up to 12 months old. Indeed, mice carrying the p.P394L change in p62 showed lesions from 8 months of age, while none were detected at 4 months (Daroszewska et al, 2011).

It is difficult to predict what the phenotype of these 12 months old *Rin3*$^{-/-}$ mice will be, from lesions to additional trabecular and cortical changes, but it will be interesting to see the evolution of the phenotypes (also considering ageing parameters) over time.

In conclusion, this work led to an insight for the role of *RIN3* in the bone microenvironment and PDB. I have described a strong candidate variant for PDB, established for the first time the expression pattern of *Rin3* in mice tissue, with a high expression in total crushed bone. RIN3 was found to be located in the cytoplasm of osteoclasts, and may be sitting in vesicles as well. *Rin3* was found to vary significantly during osteoclast differentiation, suggestive of a role in osteoclastogenesis. *Rin3* was found to be lowly expressed in calvarial osteoblasts. Mice lacking *Rin3* showed an increased bone mass and lower active resorption surface of osteoclasts in the trabecular bone, which places *RIN3* as strong candidate for a role in the normal bone microenvironment.

BIBLIOGRAPHY

REFERENCES

Adzhubei, I. A., Schmidt, S., Peshkin, L., Ramensky, V. E., Gerasimova, A., Bork, P., Kondrashov, A. S. & Sunyaev, S. R. (2010) A method and server for predicting damaging missense mutations. *Nat. Methods*, 7(4), 248-9.

Albagha, O. M., Visconti, M. R., Alonso, N., Langston, A. L., Cundy, T., Dargie, R., Dunlop, M. G., Fraser, W. D., Hooper, M. J., Isaia, G., Nicholson, G. C., Del Pino, M. J., Gonzalez-Sarmiento, R., Di, S. M., Tenesa, A., Walsh, J. P. & Ralston, S. H. (2010) Genome-wide association study identifies variants at CSF1, OPTN and TNFRSF11A as genetic risk factors for Paget's disease of bone. *Nat. Genet.*, 42, 520-524.

Albagha, O. M., Visconti, M. R., Alonso, N., Wani, S., Goodman, K., Fraser, W. D., Gennari, L., Merlotti, D., Gianfrancesco, F., Esposito, T., Rendina, D., Di, S. M., Isaia, G., Brandi, M. L., Guisti, F., Del Pino-Montes, J., Corral-Gudino, L., Gonzalez-Sarmiento, R., Ward, L., Rea, S. L., Ratajczak, T., Walsh, J. P. & Ralston, S. H. (2013) Common susceptibility alleles and SQSTM1 mutations predict disease extent and severity in a multinational study of patients with Paget's disease. *J. Bone Miner. Res.*, 28, 2238-2246.

Albagha, O. M. E., Wani, S., Visconti, M. R., Alonso, N., Goodman, K., Cundy, T., Brandi, M. L., Chung, P. Y., Dargie, R., Devogelaer, J. P., Falchetti, A., Fraser, W. D., Gennari, L., Gianfrancesco, F., Hooper, M. J., Van Hul, W., Isaia, G., Nicholson, G. C., Nuti, R., Del Pino, M. J., Ratajczak, T., Rea, S. L., Rendina, D., Gonzalez-Sarmiento, R., Di, S. M., Ward, L., Walsh, J. P. & Ralston, S. H. (2011) Genome-wide association identifies three new susceptibility loci for Paget's disease of bone. *Nat. Genet.*, 43(7), 685-689.

Allan, E. H., Hausler, K. D., Wei, T., Gooi, J. H., Quinn, J. M., Crimeen-Irwin, B., Pompolo, S., Sims, N. A., Gillespie, M. T., Onyia, J. E. & Martin, T. J. (2008) EphrinB2 regulation by PTH and PTHrP revealed by molecular profiling in differentiating osteoblasts. *J. Bone Miner. Res.*, 23(8), 1170-81.

Alliston, T., Choy, L., Ducy, P., Karsenty, G. & Derynck, R. (2001) TGF-beta-induced repression of CBFA1 by Smad3 decreases cbfa1 and osteocalcin expression and inhibits osteoblast differentiation. *EMBO J.*, 20(9), 2254-72.

Alshaikh, O. M., Almanea, H. & Alzahrani, A. S. (2011) Paget disease of the bone: does it exist in Saudi Arabia? *Ann. Saudi Med.*, 31(3), 305-10.

Altman, R. D., Bloch, D. A., Hochberg, M. C. & Murphy, W. A. (2000) Prevalence of pelvic Paget's disease of bone in the United States. *J. Bone Miner. Res.*, 15(3), 461-465.

Alvarez, L., Peris, P., Guanabens, N., Vidal, S., Ros, I., Pons, F., Filella, X., Monegal, A., Munoz-Gomez, J. & Ballesta, A. M. (2003) Serum osteoprotegerin and its ligand in Paget's disease of bone: relationship to disease activity and effect of treatment with bisphosphonates. *Arthritis Rheum.*, 48(3), 824-828.

Ao, X., Zou, L. & Wu, Y. (2014) Regulation of autophagy by the Rab GTPase network. *Cell Death Differ.*, 21(3), 348-58.

Arai, T., Nonaka, T., Hasegawa, M., Akiyama, H., Yoshida, M., Hashizume, Y., Tsuchiya, K., Oda, T. & Ikeda, K. (2003) Neuronal and glial inclusions in frontotemporal dementia with or without motor neuron disease are immunopositive for p62. *Neurosci. Lett.*, 342(1-2), 41-4.

Paget's Association, (2017) *Paget's association*, 2017. Available online: http://www.paget.org.uk/ [Accessed].

Aulchenko, Y. S., Struchalin, M. V. & van Duijn, C. M. (2010) ProbABEL package for genome-wide association analysis of imputed data. *BMC Bioinformatics*, 11, 134.

Avramidis, A., Polyzos, S. A., Moralidis, E., Arsos, G., Efstathiadou, Z., Karakatsanis, K., Grollios, G. & Kita, M. (2008) Scintigraphic, biochemical, and clinical response to zoledronic acid treatment in patients with Paget's disease of bone. *J. Bone Miner. Metab.*, 26(6), 635-41.

Axmann, R., Bohm, C., Kronke, G., Zwerina, J., Smolen, J. & Schett, G. (2009) Inhibition of interleukin-6 receptor directly blocks osteoclast formation in vitro and in vivo. *Arthritis Rheum.*, 60(9), 2747-2756.

Azzam, E., Helfrich, M. H. & Hocking, L. J. (2012) Mutations in Sequestosome-1 result in inclusion body formation. *Bone*, 50, S64-S64.

Bagi, C. M., Berryman, E. & Moalli, M. R. (2011) Comparative bone anatomy of commonly used laboratory animals: implications for drug discovery. *Comp. Med.*, 61(1), 76-85.

Balemans, W., Ebeling, M., Patel, N., Van Hul, E., Olson, P., Dioszegi, M., Lacza, C., Wuyts, W., Van Den, E. J., Willems, P., Paes-Alves, A. F., Hill, S., Bueno, M., Ramos, F. J., Tacconi, P., Dikkers, F. G., Stratakis, C., Lindpaintner, K., Vickery, B., Foernzler, D. & Van Hul, W. (2001) Increased bone density in sclerosteosis is due to the deficiency of a novel secreted protein (SOST). *Hum. Mol. Genet*, 10(5), 537-543.

Barker, D. J., Chamberlain, A. T., Guyer, P. B. & Gardner, M. J. (1980) Paget's disease of bone: the Lancashire focus. *Br. Med. J.*, 280(6222), 1105-1107.

Barker, D. J. & Gardner, M. J. (1974) Distribution of Paget's diease in England, Wales and Scotland and a possible relationship with vitamin D deficiency in childhood. *Br. J. Prev. Soc. Med.*, 28, 226-232.

Barrett, J. C., Fry, B., Maller, J. & Daly, M. J. (2005) Haploview: analysis and visualization of LD and haplotype maps. *Bioinformatics*, 21(2), 263-265.

Basle, M. F., Fournier, J. G., Rozenblatt, S., Rebel, A. & Bouteille, M. (1986) Measles virus RNA detected in Paget's disease bone tissue by in situ hybridization. *J. Gen. Virol.*, 67 (Pt 5), 907-913.

Basle, M. F., Russell, W. C., Goswami, K. K., Rebel, A., Giraudon, P., Wild, F. & Filmon, R. (1985) Paramyxovirus antigens in osteoclasts from Paget's bone tissue detected by monoclonal antibodies. *J. Gen. Virol.*, 66 (Pt 10), 2103-10.

Beauregard, M., Gagnon, E., Guay-Belanger, S., Morissette, J., Brown, J. P. & Michou, L. (2014) Identification of rare genetic variants in novel loci associated with Paget's disease of bone. *Hum. Genet.*, 133(6), 755-68.

Beckman Coulter (2017a) *PCR Purification Agencourt AMPure XP*, 2017a. Available online: http://uk.beckman.com/nucleic-acid-sample-prep/purification-clean-up/pcr-purification?geolocation=gb [Accessed].

Beckman Coulter (2017b) *Sanger Sequencing Dye Terminator Removal Agencourt CleanSEQ*, 2017b. Available online: http://uk.beckman.com/nucleic-acid-sample-prep/purification-clean-up/sanger-sequencing-dye-terminator-removal [Accessed].

Bento, C. F., Puri, C., Moreau, K. & Rubinsztein, D. C. (2013) The role of membrane-trafficking small GTPases in the regulation of autophagy. *J. Cell Sci.*, 126(Pt 5), 1059-69.

Beyens, G., Daroszewska, A., de, F. F., Fransen, E., Vanhoenacker, F., Verbruggen, L., Zmierczak, H. G., Westhovens, R., Van, O. J., Ralston, S. H., Devogelaer, J. P. & Van, H. W. (2007) Identification of sex-specific associations between polymorphisms of the osteoprotegerin gene, TNFRSF11B, and Paget's disease of bone. *J. Bone Miner. Res.*, 22(7), 1062-1071.

Bhadada, S., Bhansali, A., Unnikrishnan, A. G., Khadgawat, R., Singh, S. K., Mithal, A. & Saikia, U. N. (2006) Does Paget's disease exist in India?: A series of 21 patients. *J. Assoc. Physicians India*, 54, 530-534.

Bianco, P., Silvestrini, G., Ballanti, P. & Bonucci, E. (1992) Paramyxovirus-like nuclear inclusions identical to those of Paget's disease of bone detected in giant cells of primary oxalosis. *Virchows Archiv - A, Path. Anat. & Histo.*, 421(5), 427-433.

Bjorkoy, G., Lamark, T., Brech, A., Outzen, H., Perander, M., Overvatn, A., Stenmark, H. & Johansen, T. (2005) p62/SQSTM1 forms protein aggregates degraded by autophagy and has a protective effect on huntingtin-induced cell death. *J. Cell Biol*, 171(4), 603-614.

Bliss, J. M., Venkatesh, B. & Colicelli, J. (2006) The RIN family of Ras effectors. *Methods Enzymol.*, 407, 335-344.

Boyle, W. J., Simonet, W. S. & Lacey, D. L. (2003) Osteoclast differentiation and activation. *Nature*, 423(6937), 337-342.

Brandi, M. L., Hukkanen, M., Umeda, T., Moradi-Bidhendi, N., Bianchi, S., Gross, S. S., Polak, J. M. & MacIntyre, I. (1995) Bidirectional regulation of osteoclast function by nitric oxide synthase isoforms. *Proc. Natl. Acad. Sci. U. S. A.*, 92(7), 2954-2958.

Brandwood, C. P., Hoyland, J. A., Hillarby, M. C., Berry, J. L., Davies, M., Selby, P. L. & Mee, A. P. (2003) Apoptotic gene expression in Paget's disease: a possible role for Bcl-2. *J. Pathol.*, 201(3), 504-12.

Bucay, N., Sarosi, I., Dunstan, C. R., Morony, S., Tarpley, J., Capparelli, C., Scully, S., Tan, H. L., Xu, W., Lacey, D. L., Boyle, W. J. & Simonet, W. S. (1998) osteoprotegerin-deficient mice develop early onset osteoporosis and arterial calcification. *Genes Dev.*, 12(9), 1260-1268.

Campbell, G. M. & Sophocleous, A. (2014) Quantitative analysis of bone and soft tissue by micro-computed tomography: applications to ex vivo and in vivo studies. *Bonekey Rep.*, 3, 564.

Cao, J. J., Wronski, T. J., Iwaniec, U., Phleger, L., Kurimoto, P., Boudignon, B. & Halloran, B. P. (2005) Aging increases stromal/osteoblastic cell-induced osteoclastogenesis and alters the osteoclast precursor pool in the mouse. *J. Bone Miner. Res.*, 20(9), 1659-1668.

Chamoux, E., Couture, J., Bisson, M., Morissette, J., Brown, J. P. & Roux, S. (2009) The p62 P392L mutation linked to Paget's disease induces activation of human osteoclasts. *Mol. Endocrinol.*, 23(10), 1668-1680.

Chong, B., Hegde, M., Fawkner, M., Simonet, S., Cassinelli, H., Coker, M., Kanis, J., Seidel, J., Tau, C., Tuysuz, B., Yuksel, B., Love, D. & Cundy, T. (2003) Idiopathic hyperphosphatasia and TNFRSF11B mutations: relationships between phenotype and genotype. *J. Bone Miner. Res.*, 18(12), 2095-2104.

Chung, P. Y., Beyens, G., Boonen, S., Papapoulos, S., Geusens, P., Karperien, M., Vanhoenacker, F., Verbruggen, L., Fransen, E., Van, O. J., Goemaere, S., Zmierczak, H. G., Westhovens, R., Devogelaer, J. P. & Van, H. W. (2010) The majority of the genetic risk for Paget's disease of bone is explained by genetic variants close to the CSF1, OPTN, TM7SF4, and TNFRSF11A genes. *Hum. Genet.*, 128(6), 615-626.

Chung, P. Y., Beyens, G., de, F. F., Boonen, S., Geusens, P., Vanhoenacker, F., Verbruggen, L., Van, O. J., Goemaere, S., Zmierczak, H. G., Westhovens, R., Devogelaer, J. P. & Van, H. W. (2011) Indications for a genetic association of a VCP polymorphism with the pathogenesis of sporadic Paget's disease of bone, but not for TNFSF11 (RANKL) and IL-6 polymorphisms. *Mol. Genet. Metab.*, 103(3), 287-292.

Chung, P. Y. J. & Van Hul, W. (2012) Paget's Disease of Bone: Evidence for Complex Pathogenetic Interactions. *Semin. Arthritis Rheum.*, 41(5), 619-641.

Clarke, B. (2008) Normal bone anatomy and physiology. *Clin. J. Am. Soc. Nephrol.*, 3 Suppl 3, S131-9.

Cody, J. D., Singer, F. R., Roodman, G. D., Otterund, B., Lewis, T. B., Leppert, M. & Leach, R. J. (1997) Genetic linkage of Paget disease of the bone to chromosome 18q. *Am. J Hum. Genet.*, 61(5), 1117-1122.

Cooper, C., Schafheutle, K., Dennison, E., Kellingray, S., Guyer, P. & Barker, D. (1999) The epidemiology of Paget's disease in Britain: is the prevalence decreasing? *J. Bone Miner. Res.*, 14(2), 192-197.

Cooper, G. M., Stone, E. A., Asimenos, G., Program, N. C. S., Green, E. D., Batzoglou, S. & Sidow, A. (2005) Distribution and intensity of constraint in mammalian genomic sequence. *Genome Res.*, 15(7), 901-13.

Cundy, T. (2006) Is the prevalence of Paget's disease of bone decreasing? *J. Bone Miner. Res.*, 21 Suppl 2, P9-13.

Cundy, T., Hegde, M., Naot, D., Chong, B., King, A., Wallace, R., Mulley, J., Love, D. R., Seidel, J., Fawkner, M., Banovic, T., Callon, K. E., Grey, A. B., Reid, I. R., Middleton-Hardie, C. A. & Cornish, J. (2002) A mutation in the gene TNFRSF11B encoding osteoprotegerin causes an idiopathic hyperphosphatasia phenotype. *Hum. Mol. Genet.*, 11(18), 2119-2127.

Cundy, T., Rutland, M. D., Naot, D. & Bolland, M. (2015) Evolution of Paget's disease of bone in adults inheriting SQSTM1 mutations. *Clin. Endocrinol. (Oxf.)*.

Dai, R. M., Chen, E., Longo, D. L., Gorbea, C. M. & Li, C. C. (1998) Involvement of valosin-containing protein, an ATPase Co-purified with IkappaBalpha and 26 S proteasome, in ubiquitin-proteasome-mediated degradation of IkappaBalpha. *J. Biol. Chem.*, 273(6), 3562-3573.

Daroszewska, A., Hocking, L. J., McGuigan, F. E. A., Langdahl, B. L., Stone, M. D., Cundy, T., Nicholson, G. C., Fraser, W. D. & Ralston, S. H. (2004) Susceptibility to Paget's disease of bone is influenced by a common polymorphic variant of Osteoprotegerin. *J. Bone Miner. Res.*, 19(9), 1506-1511.

Daroszewska, A., van't Hof, R. J., Rojas, J. A., Layfield, R., Landao-Basonga, E., Rose, L., Rose, K. & Ralston, S. H. (2011) A point mutation in the ubiquitin associated domain of SQSMT1 is sufficient to cause a Paget's disease like disorder in mice. *Hum. Mol. Genet.*, 20(14), 2734-2744.

Den Dunnen, J. T. & Antonarakis, S. E. (2000) Mutation nomenclature extensions and suggestions to describe complex mutations: a discussion. *Hum. Mutat.*, 15(1), 7-12.

DeSelm, C. J., Miller, B. C., Zou, W., Beatty, W. L., van, M. E., Takahata, Y., Klumperman, J., Tooze, S. A., Teitelbaum, S. L. & Virgin, H. W. (2011) Autophagy proteins regulate the secretory component of osteoclastic bone resorption. *Dev. Cell*, 21(5), 966-974.

Detheridge, F. M., Guyer, P. B. & Barker, D. J. (1982) European distribution of Paget's disease of bone. *Br. Med. J.*, 285(6347), 1005-1008.

Divisato, G., Formicola, D., Esposito, T., Merlotti, D., Pazzaglia, L., Del Fattore, A., Siris, E., Orcel, P., Brown, J. P., Nuti, R., Strazzullo, P., Benassi, M. S., Cancela, M. L., Michou, L., Rendina, D., Gennari, L. & Gianfrancesco, F. (2016) ZNF687

Mutations in Severe Paget Disease of Bone Associated with Giant Cell Tumor. *Am. J. Hum. Genet.*, 98(2), 275-86.

Djamshidian, A., Schaefer, J., Haubenberger, D., Stogmann, E., Zimprich, F., Auff, E. & Zimprich, A. (2009) A novel mutation in the VCP gene (G157R) in a German family with inclusion-body myopathy with Paget disease of bone and frontotemporal dementia. *Muscle Nerve*, 39(3), 389-91.

Donath, J., Speer, G., Kosa, J. P., Arvai, K., Balla, B., Juhasz, P., Lakatos, P. & Poor, G. (2015) Polymorphisms of CSF1 and TM7SF4 genes in a case of mild juvenile Paget's disease found using next-generation sequencing. *Croat. Med. J.*, 56(2), 145-51.

Dougall, W. C., Glaccum, M., Charrier, K., Rohrbach, K., Brasel, K., De Smedt, T., Daro, E., Smith, J., Tometsko, M. E., Maliszewski, C. R., Armstrong, A., Shen, V., Bain, S., Cosman, D., Anderson, D., Morrissey, P. J., Peschon, J. J. & Schuh, J. (1999) RANK is essential for osteoclast and lymph node development. *Genes Dev.*, 13(18), 2412-2424.

Duplomb, L., Baud'huin, M., Charrier, C., Berreur, M., Trichet, V., Blanchard, F. & Heymann, D. (2008) Interleukin-6 inhibits receptor activator of nuclear factor kappaB ligand-induced osteoclastogenesis by diverting cells into the macrophage lineage: key role of Serine727 phosphorylation of signal transducer and activator of transcription 3. *Endocrinology*, 149(7), 3688-3697.

Erben, R. G. & Glosmann, M. (2012) Histomorphometry in rodents. *Methods Mol. Biol.*, 816, 279-303.

Erben, R. G., Scutt, A. M., Miao, D., Kollenkirchen, U. & Haberey, M. (1997) Short-term treatment of rats with high dose 1,25-dihydroxyvitamin D3 stimulates bone formation and increases the number of osteoblast precursor cells in bone marrow. *Endocrinology*, 138(11), 4629-35.

Feng, J. Q., Ward, L. M., Liu, S., Lu, Y., Xie, Y., Yuan, B., Yu, X., Rauch, F., Davis, S. I., Zhang, S., Rios, H., Drezner, M. K., Quarles, L. D., Bonewald, L. F. & White, K. E. (2006) Loss of DMP1 causes rickets and osteomalacia and identifies a role for osteocytes in mineral metabolism. *Nat. Genet.*, 38(11), 1310-1315.

Fleisch, H. (2000) *Bisphosphonates in Bone Disease: From the Laboratory to the Patient* 4edition. Academic Press.

Friedrichs, W. E., Reddy, S. V., Bruder, J. M., Cundy, T., Cornish, J., Singer, F. R. & Roodman, G. D. (2002) Sequence analysis of measles virus nucleocapsid transcripts in patients with Paget's disease. *J. Bone Miner. Res.*, 17(1), 145-151.

Galson, D. L. & Roodman, G. D. (2014) Pathobiology of Paget's Disease of Bone. *J. Bone. Metab.*, 21(2), 85-98.

Gardner, M. J., Guyer, P. B. & Barker, D. J. P. (1978) Radiological prevalance of Paget's disease of bone in British migrants to Australia. *Br. Med. J.*, 1, 1655-1657.

Gasper, T. M. (1979) Paget's disease in a treadle machine operator [letter]. *Br. Med. J.*, 1(6172), 1217-1218.

Gebhart, M., Vandeweyer, E. & Nemec, E. (1998) Paget's disease of bone complicated by giant cell tumor. *Clin. Orthop. Relat. Res.*(352), 187-93.

Geer, L. Y., Marchler-Bauer, A., Geer, R. C., Han, L., He, J., He, S., Liu, C., Shi, W. & Bryant, S. H. (2010) The NCBI BioSystems database. *Nucleic Acids Res.*, 38(Database issue), D492-6.

Geetha, T. & Wooten, M. W. (2002) Structure and functional properties of the ubiquitin binding protein p62. *FEBS Lett.*, 512(1-3), 19-24.

Gelb, B. D., Shi, G. P., Chapman, H. A. & Desnick, R. J. (1996) Pycnodysostosis, a lysosomal disease caused by cathepsin K deficiency. *Science*, 273(5279), 1236-1238.

Gianfrancesco, F., Rendina, D., Di, S. M., Mingione, A., Esposito, T., Merlotti, D., Gallone, S., Magliocca, S., Goode, A., Formicola, D., Morello, G., Layfield, R., Frattini, A., De, F. G., Nuti, R., Searle, M., Strazzullo, P., Isaia, G., Mossetti, G. & Gennari, L. (2012) A nonsynonymous TNFRSF11A variation increases NFkappaB activity and the severity of Paget's disease. *J. Bone Miner. Res.*, 27(2), 443-452.

Gianfrancesco, F., Rendina, D., Merlotti, D., Esposito, T., Amyere, M., Formicola, D., Muscariello, R., De Filippo, G., Strazzullo, P., Nuti, R., Vikkula, M. & Gennari, L. (2013) Giant cell tumor occurring in familial Paget's disease of bone: report of clinical characteristics and linkage analysis of a large pedigree. *J. Bone Miner. Res.*, 28(2), 341-50.

Girasole, G., Jilka, R. L., Passeri, G., Boswell, S., Boder, G., Williams, D. C. & Manolagas, S. C. (1992) 17 beta-estradiol inhibits interleukin-6 production by bone marrow- derived stromal cells and osteoblasts in vitro: a potential mechanism for the antiosteoporotic effect of estrogens. *J. Clin. Invest.*, 89(3), 883-891.

Gonzalez-Perez, A. & Lopez-Bigas, N. (2011) Improving the assessment of the outcome of nonsynonymous SNVs with a consensus deleteriousness score, Condel. *Am. J. Hum. Genet.*, 88(4), 440-9.

Gordon, M. T., Anderson, D. C. & Sharpe, P. T. (1991) Canine distemper virus localised in bone cells of patients with Paget's disease. *Bone*, 12, 195-201.

Grandi, P., Dang, T., Pane, N., Shevchenko, A., Mann, M., Forbes, D. & Hurt, E. (1997) Nup93, a vertebrate homologue of yeast Nic96p, forms a complex with a novel 205-kDa protein and is required for correct nuclear pore assembly. *Mol. Biol. Cell*, 8(10), 2017-2038.

Grantham, R. (1974) Amino acid difference formula to help explain protein evolution. *Science*, 185(4154), 862-4.

Grasemann, C., Schundeln, M. M., Hovel, M., Schweiger, B., Bergmann, C., Herrmann, R., Wieczorek, D., Zabel, B., Wieland, R. & Hauffa, B. P. (2013) Effects of RANK-ligand antibody (denosumab) treatment on bone turnover markers in a girl with juvenile Paget's disease. *J. Clin. Endocrinol. Metab.*, 98(8), 3121-6.

Greenbaum, D., Colangelo, C., Williams, K. & Gerstein, M. (2003) Comparing protein abundance and mRNA expression levels on a genomic scale. *Genome Biol.*, 4(9), 117.

Guerrini, M. M., Sobacchi, C., Cassani, B., Abinun, M., Kilic, S. S., Pangrazio, A., Moratto, D., Mazzolari, E., Clayton-Smith, J., Orchard, P., Coxon, F. P., Helfrich, M. H., Crockett, J. C., Mellis, D., Vellodi, A., Tezcan, I., Notarangelo, L. D., Rogers, M. J., Vezzoni, P., Villa, A. & Frattini, A. (2008) Human osteoclast-poor osteopetrosis with hypogammaglobulinemia due to TNFRSF11A (RANK) mutations. *Am. J. Hum. Genet.*, 83(1), 64-76.

Guyant-Marechal, L., Laquerriere, A., Duyckaerts, C., Dumanchin, C., Bou, J., Dugny, F., Le, B., I, Frebourg, T., Hannequin, D. & Campion, D. (2006) Valosin-containing protein gene mutations: clinical and neuropathologic features. *Neurology*, 67(4), 644-651.

Guyer, P. B. & Chamberlain, A. T. (1980) Paget's disease of bone in two American cities. *Br. Med. J.*, 280(6219), 985.

Guyer, P. B. & Chamberlain, A. T. (1988) Paget's disease of bone in South Africa. *Clin. Radiol.*, 39(1), 51-52.

Hama, H., Tall, G. G. & Horazdovsky, B. F. (1999) Vps9p is a guanine nucleotide exchange factor involved in vesicle-mediated vacuolar protein transport. *J. Biol. Chem.*, 274(21), 15284-91.

Hansen, M. F., Seton, M. & Merchant, A. (2006) Osteosarcoma in Paget's disease of bone. *J. Bone Miner. Res.*, 21, P58-P63.

Hartgers, F. C., Vissers, J. L., Looman, M. W., van, Z. C., Huffine, C., Figdor, C. G. & Adema, G. J. (2000) DC-STAMP, a novel multimembrane-spanning molecule preferentially expressed by dendritic cells. *Eur. J. Immunol.*, 30(12), 3585-3590.

Harvey, L., Gray, T., Beneton, M. N. C., Douglas, D. L., Kanis, J. A. & Russell, R. G. G. (1982) Ultrastructural features of the osteoclasts from Paget's disease of bone in relation to a viral aetiology. *J. Clin. Path.*, 35, 771-779.

Hashimoto, J., Ohno, I., Nakatsuka, K., Yoshimura, N., Takata, S., Zamma, M., Yabe, H., Abe, S., Terada, M., Yoh, K., Fukunaga, M., Cooper, C., Morii, H. & Yoshikawa, H. (2006) Prevalence and clinical features of Paget's disease of bone in Japan. *J. Bone Miner. Metab.*, 24(3), 186-190.

Haubenberger, D., Bittner, R. E., Rauch-Shorney, S., Zimprich, F., Mannhalter, C., Wagner, L., Mineva, I., Vass, K., Auff, E. & Zimprich, A. (2005) Inclusion body myopathy and Paget disease is linked to a novel mutation in the VCP gene. *Neurology*, 65(8), 1304-1305.

Helfrich, M. H., Hobson, R. P., Grabowski, P. S., Zurbriggen, A., Cosby, S. L., Dickson, G. R., Fraser, W. D., Ooi, C. G., Selby, P. L., Crisp, A. J., Wallace, R. G., Kahn, S. & Ralston, S. H. (2000) A negative search for a paramyxoviral etiology of Paget's disease of bone: molecular, immunological, and ultrastructural studies in UK patients. *J. Bone Miner. Res.*, 15(12), 2315-2329.

Hennies, H. C., Kornak, U., Zhang, H., Egerer, J., Zhang, X., Seifert, W., Kuhnisch, J., Budde, B., Natebus, M., Brancati, F., Wilcox, W. R., Muller, D., Kaplan, P. B., Rajab, A., Zampino, G., Fodale, V., Dallapiccola, B., Newman, W., Metcalfe, K., Clayton-Smith, J., Tassabehji, M., Steinmann, B., Barr, F. A., Nurnberg, P., Wieacker, P. & Mundlos, S. (2008) Gerodermia osteodysplastica is caused by mutations in SCYL1BP1, a Rab-6 interacting golgin. *Nat. Genet.*, 40(12), 1410-1412.

Hill, T. P., Spater, D., Taketo, M. M., Birchmeier, W. & Hartmann, C. (2005) Canonical Wnt/beta-catenin signaling prevents osteoblasts from differentiating into chondrocytes. *Dev. Cell*, 8(5), 727-738.

Hiruma, Y., Kurihara, N., Subler, M. A., Zhou, H., Boykin, C. S., Zhang, H., Ishizuka, S., Dempster, D. W., Roodman, G. D. & Windle, J. J. (2008) A SQSTM1/p62 mutation linked to Paget's disease increases the osteoclastogenic potential of the bone microenvironment. *Hum. Mol. Genet.*, 17(23), 3708-3719.

Hocking, L. J., Herbert, C. A., Nicholls, R. K., Williams, F., Bennett, S. T., Cundy, T., Nicholson, G. C., Wuyts, W., Van Hul, W. & Ralston, S. H. (2001) Genomewide search in familial paget disease of bone shows evidence of genetic heterogeneity with candidate loci on chromosomes 2q36, 10p13, and 5q35. *Am. J Hum. Genet.*, 69(5), 1055-1061.

Hocking, L. J., Lucas, G. J. A., Daroszewska, A., Cundy, T., Nicholson, G. C., Donath, J., Walsh, J. P., Finlayson, C., Cavey, J. R., Ciani, B., Sheppard, P. W., Searle, M. S., Layfield, R. & Ralston, S. H. (2004) Novel UBA domain mutations of SQSTM1 in Paget's disease of bone: genotype phenotype correlation, functional analysis and structural consequences. *J. Bone Miner. Res.*, 19(7), 1122-1127.

Hocking, L. J., Whitehouse, C. & Helfrich, M. H. (2012) Autophagy: a new player in skeletal maintenance? *J. Bone Miner. Res.*, 27(7), 1439-47.

Houston, B., Stewart, A. J. & Farquharson, C. (2004) PHOSPHO1-A novel phosphatase specifically expressed at sites of mineralisation in bone and cartilage. *Bone*, 34(4), 629-37.

Hu, H., Bliss, J. M., Wang, Y. & Colicelli, J. (2005) RIN1 is an ABL tyrosine kinase activator and a regulator of epithelial-cell adhesion and migration. *Curr. Biol.*, 15(9), 815-823.

Hughes, A. E. & Barr, R. J. (1996) Familial Expansile Osteolysis: A genetic model of Paget's disease, in Sharpe, P. T. (ed), *The molecular biology of Paget's Disease*. London: R.G.Landes Company, 179-199.

Hughes, A. E., Ralston, S. H., Marken, J., Bell, C., MacPherson, H., Wallace, R. G., Van Hul, W., Whyte, M. P., Nakatsuka, K., Hovy, L. & Anderson, D. M. (2000) Mutations in TNFRSF11A, affecting the signal peptide of RANK, cause familial expansile osteolysis. *Nat. Genet.*, 24(1), 45-48.

Hughes, A. E., Shearman, A. M., Weber, J. L., Barr, R. J., Wallace, R. G., Osterberg, P. H., Nevin, N. C. & Mollan, R. A. (1994) Genetic linkage of familial expansile osteolysis to chromosome 18q. *Hum. Mol. Genet.*, 3(2), 359-361.

Hultgren, H. N. (1998) Osteitis deformans (Paget's disease) and calcific disease of the heart valves. *Am. J. Cardiol.*, 81(12), 1461-1464.

Ishida, T. & Kinoshita, K. (2008) Prediction of disordered regions in proteins based on the meta approach. *Bioinformatics*, 24(11), 1344-8.

Itzstein, C., Coxon, F. P. & Rogers, M. J. (2011) The regulation of osteoclast function and bone resorption by small GTPases. *Small GTPases*, 2(3), 117-130.

Janson, C., Kasahara, N., Prendergast, G. C. & Colicelli, J. (2012) RIN3 is a negative regulator of mast cell responses to SCF. *PLoS One*, 7(11), e49615.

Janssens, K., de Vernejoul, M. C., de, F. F., Vanhoenacker, F. & Van, H. W. (2005) An intermediate form of juvenile Paget's disease caused by a truncating TNFRSF11B mutation. *Bone*, 36(3), 542-548.

Jin, W., Chang, M., Paul, E. M., Babu, G., Lee, A. J., Reiley, W., Wright, A., Zhang, M., You, J. & Sun, S. C. (2008) Deubiquitinating enzyme CYLD negatively regulates RANK signaling and osteoclastogenesis in mice. *J. Clin. Invest.*, 118, 1858-1866.

Johnson, J. O., Mandrioli, J., Benatar, M., Abramzon, Y., Van Deerlin, V. M., Trojanowski, J. Q., Gibbs, J. R., Brunetti, M., Gronka, S., Wuu, J., Ding, J. H., McCluskey, L., Martinez-Lage, M., Falcone, D., Hernandez, D. G., Arepalli, S., Chong, S., Schymick, J. C., Rothstein, J., Landi, F., Wang, Y. D., Calvo, A., Mora, G., Sabatelli, M., Monsurro, M. R., Battistini, S., Salvi, F., Spataro, R., Sola, P., Borghero, G., Galassi, G., Scholz, S. W., Taylor, J. P., Restagno, G., Chio, A., Traynor, B. J. & Consortium, I. (2010) Exome Sequencing Reveals VCP Mutations as a Cause of Familial ALS. *Neuron*, 68(5), 857-864.

Ju, J. S., Fuentealba, R. A., Miller, S. E., Jackson, E., Piwnica-Worms, D., Baloh, R. H. & Weihl, C. C. (2009) Valosin-containing protein (VCP) is required for autophagy and is disrupted in VCP disease. *J. Cell Biol.*, 187(6), 875-888.

Kajiho, H., Saito, K., Tsujita, K., Kontani, K., Araki, Y., Kurosu, H. & Katada, T. (2003) RIN3: a novel Rab5 GEF interacting with amphiphysin II involved in the early endocytic pathway. *J. Cell Sci.*, 116(Pt 20), 4159-68.

Kajiho, H., Sakurai, K., Minoda, T., Yoshikawa, M., Nakagawa, S., Fukushima, S., Kontani, K. & Katada, T. (2011) Characterization of RIN3 as a guanine nucleotide exchange factor for the Rab5 subfamily GTPase Rab31. *J. Biol. Chem.*, 286(27), 24364-73.

Kan, C. W., Fredlake, C. P., Doherty, E. A. & Barron, A. E. (2004) DNA sequencing and genotyping in miniaturized electrophoresis systems. *Electrophoresis*, 25(21-22), 3564-88.

Kaplan, F. S. (1994) Paget's disease of bone: orthopedic complications. *Semin. Arthritis Rheum.*, 23(4), 250-2.

Kay, B. K., Williamson, M. P. & Sudol, M. (2000) The importance of being proline: the interaction of proline-rich motifs in signaling proteins with their cognate domains. *FASEB J.*, 14(2), 231-41.

Kemp, J. P., Medina-Gomez, C., Estrada, K., St Pourcain, B., Heppe, D. H. M., Warrington, N. M., Oei, L., Ring, S. M., Kruithof, C. J., Timpson, N. J., Wolber, L. E., Reppe, S., Gautvik, K., Grundberg, E., Ge, B., van der Eerden, B., van de Peppel, J., Hibbs, M. A., Ackert-Bicknell, C. L., Choi, K., Koller, D. L., Econs, M. J., Williams, F. M. K., Foroud, T., Zillikens, M. C., Ohlsson, C., Hofman, A., Uitterlinden, A. G., Smith, G. D., Jaddoe, V. W. V., Tobias, J. H., Rivadeneira, F. & Evans, D. M. (2014) Phenotypic Dissection of Bone Mineral Density Reveals Skeletal Site Specificity and Facilitates the Identification of Novel Loci in the Genetic Regulation of Bone Mass Attainment. *PLoS Genet.*, 10(6).

Kibbe, W. A. (2007) OligoCalc: an online oligonucleotide properties calculator. *Nucleic Acids Res.*, 35(Web Server issue), W43-6.

Kim, H. J., Kim, N. C., Wang, Y. D., Scarborough, E. A., Moore, J., Diaz, Z., MacLea, K. S., Freibaum, B., Li, S., Molliex, A., Kanagaraj, A. P., Carter, R., Boylan, K. B., Wojtas, A. M., Rademakers, R., Pinkus, J. L., Greenberg, S. A., Trojanowski, J. Q., Traynor, B. J., Smith, B. N., Topp, S., Gkazi, A. S., Miller, J., Shaw, C. E., Kottlors, M., Kirschner, J., Pestronk, A., Li, Y. R., Ford, A. F., Gitler, A. D., Benatar, M., King, O. D., Kimonis, V. E., Ross, E. D., Weihl, C. C., Shorter, J. & Taylor, J. P. (2013) Mutations in prion-like domains in hnRNPA2B1 and hnRNPA1 cause multisystem proteinopathy and ALS. *Nature*, 495(7442), 467-473.

Kong, Y. Y., Yoshida, H., Sarosi, I., Tan, H. L., Timms, E., Capparelli, C., Morony, Oliveira, d. S. A., Van, G., Itie, A., Khoo, W., Wakeham, A., Dunstan, CR, Lacey, D. L., Mak, T. W., Boyle, W. J. & Penninger, J. M. (1999) OPGL is a key regulator of osteoclastogenesis, lymphocyte development and lymph-node organogenesis. *Nature*, 397(6717), 315-323.

Kornak, U., Kasper, D., Bosl, M. R., Kaiser, E., Schweizer, M., Schulz, A., Friedrich, W., Delling, G. & Jentsch, T. J. (2001) Loss of the ClC-7 chloride channel leads to osteopetrosis in mice and man. *Cell*, 104(2), 205-215.

Kotake, S., Sato, K., Kim, K. J., Takahashi, N., Udagawa, N., Nakamura, I., Yamaguchi, A., Kishimoto, T., Suda, T. & Kashiwazaki, S. (1996) Interleukin-6 and soluble interleukin-6 receptors in the synovial fluids from rheumatoid arthritis patients are responsible for osteoclast-like cell formation. *J. Bone Miner. Res.*, 11(1), 88-95.

Kovach, M. J., Waggoner, B., Leal, S. M., Gelber, D., Khardori, R., Levenstien, M. A., Shanks, C. A., Gregg, G., Al Lozi, M. T., Miller, T., Rakowicz, W., Lopate, G., Florence, J., Glosser, G., Simmons, Z., Morris, J. C., Whyte, M. P., Pestronk, A. & Kimonis, V. E. (2001) Clinical delineation and localization to chromosome 9p13.3-p12 of a unique dominant disorder in four families: hereditary inclusion body myopathy, Paget disease of bone, and frontotemporal dementia. *Mol. Genet. Metab.*, 74(4), 458-475.

Kozlowski, L. P. & Bujnicki, J. M. (2012) MetaDisorder: a meta-server for the prediction of intrinsic disorder in proteins. *BMC Bioinformatics*, 13, 111.

Kudo, O., Sabokbar, A., Pocock, A., Itonaga, I., Fujikawa, Y. & Athanasou, N. A. (2003) Interleukin-6 and interleukin-11 support human osteoclast formation by a RANKL-independent mechanism. *Bone*, 32(1), 1-7.

Kukita, A., Chenu, C., McManus, L. M., Mundy, G. R. & Roodman, G. D. (1990) Atypical multinucleated cells form in long-term marrow cultures from patients with Paget's disease. *J. Clin. Invest.*, 85(4), 1280-1286.

Kukita, T., Wada, N., Kukita, A., Kakimoto, T., Sandra, F., Toh, K., Nagata, K., Iijima, T., Horiuchi, M., Matsusaki, H., Hieshima, K., Yoshie, O. & Nomiyama, H. (2004) RANKL-induced DC-STAMP is essential for osteoclastogenesis. *J. Exp. Med.*, 200(7), 941-946.

Kumar, P., Henikoff, S. & Ng, P. C. (2009) Predicting the effects of coding non-synonymous variants on protein function using the SIFT algorithm. *Nat. Protoc.*, 4(7), 1073-81.

Kurihara, N., Hiruma, Y., Yamana, K., Michou, L., Rousseau, C., Morissette, J., Galson, D. L., Teramachi, J., Zhou, H., Dempster, D. W., Windle, J. J., Brown, J. P. & Roodman, G. D. (2011) Contributions of the measles virus nucleocapsid gene and the SQSTM1/p62(P392L) mutation to Paget's disease. *Cell Metab.*, 13(1), 23-34.

Kurihara, N., Reddy, S. V., Araki, N., Ishizuka, S., Ozono, K., Cornish, J., Cundy, T., Singer, F. R. & Roodman, G. D. (2004) Role of TAFII-17, a VDR binding protein, in the increased osteoclast formation in Paget's Disease. *J. Bone Miner. Res.*, 19(7), 1154-1164.

Kurihara, N., Reddy, S. V., Menaa, C., Anderson, D. & Roodman, G. D. (2000) Osteoclasts expressing the measles virus nucleocapsid gene display a pagetic phenotype. *J. Clin. Invest.*, 105(5), 607-614.

Kurihara, N., Zhou, H., Reddy, S. V., Garcia Palacios, V., Subler, M. A., Dempster, D. W., Windle, J. J. & Roodman, G. D. (2006) Experimental models of Paget's disease. *J. Bone Miner. Res.*, 21 Suppl 2, P55-7.

Langston, A. L., Campbell, M. K., Fraser, W. D., Maclennan, G., Selby, P. & Ralston, S. H. (2007) Clinical Determinants of Quality of Life in Paget's Disease of Bone. *Calcif. Tissue Int.*, 80(1), 1-9.

Langston, A. L., Campbell, M. K., Fraser, W. D., MacLennan, G. S., Selby, P. L. & Ralston, S. H. (2010a) Randomised Trial of Intensive Bisphosphonate Treatment Versus Symptomatic Management in Paget's Disease of Bone. *J. Bone Miner. Res.*, 25, 20-31.

Langston, A. L., Campbell, M. K., Fraser, W. D., MacLennan, G. S., Selby, P. L. & Ralston, S. H. (2010b) Randomized Trial of Intensive Bisphosphonate Treatment Versus Symptomatic Management in Paget's Disease of Bone. *J. Bone Miner. Res.*, 25(1), 20-31.

Langston, A. L. & Ralston, S. H. (2004) Management of Paget's disease of bone. *Rheumatology. (Oxford)*, 43, 955-959.

Laurin, N., Brown, J. P., Lemainque, A., Duchesne, A., Huot, D., Lacourciere, Y., Drapeau, G., Verreault, J., Raymond, V. & Morissette, J. (2001) Paget disease of bone: mapping of two loci at 5q35-qter and 5q31. *Am. J. Hum. Genet.*, 69(3), 528-543.

Laurin, N., Brown, J. P., Morissette, J. & Raymond, V. (2002) Recurrent Mutation of the Gene Encoding sequestosome 1 (SQSTM1/p62) in Paget Disease of Bone. *Am. J. Hum. Genet.*, 70(6), 1582-1588.

Lever, J. H. (2002) Paget's disease of bone in Lancashire and arsenic pesticide in cotton mill wastewater: a speculative hypothesis. *Bone*, 31(3), 434-436.

Li, H. & Durbin, R. (2009) Fast and accurate short read alignment with Burrows-Wheeler transform. *Bioinformatics*, 25(14), 1754-60.

Li, X., Romero, P., Rani, M., Dunker, A. K. & Obradovic, Z. (1999) Predicting Protein Disorder for N-, C-, and Internal Regions. *Genome Inform Ser Workshop Genome Inform*, 10, 30-40.

Li, Y., Willer, C., Sanna, S. & Abecasis, G. (2009) Genotype imputation. *Annu. Rev. Gen. Hum. Genet.*, 10, 387-406.

Life Technologies (2011) *TaqMan® SNP Genotyping Assays*, 2011. Available online: http://www3.appliedbiosystems.com/cms/groups/mcb_marketing/documents/generaldocuments/cms_040597.pdf [Accessed].

Lin, H. K., Bergmann, S. & Pandolfi, P. P. (2004) Cytoplasmic PML function in TGF-beta signalling. *Nature*, 431(7005), 205-211.

Liu, C. C., Liu, C. C., Kanekiyo, T., Xu, H. & Bu, G. (2013) Apolipoprotein E and Alzheimer disease: risk, mechanisms and therapy. *Nat. Rev. Neurol.*, 9(2), 106-18.

Liu, H., Feng, W., Yimin, Cui, J., Lv, S., Hasegawa, T., Sun, B., Li, J., Oda, K., Amizuka, N. & Li, M. (2014) Histological Evidence of Increased Osteoclast Cell Number and Asymmetric Bone Resorption Activity in the Tibiae of Interleukin-6-Deficient Mice. *J. Histochem. Cytochem.*, 62(8), 556-64.

Lopez-Abente, G., Morales-Piga, A., Elena-Ibanez, A., Rey-Rey, J. S. & Corres-Gonzalez, J. (1997) Cattle, pets, and Paget's disease of bone. *Epidemiology*, 8(3), 247-251.

Lucas, G., Riches, P., Hocking, L., Cundy, T., Nicholson, G., Walsh, J. & Ralston, S. H. (2008) Identification of a Major Locus for Paget Disease on Chromosome 10p13 in Families of British Descent. *J. Bone Miner. Res.*, 23(1), 58-63.

Lucas, G. J., Mehta, S. G., Hocking, L. J., Stewart, T. L., Cundy, T., Nicholson, G. C., Walsh, J. P., Fraser, W. D., Watts, G. D., Ralston, S. H. & Kimonis, V. E. (2006) Evaluation of the role of Valosin-containing protein in the pathogenesis of familial and sporadic Paget's disease of bone. *Bone*, 38(2), 280-285.

Malovannaya, A., Lanz, R. B., Jung, S. Y., Bulynko, Y., Le, N. T., Chan, D. W., Ding, C., Shi, Y., Yucer, N., Krenciute, G., Kim, B. J., Li, C., Chen, R., Li, W., Wang, Y., O'Malley, B. W. & Qin, J. (2011) Analysis of the human endogenous coregulator complexome. *Cell*, 145(5), 787-99.

Maruyama, H., Morino, H., Ito, H., Izumi, Y., Kato, H., Watanabe, Y., Kinoshita, Y., Kamada, M., Nodera, H., Suzuki, H., Komure, O., Matsuura, S., Kobatake, K., Morimoto, N., Abe, K., Suzuki, N., Aoki, M., Kawata, A., Hirai, T., Kato, T., Ogasawara, K., Hirano, A., Takumi, T., Kusaka, H., Hagiwara, K., Kaji, R. & Kawakami, H. (2010) Mutations of optineurin in amyotrophic lateral sclerosis. *Nature*, 465(7295), 223-226.

Matthews, B. G., Afzal, M. A., Minor, P. D., Bava, U., Callon, K. E., Pitto, R. P., Cundy, T., Cornish, J., Reid, I. R. & Naot, D. (2008) Failure to detect measles virus RNA in bone cells from patients with Paget's disease. *J. Clin. Endocrinol. Metab*, 93, 1398-1401.

Mays, S. (2010) Archaeological skeletons support a northwest European origin for Paget's disease of bone. *J. Bone Miner. Res.*, 25(8), 1839-1841.

McHugh, K. P., Hodivala-Dilke, K., Zheng, M. H., Namba, N., Lam, J., Novack, D., Feng, X., Ross, F. P., Hynes, R. O. & Teitelbaum, S. L. (2000) Mice lacking beta3 integrins are osteosclerotic because of dysfunctional osteoclasts. *J. Clin. Invest.*, 105(4), 433-440.

Mee, A. P., Dixon, J. A., Hoyland, J. A., Davies, M., Selby, P. L. & Mawer, E. B. (1998) Detection of Canine Distemper Virus in 100% of Paget's disease samples by in situ-reverse transcriptase polymerase chain reaction. *Bone*, 23, 171-175.

Menaa, C., Reddy, S. V., Kurihara, N., Maeda, H., Anderson, D., Cundy, T., Cornish, J., Singer, F. R., Bruder, J. M. & Roodman, G. D. (2000) Enhanced RANK ligand expression and responsivity of bone marrow cells in Paget's disease of bone. *J. Clin. Invest.*, 105(12), 1833-1838.

Merlotti, D., Gennari, L., Galli, B., Martini, G., Calabro, A., De, P., V, Ceccarelli, E., Nardi, P., Avanzati, A. & Nuti, R. (2005) Characteristics and familial aggregation of Paget's disease of bone in Italy. *J. Bone Miner. Res.*, 20(8), 1356-1364.

Meunier, P. J., Coindre, J. M., Edouard, C. M. & Arlot, M. E. (1980) Bone histomorphometry in Paget's disease. Quantitative and dynamic analysis of pagetic and nonpagetic bone tissue. *Arthritis Rheum.*, 23(10), 1095-1103.

Michigami, T., Kageyama, T., Satomura, K., Shima, M., Yamaoka, K., Nakayama, M. & Ozono, K. (2002) Novel mutations in the a3 subunit of vacuolar H(+)-adenosine triphosphatase in a Japanese patient with infantile malignant osteopetrosis. *Bone*, 30(2), 436-9.

Michou, L., Chamoux, E., Couture, J., Morissette, J., Brown, J. P. & Roux, S. (2010) Gene expression profile in osteoclasts from patients with Paget's disease of bone. *Bone*, 46(3), 598-603.

Middleton-Hardie, C., Zhu, Q., Cundy, H., Lin, J. M., Callon, K., Tong, P. C., Xu, J., Grey, A., Cornish, J. & Naot, D. (2006) Deletion of aspartate 182 in OPG causes juvenile Paget's disease by impairing both protein secretion and binding to RANKL. *J. Bone Miner. Res.*, 21(3), 438-445.

Mills, B. G. & Singer, F. R. (1976) Nuclear inclusions in Paget's disease of bone. *Science*, 194, 201-202.

Mills, B. G., Singer, F. R., Weiner, L. P. & Holst, P. A. (1981) Immunohistological demonstration of respiratory syncytial virus antigens in Paget's disease of bone. *Proc. Natl. Acad. Sci. U. S. A.*, 78, 1209-1212.

Miron-Canelo, J. A., Del Pino-Montes, J., Vicente-Arroyo, M., Saenz-Gonzalez & MC. (1997) Epidemiological study of Paget's disease of bone in a zone of the Province of Salamanca (Spain). The Paget's disease of the bone study group of Salamanca. *Eur. J. Epidemiol.*, 13(7), 801-805.

Mizuno, A., Amizuka, N., Irie, K., Murakami, A., Fujise, N., Kanno, T., Sato, Y., Nakagawa, N., Yasuda, H., Mochizuki, S., Gomibuchi, T., Yano, K., Shima, N., Washida, N., Tsuda, E., Morinaga, T., Higashio, K. & Ozawa, H. (1998) Severe osteoporosis in mice lacking osteoclastogenesis inhibitory factor/osteoprotegerin. *Biochem. Biophys. Res. Commun*, 247(3), 610-615.

Monsell, E. M., Cody, D. D., Bone, H. G. & Divine, G. W. (1999) Hearing loss as a complication of Paget's disease of bone. *J. Bone Miner. Res.*, 14, 92-95.

Morissette, J., Laurin, N. & Brown, J. P. (2006) Sequestosome 1: Mutation Frequencies, Haplotypes, and Phenotypes in Familial Paget's Disease of Bone. *J. Bone Miner. Res.*, 21 Suppl 2, 38-44.

Mossetti, G., Rendina, D., De, F. G., Viceconti, R., Di, D. G., Cioffi, M., Postiglione, L. & Nunziata, V. (2005) Interleukin-6 and osteoprotegerin systems in Paget's disease of bone: relationship to risedronate treatment. *Bone*, 36(3), 549-554.

Mundlos, S. (1999) Cleidocranial dysplasia: clinical and molecular genetics. *J. Med. Genet.*, 36(3), 177-182.

Nakashima, K., Zhou, X., Kunkel, G., Zhang, Z., Deng, J. M., Behringer, R. R. & de Crombrugghe, B. (2002) The novel zinc finger-containing transcription factor osterix is required for osteoblast differentiation and bone formation. *Cell*, 108(1), 17-29.

Nakatsuka, K., Nishizawa, Y. & Ralston, S. H. (2003) Phenotypic characterization of early onset Paget's disease of bone caused by a 27-bp duplication in the TNFRSF11A gene. *J. Bone Miner. Res.*, 18(8), 1381-1385.

Nalbandian, A., Donkervoort, S., Dec, E., Badadani, M., Katheria, V., Rana, P., Nguyen, C., Mukherjee, J., Caiozzo, V., Martin, B., Watts, G. D., Vesa, J., Smith, C. & Kimonis, V. E. (2011) The multiple faces of valosin-containing protein-associated diseases: inclusion body myopathy with Paget's disease of bone, frontotemporal dementia, and amyotrophic lateral sclerosis. *J. Mol. Neurosci.*, 45(3), 522-31.

Naot, D., Choi, A., Musson, D. S., Kiper, P. O. S., Utine, G. E., Boduroglu, K., Peacock, M., DiMeglio, L. A. & Cundy, T. (2014) Novel homozygous mutations in the osteoprotegerin gene TNFRSF11B in two unrelated patients with juvenile Paget's disease. *Bone*, 68, 6-10.

Narisawa, S., Harmey, D., Yadav, M. C., O'Neill, W. C., Hoylaerts, M. F. & Millan, J. L. (2007) Novel inhibitors of alkaline phosphatase suppress vascular smooth muscle cell calcification. *J. Bone Miner Res.*, 22(11), 1700-10.

Neale, S. D., Schulze, E., Smith, R. & Athanasou, N. A. (2002) The influence of serum cytokines and growth factors on osteoclast formation in Paget's disease. *QJM*, 95(4), 233-240.

Neale, S. D., Smith, R., Wass, J. A. & Athanasou, N. A. (2000) Osteoclast differentiation from circulating mononuclear precursors in Paget's disease is hypersensitive to 1,25-dihydroxyvitamin D(3) and RANKL. *Bone*, 27(3), 409-416.

Nielsen, E., Cheung, A. Y. & Ueda, T. (2008) The regulatory RAB and ARF GTPases for vesicular trafficking. *Plant Physiol.*, 147(4), 1516-26.

O'Brien, C. A., Plotkin, L. I., Galli, C., Goellner, J. J., Gortazar, A. R., Allen, M. R., Robling, A. G., Bouxsein, M., Schipani, E., Turner, C. H., Jilka, R. L., Weinstein, R. S., Manolagas, S. C. & Bellido, T. (2008) Control of bone mass and remodeling by PTH receptor signaling in osteocytes. *PLoS. One*, 3(8), e2942.

O'Driscoll, J. B. & Anderson, D. C. (1985) Past pets and Paget's disease. *Lancet*, 2, 919-921.

Obaid, R., Wani, S. E., Azfer, A., Hurd, T., Jones, R., Cohen, P., Ralston, S. H. & Albagha, O. M. (2015) Optineurin Negatively Regulates Osteoclast Differentiation by Modulating NF-kappaB and Interferon Signaling: Implications for Paget's Disease. *Cell Rep.*, 13(6), 1096-102.

Ohlsson, C. & Sjogren, K. (2015) Effects of the gut microbiota on bone mass. *Trends Endocrinol. Metab.*, 26(2), 69-74.

Ooi, C. G., Walsh, C. A., Gallagher, J. A. & Fraser, W. D. (2000) Absence of measles virus and canine distemper virus transcripts in long- term bone marrow cultures from patients with Paget's disease of bone. *Bone*, 27(3), 417-421.

Otto, F., Thornell, A. P., Crompton, T., Denzel, A., Gilmour, K. C., Rosewell, I. R., Stamp, G. W., Beddington, R. S., Mundlos, S., Olsen, B. R., Selby, P. B. & Owen, M. J. (1997) Cbfa1, a candidate gene for cleidocranial dysplasia syndrome, is essential for osteoblast differentiation and bone development [see comments]. *Cell*, 89(5), 765-771.

Paget, J. (1877) On a Form of Chronic Inflammation of Bones (Osteitis Deformans). *Med. Chir. Trans.*, 60, 37-64.

Palmio, J., Sandell, S., Suominen, T., Penttila, S., Raheem, O., Hackman, P., Huovinen, S., Haapasalo, H. & Udd, B. (2011) Distinct distal myopathy phenotype caused by VCP gene mutation in a Finnish family. *Neuromuscul. Disord.*, 21(8), 551-5.

Parvizi, J., Klein, G. R. & Sim, F. H. (2006) Surgical management of Paget's disease of bone. *J. Bone Miner. Res.*, 21, P75-P82.

Paternoster, L., Lorentzon, M., Lehtimaki, T., Eriksson, J., Kahonen, M., Raitakari, O., Laaksonen, M., Sievanen, H., Viikari, J., Lyytikainen, L. P., Mellstrom, D., Karlsson, M., Ljunggren, O., Grundberg, E., Kemp, J. P., Sayers, A., Nethander, M., Evans, D. M., Vandenput, L., Tobias, J. H. & Ohlsson, C. (2013) Genetic determinants of trabecular and cortical volumetric bone mineral densities and bone microstructure. *PLoS Genet.*, 9(2), e1003247.

Pautke, C., Schieker, M., Tischer, T., Kolk, A., Neth, P., Mutschler, W. & Milz, S. (2004) Characterization of osteosarcoma cell lines MG-63, Saos-2 and U-2 OS in comparison to human osteoblasts. *Anticancer Res.*, 24(6), 3743-8.

Pawlowski, M., Gajda, M. J., Matlak, R. & Bujnicki, J. M. (2008) MetaMQAP: a meta-server for the quality assessment of protein models. *BMC Bioinformatics*, 9, 403.

Peacock, M., Koller, D. L., Lai, D., Hui, S., Foroud, T. & Econs, M. J. (2009) Bone mineral density variation in men is influenced by sex-specific and non sex-specific quantitative trait loci. *Bone*, 45(3), 443-448.

Pruim, R. J., Welch, R. P., Sanna, S., Teslovich, T. M., Chines, P. S., Gliedt, T. P., Boehnke, M., Abecasis, G. R. & Willer, C. J. (2010) LocusZoom: regional visualization of genome-wide association scan results. *Bioinformatics*, 26(18), 2336-7.

Purcell, S., Neale, B., Todd-Brown, K., Thomas, L., Ferreira, M. A., Bender, D., Maller, J., Sklar, P., de Bakker, P. I., Daly, M. J. & Sham, P. C. (2007) PLINK: a tool set for whole-genome association and population-based linkage analyses. *Am. J. Hum. Genet.*, 81(3), 559-575.

Ralston, S. H. (2008a) Juvenile Paget's disease, familial expansile osteolysis and other genetic osteolytic disorders. *Best. Pract. Res. Clin. Rheumatol.*, 22(1), 101-111.

Ralston, S. H. (2008b) Pathogenesis of Paget's disease of bone. *Bone*, 43(5), 819-825.

Ralston, S. H., Afzal, M. A., Helfrich, M. H., Fraser, W. D., Gallagher, J. A., Mee, A. & Rima, B. (2007) Multicenter blinded analysis of RT-PCR detection methods for paramyxoviruses in relation to Paget's disease of bone. *J. Bone Miner. Res.*, 22(4), 569-577.

Ralston, S. H. & Albagha, O. M. (2014) Genetics of Paget's Disease of Bone. *Curr. Osteoporos. Rep*, 12(3), 263-271.

Ralston, S. H., Hoey, S. A., Gallacher, S. J., Adamson, B. B. & Boyle, I. T. (1994) Cytokine and growth factor expression in Paget's disease: analysis by reverse-transcription/polymerase chain reaction. *Br. J. Rheumatol.*, 33(7), 620-625.

Rea, S. L., Walsh, J. P., Layfield, R., Ratajczak, T. & Xu, J. K. (2013) New Insights Into the Role of Sequestosome 1/p62 Mutant Proteins in the Pathogenesis of Paget's Disease of Bone. *Endocr. Rev.*, 34(4), 501-524.

Rea, S. L., Walsh, J. P., Ward, L., Magno, A. L., Ward, B. K., Shaw, B., Layfield, R., Kent, G. N., Xu, J. & Ratajczak, T. (2009) Sequestosome 1 Mutations in Paget's Disease of Bone in Australia: Prevalence, Genotype/Phenotype Correlation and a Novel Non-UBA Domain Mutation (P364S) Associated with Increased NF-kappaB Signaling Without Loss of Ubiquitin-Binding. *J. Bone Miner. Res.*, 24(7), 1216-1223.

Rebel, A., Malkani, K. & Basle, M. (1974) Nuclear Anomalies in Osteoclasts in Pagets Bone-Disease. *Nouv. Presse Med.*, 3(20), 1299-1301.

Reid, I. R., Sharma, S., Kalluru, R. & Eagleton, C. (2016) Treatment of Paget's Disease of Bone with Denosumab: Case Report and Literature Review. *Calcif. Tissue Int.*, 99(3), 322-5.

Rendina, D., De, F. G., Ralston, S. H., Merlotti, D., Gianfrancesco, F., Esposito, T., Muscariello, R., Nuti, R., Strazzullo, P. & Gennari, L. (2015) Clinical characteristics and evolution of giant cell tumor occurring in Paget's disease of bone. *J. Bone Miner. Res.*, 30(2), 257-263.

Rezaie, T., Child, A., Hitchings, R., Brice, G., Miller, L., Coca-Prados, M., Heon, E., Krupin, T., Ritch, R., Kreutzer, D., Crick, R. P. & Sarfarazi, M. (2002) Adult-onset primary open-angle glaucoma caused by mutations in optineurin. *Science*, 295(5557), 1077-1079.

Roberts, S. J., Stewart, A. J., Sadler, P. J. & Farquharson, C. (2004) Human PHOSPHO1 exhibits high specific phosphoethanolamine and phosphocholine phosphatase activities. *Biochem. J.*, 382(Pt 1), 59-65.

Rodriguez, A., Duran, A., Selloum, M., Champy, M. F., Diez-Guerra, F. J., Flores, J. M., Serrano, M., Auwerx, J., Diaz-Meco, M. T. & Moscat, J. (2006) Mature-onset obesity and insulin resistance in mice deficient in the signaling adapter p62. *Cell Metab.*, 3(3), 211-22.

Roelofs, A. J., Thompson, K., Gordon, S. & Rogers, M. J. (2006) Molecular mechanisms of action of bisphosphonates: Current status. *Clin. Cancer. Res.*, 12(20), 6222S-6230S.

Romas, E. (2009) Clinical applications of RANK-ligand inhibition. *Intern. Med. J.*, 39(2), 110-6.

Roodman, G. D., Kurihara, N., Ohsaki, Y., Kukita, A., Hosking, D., Demulder, A., Smith, J. F. & Singer, F. R. (1992) Interleukin 6. A potential autocrine/paracrine factor in Paget's disease of bone. *J. Clin. Invest.*, 89(1), 46-52.

Roodman, G. D. & Windle, J. J. (2005) Paget disease of bone. *J. Clin. Invest.*, 115(2), 200-208.

Rosales-Rocabado, J. M., Kaku, M., Kitami, M., Akiba, Y. & Uoshima, K. (2014) Osteoblastic differentiation and mineralization ability of periosteum-derived cells compared with bone marrow and calvaria-derived cells. *J. Oral Maxillofac. Surg.*, 72(4), 694 e1-9.

Rosen, C. J. (2013) Primer on the Metabolic Bone Diseases and Disorders of Mineral Metabolism, in Rosen, C. J. (ed), *Primer on the Metabolic Bone Diseases and Disorders of Mineral Metabolism* John Wiley & Sons, Inc.; American Society for Bone and Mineral Research.

Rouka, E., Simister, P. C., Janning, M., Kumbrink, J., Konstantinou, T., Muniz, J. R., Joshi, D., O'Reilly, N., Volkmer, R., Ritter, B., Knapp, S., von Delft, F., Kirsch, K. H. & Feller, S. M. (2015) Differential Recognition Preferences of the Three Src Homology 3 (SH3) Domains from the Adaptor CD2-associated Protein (CD2AP) and Direct Association with Ras and Rab Interactor 3 (RIN3). *J. Biol. Chem.*, 290(42), 25275-92.

Ruddle, N. H., Li, C. B., Horne, W. C., Santiago, P., Troiano, N., Jay, G., Horowitz & Baron, R. (1993) Mice transgenic for HTLV-I LTR-tax exhibit tax expression in bone, skeletal alterations, and high bone turnover. *Virology*, 197(1), 196-204.

Saftig, P., Hunziker, E., Wehmeyer, O., Jones, S., Boyde, A., Rommerskirch, W., Moritz, J. D., Schu, P. & von Figura, K. (1998) Impaired osteoclastic bone resorption leads to osteopetrosis in cathepsin-K-deficient mice. *Proc. Natl. Acad. Sci. U. S. A.*, 95(23), 13453-13458.

Saito, K., Murai, J., Kajiho, H., Kontani, K., Kurosu, H. & Katada, T. (2002) A novel binding protein composed of homophilic tetramer exhibits unique properties for the small GTPase Rab5. *J. Biol. Chem.*, 277(5), 3412-8.

Saki, F., Karamizadeh, Z., Nasirabadi, S., Mumm, S., McAlister, W. H. & Whyte, M. P. (2013) Juvenile paget's disease in an Iranian kindred with vitamin D deficiency and novel homozygous TNFRSF11B mutation. *J. Bone Miner. Res.*, 28(6), 1501-8.

Sali, A. & Blundell, T. L. (1993) Comparative protein modelling by satisfaction of spatial restraints. *J. Mol. Biol.*, 234(3), 779-815.

Sanger, F., Nicklen, S. & Coulson, A. R. (1977) DNA sequencing with chain-terminating inhibitors. *Proc. Natl. Acad. Sci. U. S. A.*, 74(12), 5463-7.

Sanz, L., Diaz-Meco, M. T., Nakano, H. & Moscat, J. (2000) The atypical PKC-interacting protein p62 channels NF-kappaB activation by the IL-1-TRAF6 pathway. *EMBO J.*, 19(7), 1576-1586.

Schwarz, J. M., Cooper, D. N., Schuelke, M. & Seelow, D. (2014) MutationTaster2: mutation prediction for the deep-sequencing age. *Nat. Methods*, 11(4), 361-2.

Schwarz, J. M., Rodelsperger, C., Schuelke, M. & Seelow, D. (2010) MutationTaster evaluates disease-causing potential of sequence alterations. *Nat. Methods*, 7(8), 575-6.

Schwarz, P., Rasmussen, A. Q., Kvist, T. M., Andersen, U. B. & Jorgensen, N. R. (2012) Paget's disease of the bone after treatment with Denosumab: a case report. *Bone*, 50(5), 1023-5.

Schymkowitz, J., Borg, J., Stricher, F., Nys, R., Rousseau, F. & Serrano, L. (2005) The FoldX web server: an online force field. *Nucleic Acids Res.*, 33(Web Server issue), W382-8.

Seitz, S., Priemel, M., Zustin, J., Beil, F. T., Semler, J., Minne, H., Schinke, T. & Amling, M. (2009) Paget's disease of bone: histologic analysis of 754 patients. *J. Bone Miner. Res.*, 24(1), 62-69.

Selby, P. L., Davie, M. W., Ralston, S. H. & Stone, M. D. (2002) Guidelines on the management of Paget's disease of bone. *Bone*, 31(3), 366-373.

Selby, P. L., Davies, M. & Mee, A. P. (2006) Canine distemper virus induces human osteoclastogenesis through NF-kappaB and sequestosome 1/P62 activation. *J. Bone Miner. Res.*, 21(11), 1750-1756.

Servier (2017) *Servier Medical Art*, 2017. Available online: http://www.servier.com/Powerpoint-image-bank [Accessed].

Seton, M., Moses, A. M., Bode, R. K. & Schwartz, C. (2011) Paget's disease of bone: the skeletal distribution, complications and quality of life as perceived by patients. *Bone*, 48(2), 281-285.

Shapiro, I. M., Layfield, R., Lotz, M., Settembre, C. & Whitehouse, C. (2014) Boning up on autophagy: the role of autophagy in skeletal biology. *Autophagy*, 10(1), 7-19.

Siris, E. S. (1993) Paget's Disease of Bone, in Favus, M. J. (ed), *Primer on the Metabolic Bone Diseases and Disorders of Mineral Metabolism*, 2nd edition. Philadelphia: Lippincott-Raven, 375-384.

Siris, E. S. (1994) Epidemiological aspects of Paget's disease: family history and relationship to other medical conditions. *Semin. Arth. Rheum.*, 23(4), 222-225.

Sly, W. S., Hewett-Emmett, D., Whyte, M. P., Yu, Y. S. & Tashian, R. E. (1983) Carbonic anhydrase II deficiency identified as the primary defect in the autosomal recessive syndrome of osteopetrosis with renal tubular acidosis and cerebral calcification. *Proc. Natl. Acad. Sci. U. S. A.*, 80(9), 2752-6.

Smits, P., Bolton, A. D., Funari, V., Hong, M., Boyden, E. D., Lu, L., Manning, D. K., Dwyer, N. D., Moran, J. L., Prysak, M., Merriman, B., Nelson, S. F., Bonafe, L., Superti-Furga, A., Ikegawa, S., Krakow, D., Cohn, D. H., Kirchhausen, T., Warman, M. L. & Beier, D. R. (2010) Lethal skeletal dysplasia in mice and humans lacking the golgin GMAP-210. *N. Engl. J. Med.*, 362(3), 206-216.

Solomon, L. R. (1979) Billiard-player's fingers: an unusual case of Paget's disease of bone. *Br. Med. J.*, 1(6168), 931.

Sophocleous, A., Landao-Bassonga, E., Van't Hof, R. J., Idris, A. I. & Ralston, S. H. (2011) The Type 2 Cannabinoid Receptor Regulates Bone Mass and Ovariectomy-Induced Bone Loss by Affecting Osteoblast Differentiation and Bone Formation. *Endocrinology*, 152(6), 2141-2149.

St-Jacques, B., Hammerschmidt, M. & McMahon, A. P. (1999) Indian hedgehog signaling regulates proliferation and differentiation of chondrocytes and is essential for bone formation. *Genes Dev.*, 13(16), 2072-86.

Stephens, M. & Scheet, P. (2005) Accounting for decay of linkage disequilibrium in haplotype inference and missing-data imputation. *Am. J. Hum. Genet.*, 76(3), 449-62.

Stephens, M., Smith, N. J. & Donnelly, P. (2001) A new statistical method for haplotype reconstruction from population data. *Am. J. Hum. Genet.*, 68(4), 978-989.

Sutherland, M. K., Geoghegan, J. C., Yu, C., Turcott, E., Skonier, J. E., Winkler, D. G. & Latham, J. A. (2004) Sclerostin promotes the apoptosis of human osteoblastic cells: a novel regulation of bone formation. *Bone*, 35(4), 828-835.

Takano, K., Saikawa, E., Ogasawara, N. & Himi, T. (2014) Cochlear implantation in a patient with Paget's disease. *Am. J. Otolaryngol.*, 35(3), 408-410.

Tall, G. G., Barbieri, M. A., Stahl, P. D. & Horazdovsky, B. F. (2001) Ras-activated endocytosis is mediated by the Rab5 guanine nucleotide exchange activity of RIN1. *Dev. Cell*, 1(1), 73-82.

Tamura, T., Udagawa, N., Takahashi, N., Miyaura, C., Tanaka, S., Yamada, Y., Koishihara, Y., Ohsugi, Y., Kumaki, K., Taga, T. & . (1993) Soluble interleukin-6 receptor triggers osteoclast formation by interleukin 6. *Proc. Natl. Acad. Sci. U. S. A*, 90(24), 11924-11928.

Tan, A. & Ralston, S. H. (2014) Clinical Presentation of Paget's Disease: Evaluation of a Contemporary Cohort and Systematic Review. *Calcif. Tissue Int.*, 95(5), 385-392.

Teitelbaum, S. L. (2005) Osteoporosis and integrins. *J. Clin. Endocrinol. Metab.*, 90(4), 2466-8.

Teitelbaum, S. L. & Ross, F. P. (2003) Genetic regulation of osteoclast development and function. *Nat. Rev. Genet.*, 4(8), 638-49.

Teramachi, J., Nagata, Y., Mohammad, K., Inagaki, Y., Ohata, Y., Guise, T., Michou, L., Brown, J. P., Windle, J. J., Kurihara, N. & Roodman, G. D. (2016) Measles virus nucleocapsid protein increases osteoblast differentiation in Paget's disease. *J Clin Invest*, 126(3), 1012-22.

Theillet F-X., K. L., Tompa P., Han K-H., Selenko P., Dunker A.K., Daughdrill G.W., Uversky V.N. (2013) The alphabet of intrinsic disorder: I. Act like a Pro: On the abundance and roles of proline residues in intrinsically disordered proteins. *Intrinsical Disorder Proteins*, 1(1).

Tiegs, R. D., Lohse, C. M., Wollan, P. C. & Melton, L. J. (2000) Long-term trends in the incidence of Paget's disease of bone. *Bone*, 27(3), 423-427.

Tresse, E., Salomons, F. A., Vesa, J., Bott, L. C., Kimonis, V., Yao, T. P., Dantuma, N. P. & Taylor, J. P. (2010) VCP/p97 is essential for maturation of ubiquitin-containing autophagosomes and this function is impaired by mutations that cause IBMPFD. *Autophagy*, 6(2), 217-227.

Tumbarello, D. A., Waxse, B. J., Arden, S. D., Bright, N. A., Kendrick-Jones, J. & Buss, F. (2012) Autophagy receptors link myosin VI to autophagosomes to mediate Tom1-dependent autophagosome maturation and fusion with the lysosome. *Nat. Cell Biol.*, 14(10), 1024-35.

Vacic, V. & Iakoucheva, L. M. (2012) Disease mutations in disordered regions--exception to the rule? *Mol. Biosyst.*, 8(1), 27-32.

Vacic, V., Markwick, P. R., Oldfield, C. J., Zhao, X., Haynes, C., Uversky, V. N. & Iakoucheva, L. M. (2012) Disease-associated mutations disrupt functionally important regions of intrinsic protein disorder. *PLoS Comput. Biol.*, 8(10), e1002709.

Vallet, M., Soares, D. C., Wani, S., Sophocleous, A., Warner, J., Salter, D. M., Ralston, S. H. & Albagha, O. M. (2015) Targeted sequencing of the Paget's disease associated 14q32 locus identifies several missense coding variants in RIN3 that predispose to Paget's disease of bone. *Hum. Mol. Genet.*, 24(11), 3286-95.

Van't Hof, R. J., Macphee, J., Libouban, H., Helfrich, M. H. & Ralston, S. H. (2004) Regulation of bone mass and bone turnover by neuronal nitric oxide synthase. *Endocrinology*, 145(11), 5068-5074.

Van't Hof, R. J., Rose, L., Bassonga, E. & Daroszewska, A. (2017) Open source software for semi-automated histomorphometry of bone resorption and formation parameters. *Bone*, 99, 69-79.

Van Staa, T. P., Selby, P., Leufkens, H. G., Lyles, K., Sprafka, J. M. & Cooper, C. (2002) Incidence and natural history of Paget's disease of bone in England and Wales. *J. Bone Miner. Res.*, 17(3), 465-471.

Vasireddy, S. & Halsey, J. P. (2001) Incidental detection of lumbar Paget's disease by bone densitometry. *Rheumatology (Oxford)*, 40(12), 1424-5.

Visconti, M. R., Langston, A. L., Alonso, N., Goodman, K., Selby, P. L., Fraser, W. D. & Ralston, S. H. (2010) Mutations of SQSTM1 are associated with severity and clinical outcome in Paget's disease of bone. *J. Bone Miner. Res.*, 25(11), 2368-2373.

Visconti, M. R., Usategui-Martin, R. & Ralston, S. H. (2017) Antibody Response to Paramyxoviruses in Paget's Disease of Bone. *Calcif. Tissue Int.*, 101(2), 141-147.

Vu, T. H., Shipley, J. M., Bergers, G., Berger, J. E., Helms, J. A., Hanahan, D., Shapiro, S. D., Senior, R. M. & Werb, Z. (1998) MMP-9/gelatinase B is a key regulator of growth plate angiogenesis and apoptosis of hypertrophic chondrocytes. *Cell*, 93(3), 411-22.

Walters-Sen, L. C., Hashimoto, S., Thrush, D. L., Reshmi, S., Gastier-Foster, J. M., Astbury, C. & Pyatt, R. E. (2015) Variability in pathogenicity prediction programs: impact on clinical diagnostics. *Mol. Genet. Genomic. Med.*, 3(2), 99-110.

Wat, W. Z., Cheung, W. S. & Lau, T. W. (2013) A case series of Paget's disease of bone in Chinese. *Hong. Kong. Med. J.*, 19(3), 242-248.

Wat, W. Z. M. (2014) Current perspectives on bisphosphonate treatment in Paget's disease of bone. *Ther. Clin. Risk Manag.*, 10, 977-983.

Watts, G. D., Wymer, J., Kovach, M. J., Mehta, S. G., Mumm, S., Darvish, D., Pestronk, A., Whyte, M. P. & Kimonis, V. E. (2004) Inclusion body myopathy associated with Paget disease of bone and frontotemporal dementia is caused by mutant valosin-containing protein. *Nat. Genet.*, 36(4), 377-381.

Watts, G. D. J., Thomasova, D., Ramdeen, S. K., Fulchiero, E. C., Mehta, S. G., Drachman, D. A., Weihl, C. C., Jamrozik, Z., Kwiecinski, H., Kaminska, A. &

Kimonis, V. E. (2007) Novel VCP mutations in inclusion body myopathy associated with Paget disease of bone and frontotemporal dementia. *Clin. Genet.*, 72(5), 420-426.

Wellcome Trust Case Control, C. (2007) Genome-wide association study of 14,000 cases of seven common diseases and 3,000 shared controls. *Nature*, 447(7145), 661-78.

Whyte, M. P. & Hughes, A. E. (2002) Expansile skeletal hyperphosphatasia is caused by a 15-base pair tandem duplication in TNFRSF11A encoding RANK and is allelic to familial expansile osteolysis. *J. Bone Miner. Res.*, 17(1), 26-29.

Whyte, M. P., Obrecht, S. E., Finnegan, P. M., Jones, J. L., Podgornik, M. N., McAlister, W. H. & Mumm, S. (2002) Osteoprotegerin deficiency and juvenile Paget's disease. *N. Engl. J. Med.*, 347(3), 175-184.

Wiktorjedrzejczak, W., Bartocci, A., Ferrante, A. W., Ahmedansari, A., Sell, K. W., Pollard, J. W. & Stanley, E. R. (1990) Total Absence of Colony-Stimulating Factor 1 in the Macrophage-Deficient Osteopetrotic (Op Op) Mouse. *Proc. Natl. Acad. Sci. U. S. A.*, 87(12), 4828-4832.

Wild, P., Farhan, H., McEwan, D. G., Wagner, S., Rogov, V. V., Brady, N. R., Richter, B., Korac, J., Waidmann, O., Choudhary, C., Dotsch, V., Bumann, D. & Dikic, I. (2011) Phosphorylation of the autophagy receptor optineurin restricts Salmonella growth. *Science*, 333(6039), 228-233.

Wong, Y. C. & Holzbaur, E. L. (2014) Optineurin is an autophagy receptor for damaged mitochondria in parkin-mediated mitophagy that is disrupted by an ALS-linked mutation. *Proc. Natl. Acad. Sci. U. S. A.*, 111(42), E4439-48.

Wright, T., Rea, S. L., Goode, A., Bennett, A. J., Ratajczak, T., Long, J. E., Searle, M. S., Goldring, C. E., Park, B. K., Copple, I. M. & Layfield, R. (2013) The S349T mutation of SQSTM1 links Keap1/Nrf2 signalling to Paget's disease of bone. *Bone*, 52(2), 699-706.

Wuyts, W., Van Wesenbeeck, L., Morales-Piga, A., Ralston, S., Hocking, L., Vanhoenacker, F., Westhovens, R., Verbruggen, L., Anderson, D., Hughes, A. & Van Hul, W. (2001) Evaluation of the role of RANK and OPG genes in Paget's disease of bone. *Bone*, 28(1), 104-107.

Yadav, M. C., Simao, A. M., Narisawa, S., Huesa, C., McKee, M. D., Farquharson, C. & Millan, J. L. (2011) Loss of skeletal mineralization by the simultaneous ablation of PHOSPHO1 and alkaline phosphatase function: a unified model of the mechanisms of initiation of skeletal calcification. *J. Bone Miner. Res.*, 26(2), 286-297.

Yagi, M., Miyamoto, T., Sawatani, Y., Iwamoto, K., Hosogane, N., Fujita, N., Morita, K., Ninomiya, K., Suzuki, T., Miyamoto, K., Oike, Y., Takeya, M., Toyama, Y. & Suda, T. (2005) DC-STAMP is essential for cell-cell fusion in osteoclasts and foreign body giant cells. *J. Exp. Med.*, 202(3), 345-351.

Yoshida, H., Hayashi, S., Kunisada, T., Ogawa, M., Nishikawa, S., Okamura, H., Sudo, T., Shultz, L. D. & Nishikawa, S. (1990) The murine mutation osteopetrosis is in the coding region of the macrophage colony stimulating factor gene. *Nature*, 345(6274), 442-444.

Zhang, X., Goncalves, R. & Mosser, D. M. (2008) The isolation and characterization of murine macrophages. *Curr. Protoc. Immunol.*, Chapter 14, Unit 14 1.

Zhu, G., Wu, C. J., Zhao, Y. & Ashwell, J. D. (2007) Optineurin negatively regulates TNFalpha- induced NF-kappaB activation by competing with NEMO for ubiquitinated RIP. *Curr. Biol.*, 17(16), 1438-1443.

APPENDICES

APPENDIX 1. MATERIALS, REAGENTS, TECHNICAL EQUIPMENT AND SOFTWARE

Materials and reagents	Supplier
12 Well TC-treated microplates	Corning, UK
1ml pasteur pipettes	Fisher Scientific, UK
2-Propanol	Sigma Aldrich, UK
5X first-strand buffer	Invitrogen, Paisley, UK
96 Well TC-treated microplates	Corning, UK
Acetic acid glacial	Sigma Aldrich, UK
Adhesive PCR plate seals	Thermo Fisher Scientific, UK
AlamarBlue™ reagent	Thermo Fisher Scientific, UK
Alizarin red S	Sigma Aldrich, UK
Amersham hybond™-P	GE Healthcare Life Sciences, UK
α-Minimum essential medium (αMEM)	Sigma Aldrich, UK
Ammonium hydroxide	Sigma Aldrich, UK
Axygen MaxiClear microcentrifuge tubes	Corning Axygen, UK
β-glycerophosphate disodium	Sigma Aldrich, UK
BCA protein assay	Sigma Aldrich, UK
Bovine serum albumin	Sigma Aldrich, UK
Bromophenol blue.	BDH Laboratory Supplies, UK
Calcein	Sigma Aldrich, UK
Cell scrapers	Sarstedt, UK
Centrifuge tubes (15 and 50ml)	Greiner, UK
Cetylpyridinium chloride	Sigma Aldrich, UK
Chloroform	Sigma Aldrich, UK
Clarity western ECL substrate	Bio-Rad Laboratories, UK
Collagenase (Type 1A)	Sigma Aldrich, UK
Copper (II)-sulfate	Sigma Aldrich, UK
Cover slips	Scientific Laboratory supplies Ltd, UK
Criterion™ XT pre-cast gels (12% Bis-Tris)	Bio-Rad Laboratories, UK
DAPI	Sigma Aldrich, UK
DEPC treated water	Thermo Fisher Scientific, UK
Dibutyl phthalate	Sigma Aldrich, UK
Diethanolamine	Sigma Aldrich, UK
DL-Dithiothreitol (DTT)	Sigma Aldrich, UK

Materials and reagents	Supplier
DMSO	Sigma Aldrich, UK
DNA Ladder 1kb	New England Biolabs, UK
DNA loading buffer	New England Biolabs, UK
dNTPs	Thermo Fisher Scientific, UK
DPX mounting medium	Sigma Aldrich, UK
EDTA	Sigma Aldrich, UK
Embedding baskets	Leica Microsystems, UK
Embedding molds	Custom-made by the University workshop, UK
Embedding rings	Leica Microsystems, UK
Eppendorf tubes (0.5, 1.5, 2ml)	Greiner, UK
Ethanol absolute	Fisher Scientific, UK
EU non skirted 96 well qPCR plate	BIOplastics, UK
EU Optical robust flat 8-Cap Strip	BIOplastics, UK
Extra thick blot papers	Bio-Rad Laboratories, UK
Fast red salt TR	Sigma Aldrich, UK
Fetal calf serum (FCS)	Hyclone, UK
Filter paper	Thermo Fisher Scientific, UK
Filter tips axygen	Starlab, UK
Forceps	World precision instrument, UK
Glycerol	VWR, UK
Glycine	BDH Laboratory Supplies, UK
Hanks buffer (HBSS)	Sigma Aldrich, UK
HistoResin mounting medium	Leica Microsystems, UK
HotStart PCR kit with dNTPs 250U	Kapa Biosystem LTD, UK
Human recombinant RANKL	R&D, UK
Invisorb® spin tissue mini kit	Stratec, UK
Isopropanol	Sigma Aldrich, UK
Jackson ImmunoResearch anti-rabbit secondary antibody	Stratech Scientific Unit, UK
Kaleidoscope ladder	Bio-Rad Laboratories, UK
Kisol foil	Taab Lab, UK
L-Glutamine	Invitrogen, UK
Low molecular weight DNA ladder	New England Biolabs, UK
Magic marker	Thermo Fisher Scientific, UK
Magnesium chloride	Sigma Aldrich, UK
M-CSF mouse recombinant	Prospec, US

Materials and reagents	Supplier
Methanol	Thermo Fisher Scientific, UK
Methyl methacrylate (MMA)	Sigma Aldrich, UK
MicroAmp® 8-Cap strip, clear	Thermo Fisher Scientific, UK
Multiplex PCR master mix	Qiagen, UK
N,N-Dimethylformamide	Fisher Scientific, UK
Napthol-AS-BI-phosphate	Sigma Aldrich, UK
Napthol AS-TR phosphate	Sigma Aldrich, UK
Needles (19, 21 and 25G)	BD, US
Neubauer haemocytometer	Hawksley, UK
Novoscave	Novochem, The Netherlands
Optimal cutting temperature Embedding Matrix	CellPath, UK
Oligo(dt)20 primer	Thermo Fisher Scientific, UK
Paraformaldehyde	Taab Lab, UK
Pararosanilin	Sigma Aldrich, UK
PBS tablets	Thermo Fisher Scientific, UK
PCR Plate, 96-well, low profile, non-skirted	Thermo Fisher Scientific, UK
PCR primers	Thermo Fisher Scientific, UK
Penicillin/Streptomycin	Invitrogen, Paisley, UK
Perkadox 16	Akzo Nobel Polymer Chemicals, The Netherlands
Pipette tips (All sizes)	Starlab, UK
p-Nitrophenol	Sigma Aldrich, UK
p-Nitrophenol-phosphate	Sigma Aldrich, UK
QIAquick PCR Purification Kit	Qiagen, UK
Rabbit Anti-Actin IgG	Sigma Aldrich, UK
Reddy Mix Custom PCR Master mix	Thermo Scientific, Fermentas, UK
RIN3 Antibody, rabbit polyclonal	Proteintech, UK
RIPA	Santa Cruz, UK
RNA plate, PCR Plate, 96-well, low profile, skirted	Thermo Fisher Scientific, UK
RnaseOut Recombinant RNAse Inhibitor	Thermo Fisher Scientific, UK
Scalpel, disposable	VWR International LTD, UK
Scissors (Fine points and spring bow handles)	S Murray & Co Ltd, UK
SensiFAST™ Probe No-ROX Kit	Bioline, UK
Silver nitrate	Sigma Aldrich, UK
Slide press cover slips	Taab Lab, UK

Materials and reagents	Supplier
Sodium acetate anhydrous	Sigma Aldrich, UK
Sodium barbiturate	BDH Laboratory Supplies, UK
Sodium chloride	Sigma Aldrich, UK
Sodium dodecyl sulphate (SDS)	Bio-Rad Laboratories, UK
Sodium phosphate	Sigma Aldrich, UK
Sodium tartrate dihydrate	Sigma Aldrich, UK
Steel knife 16cm "c"	Leica Microsystems, UK
Sterile filter (0.45mm)	Merk Millipore, UK
Stripettes (5, 10, 25 and 50ml)	Costar, UK
SuperScript III reverse transcriptase	Thermo Fisher Scientific, UK
SYBR safe DNA gel stain	Thermo Fisher Scientific, UK
Syringes (All sizes)	BD, US
Taq DNA Polymerase	Invitrogen, Paisley, UK
TaqMan® Gene Expression Assay Mix for 18S rRNA	Applied Biosystems, UK
TBE buffer 10X	Fisher Scientific, UK
TBS	Fisher Scientific, UK
Teknovit Mounting powder	Taab Lab, UK
Tissue culture 10mm Dishes	Greiner, UK
Tissue culture 75cm^2 flasks	Greiner, UK
Tissue Tack (+ Charged) Microscope Slides	Polyscience, US
Transfer buffer	Fisher Scientific, UK
Tris	Bio-Rad Laboratories, UK
Triton X-100^{TM}	Sigma Aldrich, UK
TRizol® Reagent	Thermo Fisher Scientific, UK
Trypsin/EDTA	Thermo Fisher Scientific, UK
Tween-20	Bio-Rad Laboratories, UK
UPL probes	Roche Diagnostics Ltd., UK
Vacuum desiccator	Fisher Scientific, UK
Vitamin C (Ascorbic acid)	BDH Laboratory Supplies, UK
XT-MOPS	Bio-Rad Laboratories, UK
Xylene	Sigma Aldrich, UK

Technical equipment	Supplier
311DS Environmental shaking incubator	Labnet, UK
AA Hoefer® protein transfer apparatus	Fisher Scientific, UK
Autostainer	Leica Microsystems, UK
Axiocam 506 mono camera	Carl Zeiss Ltd., UK
Axiovert 200 inverted research microscope	Carl Zeiss Ltd., UK
Bench-top centrifuge	Sigma, Germany
Bench-top Eppendorf centrifuge	Sigma, Germany
Bio2 safety cabinets	Envair, UK
Bio-Tek Synergy HT plate reader	Fisher Scientific, UK
BX51 microscope	Olympus, UK
Captair Bio DNA/RNA flow workstation	Erlab, US
Coverslipper	Leica Microsystems, UK
Cryostat	Leica Microsystems, UK
Decalcifier II	Leica Microsystems, UK
Excelsior AS Automatic tissue processor	Leica Microsystems, UK
Explorer pro balance	Ohaus, Switzerland
Fume cabinet	Envair, UK
Grant OLS 200 water bath	Thistle Scientific, UK
Horizontal electrophoresis tanks	Fisher Scientific, UK
Hotplate/stirrer	Thistle Scientific, UK
Laminar flow biosafety hood Class II	Nuaire, UK
LSM 800 microscope	Carl Zeiss Ltd., UK
Microtome	Leica Microsystems, UK
MJ Research Chromo 4 real time PCR thermocycler	Genetic Research Instrumentation Ltd, UK
Nanodrop ND-8000	Thermoscientific, UK
Odyssey ® Fc imaging system	Li-Cor, UK
Origo PSU-400/200 power supply for electrophoresis	Anachem, UK
Pipettes (2, 10, 100, 200 and 1000ml)	Gilson, UK
PowerPac basic™	Bio-Rad Laboratories, UK

Technical equipment	Supplier
QImaging Retiga 4000R CCD camera	Media Cybernetics, UK
Rocking shaker WT 14	Biometra, Germany
Rotary microtome	Leica Microsystems, UK
Rotary tool	Dremel UK, UK
SkyScan 1172 X-ray microtomography system	SKYSCAN, Belgium
Syngene GeneGenius Gel Bio-Imaging system	Fisher Scientific, UK
Tetrad 2 thermal cyclers	Bio-Rad Laboratories, UK
Vertical Criterion™ gel tanks	Bio-Rad Laboratories, UK
Vortex	Fisher Scientific, UK

Software	Supplier
Alamut® Visual Version 2.1 software	Interactive Biosoftware, France
Bio-Tek Gen5^{TM} plate reader software	BioTek, UK
Burrows-Wheeler Aligner tool	Wellcome Trust Sanger Institute, UK
CalceinHisto software	University of Liverpool, UK
Condel	Universitat Pompeu Fabra, Spain
FoldX	EMBLEM, Spain
G*Power software	Heinrich Heine University Düsseldorf, Germany
Gen5™ software	BioTek, UK
Genome Analysis Toolkit, GATK	Broad institute, US
Genomic Evolutionary Rate Profiling (GERP)	Sidow lab, US
Haploview Version 4.2	Broad institute, US
ImageJ software	National Institutes of Health, US
LocusZoom	University of Michigan, US
Markov Chain Haplotyping	MaCH, US
Minitab	Minitab Inc., UK
MetaDisorder	Polish Ministry of Science and Higher Education, Poland
MetaPrDOS	Ministry of Education, Culture, Sports and Technology of Japan and (BIRD-JST), Japan
Modeller 9v12	UCSF, US
Mutation surveyor® V3.30 software	Softgenetics, US
MutationTaster	Charité, Germany
OligoCalc software	Northwestern University, US
Opticon Monitor analysis software version 3	Genetic Research Instrumentation Ltd, UK
PLINK v1.07	Human Longevity Inc, NIH-NIDDK, BGI Cognitive Genomics, University of Minnesota, Puracell Lab, US
PolyPhen-2	PolyPhen-2, US
PONDR VL-XT	Molecular Kinetics, US

Software	Supplier
ProbABEL	CMSB, NGI, NOW, Radboud University Medical Centre, RFBR, PolyOmica, Netherland, Russia
QCapture Pro software	Media Cybernetics UK, Berkshire, UK
SIFT	J. Craig Venter Institute, US
Skyscan 1172 microCT software	SKYSCAN, Bruker, Belgium
Skyscan CTAn analysis software	SKYSCAN, Bruker, Belgium
Skyscan CTVol software	SKYSCAN, Bruker, Belgium
Skyscan Dataviewer software	SKYSCAN, Bruker, Belgium
Skyscan NRecon reconstruction system	SKYSCAN, Bruker, Belgium
SNPcheck software	NGRL Manchester, UK
SPSS Version 22	SPSS Ltd., UK
Syngene GeneSnap software	Synoptics Ltd., UK
Syngene GeneTool software	Synoptics Ltd., UK
Taqman® genotyper Version 1.3	Thermo Fisher Scientific, UK
TrapHisto software	University of Liverpool, UK
Unified genotyper, GATK	Broad institute, US

APPENDIX 2.1. PRIMER SEQUENCES FOR RIN3 AMPLIFICATION

M13 unique sequences are showed in grey. PROM = Promoter; EX = Exon; F = Forward, R = Reverse. Letters A to F corresponds to the parts of *RIN3* amplified with this pair of primers.

Primer name	Primer sequence
RIN3_PROM_A_F	GTAGCGCGACGGCCAGTTAATTCAGCCTCTGGAGGAG
RIN3_PROM_B_F	GTAGCGCGACGGCCAGTATCACTAGAGTATTTTCTGTCTCT
RIN3_PROM_C_F	GTAGCGCGACGGCCAGTGGCCATATGCTTAACTTGACG
RIN3_PROM_D_F	GTAGCGCGACGGCCAGTTAGAGACATTTCTGGTCGTTAC
RIN3_PROM_E_F	GTAGCGCGACGGCCAGTAACACCCAGGCACTTAGAAGA
RIN3_PROM_F_F	GTAGCGCGACGGCCAGTAAGGCTGTGGCTCCGAGT
RIN3_EX01_F	GTAGCGCGACGGCCAGTTGACAAAAAAACCCTTGACCAC
RIN3_EX02_F	GTAGCGCGACGGCCAGTATAAGTAAGCGTGGCTGAATG
RIN3_EX03_F	GTAGCGCGACGGCCAGTCTCATCATTTCAGGAACCTTC
RIN3_EX04_F	GTAGCGCGACGGCCAGTTAATCTCCTGAAATCTCAATGGA
RIN3_EX05_F	GTAGCGCGACGGCCAGTAACCAAGGAGAAGCAGTGAC
RIN3_EX06_A_F	GTAGCGCGACGGCCAGTAGCACAGCAACACCTAGTCC
RIN3_EX06_B_F	GTAGCGCGACGGCCAGTCTCTTGGAAATTGCCCTGCA
RIN3_EX06_C_F	GTAGCGCGACGGCCAGTGGAAGCGATGAAGCCAGG
RIN3_EX06_D_F	GTAGCGCGACGGCCAGTAGCTCTGCACACAGGCGA
RIN3_EX06_E_F	GTAGCGCGACGGCCAGTACTTTGGCAGCCTGGTGC
RIN3_EX07_A_F	GTAGCGCGACGGCCAGTTTTCTCTTGAATAAACTGTGCTCT
RIN3_EX07_B_F	GTAGCGCGACGGCCAGTAAGGATGGTTCGCTGCAGC
RIN3_EX08_F	GTAGCGCGACGGCCAGTGTCCTCTCTGTCCTGAGAG
RIN3_EX09_F	GTAGCGCGACGGCCAGTTTGAAGCAGGTGTTTGCAGAT
RIN3_EX10_A_F	GTAGCGCGACGGCCAGTACTCGCAGACAGCTTGGC
RIN3_EX10_B_F	GTAGCGCGACGGCCAGTGGAGAAGTTCGCGGTGGA
RIN3_EX10_C_F	GTAGCGCGACGGCCAGTCTTCCTGTGAGGCCCTC
RIN3_EX10_D_F	GTAGCGCGACGGCCAGTATTCCCCATGAGTCCCCC
RIN3_EX10_E_F	GTAGCGCGACGGCCAGTCGGTTAAGAGACAGGCCTC

Primer name	Primer sequence
RIN3_PROM_A_R	CAGGGCGCAGCGATGACGTACTGGCACATGCTACACC
RIN3_PROM_B_R	CAGGGCGCAGCGATGACATCTGAGCATACACGAAAAGTC
RIN3_PROM_C_R	CAGGGCGCAGCGATGACTGCTTTGTTATTAAACCTCCTTCA
RIN3_PROM_D_R	CAGGGCGCAGCGATGACCATCAAGCCTGGCATCTAATT
RIN3_PROM_E_R	CAGGGCGCAGCGATGACGGAGAGGGAAACTTAGAGAAAA
RIN3_PROM_F_R	CAGGGCGCAGCGATGACCCTTCTACTTCCTGTATCGG
RIN3_EX01_R	CAGGGCGCAGCGATGACAAAGTTTAGCCAACATCGGGT
RIN3_EX02_R	CAGGGCGCAGCGATGACAAAGGGAAATAAACATGCAGTCAT
RIN3_EX03_R	CAGGGCGCAGCGATGACAATGTGGCCATGAGAATGCAAA
RIN3_EX04_R	CAGGGCGCAGCGATGACAAGCCTCAGAGCCAACACAT
RIN3_EX05_R	CAGGGCGCAGCGATGACGAAACTGGACAATCTCTCTATC
RIN3_EX06_A_R	CAGGGCGCAGCGATGACAGTCTCTCGCAGGTCATCAT
RIN3_EX06_B_R	CAGGGCGCAGCGATGACACTTTGGTCTTCTAAGGACAC
RIN3_EX06_C_R	CAGGGCGCAGCGATGACTCTGGAGAGCTCTGGGAAT
RIN3_EX06_D_R	CAGGGCGCAGCGATGACCTGCAGCAGGTAGCTCTTG
RIN3_EX06_E_R	CAGGGCGCAGCGATGACATGGCAGGGAGTAATTGGCA
RIN3_EX07_A_R	CAGGGCGCAGCGATGACGGTGAACTTCTGCAGGATCTT
RIN3_EX07_B_R	CAGGGCGCAGCGATGACAAGAGGGCCCAGGAATTACA
RIN3_EX08_R	CAGGGCGCAGCGATGACCTAATCTGTGAGCTCCTGCA
RIN3_EX09_R	CAGGGCGCAGCGATGACGTGGGGAGTCTCACTGCT
RIN3_EX10_A_R	CAGGGCGCAGCGATGACGGCCGGTAGACAAAGTGG
RIN3_EX10_B_R	CAGGGCGCAGCGATGACTTGGACGAGCGTCATGTTATTT
RIN3_EX10_C_R	CAGGGCGCAGCGATGACGCTCCTTCCTAGGCCAGT
RIN3_EX10_D_R	CAGGGCGCAGCGATGACAATTCTCCCCACACGATGG
RIN3_EX10_E_R	CAGGGCGCAGCGATGACTGGTTCTGATCCTAAGCTGG

APPENDIX 2.2. SOLUTIONS FOR TRACP STAINING IN CULTURE PLATES

- **Naphthol-AS-BI-phosphate**

  10mg/ml Naphthol-AS-BI-phosphate in Dimethylformamide

- **Veronal buffer**

  1.17g sodium acetate anhydrous and 2.94g sodium barbiturate both dissolved in 100ml of dH_2O

- **Acetate buffer**

  0.82g sodium acetate anhydrous dissolved in 100ml of dH_2O and pH adjusted to 5.2 with 0.6ml glacial acetic acid made up to 100ml with dH_2O

TRAcP Staining Solution was obtained by mixing the following two solutions (3ml):

- **Solution A**

  150ml of Napthol-AS-BI-phosphate

  750ml of Veronal buffer

  900ml Acetate buffer

  900ml Acetate buffer with 100mM Sodium Tartate

- **Solution B**

  120ml of Pararosanilin

  120ml of Sodium Nitrate (4% w/v)

APPENDIX 2.3. ALP ASSAY SOLUTIONS

- **Diethanolamine (DEA)/MgCl2 buffer**

  1M DEA and 1mM $MgCl_2$ made up in 100ml dH_2O and pH adjusted to 9.8

- **Lysis buffer**

  [1M DEA/1mM $MgCl_2$ buffer] + 0.05% Triton X-100

- **p-Nitrophenol standard solution**

  p-Nitrophenol standards at 0 to 30nM, prepared in lysis buffer

- **PNP Substrate solution**

  20mM p-nitrophenol-phopshate made up in [1M DEA/1mM $MgCl_2$ buffer]

APPENDIX 2.4. SOLUTION FOR CELL LYSIS

- **RIPA Lysis buffer**

  1% Triton 100X

  0.5% (w/v) Sodium Deoxycholate

  0.1% (w/v) Sodium Dodecyl Sulphate (SDS)

  50mM Tris-HCl (pH 7.4)

  150nM Sodium Chloride were dissolved in dH_2O.

- **Modified Lysis buffer**

  These reagents were added to the RIPA lysis buffer extemporaneously before use:

  2% (v/v) Protease inhibitor cocktail

  0.4% (v/v) Phosphatase inhibitor cocktail

  1mM EDTA

  20mM Sodium Fluoride

APPENDIX 2.5. WESTERN BLOT SOLUTIONS

- **Protein quantification (Pierce™ BCA Protein Assay Kit, Thermo Fisher Scientific)**

  10µl of lysed cells or pre-diluted standard (0; 0.125; 0.25; 0.5; 0.75; 1; 1.5; 2µg/ml) were loaded in a 96 well plate in duplicates of triplicates.

  200µl of Copper blue diluted at 1/50 in BCA Pierce were added to each samples and standard.

  The plate was then incubated at 37ºC for 15 minutes

  The plate was read at 562nm using the BioTek™ SynergyHT plate reader

- **Electrophoresis running buffer 1:20**

  50ml of XT-MOPS (20X) in 1L of dH_2O

- **Samples loading protein buffer (5X stock)**

  5.2ml of 1M Tris-HCl pH adjusted to 6.8, 1g of DL-dithiothreitol (DTT), 3g SDS, 6.5ml glycerol and 130ml of 10% (w/v) Bromophenol Blue. Stored at -20°C.

- **Transfer buffer**

  3.63g of Tris, 14.4g of glycine, 200ml of methanol and 3.75ml of 10% (w/v) SDS made up to 1000ml with dH_2O. Stored at room temperature.

- **10X TBS**

  87.66g Sodium Chloride and 78.8g Tris-HCl dissolved in 800ml dH_2O. Adjust pH to 7.6 and make up to final volume (1000ml). Stored at room temperature.

- **TBST**

  0.1% (v/v) Tween-20 in TBS. Stored at room temperature.

- **Stripping buffer**

  1mM DTT, 2% (w/v) SDS and 62.5mM Tris-HCl (pH 6.7). Stored at room temperature.

APPENDIX 2.6. APATHY SYRUP COMPOSITION

The syrup was obtained by mixing the following ingredients, in order:

- Hot water (Pre-warmed at 80ºC): 120ml
- Saccharose: 100g
- Gum Arabic: 100g
- Thymol: 1 crystal

The syrup is then centrifuged for 10 minutes at 3000g. The bubbles were removed using a spatula and the solution was aliquoted in syringes kept at 4ºC.

APPENDIX 4.1: HAPLOTYPE DIAGRAM

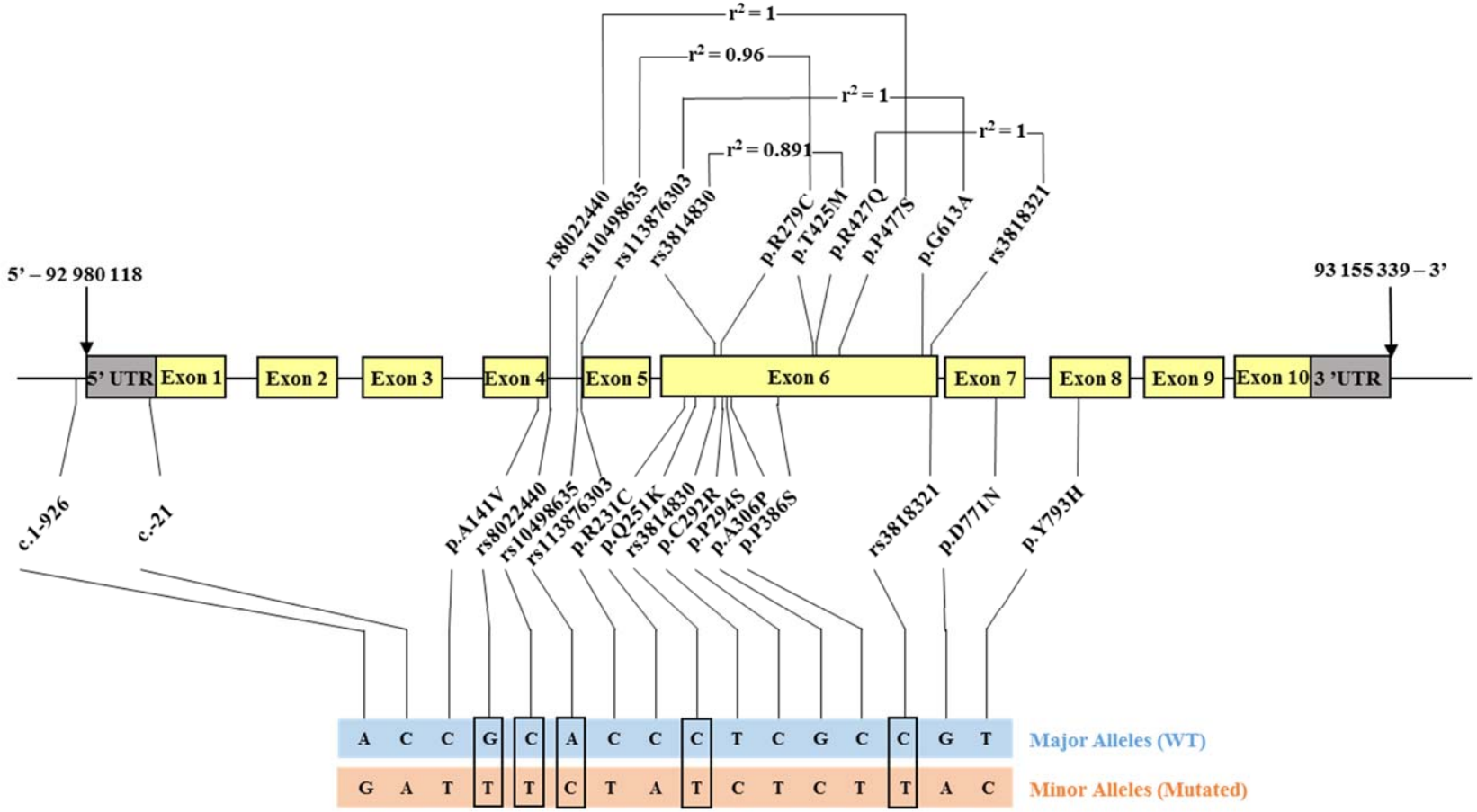

The two extreme haplotypes are presented in blue (major alleles) and in orange (minor alleles) for the 15 genotyped variants and the rs10498635 which was added from the GWAS data to represent p.R279C. The r^2 values for the 4 SNPs (And rs10498635) used as alternatives to coding variants are showed above the RIN3 sequence.

APPENDIX 4.2. ESTIMATED HAPLOTYPE FREQUENCIES FOR THE PRISM COHORT

Haplotype ID	Haplotype	Estimated frequencies (%) ± standard deviation		
		Controls and cases	Controls (*n* = 262)	Cases (*n* = 712)
1 (WT)	**ACCGACCCTCGCCGT**	**81.41 ± 0.35**	**78.97 ± 0.37**	**82.31 ± 0.38**
2	ACCGACCCTCGCCGC	0.43 ± 0.06	0.58 ± 0.03	0.37 ± 0.08
3	ACCGACCCTCGCCAT	0.05 ± 0.01	0 ± 0	0.07 ± 0.01
4	ACCGACCCTCGCTGT	1.55 ± 0.09	0.79 ± 0.16	1.83 ± 0.09
5	ACCGACCCTTGCCGT	0.06 ± 0.04	0.13 ± 0.09	0.04 ± 0.04
6 (p.425M)	**ACCGACCTTCGCCGT**	**14.43 ± 0.32**	**17.73 ± 0.34**	**13.22 ± 0.35**
7	ACCGACCTTCGCCGC	0.03 ± 0.04	0 ± 0	0.04 ± 0.06
8	ACCGACCTTCGCTGT	0.26 ± 0.08	0.19 ± 0.15	0.28 ± 0.08
9	ACCGACCTTTGCCGT	0.02 ± 0.03	0.06 ± 0.09	< 0.01%
10	ACCGACACTCGCCGT	0.03 ± 0.04	0 ± 0	0.04 ± 0.05
11	ACCGACACTCGCCGC	0.02 ± 0.03	0 ± 0	0.03 ± 0.04
12	ACCGACATTCGCCGT	0.11 ± 0.05	< 0.01%	0.15 ± 0.06
13	ACCGACATTCGCCGC	< 0.01%	0 ± 0	< 0.01%
14	ACCGATCCTCGCCGT	0.03 ± 0.03	0 ± 0	0.04 ± 0.04
15	ACCGATCCTTGCCGT	0.03 ± 0.03	0 ± 0	0.03 ± 0.04
16	ACCGCCCCTCGCCGT	0.80 ± 0.04	0.58 ± 0.03	0.89 ± 0.05
17	ACCGCCCTTCGCCGT	0.02 ± 0.03	0 ± 0	0.03 ± 0.04
18	ACCTACCCTCGCCGT	0.05 ± 0	0 ± 0	0.07 ± 0
19	ACTGACCCTCGCCGT	0.05 ± 0	0 ± 0	0.07 ± 0
20	AACGACCCTCGCCGT	0.51 ± 0.03	0.94 ± 0.10	0.35 ± 0.01
21	AACGACCTTCGCCGT	0.01 ± 0.02	0.03 ± 0.07	0 ± 0
22	GCCGACCCTCGCCGT	0.09 ± 0.03	0 ± 0	0.12 ± 0.04
23	GCCGACCTTCGCCGT	0.02 ± 0.02	0 ± 0	0.02 ± 0.03
			Frequency of SQSTM1 +	**72/699 (10.30%)**

APPENDIX 4.3. DETAILS OF THE ASSOCIATION STUDY FOR P.T425M IN THE PRISM CASES

p.T425M				
Variable	**T/T (*n* = 514)**	**T/M (*n* = 149)**	**M/M (*n* = 20)**	**p-value**
Gender (Male)	267/507 (52.66%)	85/144 (59.03%)	10/19 (52.63%)	0.398
Family history of PDB	80/506 (15.81%)	17/144 (11.81%)	4/19 (21.05%)	0.378
Orthopaedic surgery	79/507 (15.58%)	29/144 (20.14%)	4/19 (21.05%)	0.380
Any fracture	201/507 (39.64%)	60/144 (41.67%)	8/19 (42.11%)	0.895
Skull disease and hearing aid	40/507 (7.89%)	9/144 (6.25%)	2/19 (10.53%)	0.717
Bone pain	345/485 (71.13%)	101/135 (74.81%)	16/19 (84.21%)	0.350
Fracture in Pagetic bone	46/201 (22.89%)	18/60 (30%)	1/8 (12.50%)	0.389
Bisphosphonates	1.30 ± 1.06	1.21 ± 1.14	1.58 ± 1.46	0.345
Age at diagnosis	**64.74 ± 11.31**	**63.84 ± 11.68**	**55.37 ± 12.41**	**0.002**
Age at recruitment	**73.39 ± 7.87**	**73.37 ± 8.11**	**66.42 ± 9.29**	**0.001**
Number of bones affected	1.81 ± 1.03	1.83 ± 1.07	1.84 ± 1.30	0.958
Pagetic pain	1.48 ± 0.73	2.4 ± 9.73	1.44 ± 0.73	0.204
Deformity score	0.55 ± 0.93	0.56 ± 1.02	0.58 ± 0.84	0.994
Paget severity score	5.68 ± 2.43	5.70 ± 2.69	6.42 ± 3.15	0.451
Frequency of SQSTM1 +	**51/507 (10.06%)**	**11/144 (7.64%)**	**5/19 (26.32%)**	**0.039**

Values are shown as number of patients observed/total number of patients, or mean value ± SD.

APPENDIX 4.4. DETAILS OF THE ASSOCIATION STUDY FOR P.T425M IN THE PRISM CASES NOT CARRYING SQSTM1 MUTATIONS

p.T425M				
Variable	**T/T (*n* = 456)**	**T/M (*n* = 133)**	**M/M (*n* = 14)**	**p-value**
Gender (Male)	246/456 (53.95%)	77/133 (57.89%)	8/14 (57.14%)	0.713
Family history of PDB	58/455 (12.75%)	12/133 (9.02%)	1/14 (7.14%)	0.434
Orthopaedic surgery	68/456 (14.91%)	25/133 (18.80%)	3/14 (21.43%)	0.476
Any fracture	183/456 (40.13%)	55/133 (41.35%)	6/14 (42.86%)	0.952
Skull disease and hearing aid	35/456 (7.68%)	8/133 (6.02%)	0/14 (0%)	0.466
Bone pain	309/436 (70.87%)	92/125 (73.60%)	11/14 (78.57%)	0.707
Fracture in Pagetic bone	41/183 (22.40%)	16/55 (29.09%)	0/6 (0%)	0.231
Bisphosphonates	1.24 ± 1.03	1.20 ± 1.14	1.14 ± 1.23	0.867
Age at diagnosis	65.20 ± 11.29	64.03 ± 11.74	59.86 ± 9.76	0.148
Age at recruitment	**73.43 ± 7.90**	**73.53 ± 8.04**	**67.36 ± 10.30**	**0.019**
Number of bones affected	1.74 ± 1.01	1.77 ± 1.00	1.36 ± 0.74	0.334
Pagetic pain	1.45 ± 0.71	2.51 ± 10.20	1.55 ± 0.82	0.184
Deformity score	0.55 ± 0.89	0.53 ± 1.04	0.43 ± 0.65	0.879
Paget severity score	5.54 ± 2.36	5.56 ± 2.66	5.21 ± 1.76	0.875

Values are shown as number of patients observed/total number of patients, or mean value ± SD.

APPENDIX 4.5. DETAILS OF THE ASSOCIATION STUDY FOR P.T425M IN THE PRISM CASES CARRIERS OF SQSTM1 MUTATION

p.T425M				
Variable	**T/T (*n* = 51)**	**T/M (*n* = 11)**	**M/M (*n* = 5)**	**p-value**
Gender (Male)	21/51 (41.18%)	8/11 (72.73%)	2/5 (40%)	0.157
Family history of PDB	22/51 (43.14%)	5/11 (45.45%)	3/5 (60%)	0.769
Orthopaedic surgery	11/51 (21.57%)	4/11 (36.36%)	1/5 (20%)	0.567
Any fracture	18/51 (35.29%)	5/11 (45.45%)	2/5 (40%)	0.812
Skull disease and hearing aid	5/51 (9.80%)	1/11 (9.09%)	2/5 (40%)	0.132
Bone pain	36/49 (73.47%)	9/10 (90%)	5/5 (100%)	0.241
Fracture in Pagetic bone	5/18 (27.78%)	2/5 (40%)	1/2 (50%)	0.744
Bisphosphonates	1.78 ± 1.24	1.36 ± 1.12	2.8 ± 1.48	0.107
Age at diagnosis	**60.61 ± 10.68**	**61.55 ± 11.20**	**42.8 ± 10.76**	**0.003**
Age at recruitment	**73.04 ± 7.71**	**71.36 ± 9.14**	**63.8 ± 5.67**	**0.047**
Number of bones affected	2.43 ± 1.06	2.55 ± 1.57	3.2 ± 1.64	0.395
Pagetic pain	1.69 ± 0.86	1.22 ± 0.44	1.2 ± 0.43	0.153
Deformity score	0.59 ± 1.20	0.82 ± 0.75	1 ± 1.22	0.656
Paget severity score	6.92 ± 2.75	7.36 ± 2.54	9.8 ± 3.90	0.097

Values are shown as number of patients observed/total number of patients, or mean value ± SD.

APPENDIX 4.6. DETAILS OF THE ASSOCIATION STUDY FOR P.R279C IN THE PRISM CASES

p.R279C				
Variable	**R/R (*n* = 522)**	**R/C (*n* = 160)**	**C/C (*n* = 13)**	**p-value**
Gender (Male)	290/522 (55.56%)	77/160 (48.13%)	7/13 (53.85%)	0.257
Family history of PDB	85/521 (16.31%)	17/160 (10.63%)	1/13 (7.69%)	0.160
Orthopaedic surgery	82/522 (15.71%)	32/160 (20%)	1/13 (7.69%)	0.303
Any fracture	212/522 (40.61%)	61/160 (38.13%)	6/13 (46.15%)	0.773
Skull disease and hearing aid	36/522 (6.90%)	14/160 (8.75%)	1/13 (7.69%)	0.733
Bone pain	374/498 (75.10%)	104/154 (67.53%)	10/12 (83.33%)	0.131
Fracture in Pagetic bone	48/212 (22.64%)	18/61 (29.51%)	0/6 (0%)	0.208
Bisphosphonates	1.31 ± 1.10	1.21 ± 1.08	1.62 ± 1.45	0.313
Age at diagnosis	63.63 ± 11.96	65.74 ± 9.29	61.38 ± 15.59	0.088
Age at recruitment	72.97 ± 7.88	73.68 ± 8.19	74.38 ± 10.01	0.527
Number of bones affected	1.84 ± 1.07	1.76 ± 1.05	1.46 ± 0.52	0.331
Pagetic pain	1.71 ± 5.09	1.51 ± 0.79	1.2 ± 0.63	0.876
Deformity score	0.55 ± 0.93	0.59 ± 1	1 ± 1	0.233
Paget severity score	5.74 ± 2.51	5.64 ± 2.52	6.15 ± 1.86	0.754
Frequency of SQSTM1 +	55/522 (10.54%)	15/160 (9.38%)	1/13 (7.69%)	0.873

Values are shown as number of patients observed/total number of patients, or mean value ± SD.

APPENDIX 4.7. DETAILS OF THE ASSOCIATION STUDY FOR P.R279C IN THE PRISM CASES NOT CARRYING SQSTM1 MUTATIONS

p.R279C				
Variable	**R/R (*n* = 467)**	**R/C (*n* = 145)**	**C/C (*n* = 12)**	**p-value**
Gender (Male)	262/467 (56.10%)	71/145 (48.97%)	7/12 (58.33%)	0.309
Family history of PDB	59/466 (12.66%)	13/145 (8.97%)	0/12 (0%)	0.215
Orthopaedic surgery	68/467 (14.56%)	29/145 (20%)	1/12 (8.33%)	0.226
Any fracture	193/467 (41.33%)	55/145 (37.93%)	6/12 (50%)	0.617
Skull disease and hearing aid	31/467 (6.64%)	11/145 (7.59%)	1/12 (8.33%)	0.907
Bone pain	332/446 (74.44%)	92/139 (66.19%)	10/11 (90.91%)	0.064
Fracture in Pagetic bone	43/193 (22.28%)	15/55 (27.27%)	0/6 (0%)	0.298
Bisphosphonates	1.25 ± 1.06	1.17 ± 1.07	1.58 ± 1.51	0.364
Age at diagnosis	**64.24 ± 11.80**	**66.45 ± 9.11**	**59.5 ± 14.65**	**0.034**
Age at recruitment	73.02 ± 7.90	74.03 ± 8.04	73.5 ± 9.91	0.412
Number of bones affected	1.77 ± 1.02	1.66 ± 0.99	1.42 ± 0.51	0.300
Pagetic pain	1.73 ± 5.40	1.52 ± 0.79	1.2 ± 0.51	0.890
Deformity score	0.55 ± 0.95	0.53 ± 0.87	1.08 ± 1.00	0.141
Paget severity score	5.59 ± 2.48	5.41 ± 2.25	6.25 ± 1.91	0.458

Values are shown as number of patients observed/total number of patients, or mean value ± SD.

APPENDIX 4.8. DETAILS OF THE ASSOCIATION STUDY FOR P.R279C IN THE PRISM CASES CARRIERS OF SQSTM1 MUTATION

p.R279C				
Variable	**R/R (*n* = 55)**	**R/C (*n* = 15)**	**C/C (*n* = 1)**	**p-value**
Gender (Male)	28/55 (50.91%)	6/15 (40%)	0/1 (0%)	0.474*
Family history of PDB	26/55 (47.27%)	4/15 (26.67%)	1/1 (100%)	0.188
Orthopaedic surgery	14/55 (25.45%)	3/15 (20%)	0/1 (0%)	0.774*
Any fracture	19/55 (34.55%)	6/15 (40%)	0/1 (0%)	0.703*
Skull disease and hearing aid	5/55 (9.09%)	3/15 (20%)	0/1 (0%)	0.465*
Bone pain	42/52 (80.77%)	12/15 (80%)	0/1 (0%)	0.141*
Fracture in Pagetic bone	5/19 (26.32%)	3/6 (50%)	UND/1 (0%)	0.278*
Bisphosphonates	1.84 ± 1.30	1.6 ± 1.12	2 ± UND	0.804*
Age at diagnosis	58.45 ± 12.14	58.93 ± 8.50	84 ± UND	0.096*
Age at recruitment	72.53 ± 7.75	70.33 ± 9.12	85 ± UND	0.188*
Number of bones affected	2.45 ± 1.26	2.67 ± 1.18	2 ± UND	0.778*
Pagetic pain	1.57 ± 0.74	1.42 ± 0.79	UND ± UND	0.531*
Deformity score	0.53 ± 0.84	1.13 ± 1.77	0 ± UND	0.145*
Paget severity score	7.04 ± 2.47	7.87 ± 3.81	5 ± UND	0.442*

Values are shown as number of patients observed/total number of patients, or mean value ± SD. *Analysis performed on the R/R and R/C columns only. UND = Undetermined.

APPENDIX 4.9. DETAILS OF THE ASSOCIATION STUDY FOR THE RARE VARIANTS IN THE PRISM CASES

Rare variants			
Variable	**No rare variant (*n* = 653)**	**Rare variant present (*n* = 59)**	**p-value**
Gender (Male)	349/642 (54.36%)	29/57 (50.88%)	0.613
Family history of PDB	95/641 (14.82%)	8/57 (14.04%)	0.873
Orthopaedic surgery	105/642 (16.36%)	11/57 (19.30%)	0.567
Any fracture	259/642 (40.34%)	21/57 (36.84%)	0.605
Skull disease and hearing aid	48/642 (7.48%)	3/57 (5.26%)	0.538
Bone pain	450/615 (73.17%)	40/53 (75.47%)	0.716
Fracture in Pagetic bone	63/259 (24.32%)	4/21 (19.05%)	0.586
Bisphosphonates	1.29 ± 1.11	1.26 ± 1.04	0.838
Age at diagnosis	64.12 ± 11.56	64.32 ± 10.88	0.904
Age at recruitment	73.25 ± 7.88	72.53 ± 9.11	0.512
Number of bones affected	1.82 ± 1.06	1.77 ± 1.07	0.746
Pagetic pain	1.66 ± 4.65	1.63 ± 0.81	0.962
Deformity score	0.57 ± 0.97	0.46 ± 0.76	0.368
Paget severity score	5.74 ± 2.51	5.46 ± 2.46	0.410
Frequency of SQSTM1 +	65/642 (10.12%)	7/57 (12.28%)	0.608

Values are shown as number of patients observed/total number of patients, or mean value ± SD.

APPENDIX 4.10. DETAILS OF THE ASSOCIATION STUDY FOR THE RARE VARIANTS IN THE PRISM CASES NOT CARRYING SQSTM1 MUTATIONS

Rare variants			
Variable	**No rare variant (*n* = 577)**	**Rare variant present (*n* = 50)**	**p-value**
Gender (Male)	316/577 (54.77%)	27/50 (54%)	0.917
Family history of PDB	65/576 (11.28%)	7/50 (14%)	0.564
Orthopaedic surgery	89/577 (15.42%)	9/50 (18%)	0.630
Any fracture	236/577 (40.90%)	18/50 (36%)	0.498
Skull disease and hearing aid	40/577 (6.93%)	3/50 (6%)	0.802
Bone pain	402/553 (72.69%)	33/46 (71.74%)	0.889
Fracture in Pagetic bone	55/236 (23.31%)	3/18 (16.67%)	0.518
Bisphosphonates	1.24 ± 1.07	1.20 ± 1.05	0.804
Age at diagnosis	64.61 ± 11.42	66 ± 10.38	0.406
Age at recruitment	73.32 ± 7.93	73.04 ± 8.47	0.811
Number of bones affected	1.74 ± 1.00	1.68 ± 1.06	0.678
Pagetic pain	1.67 ± 4.92	1.67 ± 0.85	0.998
Deformity score	0.56 ± 0.95	0.44 ± 0.76	0.365
Paget severity score	5.58 ± 2.41	5.20 ± 2.43	0.288

Values are shown as number of patients observed/total number of patients, or mean value ± SD.

APPENDIX 4.11. DETAILS OF THE ASSOCIATION STUDY FOR THE RARE VARIANTS IN THE PRISM CASES CARRIERS OF SQSTM1 MUTATION

Rare variants			
Variable	**No rare variant (*n* = 65)**	**Rare variant present (*n* = 7)**	**p-value**
Gender (Male)	33/65 (50.77%)	2/7 (28.57%)	0.264
Family history of PDB	30/65 (46.15%)	1/7 (14.29%)	0.106
Orthopaedic surgery	16/65 (24.62%)	2/7 (28.57%)	0.818
Any fracture	23/65 (35.38%)	3/7 (42.86%)	0.696
Skull disease and hearing aid	8/65 (12.31%)	0/7 (0%)	0.325
Bone pain	48/62 (77.42%)	7/7 (100%)	0.159
Fracture in Pagetic bone	8/23 (34.78%)	1/3 (33.33%)	0.960
Bisphosphonates	1.78 ± 1.28	1.71 ± 0.95	0.888
Age at diagnosis	59.8 ± 11.97	52.29 ± 5.82	0.107
Age at recruitment	72.62 ± 7.41	68.86 ± 13.09	0.245
Number of bones affected	2.51 ± 1.25	2.43 ± 0.98	0.872
Pagetic pain	1.58 ± 0.79	1.43 ± 0.53	0.621
Deformity score	0.66 ± 1.14	0.57 ± 0.79	0.839
Paget severity score	7.18 ± 2.86	7.29 ± 1.98	0.928

Values are shown as number of patients observed/total number of patients, or mean value ± SD.

APPENDIX 4.12. ESTIMATED HAPLOTYPE FREQUENCIES FOR THE PRISM CASES, INCLUDING THE GWAS HIT IMPORTED DATA

Haplotype ID	Haplotype	Estimated frequencies (%) ± standard deviation
1 (WT)	**ACCGCACCCTCGCCGT**	**69.32 ± 0.50**
2	ACCGCACCCTCGCCGC	0.39 ± 0.05
3	ACCGCACCCTCGCCAT	0.07 ± 0.01
4	ACCGCACCCTCGCTGT	1.79 ± 0.10
5	ACCGCACCCTCHCCGT	< 0.01%
6	ACCGCACCCTTGCCGT	0.02 ± 0.03
7 (p.425M)	**ACCGCACCTTCGCCGT**	**13.14 ± 0.41**
8	ACCGCACCTTCGCCGC	0.01 ± 0.03
9	ACCGCACCTTCGCTGT	0.17 ± 0.10
10	ACCGCACACTCGCCGT	0.02 ± 0.04
11	ACCGCACACTCGCCGC	0.01 ± 0.02
12	ACCGCACATTCGCCGT	0.11 ± 0.09
13	ACCGCACATTCGCCGC	0.08 ± 0.10
14	ACCGCATCCTCGCCGT	0.02 ± 0.03
15	ACCGCATCCTTGCCGT	0.05 ± 0.03
16	ACCGCCCCCTCGCCGT	0.91 ± 0.04
17	ACCGCCCCTTCGCCGT	0.01 ± 0.03
18 (p.279C)	**ACCGTACCCTCGCCGT**	**12.84 ± 0.30**
19	ACCGTACCCTCGCCGC	< 0.01%
20	ACCGTACCCTCGCTGT	0.02 ± 0.06
21	ACCGTACCTTCGCCGT	0.25 ± 0.20
22	ACCGTACCTTCGCTGT	0.13 ± 0.05
23	ACCGTCCCCTCGCCGT	< 0.01%
24	ACCTCACCCTCGCCGT	0.04 ± 0.04
25	ACCTTACCCTCGCCGT	0.03 ± 0.03
26	ACTGCACCCTCGCCGT	0.07 ± 0
27	AACGCACCCTCGCCGT	0.31 ± 0.08
28	AACGTACCCTCGCCGT	0.04 ± 0.08
29	GCCGCACCCTCGCCGT	0.14 ± 0.03
30	GCCGCACCTTCGCCGT	0.01 ± 0.02
	Frequency of SQSTM1 +	**72/699 (10.30%)**